frontiers | Research Topics

Nuclear medicine in rheumatological diseases' therapy and diagnosis

Edited by
Giorgio Treglia and Clément Bailly

Published in
Frontiers in Medicine

ISSN 1664-8714
ISBN 978-2-83251-775-8
DOI 10.3389/978-2-83251-775-8

About Frontiers

Frontiers is more than just an open access publisher of scholarly articles: it is a pioneering approach to the world of academia, radically improving the way scholarly research is managed. The grand vision of Frontiers is a world where all people have an equal opportunity to seek, share and generate knowledge. Frontiers provides immediate and permanent online open access to all its publications, but this alone is not enough to realize our grand goals.

Frontiers journal series

The Frontiers journal series is a multi-tier and interdisciplinary set of open-access, online journals, promising a paradigm shift from the current review, selection and dissemination processes in academic publishing. All Frontiers journals are driven by researchers for researchers; therefore, they constitute a service to the scholarly community. At the same time, the *Frontiers journal series* operates on a revolutionary invention, the tiered publishing system, initially addressing specific communities of scholars, and gradually climbing up to broader public understanding, thus serving the interests of the lay society, too.

Dedication to quality

Each Frontiers article is a landmark of the highest quality, thanks to genuinely collaborative interactions between authors and review editors, who include some of the world's best academicians. Research must be certified by peers before entering a stream of knowledge that may eventually reach the public - and shape society; therefore, Frontiers only applies the most rigorous and unbiased reviews. Frontiers revolutionizes research publishing by freely delivering the most outstanding research, evaluated with no bias from both the academic and social point of view. By applying the most advanced information technologies, Frontiers is catapulting scholarly publishing into a new generation.

What are Frontiers Research Topics?

Frontiers Research Topics are very popular trademarks of the *Frontiers journals series*: they are collections of at least ten articles, all centered on a particular subject. With their unique mix of varied contributions from Original Research to Review Articles, Frontiers Research Topics unify the most influential researchers, the latest key findings and historical advances in a hot research area.

Find out more on how to host your own Frontiers Research Topic or contribute to one as an author by contacting the Frontiers editorial office: frontiersin.org/about/contact

Nuclear medicine in rheumatological diseases' therapy and diagnosis

Topic editors

Giorgio Treglia — Ente Ospedaliero Cantonale (EOC), Switzerland

Clément Bailly — Centre Hospitalier Universitaire (CHU) de Nantes, France

Citation

Treglia, G., Bailly, C., eds. (2023). *Nuclear medicine in rheumatological diseases' therapy and diagnosis*. Lausanne: Frontiers Media SA.

doi: 10.3389/978-2-83251-775-8

Table of contents

frontiers | Frontiers in Medicine

TYPE Editorial
PUBLISHED 14 March 2023
DOI 10.3389/fmed.2023.1171992

OPEN ACCESS

EDITED AND REVIEWED BY
Ronan Abgral,
Centre Hospitalier Regional Universitaire (CHU) de Brest, France

*CORRESPONDENCE
Giorgio Treglia
✉ giorgio.treglia@eoc.ch

SPECIALTY SECTION
This article was submitted to Nuclear Medicine, a section of the journal Frontiers in Medicine

RECEIVED 22 February 2023
ACCEPTED 01 March 2023
PUBLISHED 14 March 2023

CITATION
Treglia G and Bailly C (2023) Editorial: Nuclear medicine in rheumatological diseases' therapy and diagnosis. *Front. Med.* 10:1171992. doi: 10.3389/fmed.2023.1171992

Editorial: Nuclear medicine in rheumatological diseases' therapy and diagnosis

Giorgio Treglia[1,2,3]* and Clément Bailly[4,5]

[1]Division of Nuclear Medicine, Imaging Institute of Southern Switzerland, Ente Ospedaliero Cantonale, Bellinzona, Switzerland, [2]Faculty of Biomedical Sciences, Università della Svizzera italiana, Lugano, Switzerland, [3]Faculty of Biology and Medicine, University of Lausanne, Lausanne, Switzerland, [4]University of Nantes, CHU Nantes, Nantes, France, [5]Nuclear Medicine Department, University Hospital, Nantes, France

KEYWORDS

PET, nuclear medicine, rheumatology, treatment, diagnosis, radionuclides

Editorial on the Research Topic
Nuclear medicine in rheumatological diseases' therapy and diagnosis

Rheumatological diseases are common conditions in the general population and their diagnosis in clinical practice is challenging due to their unspecific clinical presentation. Nuclear medicine has a great potential for the management of the rheumatological diseases providing a tool for diagnosis, assessment of prognosis, and treatment efficacy. Furthermore, radiopharmaceuticals may be used as therapeutic options in patients with rheumatological diseases. The application of nuclear medicine techniques in the diagnosis and management of rheumatological diseases relies on the detection of *in vivo* functional abnormalities at an early stage of the diseases, earlier compared to the structural changes detected by conventional imaging (1–7).

This Research Topic comprises 11 articles (four reviews, six original articles, and one study protocol) that highlight the role of nuclear medicine techniques in the management of rheumatological diseases.

The mini-review of Wenger and Schirmer provides an overview on the current use of nuclear medicine imaging modalities in the diagnosis of rheumatological diseases. In particular the authors described that, at present, [^{18}F]FDG PET/CT is the hybrid imaging method most often used in rheumatology, in particular for diagnosis of large vessel vasculitis. Despite the current limited value of bone scintigraphy as diagnostic procedure in rheumatological diseases, this nuclear medicine technique has a role before and after radiosynovectomy. In the review of Nassarmadji et al. the evidence on the role of [^{18}F]FDG PET/CT for diagnosis, treatment monitoring and follow-up in large vessel vasculitis was summarized. [^{18}F]FDG PET/CT is currently not recommended for diagnosis of chronic inflammatory rheumatism including rheumatoid arthritis, spondyloarthritis, and polymyalgia rheumatica. However, this imaging tool seems promising in chronic inflammatory rheumatism as described in the mini-review of De Ponfilly-Sotier et al. as it may provide an overview of systemic involvement occurring in this setting. Lastly, the review of van der Geest et al. illustrates novel PET radiopharmaceuticals that may be useful for diagnosis and treatment monitoring of polymyalgia rheumatica and large vessel vasculitis.

Four original articles included in this Research Topic are focused on polymyalgia rheumatica. French researchers evaluated periarticular [^{18}F]FDG uptake scores using PET/CT images to identify polymyalgia rheumatica within a group of patients with rheumatic diseases. The presence of at least three sites with significant uptake identified polymyalgia rheumatica with a sensitivity of 86% and a specificity of 85.5%, suggesting that [^{18}F]FDG PET/CT has good performance to identify polymyalgia rheumatica within a population presenting rheumatic diseases (Amat et al.). A research article from the same group demonstrated that machine learning algorithm is useful for diagnosis of polymyalgia rheumatica using [^{18}F]FDG PET/CT in a group of patients with inflammatory rheumatisms providing accurate sensitivity and specificity (Flaus et al.).

In a large Belgian retrospective study, researchers scored [^{18}F]FDG uptake through visual analysis of PET images taking into account 12 articular regions (scores 0–2 for each articular region). A total skeletal score was calculated by summing the individual scores. These PET scores showed high diagnostic accuracy for the diagnosis of polymyalgia rheumatica (Moreel et al.).

An Italian retrospective study demonstrated that [^{18}F]FDG PET/CT performed in patients with polymyalgia rheumatica and persistent increase of acute phase reactants was able to detect persistence of active polymyalgia rheumatica, occult large vessel vasculitis, or other inflammatory diseases (Colaci et al.).

In a retrospective study from China, researchers explored the value of [^{18}F]FDG PET/CT for assessing disease activity and for predicting the prognosis of the Adult-onset Still's disease. The authors reported that increased radiopharmaceutical uptake was observed in bone marrow, lymph nodes, and spleen of patients with Adult-onset Still's disease. Taking into account the correlation among PET findings and laboratory inflammatory markers, the authors suggested to use [^{18}F]FDG PET/CT for evaluating disease activity and for predicting clinical prognosis of Adult-onset Still's disease (Li et al.).

In another retrospective study, Swiss researchers investigated the emerging role of quantification of ^{99m}Tc-labeled diphosphonates uptake by using SPECT/CT in fibrous dysplasia bone lesions; furthermore, the authors correlated SPECT/CT findings with markers of disease activity. They found that bone turnover markers were correlated with diphosphonate uptake on bone scan, suggesting that bone scan, and in particular quantification using SPECT/CT, could be useful to assess the disease burden and to guide treatment and follow-up in patients with fibrous dysplasia (Jreige et al.).

Lastly, this Research Topic also includes a study protocol on a new nuclear medicine imaging method for detecting cartilage disorders. ^{99m}Tc-NTP 15-5 is a new radiopharmaceutical that can be used to target proteoglycans, which are a component of the cartilaginous extracellular matrix. Therefore, imaging of proteoglycans could be used for diagnosis, treatment monitoring and follow-up of cartilage disorders. French researchers published a study protocol to assess ^{99m}Tc-NTP 15-5 uptake in healthy joints (Thivat et al.).

Findings provided by the articles published in this Research Topic illustrate the current role and future perspectives of nuclear medicine in rheumatological disorders. Currently, among the different nuclear medicine imaging methods, there is a growing evidence supporting the use of [^{18}F]FDG PET/CT in several rheumatological diseases even if the role of bone scintigraphy in this setting should not been underestimated (8). Even if [^{18}F]FDG uptake is non-specific for inflammatory lesions, however, the distribution and pattern of radiopharmaceutical uptake could help in the differential diagnosis of rheumatological diseases or could demonstrate the true disease extent identifying occult sites on conventional imaging, in addition to identifying sites for biopsy to obtain histological confirmation (8). Furthermore, there is an emerging role of [^{18}F]FDG PET/CT to assess the treatment response and to monitor the disease activity (8). Overall, even if there is increasing evidence on the use of [^{18}F]FDG PET/CT in the diagnosis of rheumatological diseases, multicentric prospective studies are warranted to fully understand the potential of [^{18}F]FDG PET/CT in rheumatological diseases.

About the use of nuclear medicine techniques for therapy of rheumatological diseases, radiosynovectomy involving intra-articular injection of radiolabelled colloids (which induce necrosis and fibrosis of hypertrophic synovial membrane) is a valid, safe and well-tolerated option for treating persistent joint inflammation in rheumatoid arthritis, even if other arthropathies can also benefit from this method. However, radiosynovectomy is still underutilized in rheumatological diseases (9).

Author contributions

GT and CB drafted the manuscript and revised the final version. Both authors contributed to the article and approved the submitted version.

Conflict of interest

The authors declare that the research was conducted in the absence of any commercial or financial relationships that could be construed as a potential conflict of interest.

Publisher's note

References

1. Aarntzen EHJG, Noriega-Álvarez E, Artiko V, Dias AH, Gheysens O, Glaudemans AWJM, et al. EANM recommendations based on systematic analysis of small animal radionuclide imaging in inflammatory musculoskeletal diseases. *EJNMMI Res*. (2021) 11:85. doi: 10.1186/s13550-021-00820-8

2. Slart RHJA, Writing group, Reviewer group, Members of EANM Cardiovascular, Members of EANM Infection & Inflammation, Members of Committees, SNMMI Cardiovascular, Members of Council, PET Interest Group, Members of ASNC, EANM Committee Coordinator. FDG-PET/CT(A) imaging in large vessel vasculitis and polymyalgia rheumatica: joint procedural recommendation of the EANM, SNMMI, and the PET Interest Group (PIG), and endorsed by the ASNC. *Eur J Nucl Med Mol Imaging*. (2018) 45:1250–69. doi: 10.1007/s00259-018-3973-8

3. Treglia G, Versari A, Giovanella L, Pipitone N, Salvarani C. Is 18F-FDG PET a 'potentially hazardous' or an effective tool in evaluating patients with large-vessel vasculitis? *Clin Exp Rheumatol*. (2013) 31:S93.

4. Treglia G, Mattoli MV, Leccisotti L, Ferraccioli G, Giordano A. Usefulness of whole-body fluorine-18-fluorodeoxyglucose positron emission tomography in patients with large-vessel vasculitis: a systematic review. *Clin Rheumatol*. (2011) 30:1265–75. doi: 10.1007/s10067-011-1828-9

5. van der Geest KSM, Treglia G, Glaudemans AWJM, Brouwer E, Jamar F, Slart RHJA, et al. Diagnostic value of [18F]FDG-PET/CT in polymyalgia rheumatica: a systematic review and meta-analysis. *Eur J Nucl Med Mol Imaging*. (2021) 48:1876–89. doi: 10.1007/s00259-020-05162-6

6. Treglia G, Albano D, Dondi F, Bertagna F, Gheysens O. A role of FDG PET/CT for response assessment in large vessel disease? *Semin Nucl Med*. (2023) 53:78–85. doi: 10.1053/j.semnuclmed.2022.08.002

7. van der Geest KSM, Treglia G, Glaudemans AWJM, Brouwer E, Sandovici M, Jamar F, et al. Diagnostic value of [18F]FDG-PET/CT for treatment monitoring in large vessel vasculitis: a systematic review and meta-analysis. *Eur J Nucl Med Mol Imaging*. (2021) 48:3886–902. doi: 10.1007/s00259-021-05362-8

8. Subesinghe M, Bhuva S, Arumalla N, Cope A, D'Cruz D, Subesinghe S. 2-deoxy-2[18F]fluoro-D-glucose positron emission tomography-computed tomography in rheumatological diseases. *Rheumatology*. (2022) 61:1769–82. doi: 10.1093/rheumatology/keab675

9. Chojnowski MM, Felis-Giemza A, Kobylecka M. Radionuclide synovectomy - essentials for rheumatologists. *Reumatologia*. (2016) 54:108–16. doi: 10.5114/reum.2016.61210

frontiers in Medicine

ORIGINAL RESEARCH
published: 13 August 2020
doi: 10.3389/fmed.2020.00394

Utility of ^{18}F-Fluorodeoxyglucose Positron Emission Tomography in Inflammatory Rheumatism, Particularly Polymyalgia Rheumatica: A Retrospective Study of 222 PET/CT

*Julie Amat[1], Marion Chanchou[1], Louis Olagne[2], Lucie Descamps[3], Anthime Flaus[4], Clément Bouvet[1], Bertrand Barres[1], Clemence Valla[1], Ioana Molnar[5], Arnaud Cougoul[5], Sylvain Mathieu[3], Olivier Aumaitre[2], Martin Soubrier[3], Antony Kelly[1], Charles Merlin[1] and Florent Cachin[1]**

[1] Jean Perrin Oncology Institute, Department of Nuclear Medicine, Clermont-Ferrand, France, [2] Gabriel Montpied University Hospital, Department of Internal Medicine University of Clermont-Ferrand, Clermont-Ferrand, France, [3] Gabriel Montpied University Hospital, Department of Rheumatology University of Clermont-Ferrand, Clermont-Ferrand, France, [4] North University Hospital, Department of Nuclear Medicine, University of Saint-Etienne, Saint-Etienne, France, [5] Jean Perrin Oncology Institute, Department of Biostatistics, Clermont-Ferrand, France

OPEN ACCESS

Edited by:
Ronan Abgral,
Centre Hospitalier Regional Universitaire (CHU) de Brest, France

Reviewed by:
Xavier Palard-Novello,
University of Rennes 1, France
Clément Bailly,
University Hospital of Nantes, France

***Correspondence:**
Florent Cachin
florent.cachin@clermont.unicancer.fr

Specialty section:
This article was submitted to Nuclear Medicine, a section of the journal Frontiers in Medicine

Received: 07 May 2020
Accepted: 24 June 2020
Published: 13 August 2020

Citation:
Amat J, Chanchou M, Olagne L, Descamps L, Flaus A, Bouvet C, Barres B, Valla C, Molnar I, Cougoul A, Mathieu S, Aumaitre O, Soubrier M, Kelly A, Merlin C and Cachin F (2020) Utility of ^{18}F-Fluorodeoxyglucose Positron Emission Tomography in Inflammatory Rheumatism, Particularly Polymyalgia Rheumatica: A Retrospective Study of 222 PET/CT. Front. Med. 7:394. doi: 10.3389/fmed.2020.00394

Purpose: The objective of this study was to evaluate periarticular FDG uptake scores from ^{18}F-FDG-PET/CT to identify polymyalgia rheumatica (PMR) within a population presenting rheumatic diseases.

Methods: A French retrospective study from 2011 to 2015 was conducted. Patients who underwent ^{18}F-FDG-PET/CT for diagnosis or follow-up of a rheumatism or an unexplained biological inflammatory syndrome were included. Clinical data and final diagnosis were reviewed. Seventeen periarticular sites were sorted by a visual reading enabling us to calculate two scores: mean FDG visual uptake score, number of sites with significant uptake same as that or higher than liver uptake intensity and by a semi-quantitative analysis using mean maximum standardized uptake value (SUVmax). Optimal cutoffs of visual score and SUVmax to diagnose PMR were determined using receiver operating characteristics curves.

Results: Among 222 ^{18}F-FDG PET/CT selected for 215 patients, 161 ^{18}F-FDG PET/CT were performed in patients who presented inflammatory rheumatism as a final diagnosis (of whom 57 PMR). The presence of at least three sites with significant uptake identified PMR with a sensitivity of 86% and a specificity of 85.5% (AUC 0.872, 95% CI [0.81–0.93]). The mean FDG visual score cutoff to diagnose a PMR was 0.765 with a sensitivity of 82.5% and a specificity of 75.8% (AUC 0.854; 95% CI [0.80–0.91]). The mean SUVmax cutoff to diagnose PMR was 2.168 with a sensitivity of 77.2% and a specificity of 77.6% (AUC 0.842; 95% CI [0.79–0.89]).

Conclusions: This study suggests that ^{18}F-FDG PET/CT had good performances to identify PMR within a population presenting rheumatic diseases.

Keywords: PMR, ^{18}F-FDG PET/CT, inflammatory rheumatism, uptake scores, SUVmax, bursa

KEY POINTS

- **Question:** The objective of our study was to evaluate visual and semi-quantitative periarticular scores derived from ^{18}F-FDG PET/CT for the diagnosis of PMR among rheumatic diseases.
- **Pertinent Findings:** This retrospective study showed that the presence of at least three sites with visual significant uptake and a mean SUVmax at the 17 sites equal to or greater than 2.168 had high sensitivities and specificities for the diagnosis of PMR.
- **Implications For Patient Care:** An accuracy ^{18}F-FDG PET/CT periarticular analysis guides the clinician when the clinical presentation is atypical, especially in cases of rheumatism in the elderly and, therefore, has an impact on early therapeutic management.

INTRODUCTION

Chronic inflammatory rheumatisms are common conditions among the general population. Rheumatoid arthritis (RA) is the most frequent rheumatism in France, with a prevalence of 0.35% (1). In people older than age 50, the prevalence of polymyalgia rheumatica (PMR) and giant cell arteritis (GCA) is 700/100,000 and 204/100,000, respectively (2).

The ACR/EULAR's 2010 criteria for RA (3) and its 2012 criteria for PMR (4) enable orientation of the diagnosis of these diseases; however, their sensitivities and specificities remain limited (57.9% and 88.8% for RA, 66% and 81% for PMR, respectively).

Moreover, the need to eliminate differential and associated diagnoses, such as neoplasias and vasculitis (5, 6) especially in elderly people, encourages additional examinations. Fluorodeoxyglucose positron emission tomography coupled with computerized tomography (^{18}F-FDG PET/CT) in these cases seems useful. Macrophage activation and fibroblast proliferation enhanced by proinflammatory cytokines result in an increased fluorodeoxyglucose (^{18}F-FDG) uptake in articular, periarticular, and vascular wall areas (7). Inflammation targets the synovial membrane in patients suffering from RA. In cases of PMR, it affects principally the serous bursa. Several studies demonstrated the usefulness of ^{18}F-FDG PET/CT in inflammatory rheumatism diseases (5, 6, 8–10), especially PMR and in vasculitis. ^{18}F-FDG PET/CT enables a full-body map of vascular, articular, and periarticular uptake within a single examination (9, 10).

Abbreviations: ACR/EULAR, American College of Rheumatology/European League Against Rheumatism; ASAS, Assessment of Spondyloarthritis International Society; AUC, Area under curve; BASDAI, Bath Ankylosing Spondylitis Disease Activity Index; CRP, C-reactive protein; CT, Corticotherapy; DAS28-VS or DAS28-CRP, Disease Activity Score; EORA, Elderly-onset rheumatoid arthritis; ESR, Erythrocyte sedimentation rate; ^{18}F-FDG PET/CT, Fluorodeoxyglucose positron emission tomography coupled with computerized tomography; GCA, Giant cell arteritis; IR, Inflammatory rheumatism; LVV, Large vessel vasculitis; MBq/kg, Megabecquerel per kilogram body weight; PMR, Polymyalgia rheumatica; RA, Rheumatoid arthritis; ROC, Receiver operating characteristic; ROI, Region of interest; RS3PE, Remitting symmetrical seronegative synovitis with pitting edema; SA, Spondyloarthritis; SAPHO, Synovitis-acne-pustulosis-hyperostosis-osteitis; SUVmax, Maximum standardized uptake value; TAB, Temporal artery biopsy.

Several scores have been developed for the diagnosis of vasculitis or inflammatory rheumatism and to evaluate their activity (11–13) with relatively promising results.

The objective of our study was to evaluate composite periarticular scores derived from ^{18}F-FDG PET/CT for the diagnosis of PMR among rheumatic diseases.

MATERIALS AND METHODS

Patients

In this retrospective study, 478 patients were selected. Their ^{18}F-FDG PET/CT were performed between April 2011 and December 2015 and prescribed by the Rheumatology and Internal Medicine Departments of our institution (Clermont-Ferrand, France).

^{18}F-FDG PET/CT inclusion criteria were follow-up of previously known rheumatic diseases such as PMR, RA, GCA, and spondyloarthritis (SA); diagnosis of suspected rheumatic diseases; and diagnosis of an unexplained biological inflammatory syndrome.

The following data were collected when available: indication of the ^{18}F-FDG PET/CT (initial test for inflammatory rheumatism or for an unexplained biological inflammatory syndrome, test for treatment resistance, screening for vasculitis, or a neoplasia), rheumatism's activity parameters such as C-reactive protein (CRP), erythrocyte sedimentation rate (ESR), DAS28-VS or DAS28-CRP, treatment with corticosteroids or other immunosuppressants (including duration and dose), and final diagnosis retained by a rheumatologist or an internal medicine specialist according to the patient's clinical and paraclinical data. ^{18}F-FDG PET/CT exams were not included in the paraclinical tests used for the final rheumatic diagnosis. In the majority, ^{18}F-FDG PET/CT was realized to rule out paraneoplastic rheumatism.

In case of an unclassified rheumatism, diagnosis was applied according to the 2010 ACR/EULAR's criteria for RA (3), its 2012 criteria for PMR (4), and the 2009 ASAS's criteria for SA (14). If the rheumatism did not meet these criteria, a final diagnosis was agreed upon collegially by the three principal investigators. Some patients remained with a diagnosis of unclassified rheumatism.

Patients were sorted into four groups:

- The group named "inflammatory rheumatisms" gathered patients with PMR, RA, SA, GCA, microcrystalline rheumatism, synovitis-acne-pustulosis-hyperostosis-osteitis (SAPHO), unclassified rheumatism, remitting seronegative symmetrical synovitis with pitting edema (RS3PE), paraneoplastic rheumatism, and psoriatic rheumatism.
- The group named "rheumatic diseases without inflammatory rheumatism" referred to patients who ultimately presented discopathy, vertebral collapse, prosthetic loosening, narrowing of the lumbar vertebral canal, tendinitis of the gluteus medius muscle, fracture of the pelvis, shoulder–hand syndrome, fibromyalgia, or osteoarthritis.
- The group named "infectious or inflammatory diseases" gathered a majority of patients addressed for an unexplained biological inflammatory syndrome and who ultimately

displayed infectious or inflammatory diseases, some of whom did not have musculoskeletal manifestations.
- The group named "absence of inflammatory rheumatism" included patients in the groups named "rheumatic diseases without inflammatory rheumatism" and "infectious or inflammatory diseases."

Eighty percent of GCA cases were proven histologically with a positive temporal biopsy. For the others, the diagnosis was based on clinical and paraclinical data (imaging).

The patients provided their written informed consent to participate in this study.

The study has been approved by CECIC Rhône Alpes Auvergne, Grenoble, IRB 5921 on 12 November 2019 (IRB number: 5921).

^{18}F-FDG PET/CT Imaging

After 4 h of fasting, a minimal activity of 3 MBq/kg of ^{18}F-FDG was injected into a peripheral vein. Acquisition was achieved 1 h after injection on a PET/CT scanner (Discovery ST or Discovery 710 Optima 660). In most cases, acquisition extended from the skull to the upper third of the femurs, with the upper extremities situated either along the body or above the head. Only 15% of the ^{18}F-FDG PET/CT involved the entire body. ^{18}F-FDG PET/CT acquisitions were not contrast-enhanced.

Similar to Sondag et al.'s (9) method, 17 periarticular sites were analyzed using a visual analysis to evaluate the intensity and the number of hotspots. A semi-quantitative analysis was also realized for the 17 hotspots. These involved both shoulders, both acromioclavicular and both sternoclavicular joints, the most intense interspinous bursa, both hips, both greater trochanters, both ischial tuberosities, both iliopectineal bursa, and both symphysis pubis enthesis. Each uptake was sorted by visual analysis using a four-point scale from 0 to 3 in comparison with liver uptake (0: no uptake, 1: uptake lower than the liver, 2: moderate uptake, same as that of the liver, 3: uptake higher than the liver).

Two visual composite scores were therefore analyzed: the mean FDG uptake score at the 17 sites of an exam: F_{17} and the number of sites with significant uptake [score $\geq$ 2, cutoff proposed by Goerres et al. (15): Nb].

Moreover, the maximum standardized uptake value (SUVmax) was measured at the 17 hotspots for 222 ^{18}F-FDG PET/CT by a board-certified nuclear medicine physician, blinded to the clinical and paraclinical test results, using Advantage Windows Server 3.2 (General Electric Healthcare Systems, 2016). For determination of the SUVmax, a region of interest (ROI) was manually placed over each of the 17 periarticular sites. Activity concentration within the ROI was determined and expressed as SUV, where SUV is the ratio of the activity in the tissue to the decay corrected activity injected into the patient and normalized for patient body weight. SUVmax was used as the reference measurement and was determined by considering the uptake given by the maximum pixel value within a ROI in each of the 17 hotpsots.

For PMR, RA, and all pathologies taken together, ^{18}F-FDG PET/CT was sorted into two groups (<3 sites with significant uptake, $\geq$3 sites with significant uptake) in order to compare the rheumatism's activity parameters.

Statistical Analysis

Parameters were calculated and then compared within the different groups (PMR, RA, SA, GCA, all inflammatory rheumatisms taken together, "absence of inflammatory rheumatism," and "rheumatic diseases without inflammatory rheumatism"):

- Mean FDG uptake score (F_{17}) and standard deviation,
- Number of sites with significant uptake (Nb) and standard deviation,

The means of the scores were compared using the Kruskal-Wallis test.

Some other parameters were calculated and compared between the PMR $\pm$ GCA group and other patients as follows using the Wilcoxon-Mann-Whitney test:

- Mean SUVmax for each of the 17 hotspots,
- Mean SUVmax for the 17 hotspots.

The sensitivity and specificity for the diagnosis of PMR were calculated using ROC curve.

Rheumatism's activity parameters (CRP, duration and dose of corticotherapy, DAS28-VS or DAS28-CRP) as well as age were calculated and compared based on the presence or absence of three sites with significant uptake for the groups PMR, RA and all pathologies taken together. The latter were compared using Student's test or the Kruskal-Wallis test. A bilateral p-value lower than the cutoff of 0.05 was considered statistically significant.

RESULTS

Patients

Overall, 222 ^{18}F-FDG PET/CT were selected for 215 patients as part of the testing for rheumatic diseases, vasculitis, neoplasias, or the exploration of an unexplained biological inflammatory syndrome. A flowchart is displayed in **Figure 1**.

Distribution of ^{18}F-FDG PET/CT according to the final diagnosis and characteristics of the population is given in **Tables 1**, **2**. **Table 2** summarizes the characteristics of the patients of the PMR group: median age 74.8 years (IQR 15.2), 31 women, 26 men, CRP 32 mg/L (IQR 66), 13 mg/day (IQR 5.8) corticosteroids. CRP values and corticosteroid dose were, respectively, available for 53 and 30 patients of the PMR group. In our whole population, these values were used, respectively, for 90 and 57 patients.

^{18}F-FDG PET/CT Visual Analysis

A visual score was calculated for 17 periarticular sites based on liver uptake comparison.

Summarized in **Table 3**, the mean FDG uptake score at the 17 sites (F_{17}) was significantly higher in the group of PMRs compared with the group "absence of inflammatory rheumatism," respectively, 1.32 ± 0.61 and 0.44 ± 0.31 ($p < 10^{-7}$). Likewise, the number of sites with significant uptake (Nb) was also higher, respectively, 6.9 ± 4.88 and 0.62 ± 1.2 ($p < 10^{-7}$) (**Table 3**).

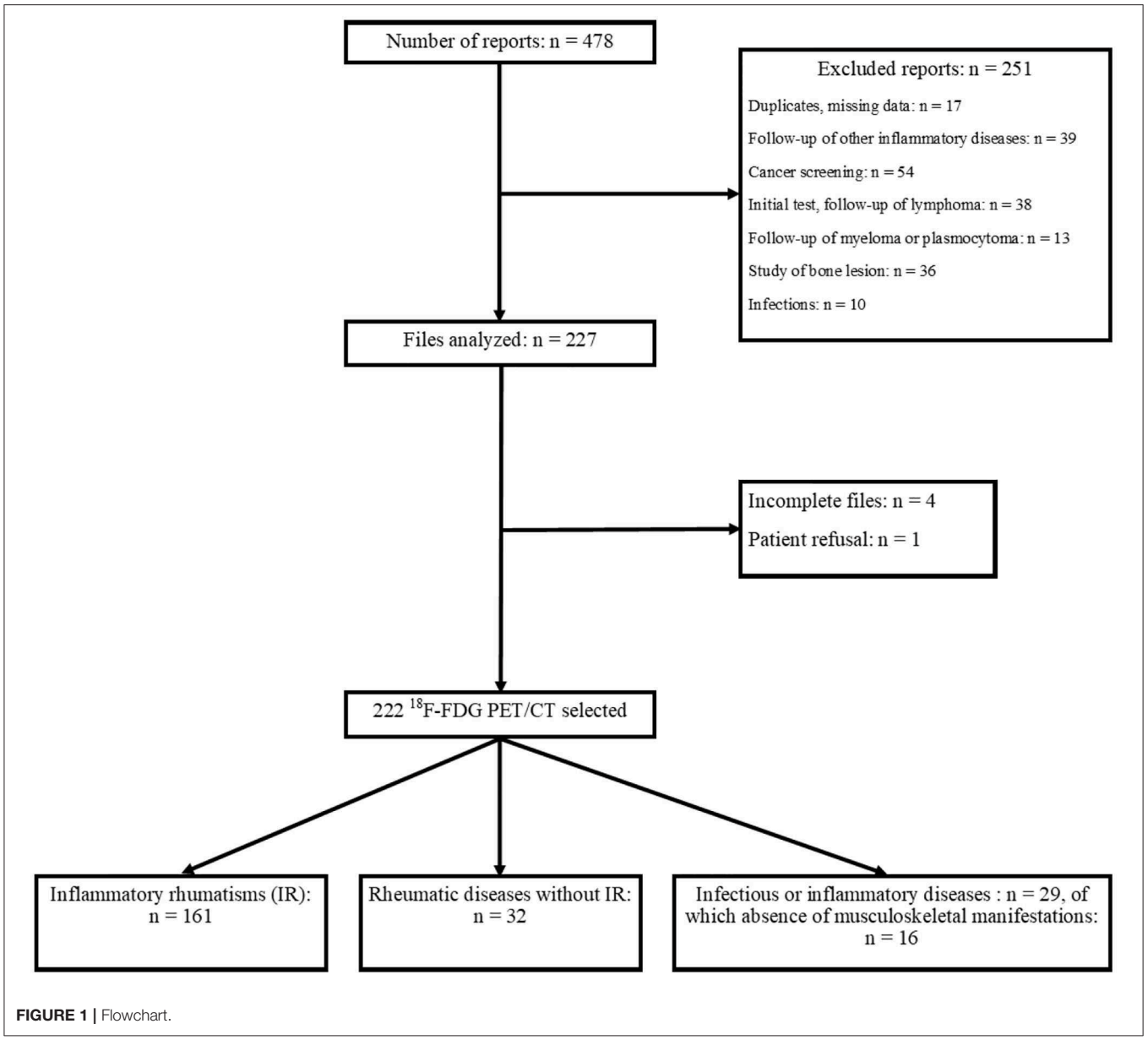

FIGURE 1 | Flowchart.

For the PMR diagnosis, the predictive cutoff values of the mean FDG uptake score (F_{17}) and the number of sites with significant uptake were determined, respectively, at 0.765 (sensitivity of 82.5%, specificity of 75.8%, AUC 0.854; 95% CI [0.80–0.91]) and ≥3 (sensitivity of 86% and specificity of 85.5%, AUC 0.872, 95% CI [0.81–0.93]).

Impairment of at least three sites (Nb $\geq$ 3) and a mean FDG uptake score >0.765 ($F_{17} > 0.765$) appeared to be the most specific criteria (respectively, 85.5 and 75.8%) for identifying PMR.

For example, this maximum-intensity projection and the axial fused ^{18}F-FDG PET/CT show a patient suffering from PMR with uptake at the 17 sites in **Figure 2**.

Relationship Between Visual FDG Uptake and Rheumatism Activity

Rheumatism activity parameters were calculated and compared in some groups according to the number of sites with visual uptake equal or superior to the liver background, which was the most sensitive and the more specific score. Results are shown in **Table 4**.

CRP values of RA and "all pathologies taken together" groups were significantly higher in patients who had at least three sites with significant uptake on their exams (respectively, $p = 0.0065$ and $p < 10^{-5}$). Likewise, DAS 28 in the RA group was significantly higher (6.0 ± 1.3 vs. 4.1 ± 1.3 with $p = 0.0045$).

TABLE 1 | Distribution of ^{18}F-FDG PET/CT according to the final diagnosis.

Final Diagnosis	Number of ^{18}F-FDG PET/CT	%
PMR	57	25.7
Of which, PMR + GCA	*10*	4.5
GCA (without PMR)	10	4.5
RA	49	22.1
SA	18	8.1
Psoriatic rheumatism	5	2.2
SAPHO	3	1.4
RS3PE	4	1.8
Paraneoplastic rheumatism	4	1.8
Microcrystalline rheumatism	5	2.2
Unclassified rheumatism	6	2.7
Rheumatic diseases without inflammatory rheumatism	32	14.4
Infectious or inflammatory diseases	29	13.1
Of which, patients without musculoskeletal manifestations	*16*	7.2
Total	222	100

TABLE 2 | Characteristics of the population.

Characteristics	All patients	PMR ± GCA
Gender, *n* (%)		
Men	89/215 (41.4)	26/57 (45.6)
Women	126/215 (58.6)	31/57 (54.4)
Age, median (IQR), years	70.4 (20.5)	74.8 (15.2)
CRP, median (IQR), mg/L	16 (49.6)	32 (66)
Steroids dose, median (IQR), mg/day	10 (9)	13 (5.8)
Total	215	57

Patients belonging to the group "all pathologies taken together" were older when there were at least three sites with significant uptake on ^{18}F-FDG PET/CT ($p = 0.034$).

Finally, we did not find any significant link between the dose and duration of corticosteroid use in patients with PMR or RA based on the number of sites with significant uptake.

^{18}F-FDG PET/CT Semi-Quantitative Analysis

SUVmax was measured on each of the 17 periarticular sites (**Table 5**). The mean SUVmax at the 17 sites was significantly higher in the PMR ± GCA group compared with the others, respectively, 2.68 (±0.63) and 1.81 (±0.69) ($p < 10^{-6}$).

The predictive cutoff of the mean SUVmax at the 17 sites for PMR was calculated at 2.168 (sensitivity of 77.2%, specificity of 77.6%, AUC 0.842; 95% CI [0.79–0.89]) (**Figure 3**).

Moreover, these results were also significantly higher in each of the 17 sites for the PMR ± Horton group.

The best predictive mean SUVmax cutoff to diagnose a PMR was determined at 2.168 (sensitivity of 77.2%, specificity of 77.6%, AUC 0.842; 95% CI [0.79–0.89]).

^{18}F-FDG PET/CT Visual and Semi-Quantitative Analysis

The sensitivities and specificities of four composite scores ($F_{17} > 0.53$, $F_{17} > 0.765$, Nb ≥ 3, SUVmax ≥ 2.168) enabling diagnosis of the studied diseases are given in **Table 6**.

DISCUSSION

Key Findings of the Study and Comparison to the Literature

To date, our study, with 222 ^{18}F-FDG PET/CT analyzed, has been one of the largest in terms of evaluating ^{18}F-FDG PET/CT in cases of inflammatory rheumatism. Visual and semi-quantitative analyses were realized on 17 periarticular sites. Also, our work consolidates various rheumatic diseases beyond cases of PMR, as was also done by Yamashita et al. (11), who included cases of PMR, RA, and SA. Yamashita et al. (11) demonstrated the usefulness of scores when categorizing cases of PMR from other rheumatic diseases (particularly RA and SA), by analyzing uptake in ischial tuberosities, in greater trochanters, and in interspinous bursa. Compared with the SA group, the ratio of FDG uptake was significantly higher in patients with PMR and lower in patients with RA in ischial tuberosities (63.2, 93.8, and 12.5%, respectively; $p < 0.001$), greater trochanters (47.4, 81.3, and 12.5%; $p < 0.001$), and interspinous bursa (52.63, 75.0, and 12.50%; $p = 0.001$). Likewise, in our study, the number of sites with significant uptake (Nb) was also higher in the PMR group compared to RA or SA, respectively, 6.9 ± 4.88, 1.53 ± 2.18, and 2.56 ± 4.34 ($p < 10^{-7}$) (**Table 3**).

Wakura et al. (12) used uptake scores in nine articular and periarticular sites (scapulohumeral and coxofemoral joints, greater trochanters, ischial tuberosities, interspinous bursa at the cervical, thoracic and lumbar levels, entheses of the pectineal muscle and the right femoral muscle) within two groups, PMR (15 patients) and EORA (seven patients). The uptake scores allowed differentiation between the cases of PMR and EORA, with the PMR group showing statistically significant higher scores. They also compared the SUVmax for abnormal FDG accumulation sites between the PMR and EORA patients and observed no significant differences between the two groups. Takahashi et al. (13) compared five articular sites uptake between PMR and EORA patients. They found a sensitivity of 92.6% and a specificity of 90% in favor of PMR when three out of the following five items were present: uptake greater than that of the liver in the shoulders, interspinous bursa, iliopectineal bursa, and ischial tuberosities associated with the absence of uptake in the wrists. In the PMR group, the results were statistically higher in the ischial tuberosities and interspinous bursa; however, the uptake was lower in the wrists. Concerning our study, the number of sites with significant uptake was higher in PMR patients than in the RA group, 6.90 ± 4.88 and 1.53 ± 2.18, respectively ($p < 10^{-7}$).

TABLE 3 | Results of the different visual composite scores (m ± s[a]) according to the final diagnosis.

Parameters	All IRs[b] taken together ($n = 161$)	PMR[c] ± GCA ($n = 57$)	RA[d] ($n = 49$)	SA[e] ($n = 18$)	GCA[f] without PMR ($n = 10$)	Absence of IR ($n = 61$)	Rheumatic diseases without IR ($n = 32$)
F_{17}^{g}	0.88 ± 0.63	1.32 ± 0.61	0.65 ± 0.41	0.69 ± 0.67	0.32 ± 0.31	0.44 ± 0.31	0.45 ± 0.29
Nb[h]	3.52 ± 4.47	6.90 ± 4.88	1.53 ± 2.18	2.56 ± 4.34	0.3 ± 0.67	0.62 ± 1.20	0.62 ± 1.13

[a] *m ± s, Mean and standard deviation.*
[b] *IR, Inflammatory rheumatism.*
[c] *PMR, Polymyalgia rheumatic.*
[d] *RA, Rheumatoid arthritis.*
[e] *SA, Spondyloarthritis.*
[f] *GCA, Giant cell arteritis.*
[g] *F_{17} is the mean FDG uptake score studied in the 17 sites.*
[h] *Nb is the number of sites with significant uptake (≥ liver uptake).*

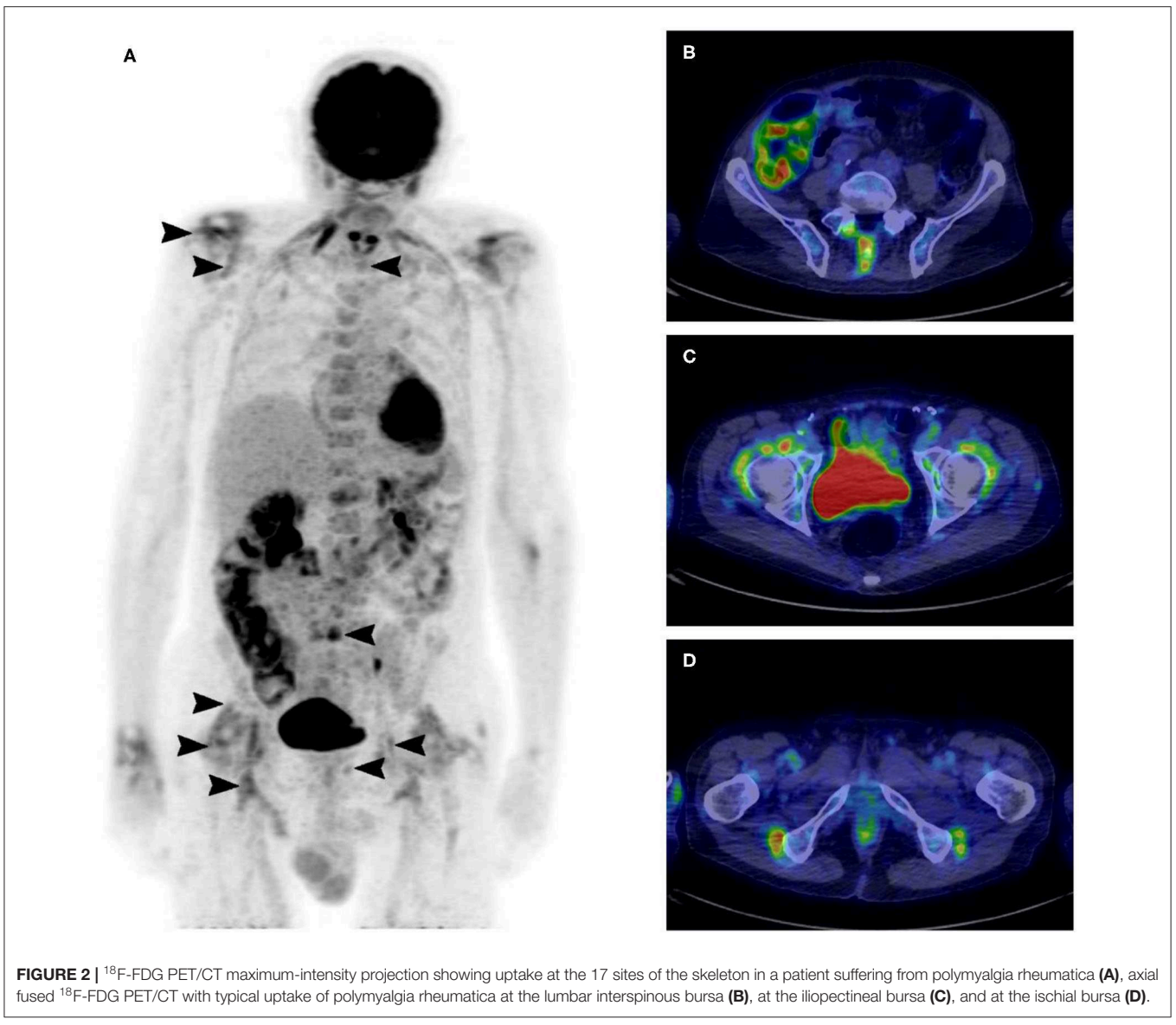

FIGURE 2 | ^{18}F-FDG PET/CT maximum-intensity projection showing uptake at the 17 sites of the skeleton in a patient suffering from polymyalgia rheumatica **(A)**, axial fused ^{18}F-FDG PET/CT with typical uptake of polymyalgia rheumatica at the lumbar interspinous bursa **(B)**, at the iliopectineal bursa **(C)**, and at the ischial bursa **(D)**.

TABLE 4 | Rheumatism activity parameters (m ± s[a]) based on the number of sites with significant uptake on ^{18}F-FDG PET/CT for PMR, RA, and all pathologies taken together.

Parameters	All pathologies taken together			RA[b]			PMR[c] ± GCA[d]		
	PET Nb[e] ≥ 3 (*n* = 73)	PET Nb < 3 (*n* = 149)	*P*[f]	PET Nb ≥ 3 (*n* = 10)	PET Nb < 3 (*n* = 39)	*p*	PET Nb ≥ 3 (*n* = 48)	PET Nb < 3 (*n* = 9)	*p*
CRP[g] (mg/L)	58.6 ± 60.9	29.9 ± 46	$<10^{-5}$	74.0 ± 49.1	32.9 ± 53.2	0.0065	53.4 ± 61.7	43.1 ± 55.9	0.54
CT[h] duration (months)		NA[i]		32.4 ± 78.8	35.4 ± 68.6	0.94	21.7 ± 53.1	6.7 ± 11.7	0.95
CT dose (mg/day)				2.9 ± 4.2	3.7 ± 5.7	0.9	5.9 ± 6.6	11.3 ± 10.0	0.18
Age (in years)	70.8 ± 12.2	64.4 ± 21.2	0.034	65.4 ± 14	64.8 ± 13.2	0.80	72.9 ± 10.9	76.7 ± 6.7	0.36
DAS28[j]		NA		6.0 ± 1.3	4.1 ± 1.3	0.0045		NA	

[a] *m ± s, Mean and standard deviation.*
[b] *RA, Rheumatoid arthritis.*
[c] *PMR, Polymyalgia rheumatica.*
[d] *GCA, Giant cell arteritis.*
[e] *Nb is the number of sites with significant uptake (≥ liver uptake).*
[f] *p, Significance value p.*
[g] *CRP, C-reactive protein.*
[h] *CT, Corticosteroids.*
[i] *NA, Not applicable.*
[j] *DAS 28, Disease Activity Score 28.*

TABLE 5 | Results of the mean SUVmax (m ± s[a]) on ^{18}F-FDG PET/CT according to the final diagnosis.

Parameters	All PET/CT except PMR[b] ± GCA[c] (*N* = 165)	PMR[b] ± GCA[c] (*N* = 57)
	Mean SUVmax	Mean SUVmax
Right sternoclavicular	1.93 ± 0.83	2.61 ± 0.87
Left sternoclavicular	1.89 ± 0.82	2.56 ± 0.75
Right acromioclavicular	1.84 ± 0.82	2.56 ± 0.84
Left acromioclavicular	1.89 ± 0.94	2.51 ± 0.81
Right glenohumeral	2.15 ± 1.17	3.13 ± 1.09
Left glenohumeral	2.11 ± 1.12	2.96 ± 0.99
Interspinous bursa	1.95 ± 0.99	3.13 ± 1.44
Right iliopectineal bursa	1.57 ± 0.75	2.48 ± 0.8
Left iliopectineal bursa	1.68 ± 1	2.61 ± 1.12
Right hip	1.78 ± 0.87	2.61 ± 0.95
Left hip	1.93 ± 1.16	2.75 ± 1.11
Right symphysis pubis enthesis	1.53 ± 0.63	2.4 ± 0.67
Left symphysis pubis enthesis	1.54 ± 0.69	2.5 ± 0.73
Right greater trochanter	1.72 ± 0.82	2.52 ± 0.84
Left greater trochanter	1.68 ± 0.69	2.63 ± 1.08
Right ischial tuberosity	1.74 ± 0.94	2.78 ± 0.97
Left ischial tuberosity	1.76 ± 0.94	2.86 ± 1.07
17 hotspots	1.81 ± 0.69	2.68 ± 0.63

[a] *m ± s, Mean and standard deviation.*
[b] *PMR, Polymyalgia rheumatic.*
[c] *GCA, Giant cell arteritis.*

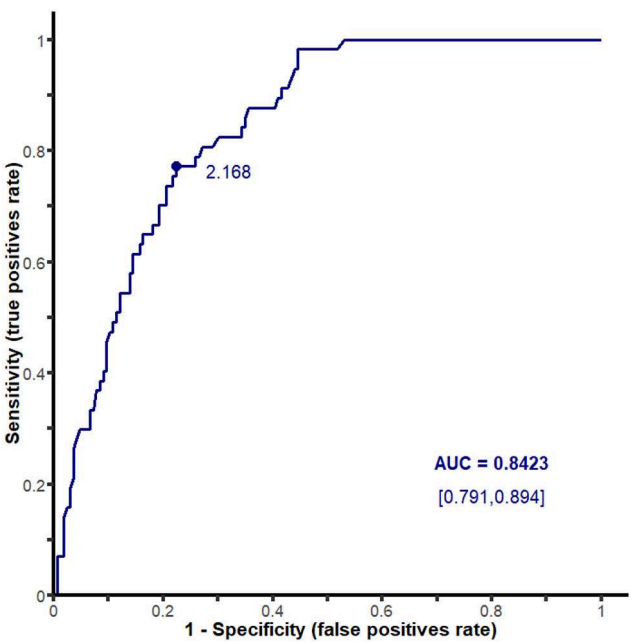

FIGURE 3 | ROC curve analyzing ^{18}F-FDG PET/CT performance for the diagnosis of polymyalgia rheumatica according to the mean SUVmax at the 17 sites.

In order to diagnose PMR, our study found sensitivity and specificity values of 86 and 85.5%, respectively, when the ^{18}F-FDG PET/CT presented at least three sites with significant uptake (Nb ≥ 3), which is higher than the results found by Sondag et al. (9) with a sensitivity of 74% and a specificity of 79% for a score Nb ≥ 3.

We found a significant link between the visual uptake intensity, an elevated CRP, and older age in the "all pathologies taken together" group when the ^{18}F-FDG PET/CT found at least three sites with significant uptake ($p \leq 0.01$). Sondag et al. (9),

TABLE 6 | Sensitivities (Se) and specificities (Sp) of the different composite scores ($F_{17} > 0.53$, $F_{17} > 0.765$, Nb ≥ 3, SUVmax > 2.168) based on the final diagnosis (all inflammatory rheumatisms taken together, PMR, RA, SA, absence of inflammatory rheumatism, and rheumatic diseases without inflammatory rheumatism).

Parameters	%	All IRs[a] (*n* = 161)	PMR[b] ± GCA[c] (*n* = 57)	RA[d] (*n* = 49)	SA[e] (*n* = 18)	Absence of IR (*n* = 61)	Rheumatic diseases without IR (*n* = 32)
$F^{f}_{17} > 0.53$	Se	61.5	91.2	51	33.3	32.8	34.4
	Sp	67.2	59.4	45.7	44.6	38.5	43.2
$F_{17} > 0.765$	Se	48.4	82.5	32.7	33.3	14.8	15.6
	Sp	85.2	75.8	59	60.3	51.6	56.8
Nb[g] ≥ 3	Se	42.9	86	20.4	27.8	6.6	6.2
	Sp	93.4	85.5	63.6	66.7	57.1	62.6
SUVmax[h] ≥ 2.168	Se	42.2	77.2	20.4	27.8	21.3	21.9
	Sp	78.7	77.6	59	62.7	57.8	61.1

[a] *IR, Inflammatory rheumatism.*
[b] *PMR, Polymyalgia rheumatic.*
[c] *GCA, Giant cell arteritis.*
[d] *RA, Rheumatoid arthritis.*
[e] *SA, Spondyloarthritis.*
[f] *F_{17} is the mean FDG uptake score studied in the 17 sites.*
[g] *Nb is the number of sites with significant uptake (≥ liver uptake).*
[h] *SUVmax is the mean SUVmax for the 17 hotspots.*

Moosig et al. (16), and Okamura et al. (17) also found that CRP rates were correlated to the uptake intensity in patients with PMR or vasculitis. We found a correlation between the intensity and number of periarticular uptake (at least three sites with significant uptake) and a higher DAS 28 score in patients with RA (6.0 ± 1.3 vs. 4.1 ± 1.3 with p at 0.0045), which was also described by Okamura et al. [15]. On the other hand, we did not highlight any significant link among the presence of at least three sites with significant uptake and the dose and duration of corticosteroids in the PMR and RA groups. This may be explained by the fact that, in our study, the rheumatism's activity parameters had not been noted on the day of the ^{18}F-FDG PET/CT. However, Blockmans et al. found a decreased uptake in the joints of the axial skeleton after 3 months of corticosteroids in 35 patients suffering from PMR (18) and in the vascular walls after 3 months of corticosteroids in 35 patients with GCA (19).

Blockmans et al. (18) did not recommend performing a ^{18}F-FDG PET/CT when following up cases of PMR because the decreased uptake was correlated to biological results. A more recent study evaluated the use of ^{18}F-FDG PET/CT for the assessment of tocilizumab as first-line treatment in PMR patients (20). FDG uptake and bioclinical parameters (physical examination, CRP, and ESR) after treatment were significantly decreased. However, the correlation between SUVmax and the other bioclinical parameters was low. This result may be explained by the low level of SUVmax variation compared to that of the other parameters. SUVmax was significantly decreased in all regions except in the shoulders, sternoclavicular joints, and cervical interspinous bursa. This persistent FDG uptake should be explained by joint remodeling during the few weeks after tocilizumab treatment. In our study, a large majority of patients (158) were free from any corticotherapy or immunosuppressive treatments at the time of ^{18}F-FDG PET/CT acquisitions guaranteeing the absence of any induced treatment modification of ^{18}F-FDG accumulation in joint sites. For the others, presence or absence of corticotherapy or immunosuppressive treatments was not clearly recorded in data files.

Our study show that the visual score is more sensitive and more specific than the semi-quantitative score (sensitivity of 86% and specificity of 85.5% when at least three sites had a significant uptake and sensitivity of 77.2% and specificity of 77.6% when the mean SUVmax at the 17 sites was equal to or greater than 2.168). Moreover, the visual score is easier to use in daily practice.

Approximately 20% of patients with apparently isolated PMR showed LVV on ^{18}F-FDG PET/CT (21). As PMR and GCA are frequently overlap, typical FDG joint uptake patterns and vascular uptake should be reported using a standardized 0-to-3 grading system (no uptake ⩽ mediastinum, low < liver, intermediate = liver, high > liver), (21–23) with grade 2 considered as possibly positive for active LVV and grade 3 positive for active LVV (23). Moreover, Slart et al. highlighted that ^{18}F-FDG PET/CT exhibited high diagnostic performance for the detection of LVV and PMR and was able to evaluate the response to treatment (17, 23, 24).

Limitations and Strengths of the Study

This study has a few limitations. One concerns missing data relating to the study's retrospective design. In this monocenter study, inclusion criteria were heterogeneous. Indeed, patients with various rheumatic diseases such as PMR, RA, SA, psoriatic rheumatism, and microcrystalline rheumatism were included and ^{18}F-FDG PET/CT were achieved either for initial diagnosis (to search for vasculitis or neoplasia) or during the follow-up (after treatment resistance). Moreover, acquisition methods were heterogeneous, performed on two different PET/CT systems leading to quantitative differences. In addition, ^{18}F-FDG PET/CT were analyzed by the same observer, which creates doubts concerning its reproducibility, which was not assessed in our

study. However, the use of a four-point scale, according to four intensity levels from 0 to 3, in comparison with liver uptake, and SUVmax values enable this variability to be reduced. This visual method was already used in the Deauville score for therapeutic evaluation of lymphomas (25).

The large number of patients included especially PMR ones and the visual and semi-quantitative assessments are part of the strengths of the study.

Integration Into the Current Understanding and Future Direction of the Research

The ^{18}F-FDG PET/CT allows us to confirm and map periarticular inflammation. Therefore, it is an exam to be prioritized in clinically contentious cases, especially rheumatism in elderly patients (26).

Infections, neoplasias, and the different rheumatic diseases can reproduce the same musculoskeletal symptoms. The importance of early diagnosis enables initiation of the proper treatment and reduction of anatomical and functional sequels.

Therefore, it is important to refine the reading of ^{18}F-FDG PET/CT by precisely indicating the number and intensity of the periarticular uptake. This allows the clinician to be guided toward a diagnosis when the clinical presentation is atypical, especially in cases of rheumatism in the elderly and, therefore, to have an impact on therapeutic management.

A prospective study should be realized to confirm these results.

CONCLUSION

The visual and semi-quantitative scores turned out to be effective in differentiating PMR from another rheumatism with a sensitivity of 86% and a specificity of 85.5% when at least three sites had a significant uptake and a sensitivity of 77.2% and a specificity of 77.6% when the mean SUVmax at the 17 sites was equal to or greater than 2.168.

DATA AVAILABILITY STATEMENT

All datasets generated for this study are included in the article/supplementary material.

ETHICS STATEMENT

The studies involving human participants were reviewed and approved by CECIC Rhône Alpes Auvergne, Grenoble, IRB 5921. The patients/participants provided their written informed consent to participate in this study.

AUTHOR CONTRIBUTIONS

MC and AF especially contributed to acquiring data. LO and LD contributed to conception and design. CB, BB, and CV contributed to revising the manuscript and approval of the final content of the manuscript. IM and AC contributed to interpreting data. SM, OA, MS, CM, AK, and FC contributed to enhancing the intellectual content. All authors contributed to the article and approved the submitted version.

ACKNOWLEDGMENTS

We want to express our gratitude to all the members of our PET staff for their contribution in performing this study.

REFERENCES

1. Fautrel B, Cukierman G, Joubert J-M, Laurendeau C, Gourmelen J, Fagnani F. Characteristics and management of rheumatoid arthritis in France: analysis of a representative French national claims database resulting in an estimated prevalence of 0.35%. *Jt Bone Spine.* (2016) 83:461–2. doi: 10.1016/j.jbspin.2015.05.010
2. Crowson CS, Matteson EL. Contemporary prevalence estimates for giant cell arteritis and polymyalgia rheumatica, 2015. *Semin Arthritis Rheum.* (2017) 47:253–6. doi: 10.1016/j.semarthrit.2017.04.001
3. Cornec D, Varache S, Morvan J, Devauchelle-Pensec V, Berthelot J-M, Le Henaff-Bourhis C, et al. Comparison of ACR 1987 and ACR/EULAR 2010 criteria for predicting a 10-year diagnosis of rheumatoid arthritis. *Jt Bone Spine.* (2012) 79:581–5. doi: 10.1016/j.jbspin.2012.01.015
4. Dasgupta B, Cimmino MA, Maradit-Kremers H, Schmidt WA, Schirmer M, Salvarani C, et al. 2012 provisional classification criteria for polymyalgia rheumatica: a European League Against Rheumatism/American College of Rheumatology collaborative initiative. *Ann Rheum Dis.* (2012) 71:484–92. doi: 10.1136/annrheumdis-2011-200329
5. Dalkiliç E, Tufan AN, Hafizoglu E, Hafizoglu M, Tufan F, Oksuz F, et al. The process from symptom onset to rheumatology clinic in polymyalgia rheumatica. *Rheumatol Int.* (2014) 34:1589–92. doi: 10.1007/s00296-014-3034-y
6. Lavado-Pérez C, Martínez-Rodríguez I, Martínez-Amador N, Banzo I, Quirce R, Jiménez-Bonilla J, et al. (18)F-FDG PET/CT for the detection of large vessel vasculitis in patients with polymyalgia rheumatica. *Rev Esp Med Nucl Imagen Mol.* (2015) 34:275–81. doi: 10.1016/j.remnie.2015.07.005
7. Matsui T, Nakata N, Nagai S, Nakatani A, Takahashi M, Momose T, et al. Inflammatory cytokines and hypoxia contribute to 18F-FDG uptake by cells involved in pannus formation in rheumatoid arthritis. *J Nucl Med.* (2009) 50:920–6. doi: 10.2967/jnumed.108.060103
8. Yamashita H, Kubota K, Mimori A. Clinical value of whole-body PET/CT in patients with active rheumatic diseases. *Arthritis Res Ther.* (2014) 16:423. doi: 10.1186/s13075-014-0423-2
9. Sondag M, Guillot X, Verhoeven F, Blagosklonov O, Prati C, Boulahdour H, et al. Utility of 18F-fluoro-dexoxyglucose positron emission tomography for the diagnosis of polymyalgia rheumatica: a controlled study. *Rheumatology.* (2016) 55:1452–7. doi: 10.1093/rheumatology/kew202
10. Elzinga EH, van der Laken CJ, Comans EFI, Lammertsma AA, Dijkmans BAC, Voskuyl AE. 2-Deoxy-2-[F-18]fluoro-D-glucose joint uptake on positron emission tomography images: rheumatoid arthritis versus osteoarthritis. *Mol Imaging Biol.* (2007) 9:357–60. doi: 10.1007/s11307-007-0113-4
11. Yamashita H, Kubota K, Takahashi Y, Minamimoto R, Morooka M, Kaneko H, et al. Similarities and differences in fluorodeoxyglucose positron emission tomography/computed tomography findings in spondyloarthropathy, polymyalgia rheumatica and rheumatoid arthritis. *Joint Bone Spine.* (2013) 80:171–7. doi: 10.1016/j.jbspin.2012.04.006
12. Wakura D, Kotani T, Takeuchi T, Komori T, Yoshida S, Makino S, et al. Differentiation between Polymyalgia Rheumatica (PMR) and elderly-onset rheumatoid arthritis using 18F-fluorodeoxyglucose positron emission

tomography/computed tomography: is enthesitis a new pathological lesion in PMR? *PLoS ONE*. (2016) 11:e0158509. doi: 10.1371/journal.pone.0158509
13. Takahashi H, Yamashita H, Kubota K, Miyata Y, Okasaki M, Morooka M, et al. Differences in fluorodeoxyglucose positron emission tomography/computed tomography findings between elderly onset rheumatoid arthritis and polymyalgia rheumatica. *Mod Rheumatol.* (2015) 25:546–51. doi: 10.3109/14397595.2014.978936
14. Rudwaleit M, Van Der Heijde D, Landewé R, Listing J, Akkoc N, Brandt J, et al. The development of assessment of SpondyloArthritis international Society classification criteria for axial spondyloarthritis (part II): validation and final selection. *Ann Rheum Dis*. (2009) 68:777–83. doi: 10.1136/ard.2009.108233
15. Goerres GW, Forster A, Uebelhart D, Seifert B, Treyer V, Michel B, et al. F-18 FDG whole-body PET for the assessment of disease activity in patients with rheumatoid arthritis. *Clin Nucl Med*. (2006) 31:386–90. doi: 10.1097/01.rlu.0000222678.95218.42
16. Moosig F, Czech N, Mehl C, Henze E, Zeuner RA, Kneba M, et al. Correlation between 18-fluorodeoxyglucose accumulation in large vessels and serological markers of inflammation in polymyalgia rheumatica: a quantitative PET study. *Ann Rheum Dis.* (2004) 63:870–3. doi: 10.1136/ard.2003.011692
17. Okamura K, Yonemoto Y, Arisaka Y, Takeuchi K, Kobayashi T, Oriuchi N, et al. The assessment of biologic treatment in patients with rheumatoid arthritis using FDG-PET/CT. *Rheumatology*. (2012) 51:1484–91. doi: 10.1093/rheumatology/kes064
18. Blockmans D, De Ceuninck L, Vanderschueren S, Knockaert D, Mortelmans L, Bobbaers H. Repetitive 18-fluorodeoxyglucose positron emission tomography in isolated polymyalgia rheumatica: a prospective study in 35 patients. *Rheumatology*. (2007) 46:672–7. doi: 10.1093/rheumatology/kel376
19. Blockmans D, de Ceuninck L, Vanderschueren S, Knockaert D, Mortelmans L, Bobbaers H. Repetitive 18F-fluorodeoxyglucose positron emission tomography in giant cell arteritis: a prospective study of 35 patients. *Arthritis Rheum.* (2006) 55:131–7. doi: 10.1002/art.21699
20. Palard-Novello X, Querellou S, Gouillou M, Saraux A, Marhadour T, Garrigues F, et al. Value of 18F-FDG PET/CT for therapeutic assessment of patients with polymyalgia rheumatica receiving tocilizumab as first-line treatment. *Eur J Nucl Med Mol Imaging*. (2016) 43:773–9. doi: 10.1007/s00259-015-3287-z
21. Cimmino MA, Camellino D, Paparo F, Morbelli S, Massollo M, Cutolo M, et al. High frequency of capsular knee involvement in polymyalgia rheumatica/giant cell arteritis patients studied by positron emission tomography. *Rheumatol*. (2013) 52:1865–72. doi: 10.1093/rheumatology/ket229
22. Rehák Z, Szturz P. Comment on: FDG PET in the early diagnosis of large-vessel vasculitis. *Eur J Nucl Med Mol Imaging*. (2014) 41:579–80. doi: 10.1007/s00259-013-2662-x
23. Slart RHJA, Slart RHJA, Glaudemans AWJM, Chareonthaitawee P, Treglia G, Besson FL, et al. FDG-PET/CT(A) imaging in large vessel vasculitis and polymyalgia rheumatica: joint procedural recommendation of the EANM, SNMMI, and the PET Interest Group (PIG), endorsed by the ASNC. *Eur J Nucl Med Mol Imaging*. (2018) 45:1250–69. doi: 10.1007/s00259-018-3973-8
24. Lee YH, Choi SJ, Ji JD, Song GG. Diagnostic accuracy of 18F-FDGPET or PET/CT for large vessel vasculitis: a meta-analysis. *Z Rheumatol*. (2016) 75:924–31. doi: 10.1007/s00393-015-1674-2
25. Meignan M, Gallamini A, Meignan M, Gallamini A, Haioun C. Report on the First International Workshop on interim-PET scan in lymphoma. *Leuk Lymphoma.* (2009) 50:1257–60. doi: 10.1080/10428190903040048
26. Wendling D, Blagosklonov O, Boulahdour H, Prati C. Positron emission tomography: the ideal tool in polymyalgia rheumatica? *Joint Bone Spine.* (2014) 81:381–3. doi: 10.1016/j.jbspin.2014.04.007

Conflict of Interest: The authors declare that the research was conducted in the absence of any commercial or financial relationships that could be construed as a potential conflict of interest.

frontiers in Medicine

ORIGINAL RESEARCH
published: 17 February 2021
doi: 10.3389/fmed.2021.646974

Decision Tree With Only Two Musculoskeletal Sites to Diagnose Polymyalgia Rheumatica Using [^{18}F]FDG PET-CT

Anthime Flaus[1], Julie Amat[2], Nathalie Prevot[1,3], Louis Olagne[4], Lucie Descamps[5], Clément Bouvet[2], Bertrand Barres[2], Clémence Valla[2], Sylvain Mathieu[5], Marc Andre[4], Martin Soubrier[5], Charles Merlin[2], Antony Kelly[2], Marion Chanchou[2] and Florent Cachin[2]*

[1] Department of Nuclear Medicine, Saint-Etienne University Hospital, University of Saint-Etienne, Saint-Etienne, France, [2] Department of Nuclear Medicine, Jean Perrin Oncology Institute of Clermont-Ferrand, Clermont-Ferrand, France, [3] Institut national de la santé et de la recherche médicale, U 1059 Sainbiose, Université Jean Monnet, Saint-Etienne, France, [4] Department of Internal Medicine, Gabriel Montpied University Hospital, University of Clermont-Ferrand, Clermont-Ferrand, France, [5] Department of Rheumatology, Gabriel Montpied University Hospital, University of Clermont-Ferrand, Clermont-Ferrand, France

OPEN ACCESS

Edited by:
Giorgio Treglia, Ente Ospedaliero Cantonale (EOC), Switzerland

Reviewed by:
Kornelis van der Geest, University Medical Center Groningen, Netherlands
Domenico Albano, University of Brescia, Italy

***Correspondence:**
Anthime Flaus
anthime.flaus@gmail.com
orcid.org//0000-0001-5877-2159

Specialty section:
This article was submitted to Nuclear Medicine, a section of the journal Frontiers in Medicine

Received: *28 December 2020*
Accepted: *28 January 2021*
Published: *17 February 2021*

Citation:
Flaus A, Amat J, Prevot N, Olagne L, Descamps L, Bouvet C, Barres B, Valla C, Mathieu S, Andre M, Soubrier M, Merlin C, Kelly A, Chanchou M and Cachin F (2021) Decision Tree With Only Two Musculoskeletal Sites to Diagnose Polymyalgia Rheumatica Using [^{18}F]FDG PET-CT. Front. Med. 8:646974. doi: 10.3389/fmed.2021.646974

Introduction: The aim of this study was to find the best ordered combination of two FDG positive musculoskeletal sites with a machine learning algorithm to diagnose polymyalgia rheumatica (PMR) vs. other rheumatisms in a cohort of patients with inflammatory rheumatisms.

Methods: This retrospective study included 140 patients who underwent [^{18}F]FDG PET-CT and whose final diagnosis was inflammatory rheumatism. The cohort was randomized, stratified on the final diagnosis into a training and a validation cohort. FDG uptake of 17 musculoskeletal sites was evaluated visually and set positive if uptake was at least equal to that of the liver. A decision tree classifier was trained and validated to find the best combination of two positives sites to diagnose PMR. Diagnosis performances were measured first, for each musculoskeletal site, secondly for combination of two positive sites and thirdly using the decision tree created with machine learning.

Results: 55 patients with PMR and 85 patients with other inflammatory rheumatisms were included. Musculoskeletal sites, used either individually or in combination of two, were highly imbalanced to diagnose PMR with a high specificity and a low sensitivity. The machine learning algorithm identified an optimal ordered combination of two sites to diagnose PMR. This required a positive interspinous bursa or, if negative, a positive trochanteric bursa. Following the decision tree, sensitivity and specificity to diagnose PMR were respectively 73.2 and 87.5% in the training cohort and 78.6 and 80.1% in the validation cohort.

Conclusion: Ordered combination of two visually positive sites leads to PMR diagnosis with an accurate sensitivity and specificity vs. other rheumatisms in a large cohort of patients with inflammatory rheumatisms.

Keywords: polymyalgia rheumatica, inflammatory rheumatism, [18F]FDG PET-CT, decision-tree algorithm, machine learning

KEYPOINTS

Question

Find the best ordered combination of FDG positive musculoskeletal sites with a decision tree classifier to diagnose polymyalgia rheumatica (PMR) vs. other rheumatisms in a large cohort of patients with inflammatory rheumatisms.

Key Findings

Musculoskeletal sites, used individually or in combination of two, were highly imbalanced to diagnose PMR with a high specificity and a low sensitivity. However, machine learning classifier helped us to build a decision tree to diagnose PMR using two sites. The classifier identified an optimal ordered combination of two sites to diagnose PMR. This required a positive interspinous bursa and, if negative, a positive trochanteric bursa. Following this tree, in a validation cohort, sensitivity and specificity to diagnose PMR were respectively 78.6 and 80.1%.

Consequences on Patient Care

We proposed an ordered combination of two visually positive musculoskeletal sites to diagnose PMR vs. other inflammatory rheumatisms. It could help clinicians when reporting PET-CT.

INTRODUCTION

[^{18}F]Fluorodeoxyglucose positron emission tomography – computed tomography ([^{18}F]FDG PET-CT) plays an important role to diagnose polymyalgia rheumatica (PMR) (1) and to rule out other diseases with similar symptoms such as rheumatoid arthritis (RA), relapsing seronegative asymmetric synovitis with pitting oedema, spondylarthritis (SA), or paraneoplastic syndrome (2).

In PMR, [^{18}F]FDG can accumulate in various joints, usually shoulders or hips. But, it appeared that uptake in musculoskeletal sites such as ischial bursa, trochanteric bursa and interspinous bursa was more specifically associated with the diagnosis (3, 4). [^{18}F]FDG PET-CT used various composite articular scores which proved accurate to diagnose PMR unlike control patients whose sensitivity and specificity ranged from 74 to 90.9% and 79 to 92.4% (5–7) and patients with other rheumatic diseases whose sensitivity and specificity ranged from 85,7 to 92,6% and 85,5 to 90% (3, 4, 8, 9).

Contrary to combinations that are selections of some members of a set regardless of order, permutation of a set is an arrangement of its members into a sequence. Diagnosis values of arrangement of three positive musculoskeletal sites to diagnose PMR were only studied in a cohort of PMR patients vs. control. Results were promising with a sensitivity and specificity above 90% in cohorts of PMR patients and controls (6). However, to the best of our knowledge, no previous study has evaluated the diagnosis values of different permutations of two positive musculoskeletal sites to diagnose PMR patients in a cohort of different rheumatic diseases. Moreover, because it gives an order to assess the different sites, an ordered combination may facilitate PET reporting.

In the present study, the primary aim was to find the best ordered combination of two FDG positive musculoskeletal sites with a decision tree classifier to diagnose polymyalgia rheumatic (PMR) in a large cohort of patients with various inflammatory rheumatisms.

METHODS

Ethics Approval and Consent to Participate

All procedures performed in studies involving human participants were in accordance with the ethical standards of the institutional research committee and with the 1964 Helsinki Declaration and its later amendments or comparable ethical standards. The study was approved by CECIC Rhône-Alpes-Auvergne, Grenoble, IRB 5921 on 12 November 2019 (IRB number: 5921) and patients provided written informed consent to participate in this study.

Study Population

In this retrospective study, we reviewed 478 patients' clinical information and [^{18}F]FDG PET-CT prescription provided by the Rheumatology and Internal Medicine Departments of our hospital from April 2011 to December 2015.

Inclusion criteria were (1) unclassified diagnosis at the time of PET completion and (2) a delayed final diagnosis of RA following the 2010 American College of Rheumatology/European League Against Rheumatism's criteria (10), of PMR following its 2012 criteria (11) and of SA following the 2009 Assessment of Spondylarthritis International Society's criteria (12). If the rheumatism did not meet these criteria, rheumatologists and internists agreed on a final diagnosis. Yet, some patients remained with a diagnosis of unclassified rheumatism. [^{18}F]FDG PET-CT exams were not included in the paraclinical tests used for the final rheumatic diagnosis.

Exclusion criteria were absence of inflammatory rheumatism, namely rheumatic diseases without inflammatory rheumatism (prosthetic loosening, narrowing of the lumber vertebral canal, fracture, fibromyalgia, osteoarthritis, shoulder hand syndrome), infectious disease, inflammatory diseases without musculoskeletal manifestations. Absence of active disease at the time of the [^{18}F]FDG PET-CT was also an exclusion criteria. However, patients already treated with corticosteroids or other immunosuppressants treatments were not excluded. When available, the following data was collected: rheumatism activity parameters such as C-reactive protein (CRP), erythrocyte sedimentation rate (ESR), treatment with corticosteroids, or other immunosuppressants (including duration and dose).

Image Acquisition

Patients fasted for at least 4 h and were injected with an activity of 3–4 MBq/kg of [^{18}F]FDG according to current guidelines. Sixty minutes after injection, PET and unenhanced CT images were acquired on a PET-CT scanner: Discovery ST or Discovery 710 Optima 660 (General Electric Healthcare). 85% of the acquisitions extended from the skull to the upper third of the femurs, with the upper extremities situated either along the body or above the head and 15% of the PET/CT involved the entire

body. Images reconstruction parameters were identical for PET-CT scanner. A fully 3D time-of-flight iterative reconstruction scheme (VUE Point FX) was used (Ordered subsets expectation maximization algorithm, 24 subsets, 2 iterations) with point spread function modeling (SHARP IR) (13). A low-dose CT scan was acquired for attenuation correction. The full width at half maximum (FWHM) of the gaussian filter was 6.4 mm. The voxel size was $2.7344 \times 2.7344 \times 3.27$ mm^3. Each voxel in PET images were converted into standard uptake value (SUV) with the following formula: SUV = voxel concentration activity * patient body weight/decay corrected injected activity (14).

Image Analysis

[^{18}F]FDG uptakes were analyzed at 17 different sites (**Supplementary Figures**), both articular and peri-articular as proposed by Sondag et al. (5): two shoulders, two acromioclavicular joints (AC joint), and two sternoclavicular joints (SC joint), the most intense interspinous bursa, two hips, two trochanteric bursas (TB), two ischial bursas (IB), two iliopectineal bursas (IPB), and two symphysis pubis enthesis (SPE).

[^{18}F]FDG uptake was visually assessed by one experienced nuclear medicine physician with high training in rheumatic disease. Each site was assessed using a standardized 0 to 3 grading system in comparison with the liver uptake (0: no uptake, 1: uptake lower than the liver, 2: moderate uptake, same as that of the liver, 3: higher uptake than the liver) as suggested by the joint procedural recommendation of the European Association of Nuclear Medicine, the Society of Nuclear Medicine and Molecular Imaging and the PET Interest Group (15).

Input Data for Machine Learning Analysis

We defined a positive site as a site with a score of 2 or 3 (3–5, 15). Bilateral site was considered positive when at least one side was positive. Nine sites were therefore used as input for machine learning analysis: shoulder, AC joint, SC joint, interspinous bursa, hip, TB, IB, IPB, and SPE. So, for each patient, machine learning algorithm was supplied with a vector of 9 numbers composed of 0 or 1 values, following the positivity or not of each site.

Machine Learning Training and Validation

The machine learning algorithm used to find the best ordered combination of FDG positive musculoskeletal sites was a decision tree classifier. A decision tree is a flowchart-like tree structure in which a root node represents feature, the branch represents a decision rule, and a leaf node represents the outcome. The classifier is an algorithm that partitions the tree in a recursive manner to test which feature of each node - in this case the musculoskeletal site- divides optimally the dataset in two subsets in PMR patients vs. other patients.

The classification method was based on an optimized version of the Classification and Regression Tree (CART) algorithm (16). Heuristic for selecting the splitting criterion is Gini index. It provided a rank to each attribute by explaining the given dataset. Best score attribute was selected as a splitting attribute. The maximum depth of the decision tree was set to two. This machine learning approach was performed using Python (version 3.7) and the open source Scikit-learn package (17).

In order to train and validate decision tree classifier, the study cohort was randomized, stratified on the final diagnosis, on ratio 3: 1 into training and validation cohorts (18). So, classifiers were developed on the training cohort and diagnosis performances were evaluated on the validation cohort.

Statistical Analysis

Firstly, sensitivity (Se) and specificity (Sp) values for PMR diagnosis vs. other inflammatory rheumatisms were calculated at each site and in combinations of 2 sites (considered positive if both sites were positive).

Secondly, we built a decision tree in order to get the best ordered combination of two sites and measured its Se and Sp values.

Thirdly, we evaluated the diagnostic performance of our algorithm with Se, Sp, positive likelihood ratio (LR+) and negative likelihood ratio (LR–).

Statistical analysis was performed using R software version 3.5.2 (19). Continuous variables were reported as mean (± standard deviation) or median ([range]). Categorical variables were represented as proportions (percentages). All tests were two-sided. Confidence intervals (Cis) were reported at the 95% level, and $p < 0.05$ was considered statistically significant.

RESULTS

Patient Characteristics

140 patients with a final diagnosis of inflammatory rheumatisms were selected. **Table 1** compares PMR patients' characteristics to patients with other inflammatory rheumatism. No significant difference was found between PMR and other patients as far as age, sex, inflammatory parameters [e.g., C-reactive protein (CRP), erythrocyte sedimentation rate (ESR)] and steroids dose were concerned. Twenty nine (52.7%) patients in the PMR group and 25 (29.4%) among the other inflammatory rheumatisms patients received steroids before [^{18}F]FDG PET-CT.

The cohort was composed of 55 patients with PMR (39,3%), 42 patients with RA (30%), 17 patients with SA (12,1%), 6 patients with unclassified rheumatism (4.3%), 3 patients with SAPHO (2.1%), and an equal number of 4 patients (2,9%) with RS3PE, psoriatic rheumatism and paraneoplastic rheumatism. Among those diagnosed with PMR, 10 patients were also diagnosed with Giant Cell Arteritis (GCA).

The training cohort was composed of 105 patients, the validation cohort was composed of 35 patients and both stratified based on the final diagnosis. No significant difference was found between both cohorts as far as age, sex, inflammatory parameters, and steroids dose are concerned.

PMR Diagnostic Value of Musculoskeletal Sites Analyzed Individually

Se and Sp values of each musculoskeletal sites were detailed in **Table 2**. Proportion of positive musculoskeletal site for each group is in **Supplementary Table 1**. Mean Sp and mean Se of musculoskeletal sites analyzed individually to diagnose PMR

TABLE 1 | Patient characteristics from the polymyalgia rheumatica and other inflammatory rheumatisms groups.

Characteristics	PMR patients ($n = 55$)[#]	Other inflammatory rheumatisms ($n = 85$)	*p*
Age (median, min-max range), years	70.4 [41–91]	69.0 [34–96]	0.97
Male (*n*, %)	25 (45%)	36 (42%)	0.28
CRP (median, min-max range), (mg/L)	32 [0–270]	17 [0–255]	0.10
ESR (median, min-max range), (mm/h)	41 [3–138]	35.5 [0–165]	0.88
Steroids dose (median, min-max range), (mg/day)	10.5 [2–30] *	8 [4–20]*	0.19
Rheumatoid arthritis (*n*, %)	-	42 (30%)	
Spondylarthritis (*n*, %)	-	17 (12.1%)	
Unclassified rheumatism (*n*, %)	-	6 (4,3%)	
Remitting seronegative symmetrical synovitis with pitting oedema (RS3PE) (*n*, %)	-	4 (2,9%)	
Psoriatic rheumatism (*n*, %)	-	4 (2,9%)	
Paraneoplastic rheumatism (*n*, %)	-	4 (2,9%)	
Synovitis-acne-pustulosis-hyperostosis-osteitis (SAPHO) (*n*, %)	-	3 (2.1%)	

PMR, Polymyalgia rheumatica; CRP, C-reactive protein; ESR, erythrocyte sedimentation rate.
**29 patients in the PMR group and 25 in the other inflammatory rheumatisms group.*
[#]Among those diagnosed with PMR, 10 patients were also diagnosed with Giant Cell Arteritis (GCA).

TABLE 2 | Sensibility, specificity at each musculoskeletal site and at the only combinations of 2 sites with sensitivity above 50% to diagnose patients with polymyalgia rheumatica in the whole cohort of patients with various inflammatory rheumatisms ($n = 140$).

Musculoskeletal site	Sensitivity (95% CI)	Specificity (95% CI)
Shoulder	0.71 (0.59–0.83)	0.65 (0.55–0.75)
Acromioclavicular joint	0.47 (0.34–0.6)	0.82 (0.74–0.9)
Sternoclavicular joint	0.44 (0.3–0.57)	0.86 (0.79–0.93)
Interspinous bursa	0.6 (0.47–0.73)	0.91 (0.84–0.97)
Trochanteric bursa	0.58 (0.45–0.71)	0.93 (0.87–0.98)
Hip	0.42 (0.29–0.55)	0.81 (0.73–0.9)
Ischial bursa	0.6 (0.47–0.73)	0.86 (0.79–0.93)
Symphysis pubis enthesis	0.36 (0.24–0.49)	0.94 (0.89–0.99)
Iliopectineal bursa	0.24 (0.12–0.35)	0.87 (0.8–0.94)
Shoulder + ischial bursa	0.51 (0.37–0.63)	0.92 (0.86–0.98)
Trochanteric bursa+ ischial bursa	0.51 (0.37–0.63)	0.95 (0.91–1)

CI, Confidence interval.

were respectively 85 and 49.1%. Symphysis pubis enthesis was the most specific site (94.1 with 95% CI 0.89–0.99) and shoulder was the most sensitive site (71 with 95% CI 0.59–0.83).

PMR Diagnostic Value of Two Concomitant Positive Musculoskeletal Sites

Combinations of two positive sites were all imbalanced. Indeed, only two combinations had a Se slightly above 50% namely shoulder + ischial bursa with a Se of 51% (95% CI 0.37–0.63) and a Sp of 91.8% (95% CI 0.86–0.98) and trochanteric bursa + ischial bursa with a Se and a Sp of 51% (95% CI 0.37–0.63) and 95.3% (95% CI 0.91–1) (**Table 2**).

PMR Diagnostic Value of Machine Learning Analysis

According the machine learning classifier output, the optimal way to diagnose PMR was first to evaluate tracer accumulation in interspinous bursa and then, if negative, to evaluate trochanteric bursa tracer uptake. Both musculoskeletal sites are shown on **Figure 1** and decision tree is shown on **Figure 2**. Using this method, Se and Sp to diagnose PMR were respectively 73.2% (95% CI 0.60–0.87) and 87.5% (95% CI 0.77–0.98) in the training cohort and 78.6% (95% CI 0.57–0.1) and 80.1% (95% CI 0.59–1) in the validation cohort. LR+ and LR– were respectively 5.85 (95% CI 2.98–11.49) and 0.31 (95% CI 0.18–0.51) in the training cohort and 3.95 (95% CI 1.6–9.72) and 0.27 (95% CI 0.1–0.75) in the validation cohort. Pooled results are summarized in **Supplementary Table 2**.

DISCUSSION

We used machine learning to define a short decision tree able to detect PMR patients among a large retrospective cohort of patients with inflammatory rheumatisms. Machine learning enabled to enhance the diagnostic value of musculoskeletal site assessed visually. Indeed, used individually or in combination of two concomitant positive sites, sensitivity and specificity were highly imbalanced and inappropriate to diagnose PMR. On the other hand, machine learning defined order of two sites allowed accurate specificity and sensitivity to diagnose PMR. We purposely used a decision tree classifier as a white box model, a system in which the inner logic is intelligible thus, results were easily explained and interpreted. It eased clinical translation of machine learning approaches to the clinics (20). Indeed, assessment of the musculoskeletal sites should be prioritized in clinical routine thanks to the created decision tree.

Splitting rules of the decision tree were based on a positive interspinous bursa or, if negative, a positive trochanteric bursa. The selected sites in decision tree were already explored in the context of patients diagnosed with PMR. Firstly, interspinous [^{18}F]FDG uptake was correlated with MRI to interspinous bursitis (21). It is also described as a very informative site to diagnose PMR, with a specificity ranging from 82.4 to 100% (3, 7). Its pooled LR+ 4 (95% CI 1.84–8.71) for diagnosis of PMR is the highest among all musculoskeletal sites according to a recent review (22). Therefore, our study results are in accordance with the literature. Secondly, [^{18}F]FDG uptake at trochanteric bursa was due to the trochanteric bursitis. It was one of the most consistent findings in PMR so its inclusion in decision tree is in accordance with the literature

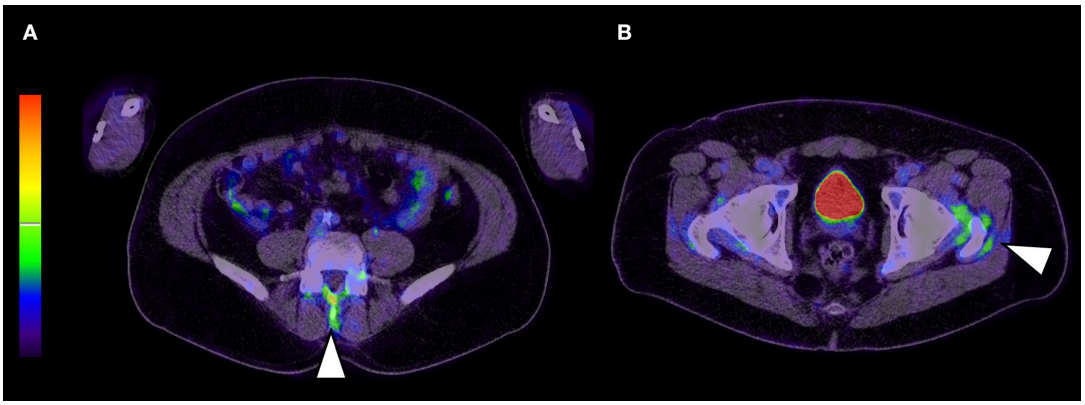

FIGURE 1 | Musculoskeletal sites part of the decision tree are interspinous bursa (**A**; arrow head) and if negative trochanteric bursa (**B**; arrow head).

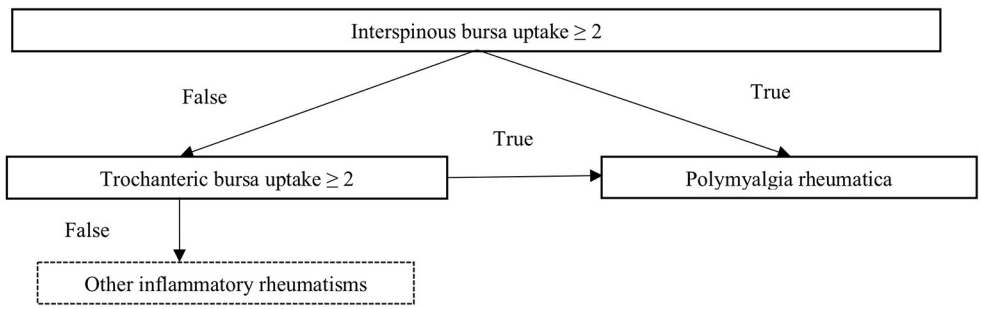

FIGURE 2 | Decision tree to diagnose polymyalgia rheumatica among a group of patients with inflammatory rheumatisms. (2: moderate uptake, same as that of the liver).

(3, 23). Although easy to apply, these splitting rules gave visual score-based decision tree a good accuracy. Its LR+ and LR– are consistent with those of pooled composite [^{18}F]FDG-PET/CT scores which were respectively 3.91 (95% CI 2.42–6.32) and 0.19 (95% CI 0.10–0.36) in a recent systemic review about the diagnostic value of [^{18}F]FDG-PET/CT in PMR (22).

In the literature, global performance of [^{18}F]FDG PET for PMR diagnostic whatever criteria used, ranges from 74 to 92.4% for Se and from 79 to 92.6% for Sp (3–9). This is in line with our results, in a large cohort and even after validation in an independent cohort. Studies proposed various composite articular scores in two different conditions: either vs. control patients or vs. patients with other rheumatic disease. For example, one approach was to define the total skeletal score, which reflected uptake in the 12 studied articular regions. Sensitivity and specificity were respectively measured at 85.1 and 87.5%, controls being non-PMR-rheumatic or inflammatory disease (7). Another approach was to look for a minimum number of positive sites - at least 3 out of 17- in order to be more effective in clinical routine. Sensitivity and specificity to diagnose PMR patients vs. control group were respectively of 74 and 79% (5). Regarding patients with other rheumatic or inflammatory disease, sensitivity, and specificity were respectively 86 and 85,5% (9). However, in both studies, the diagnostic value of each site individually was not taken into account. Recent studies encouraged to focus on positivity of musculoskeletal sites more specifically associated with the diagnosis of PMR. One study identified ischial tuberosities, peri articular shoulder and interspinous bursa as 3 specific sites allowing a PMR diagnosis. It suggested positivity of these 3 sites resulted in a high sensitivity of 90.9% and a high specificity of 92.4% vs. control patients (5, 6). However, it was unusual to find the peri-articular shoulder site among the three, as its specificity was usually low in various studies (3, 7). Furthermore, diagnostic accuracy of more specific musculoskeletal sites was evaluated in a small cohort of patients with various rheumatic diseases. It suggested positivity of 2 sites among 3 assessed (ischial tuberosity, greater trochanter, and lumbar spinous process) resulted in a high sensitivity (85.7%) and specificity (88.2%) (3). It was close to the ordered combination of musculoskeletal sites established by machine learning to assess PMR diagnosis in our large cohort. Splitting rules were based on a positive interspinous bursa or, if negative, a positive trochanteric bursa.

There were some limitations to our study, the first being its retrospective design and descriptive nature. Inclusion criteria were heterogeneous as various rheumatic diseases were

considered. Moreover, whole body examination was not always performed as some patients were not referred for rheumatic pathology and [^{18}F]FDG PET-CT were not always performed at the same time as the disease evolved, both at initial evaluation or during follow up. Besides, 29/55 (53%) of PMR patients had already received glucocorticoids when [^{18}F]FDG PET-CT was performed. Glucocorticoids may have decreased sensitivity of [^{18}F]FDG PET-CT with reduced incidence of abnormal finding and FDG uptake intensity (5) however, our diagnostic accuracy remains reliable. In addition, although decision tree suggests preferential articular or peri-articular sites to analyse to differentiate PMR in a large cohort of patients with inflammatory rheumatisms, assessment of PET should not be limited to 2 sites: full examination of all sites must be done. Lastly, we did not include any quantitative analysis in this machine learning approach because the objective was to propose a robust and reproductive clinic visual method known to be less sensitive to acquisition conditions than quantification methods (24). Finally, our findings have to be validated in multicentric prospective studies with larger cohorts. Methodological improvement would be to develop an automatic segmentation of each musculoskeletal site with automatic ratio quantification to liver uptake.

CONCLUSION

We proposed an ordered combination of two visually positive musculoskeletal sites to diagnose PMR thanks to machine learning. Splitting rules were based on a positive interspinous bursa or, if negative, a positive trochanteric bursa. It was validated in a large cohort of patients with inflammatory rheumatisms and was able to diagnose patient with an accurate sensitivity and specificity. It could help clinicians with PET-CT reporting.

DATA AVAILABILITY STATEMENT

The original contributions presented in the study are included in the article/**Supplementary Material**, further inquiries can be directed to the corresponding author.

ETHICS STATEMENT

The studies involving human participants were reviewed and approved by CECIC Rhône Alpes Auvergne, Grenoble, IRB 5921. The patients/participants provided their written informed consent to participate in this study.

AUTHOR CONTRIBUTIONS

JA, MC, and AF especially contributed to acquire data. MA, MS, LO, SM, and LD performed the clinical evaluations, treatments, and follow-up evaluations of the patients. FC, JA, and AF contributed to conception and design. CB, BB, and CV to revised the manuscript and approved the final content of the manuscript. AF contributed to interpret data. NP, CM, AK, and FC to enhanced the intellectual content. All authors read and approved the final manuscript.

ACKNOWLEDGMENTS

The authors would like to thank Sandrine Sotton for her precious help.

SUPPLEMENTARY MATERIAL

The Supplementary Material for this article can be found online at: https://www.frontiersin.org/articles/10.3389/fmed.2021.646974/full#supplementary-material

REFERENCES

1. Hotta M, Minamimoto R, Kaneko H, Yamashita H. Fluorodeoxyglucose PET/CT of arthritis in rheumatic diseases: a pictorial review. *RadioGraphics*. (2020) 40:223–40. doi: 10.1148/rg.2020190047
2. Kubota K, Yamashita H, Mimori A. Clinical value of FDG-PET/CT for the evaluation of rheumatic diseases: rheumatoid arthritis, polymyalgia rheumatica, and relapsing polychondritis. *Semin Nucl Med*. (2017) 47:408–24. doi: 10.1053/j.semnuclmed.2017.02.005
3. Yamashita H, Kubota K, Takahashi Y, Minaminoto R, Morooka M, Ito K, et al. Whole-body fluorodeoxyglucose positron emission tomography/computed tomography in patients with active polymyalgia rheumatica: evidence for distinctive bursitis and large-vessel vasculitis. *Mod Rheumatol*. (2012) 22:705–11. doi: 10.3109/s10165-011-0581-x
4. Takahashi H, Yamashita H, Kubota K, Miyata Y, Okasaki M, Morooka M, et al. Differences in fluorodeoxyglucose positron emission tomography/computed tomography findings between elderly onset rheumatoid arthritis and polymyalgia rheumatica. *Mod Rheumatol*. (2015) 25:546–51. doi: 10.3109/14397595.2014.978936
5. Sondag M, Guillot X, Verhoeven F, Blagosklonov O, Prati C, Boulahdour H, et al. Utility of 18F-fluoro-dexoxyglucose positron emission tomography for the diagnosis of polymyalgia rheumatica: a controlled study. *Rheumatology*. (2016) 55:1452–7. doi: 10.1093/rheumatology/kew202
6. Owen CE, Poon AMT, Yang V, McMaster C, Lee ST, Liew DFL, et al. Abnormalities at three musculoskeletal sites on whole-body positron emission tomography/computed tomography can diagnose polymyalgia rheumatica with high sensitivity and specificity. *Eur J Nucl Med Mol Imaging*. (2020) 47:2461–8. doi: 10.1007/s00259-020-04731-z
7. Henckaerts L, Gheysens O, Vanderschueren S, Goffin K, Blockmans D. Use of 18F-fluorodeoxyglucose positron emission tomography in the diagnosis of polymyalgia rheumatica—a prospective study of 99 patients. *Rheumatology*. (2018) 57:1908–16. doi: 10.1093/rheumatology/kex376
8. Wakura D, Kotani T, Takeuchi T, Komori T, Yoshida S, Makino S, et al. Differentiation between Polymyalgia Rheumatica (PMR) and elderly-onset rheumatoid arthritis using 18F-fluorodeoxyglucose positron emission tomography/computed tomography: is enthesitis a new pathological lesion in PMR? *PLoS ONE*. (2016) 11:e0158509. doi: 10.1371/journal.pone.0158509
9. Amat J, Chanchou M, Olagne L, Descamps L, Flaus A, Bouvet C, et al. Utility of 18F-fluorodeoxyglucose positron emission tomography in inflammatory rheumatism, particularly polymyalgia rheumatica: a retrospective study of 222 PET/CT. *Front Med*. (2020) 7:394. doi: 10.3389/fmed.2020.00394
10. Kay J, Upchurch KS. ACR/EULAR (2010) rheumatoid arthritis classification criteria. *Rheumatology*. (2012) 51:vi5–9. doi: 10.1093/rheumatology/kes279
11. Dasgupta B, Cimmino MA, Maradit-Kremers H, Schmidt WA, Schirmer M, Salvarani C, et al. Provisional classification criteria for polymyalgia rheumatica: a European League Against Rheumatism/American College

of Rheumatology collaborative initiative. *Ann Rheum Dis*. (2012) 71:484–92. doi: 10.1016/j.ymed.2012.09.009
12. Rudwaleit M, Jurik AG, Hermann K-GA, Landewe R, van der Heijde D, Baraliakos X, et al. Defining active sacroiliitis on magnetic resonance imaging (MRI) for classification of axial spondyloarthritis: a consensual approach by the ASAS/OMERACT MRI group. *Ann Rheum Dis*. (2009) 68:1520–7. doi: 10.1136/ard.2009.110767
13. Vennart NJ, Bird N, Buscombe J, Cheow HK, Nowosinska E, Heard S. Optimization of PET/CT image quality using the GE 'Sharp IR' point-spread function reconstruction algorithm. *Nucl Med Commun*. (2017) 38:471–9. doi: 10.1097/MNM.0000000000000669
14. Thie JA. Understanding the standardized uptake value, its methods, and implications for usage. *J Nucl Med*. (2004) 45:1431–4.
15. Slart RHJA; Writing group; Reviewer group; Members of EANM Cardiovascular; Members of EANM Infection & Inflammation; Members of Committees, SNMMI Cardiovascular; Members of Council, PET Interest Group; Members of ASNC; EANM Committee Coordinator. FDG-PET/CT(A) imaging in large vessel vasculitis and polymyalgia rheumatica: joint procedural recommendation of the EANM, SNMMI, and the PET Interest Group (PIG), and endorsed by the ASNC. *Eur J Nucl Med Mol Imaging*. (2018) 45:1250–69. doi: 10.1007/s00259-018-3973-8
16. Azar AT, El-Metwally SM. Decision tree classifiers for automated medical diagnosis. *Neural Comput Applic*. (2013) 23:2387–403. doi: 10.1007/s00521-012-1196-7
17. Pedregosa F, Varoquaux G, Gramfort A, Michel V, Thirion B, Grisel O, et al. Scikit-learn: machine learning in python. Machine learning in python. *J Mach Learn Res*. (2011) 12:2825–30.
18. Goodfellow I, Bengio Y, Courville A. Machine learning basics. *Deep Learn*. (2016) 1:98–164.
19. Team RC. *R: A Language and Environment for Statistical Computing (Version 3.5.2)*. Vienna: R Foundation for Statistical Computing (2018).
20. Wongvibulsin S, Wu KC, Zeger SL. Improving clinical translation of machine learning approaches through clinician-tailored visual displays of black box algorithms: development and validation. *JMIR Med Inform*. (2020) 8:e15791. doi: 10.2196/15791
21. Salvarani C, Barozzi L, Boiardi L, Pipitone N, Bajocchi GL, Macchioni PL, et al. Lumbar interspinous bursitis in active polymyalgia rheumatica. *Clin Exp Rheumatol*. (2013) 31:526–31.
22. Van der Geest KSM, Treglia G, Glaudemans AWJM, Brouwer E, Jamar F, Slart RHJA, et al. Diagnostic value of [18F]FDG-PET/CT in polymyalgia rheumatica: a systematic review and meta-analysis. *Eur J Nucl Med Mol Imaging*. (2020). doi: 10.1007/s00259-020-05162-6
23. Camellino D, Cimmino MA. Imaging of polymyalgia rheumatica: indications on its pathogenesis, diagnosis and prognosis. *Rheumatology*. (2012) 51:77–86. doi: 10.1093/rheumatology/keq450
24. Adams MC, Turkington TG, Wilson JM, Wong TZ. A systematic review of the factors affecting accuracy of SUV measurements. *AJR Am J Roentgenol*. (2010) 195:310–20. doi: 10.2214/AJR.10.4923

Conflict of Interest: The authors declare that the research was conducted in the absence of any commercial or financial relationships that could be construed as a potential conflict of interest.

frontiers in Medicine

ORIGINAL RESEARCH
published: 11 May 2021
doi: 10.3389/fmed.2021.668323

^{18}F-FDG PET/CT Associates With Disease Activity and Clinical Recurrence of AOSD Patients

Xian Li, Chuning Dong, Xiaowei Ma and Yunhua Wang**

Department of Nuclear Medicine, The Second Xiangya Hospital, Central South University, Changsha, China

Objective: The purpose of this study was to explore the value of ^{18}F-FDG PET/CT in monitoring the disease activity and predicting the prognosis of the Adult-onset Still's disease (AOSD).

Methods: We retrospectively analyzed the electronic medical records of 45 AOSD patients who underwent ^{18}F-FDG PET/CT in the Second Xiangya Hospital. PET/CT imaging and clinical information were retrospectively reviewed and analyzed. ^{18}F-FDG uptake was assessed by measuring standard uptake value (SUV) in the spleen, liver, bone marrow, and lymph nodes. The spleen-to-liver ratio of the SUVmax (SLRmax) and SUVmean (SLRmean), the bone-to-liver ratio of the SUVmax (BLRmax), and SUVmean (BLRmean), and the lymph nodes-to-liver ratio of the SUVmax (LyLRmax) were calculated. Clinical and laboratory information were collected and evaluated for association with metabolic parameters of ^{18}F-FDG PET/CT. The influencing factors for recurrence within 1 year were analyzed to determine whether ^{18}F-FDG PET/CT can predict the prognosis of AOSD patients.

Results: Elevated ^{18}F-FDG uptake could be observed in bone marrow, spleen, and lymph nodes of AOSD patients. Correlation analysis between ^{18}F-FDG uptake of organs and laboratory examinations showed that SLRmean positively correlated with LDH, AST, ferritin, and the systemic score ($r = 0.572$, 0.353, 0.586, and 0.424, $P < 0.05$). The SLRmean had the highest correlation with ferritin ($r = 0586$, $P < 0.001$). All metabolic parameters in spleen, including SUVmax, SUVmean, SLRmax, and SLRmean, are positively correlated with LDH level ($r = 0.405$, 0.539, 0.481, and 0.572, $P < 0.05$). Bone marrow SUVmax, BLRmax, and BLRmean were correlated with C-reactive protein (CRP) level ($r = 0.395$, 0.437, and 0.469, $P < 0.05$). Analysis of the influencing factors of recurrence within 1 year showed that the spleen SUVmax, spleen SUVmean, SLRmax, SLRmean, ferritin, and the systemic score of the recurrence group was significantly higher than the non-recurrence group ($P < 0.05$). The SLRmean cutoff of 1.66 with a sensitivity of 72.7% and specificity of 80.0% had the highest performance in predicting recurrence.

Conclusion: The glucose metabolism of the liver, spleen, and bone marrow of AOSD patients were correlated with laboratory inflammatory indicators and system score, suggesting that ^{18}F-FDG PET/CT could be applied to evaluate disease activity. Moreover, spleen ^{18}F-FDG uptake may be a potential biomarker for predicting clinical prognosis of AOSD patients.

Keywords: ^{18}F-FDG, AOSD, disease activity, recurrence, PET/CT, still's disease

OPEN ACCESS

Edited by:
Giorgio Treglia,
Ente Ospedaliero Cantonale (EOC), Switzerland

Reviewed by:
Domenico Albano,
University of Brescia, Italy
Maria Vittoria Mattoli,
University of Studies G. d'Annunzio Chieti and Pescara, Italy

****Correspondence:***
Yunhua Wang
wangyunhua0801@csu.edu.cn
Xiaowei Ma
maxiaowei@csu.edu.cn

Specialty section:
This article was submitted to Nuclear Medicine, a section of the journal Frontiers in Medicine

Received: *18 February 2021*
Accepted: *06 April 2021*
Published: *11 May 2021*

Citation:
Li X, Dong C, Ma X and Wang Y (2021) ^{18}F-FDG PET/CT Associates With Disease Activity and Clinical Recurrence of AOSD Patients. Front. Med. 8:668323. doi: 10.3389/fmed.2021.668323

INTRODUCTION

AOSD is a multisystemic autoinflammation disorder usually affecting young adults, which is associated with many inflammatory factors including IL-1 (inetleukin-1, IL-1), IL-6, IL-8, tumor necrosis factor alpha (TNF-α), and interferon gamma (IFN-γ) (1, 2). AOSD is characterized by four cardinal symptoms, fever, rash, arthralgia, and increased leukocyte and neutrophil counts. Many other manifestations can also occur, such as odynophagia, myalgia, myositis, lymphadenopathy, and splenomegaly. However, nonspecific clinical sign or biological abnormality is unable to ascertain the diagnosis of AOSD. The most widely used diagnosis criteria of AOSD is Yamaguchi criteria, but the criteria ought to exclude infections, malignant tumors, and other rheumatic diseases. Then performing a comprehensive diagnostic work-up is challenging in clinical practice.

Accompanied with activation of systemic inflammation, AOSD is closely related to inflammatory activity and may develop severe and life-threatening complications, such as macrophage syndrome, disseminated intravascular coagulopathy (DIC), thrombotic thrombocytopenic purpura (TTP) (3–5). The most common methods for assessing AOSD activity are systemic score and laboratory tests, such as erythrocyte sedimentation rate (ESR), C-reactive protein (CRP), lactate dehydrogenase (LDH), aspartate aminotransferase (AST), alanine aminotransferase (ALT), and plasma ferritin (6, 7). ^{18}F-FDG PET/CT, which reflect the glucose metabolism of organs, can be used in differential diagnosis of AOSD and malignant tumors and other autoimmune diseases (8, 9). However, ^{18}F-FDG PET/CT imaging for assessing AOSD disease activity have not been well-established. Some researches have demonstrated ^{18}F-FDG PET/CT may be associated with the activity of the disease (10, 11), but their limitation is a small sample sized. Thus, more investigations are required to certify its value for accessing disease activity. Besides, a reliable method for predicting the therapeutic response and outcome has not been established (12). Therefore, it is critically important to develop new tools for effectively monitoring disease activity and predicting the outcome of AOSD in order to prevent fatal complications.

In this study, we retrospectively investigated a group of patients with AOSD to explore the role of ^{18}F-FDG PET/CT imaging in evaluating the disease activity and predicting prognosis.

MATERIALS AND METHODS

Patient Selection

The medical records and PET/CT images of 45 AOSD patients at the Second Xiangya Hospital, Central South University, from January 2015 to June 2019 were reviewed. Inclusion criteria: (1) Met the Japan's Yamaguehi criteria (13), it contains four major criteria (fever, rash, arthritis, and leukocytosis) and five minor criteria (sore throat, lymphadenopathy, hepatomegaly/splenomegaly, altered liver function test, and negative for antinuclear antibodies and rheumatoid arthritis) criteria. A total of five or more criteria are required to make the diagnosis, including at least two major criteria; (2) Followed up by telephone or outpatient service for more than 6 months; (3) Complete laboratory examinations within 3 days before and after ^{18}F-FDG PET/CT examination; (4) No previous history of malignant tumor; (5) Complete clinical data. Exclusion criteria: (1) previous history of tumors; (2) patients who had progressed to other rheumatic diseases or malignant tumors; (3) Incomplete clinical data. This retrospective study was approved by Medical Ethical Committee of The Second Xiangya Hospital.

Clinical Information and Laboratory Data and Therapeutic Data Collection

Clinical information included age, sex, and length of disease. Laboratory data included cell counts of white blood cell, neutrophil, lymphocyte, monocyte, and platelet and hemoglobin, ALT, AST, ESR, CRP, LDH, and ferritin levels. All laboratory tests were measured within 3 days of the date of the PET/CT scan. Other tests included bone marrow aspiration and lymph node biopsy. Therapeutic Data included drug category (glucocorticoids or nonsteroidal anti-inflammatory drugs or antirheumatic drugs), medication time, sequence of drug therapy and PET/CT examination.

The systemic score standard is mainly based on clinical manifestation scores for disease activity evaluation (14), with a score of 0–12, and 1 point for each of the following clinical manifestations: fever, typical rash, pleurisy, pneumonia, pericarditis, hepatomegaly, or abnormal liver function, splenomegaly, large lymph nodes, sore throat, myalgia, abdominal pain, and white blood cell count $\geq 15 \times 10^9$/L. The total score ≥ 2 points is regarded as an active stage of AOSD.

Criteria for Recurrence

All patients were followed up for at least 6 months to exclude other rheumatic diseases or malignant tumors. Recurrence refers to the disappearance of clinical manifestations such as fever and rash after systemic treatment and the discharge of related laboratory indicators to the normal range. During the one-year follow-up period after discharge from the hospital, under the premise of taking regular medication and eliminating other pathogenic factors such as infection, patients recurred fever, rash, arthralgia, sore throat, lymphadenopathy, splenomegaly and other AOSD-related clinical symptoms, accompanied by relevant laboratory indicators and abnormalities in imaging examinations (X-ray, CT or MRI).

^{18}F-FDG PET/CT Image Acquisition

All ^{18}F-FDG PET/CT images were acquired with a standard protocol on a dedicated PET/CT scanner (Biography mCT, Siemens Medical Systems, Germany). Patients fasted for 6 h before the PET/CT scan, and a blood glucose level below 140 mg/dL was confirmed. The PET/CT scan was performed 60 min after the intravenous administration of 5.0 MBq/Kg body weight of ^{18}F-FDG. The first procedure of scanning is CT scan (120 kV, 200 mA, and layer thickness 3.0 mm). Then the PET scan was performed with an acquisition time of 1.5 min per bed position in 3-dimensional mode. Imaging ranging from the base of the skull to the middle of the thighs was acquired for each patient, then the image is reconstructed by the iterative method, and the data is transferred to the MMWP image post-processing workstation.

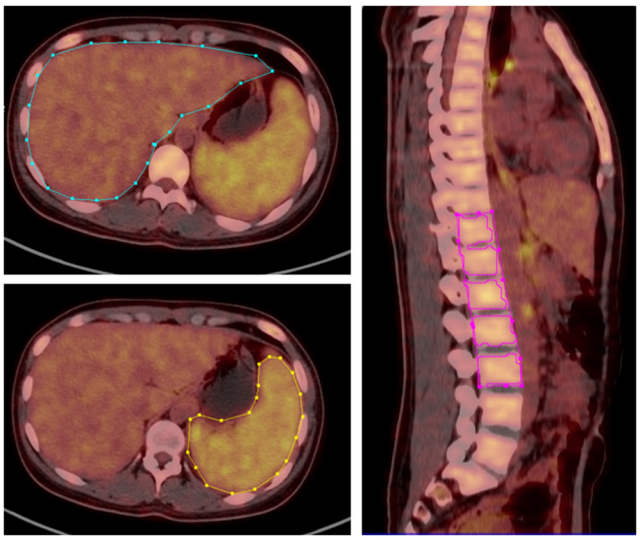

FIGURE 1 | 3D ROI was manually delineated according to the contours of liver, spleen and spine, SUVmax, and SUVmean of corresponding regions was obtained.

TABLE 1 | Baseline characteristics of AOSD patients.

Variable	*n*	Minimum	Maximum	$x \pm s$
WBC count (/μL)	45	2.9	31.3	13.7 ± 6.4
Neutrophil count (/μL)	45	2.1	29.3	11.4 ± 6.2
Lymphocyte count (/μL)	45	0.4	5.8	1.5 ± 1.0
Monocyte count (/μL)	45	0.1	0.9	0.5 ± 0.2
Hemoglobin (g/dL)	45	49.0	127.0	96.0 ± 18.4
Platelet count (1,000/μL)	45	81.0	531.0	256.2 ± 113.9
ESR (mm/h)	35	7.0	274.0	74.1 ± 48.4
CRP (mg/L)	36	0.8	215.0	70.5 ± 51.2
LDH(IU/L)	33	210.0	1863.8	655.1 ± 404.6
Ferritin (ng/mL)	32	2005.4	40000.0	22120.5 ± 15390.3
ALT (IU/L)	38	9.6	298.1	50.9 ± 59.9
AST (IU/L)	38	18.6	142.9	59.8 ± 34.3
Systemic score	45	2.0	10.0	6.3 ± 1.4

WBC, white blood cell; ESR, erythrocyte sedimentation rate; CRP, C-reactive protein; AST, aspartate aminotransferase; ALT, alanine aminotransferase; LDH, lactate dehydrogenase.

PET/CT Imaging Analysis

PET/CT imaging was firstly visually analyzed by two experienced nuclear medicine physicians to determine whether there was abnormal ^{18}F-FDG uptake and/or structural changes in the imaging. Secondly, the location, number, ^{18}F-FDG uptake, and systemic distribution of abnormal lesions were recorded. Thirdly, the maximum standardized uptake value (SUVmax) and mean standardized uptake value (SUVmean) of the liver, spleen, and bone marrow was measured and recorded by a fixed physician, using the three-dimensional region of interest (3D ROI) technique manually. The ROIs on liver, spleen, and spine were manually delineated according to the contours of target organs slice-by-slice and then reconstructed to three-dimensional region of interest (3D ROI). The bone marrow SUV measurement is obtained by delineating the ROI of five adjacent vertebral bodies (from T11-L3 spine, except for compression fractures or severe osteoarthritis changes, or those undergoing surgery due to spinal diseases Patient) (**Figure 1**). When an abnormal lymph node was found, the SUVmax was measured and recorded. The spleen-to-liver ratio of the SUVmax (SLRmax) and SUVmean (SLRmean) was calculated by dividing the spleen SUVmax and SUVmean by the liver SUVmax and liver SUVmean, respectively, and the bone marrow-to-liver ratio of the SUV max (BLRmax) and SUVmean (BLRmean) was calculated by dividing the bone marrow SUVmax and SUVmean by the liver SUVmax and liver SUVmean, respectively. The lymph node-to-liver ratio of SUVmax (LyLRmax) was calculated by dividing lymph node SUVmax by the liver SUVmax.

Statistical Analysis

Data were analyzed using SPSS, version 25 (SPSS Inc.). Continuous variables are expressed as mean with SD, and continuous variables data were compared using the Student *t*-test. Categoric variables are expressed as frequencies and percentages, compared using the x^2 test. Correlations between laboratory variables and metabolic parameters (SUVmax, SUVmean, SLRmean, SLRmax, BLRmean, BLRmax, and LyLRmax) were calculated by the Pearson correlation analysis. The discriminative ability of spleen SUVmax, spleen SUVmean, SLRmax, SLRmean for predicting recurrence was analyzed using area under the receiver-operating-characteristic (ROC) curve. The area under the ROC curve was presented with 95% confidence interval (CI), and the Youden index was used to identify the maximal cutoff. When *P* value was less than 0.05, the difference was considered statistically significant.

RESULTS

Baseline Characteristics of Patients and Pathology and Therapeutic Data

Thirty-one female and 14 male patients with a mean age of 36.4 years (range, 16–74 years) took part in the present study. The duration of the disease ranged from 1 week to 2 years, with a mean of 109 days. The laboratory data and systemic score of 45 patients are shown in **Table 1**. Twenty-seven patients underwent bone marrow biopsy, all of which were myelohyperplasia. Nineteen patients underwent lymph node biopsy, of which 2 cases showed necrotizing lymphadenitis, 1 case had lymph node structural disorder, and the rest had lymph node reactive hyperplasia. Nine skin biopsies were performed, and there were no apparent abnormalities.

Of the 45 patients, 17 patients did not receive drug therapy before PET/CT examination, and 28 patients received medical treatment within 3 days before PET/CT examination, of which 19 patients received monotherapy (glucocorticoids/nonsteroidal anti-inflammatory drugs/conventional synthetic DMARDs) and 9 patients received combination therapy. Among all treated patients, the mean duration of treatment was 7 days, the shortest treatment time was 2 days and the longest was 30 days.

TABLE 2 | ^{18}F-FDG uptakes in AOSD patients.

Lesion	*n*	SUVmax		SUVmean	
		Range	$x \pm s$	Range	$x \pm s$
Spleen	42 (93.3%)	2.28–10.52	4.82 ± 1.64	1.07–6.30	2.73 ± 1.05
Bone marrow	41 (91.1%)	2.46–10.81	5.66 ± 1.90	1.12–4.87	2.38 ± 0.83
Lymph node	42 (93.3%)	2.33–42.67	10.32 ± 7.68	–	–
Joint	7 (15.6%)	3.30–6.10	4.3 ± 0.68	–	–
Parotid gland/Salivary gland	3 (6.7%)	2.60–4.50	3.70 ± 0.98	–	–

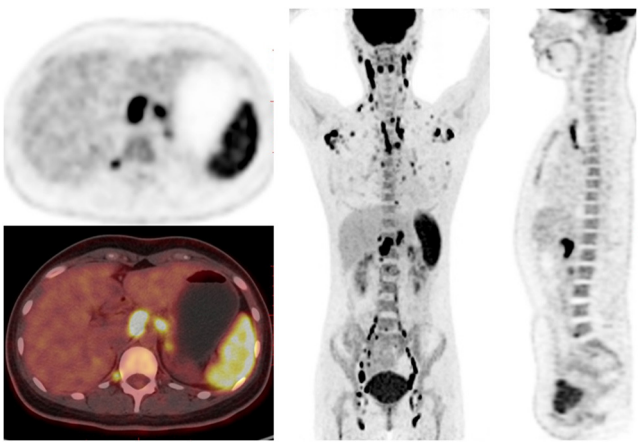

FIGURE 2 | ^{18}F-FDG PET/CT images in a 23-year-old female of AOSD patient. PET/CT showed diffusely increased ^{18}F-FDG uptake in spleen, bone marrow and lymph nodes, and reactive hyperplastic lymph nodes symmetrically distributed in the whole body.

During the follow-up period, 41 patients were followed up for more than 1 year. Of those 41 patients, 37 patients received glucocorticoids as first-line treatment, 20 of whom received nonsteroidal anti-inflammatory drugs simultaneously, and 17 of whom received conventional synthetic DMARDs. Two patients received single nonsteroidal anti-inflammatory drugs and antirheumatic drugs as first-line treatment, respectively. The average treatment time for all patients was 8.2 months, the shortest was 3 months, and the longest was 25.3 months.

Characteristics of ^{18}F-FDG PET/CT Imaging in AOSD Patients

In AOSD patients, the main manifestations of PET/CT images are diffusely increased FDG uptake in the spleen, bone marrow, and lymph nodes (**Table 2** and **Figure 2**). The spleen glucose metabolism increased in 42 patients, all accompanied by splenomegaly. Reactive hyperplastic lymph nodes with increased ^{18}F-FDG uptake of 42 patients were distributed in the whole body, most of them located in the neck and axilla. All lymph nodes were regular and oval; there was almost no fusion or calcification, and only 1 case had a tendency of fusion. Seven patients had increased FDG uptake in the joints, mainly involving the shoulder and hip joints, with joint pain in all cases. In addition, 10 patients had pleural effusion, and 2 patients had pericardial effusion.

Association of Laboratory Variables With Metabolic Parameters

In AOSD patients, correlation analysis between metabolic parameters and laboratory examination showed that SLRmean correlated positively with LDH, AST, ferritin, and the systemic score ($r = 0.572$, 0.353, 0.586, and 0.424, $P < 0.05$; **Figure 3**), and SLRmean had the highest correlation with ferritin ($r =$ 0586, $P < 0.001$). LDH was positively correlated with spleen SUVmax, spleen SUVmean, SLRmax, SLRmean ($r = 0.405$, 0.539, 0.481, 0.572, and $P < 0.05$; **Figure 4**). In addition, bone marrow SUVmax, BLRmax, and BLRmean were correlated with C-reactive protein ($r = 0.395$, 0.437, 0.469, and $P < 0.05$; **Supplementary Table 1**). We also analyzed the association of laboratory variables between LDH, liver enzyme, ferritin, and the systemic score (**Supplementary Table 2**). ESR, CRP, LDH, AST, ferritin, and the systemic score are related to each other.

Differentiation Between AOSD Recurrence Group and Non-recurrence Group

Forty-one AOSD patients completed more than 1 year follow-up, of which 25 patients (60.98%) relapsed, 16 patients (39.02%) did not relapse. Analysis of the influencing factors of recurrence within 1 year showed that spleen metabolic parameters (spleen SUVmax, spleen SUVmean, SLRmax, and SLRmean), ferritin, and systemic score of the recurrence group was significantly higher than the nonrecurrence group ($P < 0.05$; **Table 3**). ROC analysis of spleen metabolic parameters (spleen SUVmax, spleen SUVmean, SLRmax, and SLRmean), ferritin, and systemic score were performed to differentiate AOSD recurrence and nonrecurrence (**Figure 5**). SLRmean had the highest ROC value, and a SLRmean cutoff of 1.66 had a sensitivity of 72.7% and specificity of 80.0% (area under the ROC curve, 0.824; 95% CI, 0.692–0.957; $P < 0.001$; **Table 4** and **Figure 6**). In addition, treatment prior to PET/CT examination did not change the metabolic parameters of the organs, there was no significant difference of metabolic parameters between the AOSD treatment group and the untreated group (**Supplementary Table 3**).

DISCUSSION

AOSD is an autoinflammation disease of unknown etiology. Its clinical symptoms are varied, typically characterized by

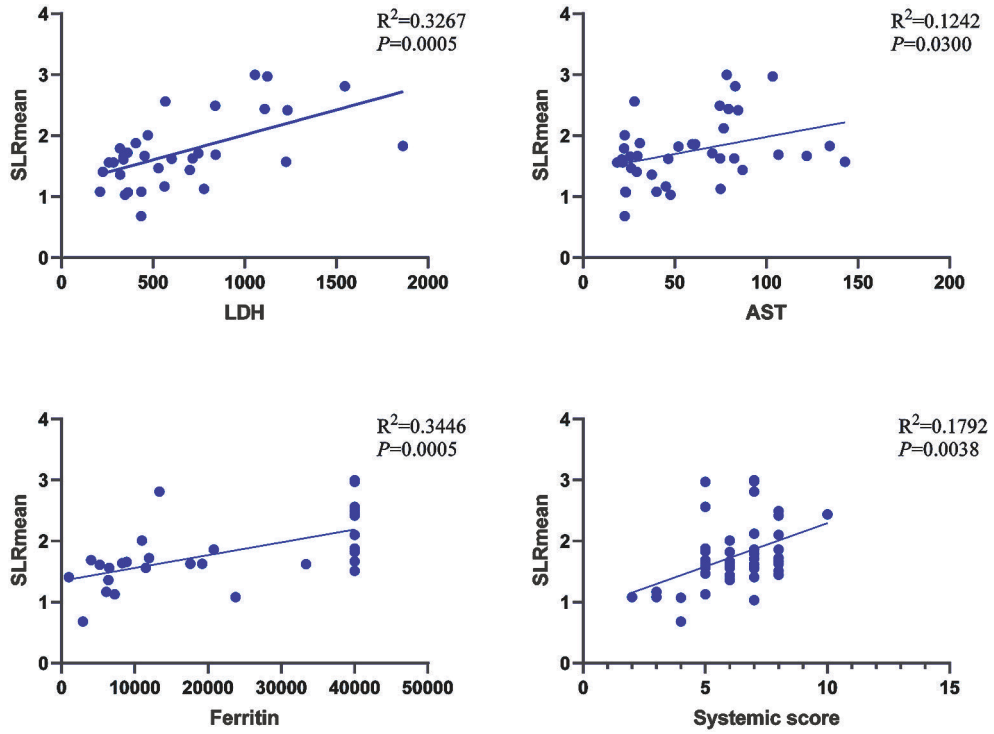

FIGURE 3 | SLRmean correlated positively with LDH, AST, ferritin, and systemic score ($P < 0.05$).

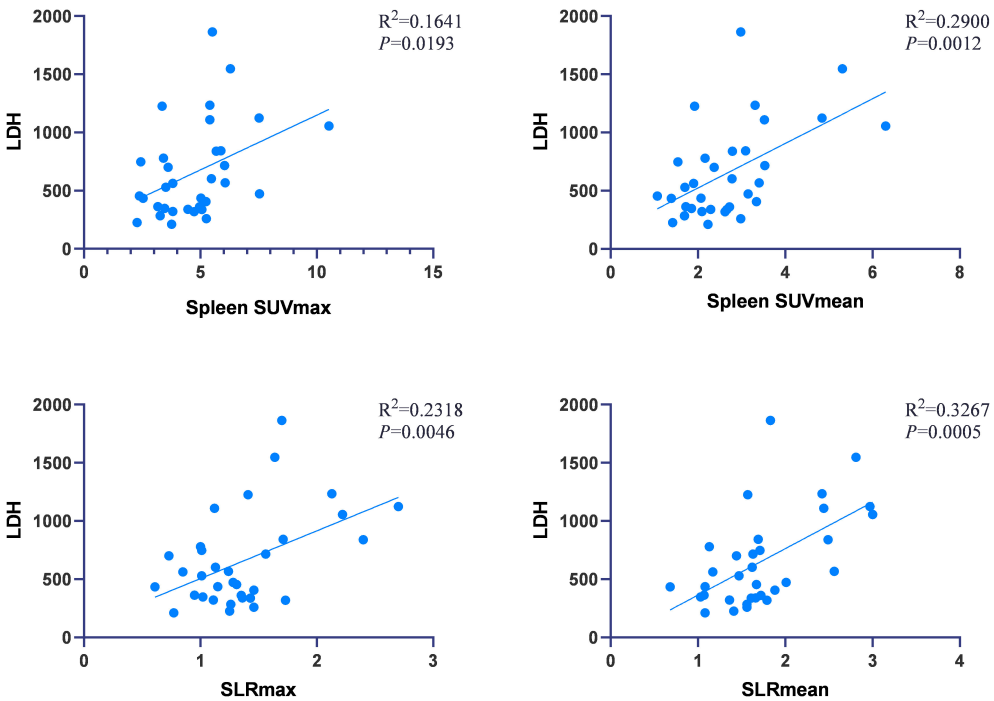

FIGURE 4 | LDH was positively correlated with spleen SUVmax, spleen SUVmean, SLRmax, SLRmean, and LDH ($P < 0.05$).

fever, rash, arthralgia, increased leukocyte, and neutrophil counts. These manifestations and relevant laboratory tests lack specificity, so early diagnosis is problematic in clinical work. Increased ^{18}F-FDG uptake involving various pathologic conditions, including malignancies, infections, and non-infectious, is greatly beneficial to the diagnosis of clinical diseases. Some studies have demonstrated the role of ^{18}F-FDG PET/CT in assisting the diagnosis of ASOD (8, 9, 15). However, researches for ^{18}F-FDG PET/CT evaluating AOSD disease activity are limited and whether it can assess prognosis remains unknown. In our study, we found that the glucose metabolism of the liver, spleen, and bone marrow of AOSD patients correlated with laboratory inflammatory indicators and systemic score, suggesting ^{18}F-FDG PET/CT may be a useful imaging method for the assessment of disease activity throughout the body. Furthermore, our study demonstrated that ^{18}F-FDG PET/CT might predict AOSD prognosis, with spleen uptake is elevated in AOSD recurrence group compared with the nonrecurrence group.

TABLE 3 | Comparison of laboratory variables and metabolic parameters between AOSD recurrence group and non-recurrence group.

Variable	Recurrence group	Non-recurrence group	*P*
n	25 (60.98%)	16 (39.02%)	/
Clinical variables			
Age	37.20 ± 14.18	35.75 ± 17.08	0.770
Sex			
Male	4 (16.00%)	9 (56.25%)	0.018*
Female	21 (84.00%)	7 (43.75%)	
Laboratory variables			
WBC count ($\times 10^9$/L)	14.09 ± 5.76	11.24 ± 5.90	0.133
Neutrophil count ($\times 10^9$/L)	11.66 ± 5.89	9.27 ± 5.10	0.186
ESR# (mm/h)	67.53 ± 26.50	76.14 ± 68.41	0.619
CRP# (mg/L)	71.77 ± 50.87	59.59 ± 41.51	0.463
LDH* (U/L)	743.30 ± 379.65	619.49 ± 450.40	0.421
Ferritin† (ng/mL)	27416.00 ± 15096.67	14542.14 ± 13378.14	0.033*
Systemic score	6.76 ± 1.51	5.50 ± 1.59	0.015*
Metabolic parameters			
Liver SUVmax	3.54 ± 1.01	3.56 ± 0.92	0.941
Liver SUVmean	1.53 ± 0.32	1.64 ± 0.31	0.285
Spleen SUVmax	5.43 ± 1.77	4.01 ± 1.07	0.006**
Spleen SUVmean	3.12 ± 1.17	2.24 ± 0.57	0.008**
Bone SUVmax	5.91 ± 2.03	5.07 ± 1.39	0.158
Bone SUVmean	2.53 ± 0.97	2.18 ± 0.55	0.149
Lymph node SUVmax	11.48 ± 8.90	8.92 ± 6.23	0.322
SLRmax	1.59 ± 0.52	1.18 ± 0.39	0.011*
BLRmax	1.70 ± 0.53	1.53 ± 0.59	0.334
LLRmax	3.37 ± 2.62	2.60 ± 2.01	0.305
SLRmean	2.02 ± 0.54	1.39 ± 0.34	0.000***
BLRmean	1.65 ± 0.51	1.38 ± 0.47	0.107

*WBC, white blood cell; ESR, erythrocyte sedimentation rate; CRP, C-reactive protein; AST, aspartate aminotransferase; ALT, alanine aminotransferase; LDH, lactate dehydrogenase; #33 patients; *30 patients; †28 patients. *P < 0.05, **P < 0.01, ***P < 0.001.*

For the ^{18}F-FDG PET/CT imaging of AOSD, it's common that ^{18}F-FDG uptake of spleen, bone, and lymph nodes is elevated, with hepatosplenomegaly. These manifestations are consistent with previous reports (9, 11). Other lesions such as joints and glands may also accumulate a high level of ^{18}F-FDG, which helps the diagnosis (16). Due to the diagnosis of AOSD is exclusive, it's necessary to rule out cancers, infections, and other autoimmune diseases firstly. Most notable is that the ^{18}F-FDG PET/CT imaging of AOSD is similar to lymphoma. It's widely known that ^{18}F-FDG PET/CT is essential in detecting malignant lesions. For differential diagnosis of AOSD and lymphoma, studies have shown the morphology of lymphoma's enlarged lymph nodes is variable and different, and the degree of ^{18}F-FDG uptake of lymphoma is higher than AOSD (9). Moreover, ^{18}F-FDG PET/CT could facilitate accurate localization of the high radioactive concentration to guide pathologic puncture to further diagnosis.

In the current study, the comparison of metabolic parameters with laboratory tests manifested distinct patterns. Metabolic parameters of the spleen (SUVmax, SUVmean, SLRmean, and SLRmax) were associated with ferritin level, liver enzymes, LDH, and systemic score, whereas bone marrow glucose metabolism was associated with CRP. Serum ferritin is an acute-phase reactant, which can elevate in various autoimmune and autoinflammation diseases, such as AOSD and systemic lupus erythematosus. An increase of more than five times of ferritin has a high specificity in the diagnosis of AOSD, and

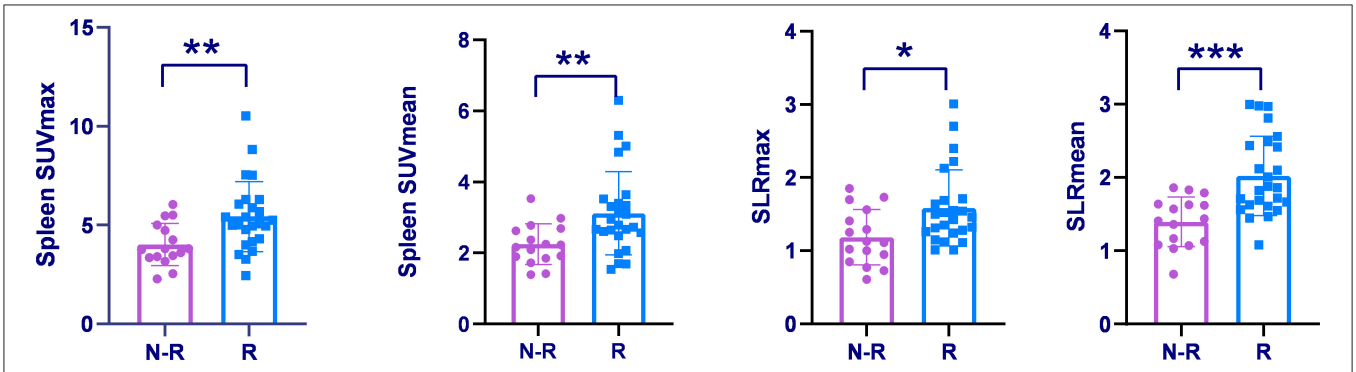

FIGURE 5 | Spleen SUVmax, Spleen SUVmean, and SLRs were compared among the recurrence group and non-recurrence group. *$P < 0.05$, **$P < 0.01$, ***$P < 0.001$.

TABLE 4 | Comparison of metabolic parameters and ferritin and the systemic score in differentiating between AOSD recurrence group and non-recurrence group.

Variable	Cutoff	Sensitivity	Specificity	Area under curve
Sleen SUVmax	4.76	72.0	75.0	0.758 (0.606–0.909)
Sleen SUVmean	2.53	80.0	69.0	0.745 (0.592–0.898)
SLRmax	1.14	84.0	56.2	0.725 (0.556–0.894)
SLRmean	1.66	72.7	80.0	0.824 (0.692–0.957)
Ferritin	36690.00	52.6	90.0	0.737 (0.547–0.927)
The systemic score	7.50	37.0	100.0	0.718 (0.533–0.904)

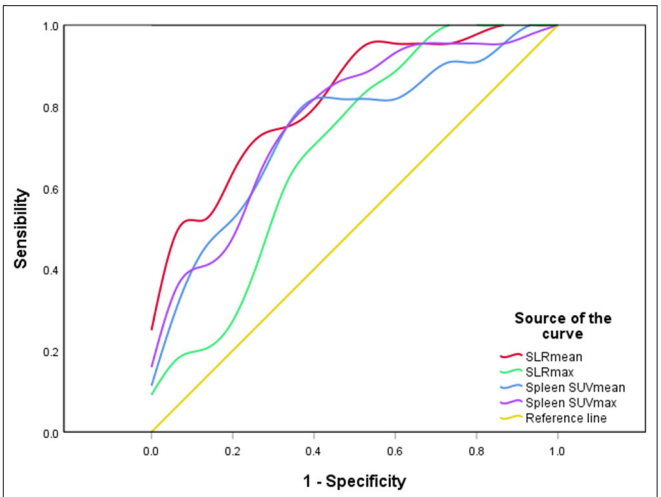

FIGURE 6 | A ROC curve of spleen metabolic parameters. SLRmean had the highest ROC value ($P < 0.001$).

it is closely related to the activity state of the disease (6, 17). AOSD can affect a variety of lesions, of which the liver is a commonly involved organ. The mechanisms are not yet clear but may be related to the continuous activation of macrophages and the production of cytokines (18). The primary manifestation of liver damage is transaminase elevate, which may relative to the activity of AOSD disease (19). Besides, AOSD patients are often accompanied by increased LDH. Our finding showed a significant correlation between ferritin, liver enzymes, and LDH, suggesting these indicators interact with each other and are closely related to the body's inflammatory response. As the largest organ in the lymphatic system of the whole body, the spleen is responsible for filtering blood and monitoring blood-borne antigens. When an inflammatory reaction occurs, the dendritic cells and T cells of the spleen process antigen and directly contact the pro-inflammatory cytokines in the blood (20). During the activation process, the metabolism of dendritic cells and T cells changes, from oxygen metabolism to glycolysis for energy (21, 22). Therefore, it is feasible to assess spleen immunometabolism through ^{18}F-FDG uptake in systemic inflammation (23, 24). Our study demonstrates there is a significant correlation between splenic ^{18}F-FDG uptake and laboratory inflammatory parameters. In addition, ^{18}F-FDG uptake of bone marrow was associated with CRP, which may be due to the regulation of bone marrow metabolism induced by inflammatory factors (25), suggesting that spleen ^{18}F-FDG uptake may provide more comprehensive information in accessing the inflammatory condition of the whole body than traditional laboratory examinations.

Identification of prognostic factors is extremely vital for the proper treatment of AOSD. ^{18}F-FDG PET/CT, currently the most commonly used whole-body molecular imaging technology, can not only discover inflammatory reactions and early changes in a disease that cannot be detected by routine laboratory tests but also has significant potential in predicting disease outcome. Since the spleen plays a crucial role in the innate and adaptive immune response, some scholars have indicated that splenic ^{18}F-FDG uptake is related to the prognosis of rheumatic immune disease, melanoma, and other diseases (24, 26). In this study, spleen ^{18}F-FDG uptake of the AOSD recurrence group was significantly higher than the non-recurrence group, and metabolic parameters of spleen had higher ROC values than ferritin and systemic score, demonstrating splenic radiological uptake may be a potential indicator for predicting AOSD recurrence. Increased spleen ^{18}F-FDG uptake may be an overall reflection of the inflammatory state, or it may be an early sign of severe systemic inflammation that has not been detected by traditional laboratory tests (24). Therefore, closer monitoring is required and necessary for AOSD patients with high spleen ^{18}F-FDG uptake.

Previous studies revealed that ^{18}F-FDG PET/CT could help differentiate AOSD from other febrile autoimmune diseases, and ^{18}F-FDG PET/CT may evaluate the therapeutic effect of AOSD (8, 27). Our study further extended the application of ^{18}F-FDG PET/CT in assessing AOSD disease activity and predicting of recurrence.

Our study has several limitations. Firstly, it is a single-institution retrospective observational study, with bias in patient selection and analysis. Secondly, only AOSD patients were included. Other differential diagnoses, such as cancer or infection, may present different splenic glucose metabolism patterns and changes.

CONCLUSION

The glucose metabolism of the liver, spleen, and bone marrow of AOSD patients were correlated with laboratory inflammatory indicators and systemic score, suggesting that ^{18}F-FDG PET/CT could be applied to evaluate disease activity. Moreover, spleen ^{18}F-FDG uptake may be a potential biomarker for predicting clinical prognosis of AOSD patients.

DATA AVAILABILITY STATEMENT

The original contributions presented in the study are included in the article/**Supplementary Material**, further inquiries can be directed to the corresponding author/s.

ETHICS STATEMENT

The studies involving human participants were reviewed and approved by Medical Ethical Committee of Second Xiangya

Hospital. Written informed consent to participate in this study was provided by the participants' legal guardian/next of kin. Written informed consent was obtained from the individual(s) for the publication of any potentially identifiable images or data included in this article.

AUTHOR CONTRIBUTIONS

XL: conceptualization, methodology, formal analysis, and writing–original draft. CD: data curation and validation. XM: review and editing, supervision, and writing–review and editing. YW: conceptualization, methodology, supervision, and writing–review and editing. All authors contributed to the article and approved the submitted version.

SUPPLEMENTARY MATERIAL

The Supplementary Material for this article can be found online at: https://www.frontiersin.org/articles/10.3389/fmed.2021.668323/full#supplementary-material

REFERENCES

1. Gerfaud-Valentin M, Jamilloux Y, Iwaz J, Seve P. Adult-onset Still's disease. *Autoimmun Rev.* (2014) 13:708–22. doi: 10.1016/j.autrev.2014.01.058
2. Jung JY, Kim JW, Suh CH, Kim HA. Roles of interactions between toll-like receptors and their endogenous ligands in the pathogenesis of systemic juvenile idiopathic arthritis and adult-onset still's disease. *Front Immunol.* (2020) 11:583513. doi: 10.3389/fimmu.2020.583513
3. Ruscitti P, Iacono D, Ciccia F, Emmi G, Cipriani P, Grembiale RD, et al. Macrophage activation syndrome in patients affected by adult-onset still disease: analysis of survival rates and predictive factors in the Gruppo Italiano di Ricerca in Reumatologia Clinica e Sperimentale Cohort. *J Rheumatol.* (2018) 45:864–72. doi: 10.3899/jrheum.170955
4. Efthimiou P, Kadavath S, Mehta B. Life-threatening complications of adult-onset Still's disease. *Clin Rheumatol.* (2014) 33:305–14. doi: 10.1007/s10067-014-2487-4
5. Tristano AG. Macrophage activation syndrome: a frequent but under-diagnosed complication associated with rheumatic diseases. *Med Sci Monit.* (2008) 14:RA27-36
6. Giacomelli R, Ruscitti P, Shoenfeld Y. A comprehensive review on adult onset Still's disease. *J Autoimmun.* (2018) 93:24–36. doi: 10.1016/j.jaut.2018.07.018
7. Mitrovic S, Fautrel B. New markers for adult-onset Still's disease. *Joint Bone Spine.* (2018) 85:285–93. doi: 10.1016/j.jbspin.2017.05.011
8. Zhou X, Li Y, Wang Q. FDG PET/CT used in identifying adult-onset Still's disease in connective tissue diseases. *Clin Rheumatol.* (2020) 39:2735–42. doi: 10.1007/s10067-020-05041-3
9. Dong MJ, Wang CQ, Zhao K, Wang GL, Sun ML, Liu ZF, et al. 18F-FDG PET/CT in patients with adult-onset Still's disease. *Clin Rheumatol.* (2015) 34:2047–56. doi: 10.1007/s10067-015-2901-6
10. Yamashita H, Kubota K, Takahashi Y, Minamimoto R, Morooka M, Kaneko H, et al. Clinical value of ^{18}F-fluoro-dexoxyglucose positron emission tomography/computed tomography in patients with adult-onset Still's disease: a seven-case series and review of the literature. *Mod Rheumatol.* (2014) 24:645–50. doi: 10.3109/14397595.2013.850998
11. An YS, Suh CH, Jung JY, Cho H, Kim HA. The role of 18F-fluorodeoxyglucose positron emission tomography in the assessment of disease activity of adult-onset Still's disease. *Korean J Intern Med.* (2017) 32:1082–9. doi: 10.3904/kjim.2015.322
12. Feist E, Mitrovic S, Fautrel B. Mechanisms, biomarkers and targets for adult-onset Still's disease. *Nat Rev Rheumatol.* (2018) 14:603–18. doi: 10.1038/s41584-018-0081-x
13. Yamaguchi M, Ohta A, Tsunematsu T, Kasukawa R, Mizushima Y, Kashiwagi H, et al. Preliminary criteria for classification of adult Still's disease. *J Rheumatol.* (1992) 19:424–30.
14. Ruscitti P, Cipriani P, Masedu F, Iacono D, Ciccia F, Liakouli V, et al. Adult-onset Still's disease: evaluation of prognostic tools and validation of the systemic score by analysis of 100 cases from three centers. *BMC Med.* (2016) 14:194. doi: 10.1186/s12916-016-0738-8
15. Jiang L, Xiu Y, Gu T, Dong C, Wu B, Shi H. Imaging characteristics of adult onset Still's disease demonstrated with 18F-FDG PET/CT. *Mol Med Rep.* (2017) 16:3680–6. doi: 10.3892/mmr.2017.7022
16. Ahn BC, Lee SW, Lee J. Intense accumulation of F-18 FDG in colonic wall in adult onset still disease with pseudomembranous colitis. *Clin Nucl Med.* (2008) 33:806–8. doi: 10.1097/RLU.0b013e318187eec4
17. Fardet L, Coppo P, Kettaneh A, Dehoux M, Cabane J, Lambotte O. Low glycosylated ferritin, a good marker for the diagnosis of hemophagocytic syndrome. *Arthritis Rheum.* (2008) 58:1521–7. doi: 10.1002/art.23415
18. Arlet JB, Le TH, Marinho A, Amoura Z, Wechsler B, Papo T, et al. Reactive haemophagocytic syndrome in adult-onset Still's disease: a report of six patients and a review of the literature. *Ann Rheum Dis.* (2006) 65:1596–601. doi: 10.1136/ard.2005.046904
19. Muller R, Briantais A, Faucher B, Borentain P, Nafati C, Blasco V, et al. Acute severe hepatitis in adult-onset Still's disease: case report and comprehensive review of a life-threatening manifestation. *Clin Rheumatol.* (2020). doi: 10.1007/s10067-020-05383-y. [Epub ahead of print].
20. Yin Y, Choi SC, Xu Z, Perry DJ, Seay H, Croker BP, et al. Normalization of CD^{4+} T cell metabolism reverses lupus. *Sci Transl Med.* (2015) 7:274ra218. doi: 10.1126/scitranslmed.aaa0835
21. Everts B, Pearce EJ. Metabolic control of dendritic cell activation and function: recent advances and clinical implications. *Front Immunol.* (2014) 5:203. doi: 10.3389/fimmu.2014.00203
22. Park BV, Pan F. Metabolic regulation of T cell differentiation and function. *Mol Immunol.* (2015) 68:497–506. doi: 10.1016/j.molimm.2015.07.027
23. Mathis D, Shoelson SE. Immunometabolism: an emerging frontier. *Nat Rev Immunol.* (2011) 11:81. doi: 10.1038/nri2922
24. Ahn SS, Hwang SH, Jung SM, Lee SW, Park YB, Yun M, et al. Evaluation of spleen glucose metabolism using (18)F-FDG PET/CT in patients with febrile autoimmune disease. *J Nucl Med.* (2017) 58:507–13. doi: 10.2967/jnumed.116.180729
25. Prevost S, Boucher L, Larivee P, Boileau R, Benard F. Bone marrow hypermetabolism on 18F-FDG PET as a survival prognostic factor in non-small cell lung cancer. *J Nucl Med.* (2006) 47:559–65.
26. Wong A, Callahan J, Keyaerts M, Neyns B, Mangana J, Aberle S, et al. (18)F-FDG PET/CT based spleen to liver ratio associates with clinical outcome to ipilimumab in patients with metastatic melanoma. *Cancer Imaging.* (2020) 20:36. doi: 10.1186/s40644-020-00313-2
27. Yamashita H, Kubota K, Mimori A. Clinical value of whole-body PET/CT in patients with active rheumatic diseases. *Arthrit Res Ther.* (2014) 16:423. doi: 10.1186/s13075-014-0423-2

Conflict of Interest: The authors declare that the research was conducted in the absence of any commercial or financial relationships that could be construed as a potential conflict of interest.

frontiers | Frontiers in Medicine

REVIEW
published: 06 June 2022
doi: 10.3389/fmed.2022.902155

Novel PET Imaging of Inflammatory Targets and Cells for the Diagnosis and Monitoring of Giant Cell Arteritis and Polymyalgia Rheumatica

*Kornelis S. M. van der Geest[1], Maria Sandovici[1], Pieter H. Nienhuis[2], Riemer H. J. A. Slart[2,3], Peter Heeringa[4], Elisabeth Brouwer[1] and William F. Jiemy[1]**

[1] Department of Rheumatology and Clinical Immunology, University of Groningen, University Medical Center Groningen, Groningen, Netherlands, [2] Department of Nuclear Medicine and Molecular Imaging, Medical Imaging Center, University Medical Center Groningen, University of Groningen, Groningen, Netherlands, [3] Department of Biomedical Photonic Imaging Group, University of Twente, Enschede, Netherlands, [4] Department of Pathology and Medical Biology, University of Groningen, University Medical Center Groningen, Groningen, Netherlands

OPEN ACCESS

Edited by:
Giorgio Treglia,
Ente Ospedaliero Cantonale (EOC), Switzerland

Reviewed by:
Gaurav Malviya,
University of Glasgow, United Kingdom
Lucia Leccisotti,
Agostino Gemelli University Polyclinic (IRCCS), Italy

***Correspondence:**
William F. Jiemy
w.f.jiemy@umcg.nl

Specialty section:
This article was submitted to Nuclear Medicine, a section of the journal Frontiers in Medicine

Received: 22 March 2022
Accepted: 13 May 2022
Published: 06 June 2022

Citation:
van der Geest KSM, Sandovici M, Nienhuis PH, Slart RHJA, Heeringa P, Brouwer E and Jiemy WF (2022) Novel PET Imaging of Inflammatory Targets and Cells for the Diagnosis and Monitoring of Giant Cell Arteritis and Polymyalgia Rheumatica. Front. Med. 9:902155. doi: 10.3389/fmed.2022.902155

Giant cell arteritis (GCA) and polymyalgia rheumatica (PMR) are two interrelated inflammatory diseases affecting patients above 50 years of age. Patients with GCA suffer from granulomatous inflammation of medium- to large-sized arteries. This inflammation can lead to severe ischemic complications (e.g., irreversible vision loss and stroke) and aneurysm-related complications (such as aortic dissection). On the other hand, patients suffering from PMR present with proximal stiffness and pain due to inflammation of the shoulder and pelvic girdles. PMR is observed in 40–60% of patients with GCA, while up to 21% of patients suffering from PMR are also affected by GCA. Due to the risk of ischemic complications, GCA has to be promptly treated upon clinical suspicion. The treatment of both GCA and PMR still heavily relies on glucocorticoids (GCs), although novel targeted therapies are emerging. Imaging has a central position in the diagnosis of GCA and PMR. While [^{18}F]fluorodeoxyglucose (FDG)-positron emission tomography (PET) has proven to be a valuable tool for diagnosis of GCA and PMR, it possesses major drawbacks such as unspecific uptake in cells with high glucose metabolism, high background activity in several non-target organs and a decrease of diagnostic accuracy already after a short course of GC treatment. In recent years, our understanding of the immunopathogenesis of GCA and, to some extent, PMR has advanced. In this review, we summarize the current knowledge on the cellular heterogeneity in the immunopathology of GCA/PMR and discuss how recent advances in specific tissue infiltrating leukocyte and stromal cell profiles may be exploited as a source of novel targets for imaging. Finally, we discuss prospective novel PET radiotracers that may be useful for the diagnosis and treatment monitoring in GCA and PMR.

Keywords: PET/CT, giant cell arteritis (GCA), polymyalgia rheumatica (PMR), radiotracer, imaging, large-vessel vasculitis (LVV)

INTRODUCTION

Giant cell arteritis (GCA) and polymyalgia rheumatica (PMR) are two related inflammatory diseases exclusively affecting adults above the age of 50, with a peak incidence between 75 and 79 years of age (1). GCA is a vasculitis affecting medium- to large-sized arteries which can be subclassified into a spectrum that includes cranial GCA (C-GCA) and large-vessel GCA (LV-GCA) (2). C-GCA mainly affects the cranial arteries and leads to ischemic symptoms such as jaw claudication, vision loss, and stroke (3, 4). LV-GCA mainly affects the aorta and its main branches and may lead to aneurysm formation and aortic dissection. Up to 83% of GCA patients present with overlapping C-GCA and LV-GCA (5). PMR is a rheumatic inflammatory disorder characterized by inflammation of bursae, tendon sheaths, and joints primarily affecting the shoulder and pelvic girdles (6). GCA and PMR commonly coexist; up to 60% of GCA patients are diagnosed with PMR while up to 21% of PMR patients present with overlapping GCA (7). To date, glucocorticoid (GC) therapy remains the mainstream treatment for the management of GCA and PMR (8). Although GC treatment is effective in inducing and maintaining remission, it can cause substantial toxicity in patients (9). Recently, IL-6 receptor blocking therapy has shown positive results as GC sparing therapy in GCA (10). Promising results with this therapy have also been reported in PMR (11, 12). However, tocilizumab monotherapy is not recommended for these diseases and combination treatment with GC is still imperative, especially in GCA.

Historically, the diagnosis of GCA solely relied on the assessment of clinical signs and symptoms, laboratory assessment of inflammatory markers such as elevated C-reactive protein (CRP) and erythrocyte sedimentation rate (ESR), and positive histological evidence of giant cell arteritis in the temporal artery biopsy (TAB) (13). Similarly, diagnosis of PMR also relies heavily on the assessment of clinical signs and symptoms, and laboratory assessment of inflammatory markers (14). More recently, imaging techniques such as ultrasonography and [^{18}F]fluorodeoxyglucose (FDG)-positron emission tomography (PET) have gained importance as diagnostic tools for GCA and PMR, whereas these imaging techniques are also increasingly used for treatment monitoring (11, 15–18). Previously, [^{18}F]FDG-PET/CT was only utilized for the detection of LV-GCA due to its limitation in resolution. However, [^{18}F]FDG-PET/CT employing new generation scanners with improved resolution has been shown to be able to detect C-GCA. Recent reports have shown that C-GCA can be effectively detected by PET/CT (up to 83% sensitivity and 100% specificity) (19, 20). However, despite its utility, there are several important clinical drawbacks posed by [^{18}F]FDG-PET as a diagnostic tool in the diagnosis of GCA and PMR. Firstly, [^{18}F]FDG uptake is non-specific and only indicates increased glucose metabolism. Therefore, it may be present in the context of neoplasia, inflammation, degenerative disease, and increased muscle use (21). In the context of vascular inflammation, [^{18}F]FDG may also be taken up due to atherosclerotic activity (21). In addition, [^{18}F]FDG shows intense uptake in several organs that may hamper its diagnostic accuracy. One example is the high brain uptake of [^{18}F]FDG that may result in a low target-to-background ratio (TBR) in cranial vessels and limit the diagnostic accuracy of C-GCA. Furthermore, the diagnostic accuracy of [^{18}F]FDG-PET in patients undergoing GC treatment is significantly reduced as exemplified by one study reporting that only 36% of LV-GCA patients showed a positive [^{18}F]FDG-PET scan after 10 days of GC treatment (22). A reduction in diagnostic accuracy has also been shown in PMR patients undergoing GC treatment albeit to a lesser extent as compared to GCA (17). GC rapidly blocks glycolysis pathways important for FDG uptake in inflammatory cells (23, 24). It is imperative to start GC treatment upon suspicion of GCA while postponing the GC treatment can be difficult in patients with suspected PMR. Unfortunately, diagnostic imaging of these patients is often not feasible within a narrow timeframe due to limited hospital capacities. Therefore, there is a strong clinical need to identify novel radiotracers that (1) have low background radioactivity in non-target organs and blood pool, and (2) can still accurately detect ongoing inflammation for a prolonged period (e.g., up to weeks) after initiation of GC treatment. Such radiotracers could potentially help to firmly rule in or rule out GCA/PMR and would provide an important benefit to patients in which the diagnosis remains uncertain despite routine clinical evaluation. With the expanding knowledge regarding the cellular heterogeneity at the site of inflammation in GCA and PMR, novel radiotracers targeting these specific cell subsets may prove to be useful for the diagnosis and eventually treatment monitoring in GCA and PMR patients.

IMMUNOPATHOLOGY OF GCA AND PMR

C-GCA

The immunopathology of GCA is characterized by leukocyte infiltration at the site of inflammation. Although not yet fully understood, decades of efforts in characterizing and understanding the cellular heterogeneity in the inflamed GCA vessels have led us to better understand the pathogenesis of this disease. Based on these data, a pathogenic model has been established in which the initiation of GCA is believed to start with the activation of vascular dendritic cells (vasDCs) through toll-like receptors (TLRs) stimulation by still unknown triggers. Upon activation, these vasDCs adopt a phenotype characterized by the expression of the activation marker CD83 and elevated expression of the costimulatory molecule CD86 (25). These activated vasDCs express the chemokines CCL19 and CCL21 while simultaneously expressing the receptor CCR7, causing these activated vasDCs to be trapped in the vessel wall. Moreover, these activated vasDCs produce CCL20 and a range of proinflammatory cytokines (IL-1β, IL-6, IL-18, IL-23, and IL-33) leading to the recruitment of CD4+ T cells into the vessel-wall, their subsequent co-stimulation and activation, and their polarization into Th1 and Th17 cells (26–29). Although infiltrating T cells in the vessel wall show expression of the inhibitory checkpoint molecule PD-1, vasDCs exhibit low expression of the coinhibitory ligand PD-L1 resulting in dampened negative regulation of T cell activation (30,

31). Activated Th1 and Th17 cells produce high amounts of IFNγ and IL-17, respectively, which in turn activate the resident vascular smooth muscle cells (VSMCs) and endothelial cells (ECs). Activated ECs express high levels of adhesion molecules (VCAM-1, ICAM-1 and E-selectin) enabling leukocyte adhesion and transmigration to the vessel wall (32). Activated VSMCs produce several crucial chemokines such as CXCL9, CXCL10, CXCL11, CXCL13, CCL2, and CX3CL1 augmenting the infiltration of CXCR3+ CD8+ T cells, CXCR3+/CXCR5+ B cells, and CCR2+/CX3CR1+ monocytes to the vessel wall (33–37). Infiltrating CD20+ B cells organize themselves into tertiary lymphoid organs (TLOs) where they produce proinflammatory cytokines which perpetuate the inflammatory processes (38, 39). Infiltrating CD8+ T cells start to produce cytokines such as IFN-γ and IL-17 which triggers a positive feedback loop recruiting more CD4+ and CD8+ T cells as well as monocytes to the vessel wall (36). Notably, activated VSMCs, ECs, CD4+ and CD8+ T cells also produce GM-CSF, a potent hematopoietic growth factor that induces the differentiation and maturation of infiltrating monocytes into proinflammatory CD206+ macrophages (40, 41). These CD206+ macrophages express the collagenase matrix metalloproteinase (MMP)-9 and proangiogenic factor YKL-40 (42). These CD206+/YKL-40+/MMP-9+ macrophages are mainly located in the media and media borders promoting collagen degradation and neovessel formation, enabling more invasion of T cells and monocytes into the vessel wall (42–45). In addition, these CD206+ macrophages express high levels of the growth factor M-CSF, priming adjacent macrophages to become FRβ+ macrophages (41). These M-CSF primed FRβ+ macrophages produce high levels of platelet-derived growth factor (PDGF)-AA which promotes fibroblast migration and proliferation. Furthermore, macrophages are incredibly plastic cells that may change their phenotype in response to cues from the microenvironment. Proinflammatory cytokines such as IFNγ, IL-17, and IL-6 that are abundantly present in the inflamed vessel wall may trigger the expression of a multitude of macrophage markers (5). Notably, abundant numbers of CD64+, CD86+, iNOS+ and CD163+ macrophages have been reported in GCA-affected vessels (41, 46–48). Moreover, these activated macrophages themselves produce a wide range of proinflammatory cytokines (including IL-6, TNF-α, IL-1β, GM-CSF) and growth factors (TGF-β, VEGF, PDGFs) (5). Macrophage secreted proinflammatory cytokines contribute to a positive feedback loop amplifying the inflammatory process. Macrophage secreted growth factors promote fibroblasts and VSMCs activation and differentiation into α-smooth muscle actin (SMA)+ myofibroblasts and subsequently their migration and proliferation in the intima layer which results in intimal hyperplasia and ultimately vessel-wall occlusion (49, 50). Of note, this pathogenic model has largely been constructed from studies on TAB obtained from C-GCA patients.

LV-GCA

Our understanding of the pathogenesis of LV-GCA is derived from studies with aortic specimens obtained during aortic aneurysm surgery. Aortitis in GCA is characterized by granulomatous inflammation largely occurring in the medial layer of the aorta. This granulomatous inflammation leads to medial necrosis which is responsible for aortic aneurysm and may ultimately lead to aortic dissection. Although the final consequences of LV-GCA may differ from C-GCA, the cellular infiltrates are largely similar. Infiltrating leukocytes in the inflamed aorta largely dominate the adventitia and the media layer of the aorta. Infiltration of both activated CD4+ and CD8+ T cells has been reported in GCA affected aorta (51). While the infiltration of T cells in adventitia and media of the aorta has been described, infiltration of CD20+ B cells mainly localizes in the adventitia where these cells are organized into TLOs (38). Macrophages expressing CD64, CD86, CD206, and FRβ are abundant in the adventitia and the media of GCA-affected aortas (41). CD206+/MMP-9+/YKL-40+ macrophages surround the necrotic areas in the media indicating a role in medial destruction (41). Notably, a reduction of α-SMA+ cells has been reported in the media of GCA-affected aortas due to medial necrosis which differs from the increase of adventitial and intimal α-SMA+ myofibroblasts in temporal arteries (52).

PMR

In contrast to GCA, not much is currently known regarding the immunopathology of PMR. One of the first reports studying synovial tissue biopsies of PMR patients was published in 1964 in which hyperplasia of synovial lining cells, increased vascularity, and leukocyte infiltration mainly consisting of lymphocytes and macrophages were described (53). In the 1990s, immunohistological investigation on glenohumeral synovial tissue of patients with PMR revealed that CD68+ macrophages comprise the majority of the infiltrating cells followed by T cells and a small percentage of neutrophils (54). The T cell infiltrates were mainly comprised of CD45RO+ memory CD4+ T cells although small numbers of CD8+ T cells were also detected. B cells were not detected in the synovial tissue. In another report, the same group showed elevated VEGF expression by both CD3+ T cells and CD68+ macrophages in synovial biopsy tissues which correlated with vessel density indicating that these cells are involved in vasa vasorum formation and subsequently enhanced leukocyte infiltration in the synovium of PMR patients (55). More recently, enrichment of both CD4+ and CD8+ T cells in the synovial fluid of PMR patients have been reported (56). These T cells show a high IFNγ producing capacity pointing toward Th1 and Tc1 subsets. To date, no further cellular profiling has been done in the synovial tissues of PMR patients. Taking clues from other inflammatory diseases of the joint such as rheumatoid arthritis (RA) and osteoarthritis (OA), infiltration of CD206+, FRβ+, CD163+, MMP-9+ and iNOS+ macrophages has been reported (57, 58). Whether or not these cells are also involved in the immunopathology of PMR remains to be elucidated. Therefore, it is warranted for future studies to focus on deeper phenotyping of the cellular infiltrates in PMR synovial biopsies to better understand their roles in the immunopathology of PMR and subsequently target these cells for imaging and therapeutic purposes.

POTENTIAL NOVEL PET TRACERS FOR DIAGNOSIS AND MONITORING OF GCA AND PMR

The knowledge regarding the cellular heterogeneity in the pathogenesis of GCA and PMR may allow us to target these specific cells for imaging purposes. For a long time, [^{18}F]FDG-PET has dominated the imaging landscape in oncology and inflammatory diseases alike. However, more recent efforts have shifted the trend toward targeting a specific cellular population. Targeting specific cell populations may provide the following advantages compared to [^{18}F]FDG-PET:

(1) Lower background activity, thereby increasing target-to-background ratio and the imaging accuracy.

(2) Ability to evaluate specific cell populations as prognostic markers for disease progression and treatment response, thereby aiding the design of personalized treatment regimens, especially with emerging novel immunotherapies.

(3) Better insight into treatment effects. Novel immunotherapies often specifically target cellular pathways which may alter specific cell populations at the site of inflammation.

(4) Cellular infiltrates are unlikely to disappear immediately upon initiation of treatments in patients with immune-mediated inflammatory diseases including GCA and PMR (54, 59, 60), whereas especially glucocorticoid treatment may promptly impact the glucose metabolism by infiltrating immune cells and liver. Thus, the time interval of diagnostic scanning for cell-specific PET tracers might potentially be longer.

As the efforts in developing PET radiotracers targeting specific cell populations are increasing, these radiotracers may also prove to be useful for the imaging of GCA and PMR which is summarized below (**Figure 1**).

T Cell-Targeted Radiotracers

T cells are one of the most abundant infiltrating cell types in the inflamed GCA vessels (61). In the synovium of PMR patients, although not the most abundant cells, infiltration of T cells has been documented as well (54). Several radiotracers targeting T cells have been developed and are currently undergoing clinical trials for imaging other diseases, primarily oncology (**Table 1**). These radiotracers may also prove to be useful for the imaging of GCA and PMR patients.

IL-2 is a pleiotropic cytokine highly secreted by activated T cells which promotes T cell survival, expansion and differentiation into effector cells (72). The IL-2 receptor consists of three subunits including IL-2Rα (CD25), IL-2Rβ (CD122), and IL-2Rγ (CD132). IL-2 signals through the intermediary IL-2 receptor comprising the IL-2Rβ and IL-2Rγ chain. Upon activation, T cells gain elevated expression of CD25, completing the high-affinity receptor with the three subunits (72, 73). As a crucial cytokine in T cell functions, IL-2 is rapidly consumed by activated T cells making it an attractive cytokine for targeted imaging of activated T cells. The IL-2 targeted SPECT radiotracers, [^{99m}Tc]IL-2 and [^{99m}Tc]HYNIC-IL-2, have already been applied successfully for the visualization of vulnerable atherosclerotic plaques, transplant rejection and autoimmune thyroid disease (74–76). Furthermore, visualization of Takayasu arteritis has been reported in a case study utilizing [^{99m}Tc]IL-2 scintigraphy (77), pointing toward the possible utility of IL-2 based lymphocyte targeted imaging in the detection of GCA.More recently, several PET radiotracers based on radionuclide tagged IL-2 have been reported. The first-generation IL-2 tracer, [^{18}F]FB-IL-2, was reported to show high-affinity binding to activated human peripheral blood mononuclear cells (hPBMCs). The reports showed a high correlation of [^{18}F]FB-IL-2 uptake with the number of CD25+ cells *in vitro* and in matrigel implants with activated hPBMCs (62–64). In a recent study, [^{18}F]FB-IL-2 imaging successfully detected tumor lesions in metastatic melanoma patients (63). Biodistribution data showed high uptake in secretion organs (liver and kidneys), lymphoid organs (spleen and bone marrow) and the blood pool (myocardial and aortic) but low uptake in other non-target organs including the brain. The high blood pool radioactivity, however, may mask the detection of arterial inflammation in GCA. Recently, second-generation IL-2 based tracers, [^{18}F]AIF-RESCA-IL2 and [^{68}Ga]Ga-NODAGA-IL2 have been developed (65). Although yet to be tested in humans, both radiotracers showed high specific uptake in lymphoid tissue and hPBMC xenografts in a mouse model. In addition, both second-generation radiotracers showed no brain uptake and lower blood pool radioactivity compared to [^{18}F]FB-IL-2 which may be advantageous for the detection of aortic and arterial inflammation in GCA. Furthermore, as T cell infiltration in the synovium of PMR patients has been documented, these radiotracers may also prove to be useful for PMR imaging.

Dominant CD4+ T cell infiltration over CD8+ T cells at the site of inflammation has been reported for both GCA and PMR (51, 54), making CD4+ T cells an attractive target for imaging of these diseases. Two ImmunoPET tracers targeting human CD4 T cells have been recently reported. Nanobody-based [^{64}Cu]CD4-Nb1 showed specific uptake in organs with high numbers of CD4+ T cells including lymph nodes, thymus, spleen, and liver with rapid blood and lung clearance *via* renal elimination in a human CD4 knock-in mouse model (66). Similarly, minibody based [^{64}Cu]NOTA-IAB41 showed specific uptake in CD4+ T cells infiltrated lungs, spleen, liver and kidney in hPBMC injected humanized mice (67). Interestingly, the report also showed successful visualization of CD4+ T cell infiltration in a humanized brain tumor mouse model compared to no brain uptake in the non-disease control group. Both radiotracers may potentially be useful in imaging GCA and PMR patients.

Lower numbers of infiltrating CD8+ T cells compared to CD4+ T cells have been reported in the inflamed vessels of GCA patients. However, CD8 targeted imaging may still be valuable for this disease since the presence of large arterial CD8 T cell infiltrates is associated with disease severity (51). A minibody based CD8+ T cell-targeted radiotracer, [^{89}Zr]Df-IAB22M2C, has been developed and is currently actively investigated in several clinical trials. Reports of CD8+ T cells imaging in patients with solid tumors have shown successful visualization of tumor-infiltrating CD8+ T cells and specific uptake in CD8+ rich lymphoid organs (70, 71). Moreover, low blood pool radioactivity

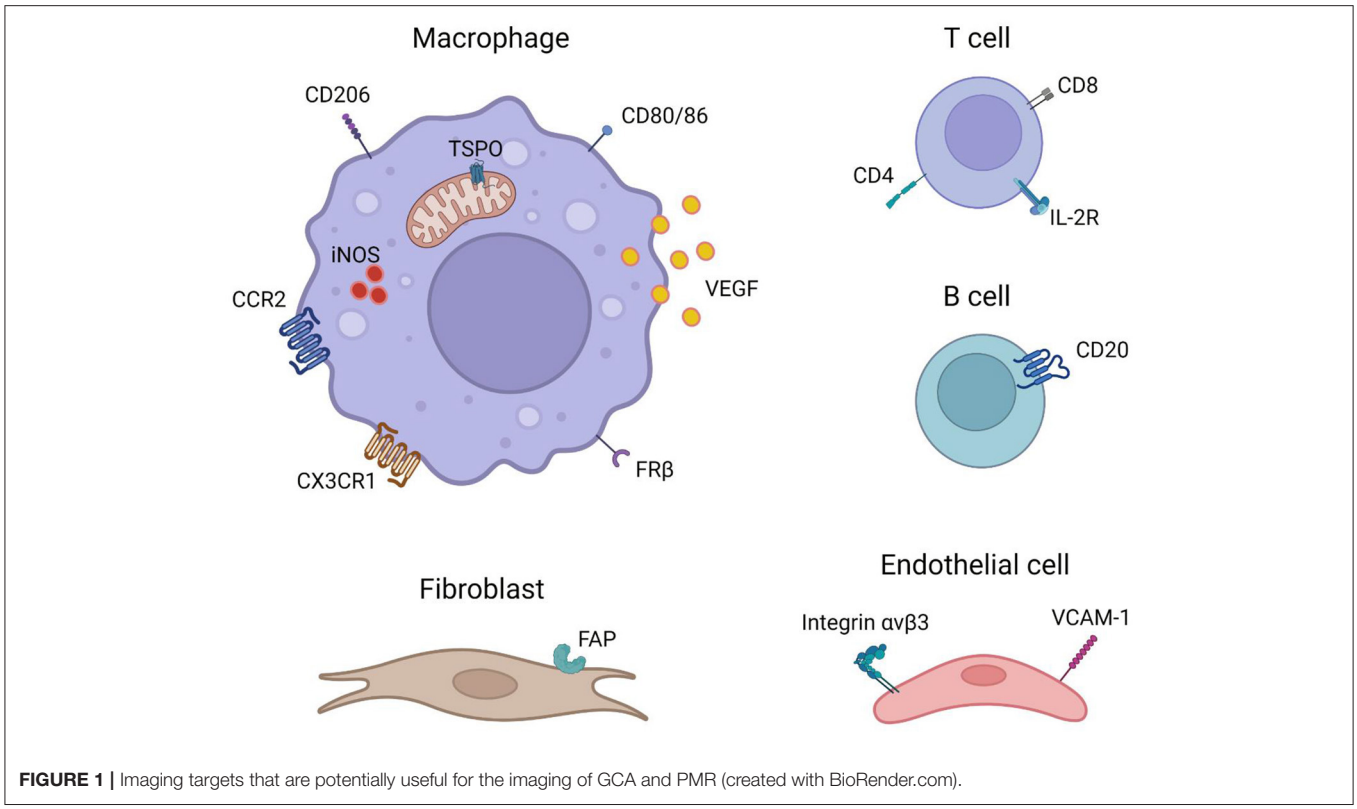

FIGURE 1 | Imaging targets that are potentially useful for the imaging of GCA and PMR (created with BioRender.com).

TABLE 1 | T cell targeted PET radiotracers.

Target cell	Target marker/ pathway	Radiotracer	Class	Clinical/ preclinical	Active clinical trials	References
Activated T cells	IL-2R	[^{18}F]FB-IL-2	Cytokine	Clinical	NCT04163094 NCT02478099	(62–64)
	IL-2R	[^{18}F]AlF-RESCA-IL2	Cytokine	Preclinical	–	(65)
	IL-2R	[^{68}Ga]Ga-NODAGA-IL2	Cytokine	Preclinical	–	(65)
CD4+ T cells	CD4 molecule	[^{64}Cu]CD4-Nb1	Nanobody	Preclinical	–	(66)
		[^{64}Cu]NOTA-IAB41	Minibody	Preclinical	–	(67)
CD8+ T cells	CD8 molecule	[^{89}Zr]-Df-IAB22M2C	Minibody	Clinical	NCT03802123 NCT04874818 NCT04826393 NCT05013099 NCT04606316 NCT04180215 NCT03533283	(68–71)

and no brain uptake were detected in these patients making it suitable for imaging C-GCA and LV-GCA. The infiltration of CD8+ T cells in the synovium of PMR patients is scarce and therefore CD8+ T cell-targeted imaging may be less suitable for PMR.

Although PD-1 expressing T cell infiltration has been reported in GCA (30, 31), only two radiotracers targeting PD-1 based on PD-1 antagonist nivolumab and pembrolizumab are currently available (78). Since the development of both GCA and PMR as consequences of PD-1/PD-L1 inhibition therapy of cancer patients has been reported (79, 80), the use of these radiotracers for the imaging of GCA and PMR may potentially worsen the disease and is therefore not feasible. However, with the rise of PD-1 agonists (81–84), future applications of these PD-1 agonist-based radiotracers may prove to be useful as a theranostic approach in these diseases.

Macrophage Targeted Radiotracers

Macrophages play vital roles and are one of the most abundant cell types infiltrating the inflamed vessels and synovial tissue of GCA and PMR patients making them attractive targets for cell-specific imaging (5, 54). As macrophages are incredibly

plastic cells, not all tracers are suitable for the imaging of macrophages in GCA and PMR patients. As our knowledge regarding macrophage heterogeneity in the pathogenesis of GCA has improved considerably, we will focus on a selected number of radiotracers targeting macrophage phenotypes that have been proven to be involved in the vasculopathy of GCA (**Table 2**).

Macrophage-targeted imaging of translocator protein (TSPO; also known as PBR or peripheral benzodiazepine receptor) was first developed for the targeted imaging of microglia in neuroinflammation. It was later found that TSPO targeted imaging could be utilized for the imaging of non-neuronal inflammatory diseases such as rheumatoid arthritis (RA), atherosclerosis, Takayasu arteritis (TAK), systemic lupus erythematosus (SLE), and GCA (88, 94, 98–100, 103, 106, 185, 190, 193). In 2010, Pugliese et al. successfully showed the utility of [^{11}C]PK11195, a first-generation TSPO targeted radiotracer, in the detection of large-vessel vasculitis including GCA (94). Shortly after, another study led by Lamare et al. utilizing the radiotracer [^{11}C]-(R)-PK11195 showed a similar result in detecting vascular inflammation in patients suffering from large-vessel vasculitis (106). Additionally, studies have shown high uptake of a second-generation TSPO tracer, [^{11}C]DPA-713, in inflamed joints of RA patients pointing to the potential in imaging PMR (185, 193). Although the utility has been shown in imaging GCA, older generation TSPO targeted radiotracers possess several disadvantages. The major drawback of these radiotracers is the significantly lower binding capability to TSPO in patients with a common TSPO gene polymorphism (*rs6971*), which resulted in variability in the imaging signal (324, 325). Furthermore, these older generation TSPO targeted tracers are not very specific and show high background radioactivity, which may hamper the imaging capability (326). The third generation of TSPO targeted radiotracers, such as [^{18}F]FEBMP, [^{18}F]ER176 and [^{18}F]-(S)-GE387, are designed to overcome these drawbacks. Notably, a recent study using another second-generation tracer, [^{11}C]PBR28, documented no vascular uptake in patients suffering from large-vessel vasculitis (Takayasu arteritis and GCA) (327). It is unclear whether this discrepancy was caused by the unspecific binding of the first-generation TSPO tracers in the inflamed tissues. This discrepancy warrants a more detailed investigation into the feasibility of new generation TSPO targeted tracers in imaging GCA.

The mannose receptor (CD206) is a C-type lectin receptor highly expressed by certain populations of macrophages. Several CD206 targeted radiotracers have been developed and some have been used in clinical applications (**Table 2**). Employing the receptor-ligand binding approach, tracers based on mannose derivatives, mannose coated liposome, and mannosylated protein have shown reliable CD206 targeting. [^{18}F]FDM based on fluorodeoxy-mannose have been shown to have lower non-specific brain uptake compared to [^{18}F]FDG in patients with brain infarction (241). Furthermore, this radiotracer has been successfully used in preclinical imaging of atherosclerotic lesions in a rabbit model supporting its potential in vascular imaging (328). More recently, anti-CD206 nanobody-based radiotracers have been developed which are more specific compared to the mannose derivatives-based tracers. In animal models of atherosclerosis and cancer, these radiotracers have shown rapid blood clearance and low radioactivity in non-target organs including the brain (243, 245, 246). The abundance of CD206+ macrophages responsible for expressing high levels of YKL-40 and MMP-9, a proangiogenic and tissue destructive collagenase, respectively, has been documented in affected vessels of GCA patients (41, 42). These macrophages are likely skewed by GM-CSF in the microenvironment and are considered to be responsible for media destruction in GCA. Given their prominent roles, targeted imaging of CD206+ macrophages may be beneficial for the diagnosis and prognosis of GCA.

The interest in folate-based imaging started over two decades ago when folate receptor-expressing tumors were discovered (329). This led to the rapid development of numerous folate receptor-targeted radiopharmaceuticals. Of note, some of these radiotracers are tagged with highly radioactive nuclides or toxic particles intended as radiotherapeutics for cancers (330–333). More recently, it has been demonstrated that some macrophages involved in autoimmune and inflammatory diseases, including GCA, express high levels of folate receptor beta (FRβ) as well. Interestingly, the degree of FRβ+ macrophage infiltration in the intima of the GCA affected vessels has been linked to intimal hyperplasia (41). Patients with intimal hyperplasia in their biopsy may be more likely to develop ischemic complications than those without (334). Imaging FRβ may potentially reveal the degree of vessel wall occlusion in C-GCA and may signal the need for the rapid induction of high-dose GC therapy to lower the risk of vision loss in these patients. Among the plethora of FR-targeted radiotracers, [^{18}F]fluoro-PEG-folate and [^{18}F]AzaFol have been used in clinical applications (259, 263). [^{18}F]fluoro-PEG-folate was assessed in patients with RA and showed specific uptake in inflamed joints with low brain uptake. The infiltration of FRβ+ macrophages in the synovial tissue of RA patients has been well-documented. On the other hand, the utility of [^{18}F]AzaFol was assessed in patients with FRα+ adenocarcinoma of the lungs. These studies demonstrate the utility of these novel folate receptor-targeted radiotracers in human subjects, but at the same time revealed that folate receptor imaging may not be very specific due to uptake by both FRα+ and FRβ+ cells. Nevertheless, folate receptor imaging may still prove to be useful in patients suffering from GCA especially in the detection of patients at risk of developing ischemic events due to severe intimal hyperplasia.

Immunotherapy targeting T cell activation by blocking CD80/86 on antigen-presenting cells (APCs) with a CTLA-4Ig fusion protein (abatacept) is currently evaluated in GCA (NCT04474847). An earlier phase II randomized control trial of abatacept for the treatment of GCA showed promising results with significant proportions of patients achieving relapse-free survival rate at 12 months compared to placebo (48% abatacept vs. 31% placebo; $p = 0.049$) (335). Separately, a case report has shown the potential application of abatacept for the treatment of PMR (336). Together, these encouraging results may point toward the potential application of radionuclide tagged [^{64}Cu]NODAGA-abatacept in GCA and PMR.

TABLE 2 | Macrophage targeted PET radiotracer.

Target marker/ pathway	Radiotracer	Class	Clinical/ preclinical	Active clinical trials	References
TSPO	[^{11}C]PK11195	TSPO antagonist	Clinical	NCT03368677 NCT04239820 NCT05111678	(85–94)
	[^{11}C]-(R)-PK11195	TSPO antagonist	Clinical	–	(95–114)
	[^{11}C]DAA1106	TSPO agonist	Clinical	–	(115–121)
	[^{18}F]DAA1106	TSPO agonist	Preclinical	–	(122–124)
	[^{18}F]FEDAA1106	TSPO agonist	Clinical	–	(125–130)
	[^{18}F]FMDAA1106	TSPO agonist	Preclinical	–	(125)
	[^{11}C]PBR28	TSPO agonist	Clinical	NCT04274998 NCT05205291 NCT04230174 NCT03705715 NCT04490096 NCT02649985 NCT04236986 NCT04398719 NCT04811404 NCT04066244 NCT04233593 NCT03106740 NCT05066308 NCT04486118 NCT05183087	(131–145)
	[^{18}F]PBR06	TSPO agonist	Clinical	NCT04510220 NCT03983252 NCT04144257 NCT02649985	(146–150)
	[^{11}C]PBR06	TSPO agonist	Preclinical	–	(147)
	[^{11}C]PBR01	TSPO agonist	Preclinical	–	(151, 152)
	[^{18}F]FEPPA	TSPO agonist	Clinical	NCT02945774 NCT04814355 NCT04307667 NCT04854785	(153–163)
	[^{18}F]PBR111	TSPO antagonist	Clinical	–	(164–169)
	[^{18}F]PBR102	TSPO antagonist	Preclinical	–	(166, 169, 170)
	[^{11}C]CB184	TSPO antagonist	Clinical	–	(171–174)
	[^{11}C]CLINME	TSPO ligand	Preclinical	–	(167, 175, 176)
	[^{18}F]CB251	TSPO ligand	Preclinical	–	(177–179)
	[^{11}C]AC-5216	TSPO agonist	Preclinical	–	(180)
	[^{11}C]DAC	TSPO agonist	Preclinical	–	(181, 182)
	[^{11}C]DPA-713	TSPO agonist	Clinical	–	(183–193)
	[^{18}F]DPA-714	TSPO agonist	Clinical	NCT03759522 NCT03754348 NCT03457493 NCT04362644 NCT03999164 NCT04364672 NCT04542603 NCT03230526 NCT03968445 NCT05238961 NCT04520802 NCT05147532 NCT03691077 NCT04171882 NCT03482115 NCT03314155	(193–195)

(Continued)

TABLE 2 | Continued

Target marker/ pathway	Radiotracer	Class	Clinical/ preclinical	Active clinical trials	References
				NCT05128903 NCT03435861 NCT05233605 NCT04785157	
	[^{18}F]DPA-C5yne	TSPO agonist	Preclinical	–	(196)
	[^{18}F]FDPA	TSPO agonist	Preclinical	–	(197–200)
	[^{18}F]VUIIS1018A	TSPO agonist	Preclinical	–	(201, 202)
	[^{18}F]FEDAC	TSPO ligand	Preclinical	–	(203–205)
	[^{11}C]SSR180575	TSPO agonist	Preclinical	–	(206)
	[^{18}F]SSR180575	TSPO agonist	Preclinical	–	(207)
	[^{18}F]FEMPA	TSPO ligand	Clinical	NCT05039268	(208–210)
	[^{18}F]FETEM	TSPO ligand	Preclinical	–	(211)
	[^{18}F]FEBMP	TSPO ligand	Preclinical	–	(212, 213)
	[^{18}F]GE180	TSPO ligand	Clinical	NCT04412187 NCT03702816	(214–223)
	(R)-[^{18}F]NEBIFQUINIDE	TSPO ligand	Preclinical	-	(224)
	[^{11}C]ER176	TSPO ligand	Clinical	NCT04762719 NCT04840979 NCT03705715 NCT04576793 NCT03958630 NCT03912428 NCT04510168 NCT04786548	(225–228)
	[^{18}F]ER176 analogs	TSPO ligand	Preclinical	–	(229, 230)
	[^{18}F]-(S)-GE387	TSPO ligand	Preclinical	–	(223, 231)
	[^{18}F]LW223	TSPO ligand	Preclinical	–	(232, 233)
	[^{18}F]BS224	TSPO ligand	Preclinical	–	(234)
CD206	[^{64}Cu]MAN-LIPs	Mannose coated liposome	Preclinical	–	(235)
	[^{68}Ga]NOTA-MSA	Mannosylated protein	Clinical	–	(236–239)
	[^{18}F]FDM	Mannose derivative	Clinical	–	(240, 241)
	[^{68}Ga]IRDye800-tilmanocept	Mannose derivative	Preclinical	–	(242)
	[^{18}F]FB-anti-MMR 3.49 sdAb	Nanobody	Preclinical	–	(243)
	[^{68}Ga]MMR	Nanobody	Preclinical	–	(244)
	[^{68}Ga]Ga-NOTA-anti-MMR-sdAb	Nanobody	Preclinical	–	(245)
	[^{68}Ga]Ga-NOTA-MMR Nb	Nanobody	Preclinical	–	(246)
	[^{68}Ga]Ga-NOTA-anti-MMR-VHH2	Nanobody	Clinical	NCT04168528 NCT04758650	–
FRβ	[^{18}F]α/γ-FBA-Folate	Folate derivative	Preclinical	–	(247)
	[^{18}F]click-folate	Folate derivative	Preclinical	–	(248)
	[^{68}Ga]DOTA-folate	Folate derivative	Preclinical	–	(249)
	2'-[^{18}F]fluorofolic acid	Folate derivative	Preclinical	–	(250)
	[^{18}F]fluorobenzene-folate	Folate derivative	Preclinical	–	(251)
	[^{18}F]pyridinecarbohydrazide-folate	Folate derivative	Preclinical	–	(251)
	[^{18}F]fluorodeoxy-glucose-folate	Folate derivative	Preclinical	–	(252–254)
	[^{68}Ga]NODAGA-folate	Folate derivative	Preclinical	–	(255)
	[^{68}Ga]DO3A-EA-Pte	Pteroic acid derivative	Preclinical	–	(256)
	3′-aza-2′[^{18}F]fluorofolicacid/[^{18}F]AzaFol	Folate derivative	Clinical	–	(257–259)
	[^{18}F]fluoro-PEG-folate	Folate derivative	Clinical	NCT05215496	(260–263)
	4-[^{18}F]-fluorophenylfolate	Folate derivative	Preclinical	–	(264)
	[^{68}Ga]NOTA-folate	Folate derivative	Preclinical	–	(265, 266)
	α/β-click[^{18}F]FDG-folate	Folate derivative	Preclinical	–	(267)
	α/β-click[^{18}F]FE-folate	Folate derivative	Preclinical	–	(267)

(Continued)

TABLE 2 | Continued

Target marker/ pathway	Radiotracer	Class	Clinical/ preclinical	Active clinical trials	References
	α/β-click[^{18}F]FB-folate	Folate derivative	Preclinical	–	(267)
	Folate-NOTA-Al[^{18}F]	Folate derivative	Preclinical	–	(268)
	[^{64}Cu]rf42	Folate derivative	Preclinical	–	(269)
	[^{68}Ga]rf42	Folate derivative	Preclinical	–	(269)
	[^{68}Ga]DOTA-Lys-Pteroyl	Pteroyl-Lys derivatives	Preclinical	–	(270)
	[^{68}Ga]DOTA-DAV-Lys-Pteroyl	Pteroyl-Lys derivatives	Preclinical	–	(270)
	[^{68}Ga]NOTA-folic acid	Folate derivative	Preclinical	–	(271)
	[^{89}Zr]FA-DFO-liposome	Folate coated liposome	Preclinical	–	(272)
	[^{68}Ga]HCEF	Folate derivative	Preclinical	–	(273)
	Folate-PEG12-NOTA-Al[^{18}F]	Folate derivative	Preclinical	–	(274)
	[^{64}Cu]DOTA-FA-FI-G5·NHAc dendrimers	Folate tagged dendrimers	Preclinical	–	(275)
	[^{18}F]Ala-folate	Folate derivative	Preclinical	–	(276)
	[^{18}F]DBCO-folate	Folate derivative	Preclinical	–	(276)
	[^{18}F]FOL	Folate derivative	Preclinical	–	(277, 278)
	[^{68}Ga]NODAGA-FA	Folate modified polymer	Preclinical	–	(279)
	[^{55}Co]Co-cm10	Folate derivative	Preclinical	–	(280)
	[^{55}Co]Co-rf42	Folate derivative	Preclinical	–	(280)
	[^{68}Ga]Ga-FA-I	Folate derivative	Preclinical	–	(281)
	[^{68}Ga]Ga-FA-II	Folate derivative	Preclinical	–	(281)
	[^{89}Zr]SFT-1	Folate coated nanoparticle	Preclinical	–	(282)
	[^{68}Ga]FOL	Folate derivative	Preclinical	–	(283)
	[^{89}Zr]FA-SMWs	Folate coated micro-silica	Preclinical	–	(284)
CD80/86	[^{64}Cu]NODAGA-abatacept	Biologic	Preclinical	–	(285)
iNOS	S-[^{11}C]methylisothiourea	iNOS inhibitor	Preclinical	–	(286)
	S-(2-[^{18}F]fluoroethyl)-isothiourea	iNOS inhibitor	Preclinical	–	(286)
	[^{18}F]FFDI	iNOS inhibitor	Preclinical	–	(287)
	[^{18}F]6-(2-fluoropropyl)-4-methyl-pyridin-2-amine	iNOS inhibitor	Preclinical	–	(288)
	[^{18}F]NOS	iNOS inhibitor	Clinical	NCT04062526	(289, 290)
	[^{18}F]FBAT	iNOS inhibitor	Preclinical	–	(291)
CCR2	[^{64}Cu]DOTA-ECL1i	Peptide	Clinical	NCT04217057 NCT03492762 NCT05107596 NCT04592991 NCT04537403 NCT03851237 NCT04586452	(292–300)
	[^{64}Cu]AuNCs-ECL1i	Peptide	Preclinical	–	(293)
	[^{64}Cu]Cu@CuO_x	Nanoparticle	Preclinical	–	(301)
	[^{18}F]6b	Chemical compound	Preclinical	–	(302)
CX3CR1	[^{11}C]methyl(2-amino-5(benzylthio)thiazolo[4,5-d]pyrimidin-7-yl)-d-leucinate	Chemical compound	Preclinical	–	(303)
VEGF	[^{124}I]HuMV833	Antibody	Clinical	–	(304)
	[^{124}I]iodinated-VG76e	Antibody	Preclinical	–	(305)
	[^{89}Zr]bevacizumab	Antibody	Clinical	–	(306–317)
	[^{64}Cu]DOTA-bevacizumab	Antibody	Preclinical	–	(318)
	[^{89}Zr]ranibizumab	Antibody	Preclinical	–	(319)
	[^{64}Cu] NOTA-Bev-800CW	Antibody	Preclinical	–	(320)
	[^{124}I]aflibercept	VEGF antagonist	Preclinical	–	(321)
	[^{64}Cu]NOTA-bevacizumab	Antibody	Preclinical	–	(322)
	[^{64}Cu]L19K-FDNB	Peptide	Preclinical	–	(323)

Inducible nitric oxide synthase (iNOS) is a reactive oxygen and nitrogen metabolite-metabolizing enzyme typically expressed by activated proinflammatory macrophages. The utility of [^{18}F]NOS, iNOS targeted radiotracer based on iNOS inhibitor has been reported in allograft rejection patients and patients with acute lung inflammation (289, 290). The studies also showed low brain radioactivity suitable for the imaging of C-GCA. Intimal infiltrating iNOS+ macrophages have been previously reported in GCA whereas in the adventitia of these vessels iNOS+ macrophages were absent (48). Therefore, iNOS imaging may be valuable as a tool to detect intimal macrophage infiltration and potentially intimal hyperplasia.

The chemokine receptors CCR2 and CX3CR1 are responsible for the trafficking of monocytes into the GCA affected vessel wall where these cells will then mature into macrophages (33). The radiotracer [^{64}Cu]DOTA-ECL1i specifically targeting CCR2 may be useful for imaging infiltrating monocytes/macrophages in GCA affected vessels. The utility of this radiotracer has recently been investigated in patients with pulmonary fibrosis (298). The study showed specific uptake in diseased lungs with little uptake in healthy controls. Moreover, low non-specific brain uptake and low blood radioactivity may be beneficial for imaging both LV-GCA and C-GCA. On the other hand, the radiotracer [^{11}C]methyl(2-amino-5(benzylthio)thiazolo[4,5-d]pyrimidin-7-yl)-d-leucinate designed to target CX3CR1, failed to show specific binding to CX3CR1 and therefore is not suitable for imaging GCA at the current state (303). As CX3CR1+ monocyte infiltration was reported to be higher than CCR2+ monocytes, future radiotracers targeting CX3CR1 may be beneficial for the imaging of GCA.

The abundance of vascular endothelial growth factor (VEGF), a potent pro-angiogenic growth factor, has been reported in the synovium of PMR patients (55). Macrophages have been implicated as the major source of VEGF as these cells are the major cellular infiltrates in the inflamed synovium (55). The antibody-based radiotracer [^{89}Zr]bevacizumab targeting VEGF has been successfully used to visualize VEGF expression in multiple oncological conditions (308, 314–317). Additionally, the utility of [^{89}Zr]bevacizumab in detecting VEGF expression in atherosclerotic plaques has been shown in *ex vivo* imaging studies of human carotid endarterectomy (CEA) specimens (309). Since the increased expression of VEGF has been reported in PMR, [^{89}Zr]bevacizumab imaging may be useful for imaging PMR patients. Of note, although inflammatory macrophages are major producers of VEGF in PMR, infiltrating T cells are also capable of producing VEGF (55). Hence, VEGF-targeted imaging may not be specific for macrophages. In GCA, heightened VEGF expression has been documented especially in the adventitia of GCA-affected vessels (337). However, whether macrophages or T cells are the main producers of VEGF in GCA lesions remains to be further explored. Nevertheless, VEGF imaging may potentially also be useful for imaging GCA.

Most of the macrophage-targeted radiotracers discussed above may be suitable for imaging GCA. However, whether similar macrophage phenotypes are involved in the pathogenesis of PMR remains to be proven since, to our knowledge, no study to date has explored macrophage heterogeneity in PMR.

B Cell-Targeted Radiotracers

B cell infiltration and organization into TLOs have been well-documented in GCA (38, 338). However, B cell appear to be absent in the synovial tissue of PMR patients (54). Therefore, B cell-targeted imaging may only be suitable for GCA. Several B cells targeted radiotracers have been developed (**Table 3**).

A case report has documented the resolution of vascular inflammation in a GCA patient with rituximab B cell depletion therapy (354). However, no further trials are currently ongoing for rituximab therapy in GCA. Rituximab-based radiotracer [^{89}Zr]rituximab has been successfully used to image B cells in lymphoma and RA patients (347, 348). The radiotracer showed low background activity in the blood pool which may support its suitability for application in imaging GCA.

Activated Fibroblast Targeted Radiotracers

Remodeling of the arterial wall secondary to inflammation may cause vessel occlusion and hence, be responsible for the ischemic events in GCA. Fibroblast activation, migration, and proliferation in the intima have been reported as one of the causes of intimal hyperplasia (50). Currently, the targeted imaging of fibroblast activation protein alpha (FAP), a serine protease expressed mainly by activated fibroblast, is gaining tremendous interest in cancer and inflammatory diseases (355). The interest in FAP targeted imaging started with the development of radiolabeled FAP inhibitor [^{125}I]MIP-1232 for single-photon emission computed tomography (SPECT) imaging of atherosclerosis (356). However, *ex vivo,* the radiotracer showed uptake in normal arteries as well hampering its utility for atherosclerotic imaging. Since then, more specific FAP inhibitors (FAPIs) have been rapidly developed and radiolabeled as PET radiotracers (**Table 4**).

From these FAPI based radiotracers, [^{68}Ga]FAPI-04 has been rapidly implemented in clinical trials and has shown superiority compared to the long-time gold standard [^{18}F]FDG for imaging cancer and inflammation as recently summarized by Li et al. (355). These reports showed high and specific uptake in tumors as well as at sites of fibrosis and inflammation while displaying negligible blood pool and brain radioactivity supporting its potential application for imaging both C-GCA and LV-GCA. Although FAP expression has not yet been investigated in the context of GCA and PMR, a case report has shown successful visualization of aortic and arterial inflammation in a patient suffering from GCA using [^{68}Ga]FAPI-04 (368). Interestingly [^{68}Ga]FAPI-04 imaging showed negligible radioactivity in non-target organs including the brain, background tissue, and in the blood pool, which may allow accurate detection of C-GCA. This case report demonstrates the potential of FAP targeted imaging for visualization of vascular inflammation in GCA warranting further investigation especially in comparison with the current gold standard [^{18}F]FDG-PET. No reports have shown the utility of FAP targeted imaging in PMR patients to date. Yet, successful FAP targeted imaging has been demonstrated in RA patients which may point to its potential to image inflammation in PMR patients as well (369).

TABLE 3 | B cell targeted PET radiotracers.

Target marker/ pathway	Radiotracer	Class	Clinical/ preclinical	Active clinical trials	References
CD20	[^{64}Cu]DOTA-minibody (based on rituximab)	Minibody	Preclinical	–	(339)
	[^{124}I]anti-CD20-Cys-Db (based on rituximab)	Diabody	Preclinical	–	(340)
	[^{124}I]rituximab	Antibody	Clinical	–	(341, 342)
	[^{89}Zr]rituximab	Antibody	Clinical	–	(343–348)
	[^{64}Cu]DOTA-rituximab	Antibody	Preclinical	–	(349, 350)
	[^{64}Cu]FN3(CD20)	Protein	Preclinical	–	(351)
	[^{18}F]FB-GAcDb (based on obinutuzumab)	Diabody	Preclinical	–	(352)
	[^{89}Zr]GacDb (based on obinutuzumab)	Diabody	Preclinical	–	(353)
	[^{89}Zr]GacMb (based on obinutuzumab)	Minibody	Preclinical	–	(353)

TABLE 4 | Fibroblast activation protein alpha (FAP) targeted PET radiotracers.

Radiotracer	Class	Clinical/preclinical	Active clinical trials	References
[^{68}Ga]FAPI-02	FAP inhibitor	Preclinical	–	(357)
[^{68}Ga]DOTA.SA.FAPI	FAP inhibitor	Clinical	–	(358, 359)
[^{68}Ga]FAPI-04/[^{68}Ga]DOTA-FAPI-04	FAP inhibitor	Clinical	NCT05003427 NCT04504110 NCT04533828 NCT04441606 NCT04499365 NCT04831034 NCT04416165 NCT05121779 NCT05140746	(357)
[^{68}Ga]NOTA-FAPI-04	FAP inhibitor	Clinical	NCT04499365 NCT04367948 NCT04750772 NCT05004961	(360)
[^{68}Ga]FAPI-21	FAP inhibitor	Clinical	–	(361)
[^{68}Ga]FAPI-46	FAP inhibitor	Clinical	NCT05160051 NCT04941872 NCT04457258 NCT04457232 NCT04459273 NCT04147494 NCT05172310	(361)
[^{68}Ga]TEFAPI-06	FAP inhibitor	Preclinical	–	(362)
[^{68}Ga]TEFAPI-07	FAP inhibitor	Preclinical	–	(362)
[^{68}Ga]FAPI-C12	FAP inhibitor	Preclinical	–	(363)
[^{68}Ga]FAPI-C16	FAP inhibitor	Preclinical	–	(363)
[^{68}Ga]FAPtp	FAP inhibitor	Preclinical	–	(364)
[^{68}Ga]Aib-FAPtp-01	FAP inhibitor	Preclinical	–	(364)
[^{68}Ga]DOTA-2P(FAPI)$_2$	FAP inhibitor	Clinical	NCT04941872	(365)
[^{18}F]FGlc-FAPI	FAP inhibitor	Preclinical	–	(366)
Al[^{18}F]NOTA-FAPI	FAP inhibitor	Clinical		(367)
[^{18}F]NOTA-FAPI-04	FAP inhibitor	Clinical	NCT04367948 NCT04750772 NCT05004961	–

Endothelial Cell-Targeted Radiotracers

Neoangiogenesis is one of the crucial pathogenic features of GCA and PMR. Increased vascularity in the vessel wall and synovium of GCA and PMR patients further enables the invasion of leukocytes thereby fueling the inflammatory process (32, 54, 55). In uninflamed vessels, the luminal endothelium does not express the inducible adhesion molecules VCAM-1. In inflamed GCA-affected vessels, the intense expression of VCAM-1 has been

reported on neovessel endothelial cells making this adhesion molecule suitable for targeted imaging (32). Several radiotracers targeting VCAM-1 have been developed (**Table 5**) which may be useful for imaging GCA.

An alternative approach to image angiogenesis is to target the integrin αvβ3 and specific radiotracers for this integrin have already been applied in clinical practice for imaging tumor metastasis (374–376). However, whether this approach is suitable for imaging GCA is uncertain since the αvβ3 integrin is constitutively expressed on the luminal endothelium (377). Nevertheless, studies have demonstrated the enhanced uptake of αvβ3 integrin-targeted tracers in atherosclerotic plaques corresponding to neo-vessel formation indicating its potential utility in GCA (374, 378). Furthermore, imaging integrin αvβ3 may be of interest for PMR as increased vascularization has been reported in the synovial tissues from PMR patients. Of note, integrin αvβ3 imaging is not specific for angiogenesis as infiltrating leukocytes can also express this adhesion molecule (379).

FUTURE PERSPECTIVES: TOWARD DISEASE STRATIFICATION AND BETTER TREATMENT MONITORING

The molecular PET imaging technique targeting specific markers has made valuable contributions to clinical practice ranging from diagnosis, staging, and prognosis to treatment monitoring. There are clear examples in other fields of medicine, mainly from the field of oncology, supporting the use of targeted imaging in patient stratification for targeted therapy. For example, anti-human epidermal growth factor receptor 2 (HER2) targeted therapy is only effective in HER2+ breast cancer accounting for only up to 30% of newly diagnosed breast cancer patient which can be visualized by HER2 targeted PET imaging (380–383). In another study, HER2+ PET imaging using [^{89}Zr]trastuzumab in combination with [^{18}F]FDG resulted in a negative and positive predictive value of 100% for discriminating between patients with a time to treatment failure of 2.8 and 15 months (384). A recent preclinical study in a cancer mouse model, *in vivo* imaging of different receptor tyrosine kinases (RTKs) demonstrated a decrease in receptor expression levels after their respective targeted therapy (385). Beyond oncology, [^{18}F]FDOPA PET imaging of striatal dopaminergic system has been shown to effectively stratify responders and non-responders of antipsychotic treatment in schizophrenic patients (386). Collectively, these studies support the utility of targeted PET imaging in aiding patient stratification for specific treatment strategies, prognosis and precision monitoring of treatment effect in inflammatory diseases including GCA and PMR.

In imaging GCA and PMR, radiotracers targeting specific cell populations may potentially be superior compared to the current gold standard [^{18}F]FDG. The majority of the novel PET radiotracers listed above have shown low non-target organ uptake, especially in the brain, which could increase the TBR and may translate into improved detection of cranial artery inflammation in patients suffering from C-GCA. Additionally, several novel radiotracers show low blood pool radioactivity assuring optimal TBR and visualization of aortic and arterial inflammation in LV-GCA.

Since persistent T cell and macrophage infiltration has been reported in TAB of patients undergoing glucocorticoid treatment (59, 60), imaging T cell and macrophage subsets could, in theory, be superior to [^{18}F]FDG in the diagnostic imaging of GCA. Similarly, these radiotracers could also be useful for the diagnostic imaging of PMR as persistent T cell and macrophage infiltration has also been shown in PMR patients undergoing GC treatment (54).

Imaging specific leukocyte populations may have prognostic value and may help in designing personalized treatment regimens for GCA and PMR (387). The utility of immune cell targeted imaging has indeed been reported in the context of oncology and in autoimmune inflammatory diseases. An example of this was reported in a study conducted using [^{99m}TC]IL-2 scintigraphy in melanoma patients. The study showed successful visualization of tumor infiltrating lymphocytes which enables the selection of patient whom may benefit from IL-2 immunotherapy (388). Another example was reported in patients with rheumatoid arthritis (RA) using B cell targeted [^{89}Zr]rituximab (348). The study showed that patients who responded to B cells depletion therapy had higher baseline imaging signal. In the context of GCA, the higher intensity of CD8+ T cell infiltration in the vessel wall of GCA patients has been proposed as a risk factor for visual impairment and a longer GC treatment dependency. This suggests that CD8+ T cell imaging in GCA may confer prognostic value (35). In the B cell compartment, CD20-based imaging could prove to be useful as a theranostic approach to identify GCA patients that may benefit from rituximab treatment followed by a therapeutic dose of rituximab after imaging confirmation (354). In another example, we have previously reported the prognostic value of serum levels of YKL-40 in patients suffering from GCA (389). Higher levels of serum YKL-40 at baseline predicted a longer duration of GC treatment. In the GCA-affected vessel wall, YKL-40 is highly expressed by GM-CSF skewed CD206+ macrophages (42). Therefore, imaging the extent of CD206+ infiltration in the vessels may also predict the GC dependency of these patients. Recently, a phase II clinical trial with a GM-CSF receptor blocker (mavrlimumab) demonstrated GM-CSF receptor blockade to be efficacious in the treatment of GCA (390). Furthermore, *ex vivo* treatment of GCA-affected vessels with mavrilimumab documented a reduction of CD206 expression (40). Based on these studies, imaging CD206 in GCA patients may potentially identify patients that could benefit from mavrilimumab treatment. Along similar lines, the cytokine IL-6 has been reported to elevate the expression of CD163 on macrophages (5). Hence, the detection of CD163+ macrophages may reveal GCA patients that could benefit from the IL-6 receptor blocker, tocilizumab. Although no report has shown infiltration of CD163+ macrophages in PMR, IL-6 is a major cytokine involved in the pathogenesis of this disease denoting the possibility of CD163+ macrophage infiltration in the synovium of PMR patients. Unfortunately, the only CD163 targeted radiotracer currently reported was developed for preclinical imaging in rat models but does not cross-react with

TABLE 5 | Adhesion molecule VCAM-1 targeted PET radiotracers.

Target marker/ pathway	Radiotracer	Class	Clinical/ preclinical	Active clinical trials	References
VCAM-1	[^{18}F]4V	Peptide	Preclinical	–	(370)
	[^{18}F]-FB-anti-VCAM-1 Nb	Nanobody	Preclinical	–	(371)
	[^{68}Ga]NOTA-VCAM-1$_{scFv}$	Antibody fragment	Preclinical	–	(372)
	[^{68}Ga]MacroP	Peptide	Preclinical	–	(373)
	NAMP–avidin–[^{68}Ga]–BisDOTA	Peptide	Preclinical	–	(373)

human CD163 (391). Future development of CD163 targeted tracers may be beneficial for the imaging of GCA patients and potentially PMR patients.

The novel radiotracers discussed in this review may also be used for monitoring treatment efficacy. Reduced numbers of T cells and macrophages at the site of inflammation have been reported (54, 59, 60). This may translate to a gradual decrease in imaging signal during treatment which could be useful for monitoring ongoing inflammation during GC treatment. Furthermore, the reduced expression of endothelial adhesion molecules VCAM-1 and E-selectin has been reported in the vessels of GCA patients undergoing GC treatment (32). In addition, targeted imaging of specific cell populations could also be used for monitoring the efficacy of novel immunotherapies. Reduced CD206 expression and neovascularization have been reported in *ex vivo* cultured temporal artery explants of GCA patients treated with mavrilimumab (40). Therefore, tracking the dynamics of these cellular markers by imaging may be useful for treatment effect monitoring in patients undergoing mavrilimumab treatment.

Although these novel radiotracers may be useful for imaging GCA and PMR, several considerations have to be taken into account before these tracers can be applied in clinical practice. Firstly, some of these novel tracers are tagged with radionuclides with high radiation doses such as ^{89}Zr (392). Nuclides with high radioactivity are necessary for tracers based on large molecules with low tissue penetration rates such as antibodies. The long half-life of ^{89}Zr (3.3 days) allows a longer period of time for effective tissue penetration and blood clearance to ensure that the signal can be imaged after a prolonged time frame after injection. This higher radiation dose is permissible in imaging oncology patients but is not recommended for patients with autoimmune and inflammatory diseases such as GCA and PMR. Therefore, it is important to develop radiotracers with better tissue penetration rates and tagged with radionuclides with lower radiation burdens such as ^{18}F. The current emerging technology employing camelid-based nanobody is promising in this regard (393). Secondly, these novel radiotracers are not readily available due to the production complexity and cost compared to [^{18}F]FDG (394, 395). Future research into an improved methodology for the economical and rapid production of these novel tracers is imperative to bring these into clinical practice. Finally, although theoretically the novel radiotracers mentioned in this review may be useful for the imaging of GCA and PMR, clinical trials are needed to evaluate and confirm their utility in the diagnosis and monitoring of GCA and PMR.

SUMMARY AND CONCLUSION

Due to progress in our understanding of the immunopathology of GCA/PMR and the development of novel, highly specific tracers, direct imaging of immune cells/mediators by PET is now within reach. Such novel PET imaging strategies targeting a specific subset of inflammatory cells and activation markers of resident cells could be valuable diagnostic tools in GCA/PMR. Furthermore, direct imaging of infiltrating immune cells and inflammatory mediators might be useful for the treatment monitoring of GCA and PMR patients. Eventually, these novel radiotracers may also hold promise for disease stratification in GCA/PMR, since these tracers could help to select patients that may benefit from particular treatment regimens. The majority of these novel radiotracers are still mainly used as research tools in academic centers. Efforts are needed to evaluate these radiotracers in larger clinical trials to validate their utility in clinical practice. The introduction and implementation of such novel tracers will require close collaboration between patients, clinicians (e.g., rheumatologists, internists), nuclear medicine specialists and immunologists.

AUTHOR CONTRIBUTIONS

KG: conceptualization, conducted a review of the literature, and writing—review and editing. MS, PN, RS, and PH: writing—review and editing. EB: conceptualization and writing—review and editing. WJ: conceptualization, conducted a review of the literature, writing—original draft preparation, and writing—review and editing. All authors provide approval for publication of the content and agreed to be accountable for all aspects of the work.

FUNDING

This review was supported by the Immune-Image consortium. The Immune-Image project receives funding from the Innovative Medicines Initiative 2 Joint Undertaking (JU) under grant agreement No 831514 (Immune-Image). The JU receives support from the European Union's Horizon 2020 research and innovation programme and EFPIA. This review was also supported by a research grant from FOREUM Foundation for Research in Rheumatology.

REFERENCES

1. Li KJ, Semenov D, Turk M, Pope J, A. meta-analysis of the epidemiology of giant cell arteritis across time and space. *Arthritis Res Ther.* (2021) 23:1–10. doi: 10.1186/s13075-021-02450-w
2. Robinette ML, Rao DA, Monach PA. The immunopathology of giant cell arteritis across disease spectra. *Front Immunol.* (2021) 12:623716. doi: 10.3389/fimmu.2021.623716
3. Dejaco C, Brouwer E, Mason JC, Buttgereit F, Matteson EL, Dasgupta B. Giant cell arteritis and polymyalgia rheumatica: current challenges and opportunities. *Nat Rev Rheumatol.* (2017) 13:578–92. doi: 10.1038/nrrheum.2017.142
4. Van Der Geest KSM, Sandovici M, Brouwer E, Mackie SL. Diagnostic accuracy of symptoms, physical signs, and laboratory tests for giant cell arteritis: a systematic review and meta-analysis. *JAMA Intern Med.* (2020) 180:1295–304. doi: 10.1001/jamainternmed.2020.3050
5. Esen I, Jiemy WF, van Sleen Y, van der Geest KSM, Sandovici M, Heeringa P, et al. Functionally heterogenous macrophage subsets in the pathogenesis of giant cell arteritis: novel targets for disease monitoring and treatment. *J Clin Med.* (2021) 10:4958. doi: 10.3390/jcm10214958
6. Hysa E, Gotelli E, Sammorì S, Cimmino MA, Paolino S, Pizzorni C, et al. Immune system activation in polymyalgia rheumatica: which balance between autoinflammation and autoimmunity? A systematic review. *Autoimmun Rev.* (2022) 21:102995. doi: 10.1016/j.autrev.2021.102995
7. Sharma A, Mohammad A, Turesson C. Incidence and prevalence of giant cell arteritis and polymyalgia rheumatica: a systematic literature review. *Semin Arthritis Rheum.* (2020) 50:1040–8. doi: 10.1016/j.semarthrit.2020.07.005
8. Sandovici M, van der Geest N, van Sleen Y, Brouwer E. Need and value of targeted immunosuppressive therapy in giant cell arteritis. *RMD Open.* (2022) 8:e001652. doi: 10.1136/rmdopen-2021-001652
9. Pujades-Rodriguez M, Morgan AW, Cubbon RM, Wu J. Dose-dependent oral glucocorticoid cardiovascular risks in people with immune-mediated inflammatory diseases: a population-based cohort study. *PLoS Med.* (2020) 17: 3432. doi: 10.1371/journal.pmed.1003432
10. Stone JH, Tuckwell K, Dimonaco S, Klearman M, Aringer M, Blockmans D, et al. Trial of tocilizumab in giant-cell arteritis. *N Engl J Med.* (2017) 377:317–28. doi: 10.1056/NEJMoa1613849
11. Devauchelle-Pensec V, Berthelot JM, Cornec D, Renaudineau Y, Marhadour T, Jousse-Joulin S, et al. Efficacy of first-line tocilizumab therapy in early polymyalgia rheumatica: a prospective longitudinal study. *Ann Rheum Dis.* (2016) 75:1506–10. doi: 10.1136/annrheumdis-2015-208742
12. Bonelli M, Radner H, Kerschbaumer A, Mrak D, Durechova M, Stieger J, et al. Tocilizumab in patients with new onset polymyalgia rheumatica (PMR-SPARE): a phase 2/3 randomised controlled trial. *Ann Rheum Dis.* (2022) 81:838–44. doi: 10.1136/annrheumdis-2021-221126
13. Hunder GG, Bloch DA, Michel BA, Stevens MB, Arend WP, Calabrese LH, et al. The American College of Rheumatology 1990 criteria for the classification of giant cell arteritis. *Arthritis Rheum.* (2010) 33:1122–8. doi: 10.1002/art.1780330810
14. Mahmood S. Bin, Nelson E, Padniewski J, Nasr R. Polymyalgia rheumatica: an updated review. *Cleve Clin J Med.* (2020) 87:549–56. doi: 10.3949/ccjm.87a.20008
15. Aschwanden M, Schegk E, Imfeld S, Staub D, Rottenburger C, Berger CT, et al. Vessel wall plasticity in large vessel giant cell arteritis: an ultrasound follow-up study. *Rheumatology.* (2019) 58:792–7. doi: 10.1093/rheumatology/key383
16. van der Geest KSM, Treglia G, Glaudemans AWJM, Brouwer E, Sandovici M, Jamar F, et al. Diagnostic value of [18F]FDG-PET/CT for treatment monitoring in large vessel vasculitis: a systematic review and meta-analysis. *Eur J Nucl Med Mol Imaging.* (2021) 48:3886–902. doi: 10.1007/s00259-021-05362-8
17. van der Geest KSM, Treglia G, Glaudemans AWJM, Brouwer E, Jamar F, Slart RHJA, et al. Diagnostic value of [18F]FDG-PET/CT in polymyalgia rheumatica: a systematic review and meta-analysis. *Eur J Nucl Med Mol Imaging.* (2021) 48:1876–89. doi: 10.1007/s00259-020-05162-6
18. Hellmich B, Agueda A, Monti S, Buttgereit F, De Boysson H, Brouwer E, et al. 2018 Update of the EULAR recommendations for the management of large vessel vasculitis. *Ann Rheum Dis.* (2020) 79:19–130. doi: 10.1136/annrheumdis-2019-215672
19. Nienhuis PH, Sandovici M, Glaudemans AW, Slart RH, Brouwer E. Visual and semiquantitative assessment of cranial artery inflammation with FDG-PET/CT in giant cell arteritis. *Semin Arthritis Rheum.* (2020) 50:616–23. doi: 10.1016/j.semarthrit.2020.04.002
20. Nielsen BD, Hansen IT, Kramer S, Haraldsen A, Hjorthaug K, Bogsrud TV, et al. Simple dichotomous assessment of cranial artery inflammation by conventional 18F-FDG PET/CT shows high accuracy for the diagnosis of giant cell arteritis: a case-control study. *Eur J Nucl Med Mol Imaging.* (2019) 46:184–93. doi: 10.1007/s00259-018-4106-0
21. Pijl JP, Nienhuis PH, Kwee TC, Glaudemans AWJM, Slart RHJA, Gormsen LC. Limitations and pitfalls of FDG-PET/CT in infection and inflammation. *Semin Nucl Med.* (2021) 51:633–45. doi: 10.1053/j.semnuclmed.2021.06.008
22. Nielsen BD, Gormsen LC, Hansen IT, Keller KK, Therkildsen P, Hauge EM. Three days of high-dose glucocorticoid treatment attenuates large-vessel 18F-FDG uptake in large-vessel giant cell arteritis but with a limited impact on diagnostic accuracy. *Eur J Nucl Med Mol Imaging.* (2018) 45:1119–28. doi: 10.1007/s00259-018-4021-4
23. Lu Y, Liu H, Bi Y, Yang H, Li Y, Wang J, et al. Glucocorticoid receptor promotes the function of myeloid-derived suppressor cells by suppressing HIF1α-dependent glycolysis. *Cell Mol Immunol.* (2018) 15:618–29. doi: 10.1038/cmi.2017.5
24. Buentke E, Nordström A, Lin H, Björklund AC, Laane E, Harada M, et al. Glucocorticoid-induced cell death is mediated through reduced glucose metabolism in lymphoid leukemia cells. *Blood Cancer J.* (2011) 1:e31. doi: 10.1038/bcj.2011.27
25. Krupa WM, Dewan M, Jeon MS, Kurtin PJ, Younge BR, Goronzy JJ, et al. Trapping of misdirected dendritic cells in the granulomatous lesions of giant cell arteritis. *Am J Pathol.* (2002) 161:1815–23. doi: 10.1016/S0002-9440(10)64458-6
26. Weyand CM, Tetzlaff N, Björnsson J, Brack A, Younge B, Goronzy JJ. Disease patterns and tissue cytokine profiles in giant cell arteritis. *Arthritis Rheum.* (1997) 40:19–26. doi: 10.1002/art.1780400105
27. Conway R, O'Neill L, McCarthy GM, Murphy CC, Fabre A, Kennedy S, et al. Interleukin 12 and interleukin 23 play key pathogenic roles in inflammatory and proliferative pathways in giant cell arteritis. *Ann Rheum Dis.* (2018) 77:1815–24. doi: 10.1136/annrheumdis-2018-213488
28. Espígol-Frigolé G, Corbera-Bellalta M, Planas-Rigol E, Lozano E, Segarra M, García-Martínez A, et al. Increased IL-17A expression in temporal artery lesions is a predictor of sustained response to glucocorticoid treatment in patients with giant-cell arteritis. *Ann Rheum Dis.* (2013) 72:1481–7. doi: 10.1136/annrheumdis-2012-201836
29. Ciccia F, Rizzo A, Guggino G, Cavazza A, Alessandro R, Maugeri R, et al. Difference in the expression of IL-9 and IL-17 correlates with different histological pattern of vascular wall injury in giant cell arteritis. *Rheumatology.* (2015) 54:1596–604. doi: 10.1093/rheumatology/kev102
30. Cadena RH, Reitsema RD, Huitema MG, van Sleen Y, van der Geest KSM, Heeringa P, et al. Decreased expression of negative immune checkpoint VistA by CD4+ T cells facilitates T helper 1, T helper 17, and T follicular helper lineage differentiation in GCA. *Front Immunol.* (2019) 10:1638. doi: 10.3389/fimmu.2019.01638
31. Zhang H, Watanabe R, Berry GJ, Vaglio A, Liao YJ, Warrington KJ, et al. Immunoinhibitory checkpoint deficiency in medium and large vessel vasculitis. *Proc Natl Acad Sci USA.* (2017) 114:E970–9. doi: 10.1073/pnas.1616848114
32. Cid MC, Cebrián M, Font C, Coll-Vinent B, Hernández-Rodríguez J, Esparza J, et al. Cell adhesion molecules in the development of inflammatory infiltrates in giant cell arteritis: inflammation-induced angiogenesis as the preferential site of leukocyte-endothelial cell interactions. *Arthritis Rheum.* (2000) 43:184–94. doi: 10.1002/1529-0131(200001)43:1<184::AID-ANR23>3.0.CO;2-N
33. van Sleen Y, Wang Q, van der Geest KSM, Westra J, Abdulahad WH, Heeringa P, et al. Involvement of monocyte subsets in the immunopathology of giant cell arteritis. *Sci Rep.* (2017) 7:6553. doi: 10.1038/s41598-017-06826-4
34. Corbera-Bellalta M, Planas-Rigol E, Lozano E, Terrades-García N, Alba MA, Prieto-González S, et al. Blocking interferon γ reduces expression

of chemokines CXCL9, CXCL10 and CXCL11 and decreases macrophage infiltration in *ex vivo* cultured arteries from patients with giant cell arteritis. *Ann Rheum Dis.* (2016) 75:1177–86. doi: 10.1136/annrheumdis-2015-208371
35. Samson M, Ly KH, Tournier B, Janikashvili N, Trad M, Ciudad M, et al. Involvement and prognosis value of CD8(+) T cells in giant cell arteritis. *J Autoimmun.* (2016) 72:73–83. doi: 10.1016/j.jaut.2016.05.008
36. Reitsema RD, Boots AMH, van der Geest KSM, Sandovici M, Heeringa P, Brouwer E. CD8+ T cells in GCA and GPA: bystanders or active contributors? *Front Immunol.* (2021) 12:654109. doi: 10.3389/fimmu.2021.654109
37. Graver JC, Abdulahad W, van der Geest KSM, Heeringa P, Boots AMH, Brouwer E, et al. Association of the CXCL9-CXCR3 and CXCL13-CXCR5 axes with B-cell trafficking in giant cell arteritis and polymyalgia rheumatica. *J Autoimmun.* (2021) 123:102684. doi: 10.1016/j.jaut.2021.102684
38. Graver JC, Boots AMH, Haacke EA, Diepstra A, Brouwer E, Sandovici M. Massive B-cell infiltration and organization into artery tertiary lymphoid organs in the aorta of large vessel giant cell arteritis. *Front Immunol.* (2019) 10:83. doi: 10.3389/fimmu.2019.00083
39. Graver JC, Jiemy WF, Altulea D, Boots A, Heeringa P, Abdulahad W, Brouwer E, Sandovici M. OP0062 cytokine producing B cells skew macrophages towards a pro-inflammatory phenotype in giant cell arteritis. *Ann Rheum Dis.* (2021) 80:33.1–34. doi: 10.1136/annrheumdis-2021-eular.1984
40. Corbera-Bellalta M, Alba-Rovira R, Muralidharan S, Espígol-Frigolé G, Ríos-Garcés R, Marco-Hernández J, et al. Blocking GM-CSF receptor α with mavrilimumab reduces infiltrating cells, pro-inflammatory markers and neoangiogenesis in *ex vivo* cultured arteries from patients with giant cell arteritis. *Ann Rheum Dis.* (2022) 81:524–36. doi: 10.1136/annrheumdis-2021-220873
41. Jiemy WF, van Sleen Y, van der Geest KSM, ten Berge HA, Abdulahad WH, Sandovici M, et al. Distinct macrophage phenotypes skewed by local granulocyte macrophage colony-stimulating factor (GM-CSF) and macrophage colony-stimulating factor (M-CSF) are associated with tissue destruction and intimal hyperplasia in giant cell arteritis. *Clin Transl Immunol.* (2020) 9:e1164. doi: 10.1002/cti2.1164
42. van Sleen Y, Jiemy WF, Pringle S, van der Geest KSM, Abdulahad WH, Sandovici M, et al. Distinct macrophage subset mediating tissue destruction and neovascularization in giant cell arteritis: implication of the YKL-40/interleukin-13 receptor α2 axis. *Arthritis Rheumatol.* (2021) 73:2327–37. doi: 10.1002/art.41887
43. Esen I, Jiemy WF, van Sleen Y, Bijzet J, de Jong DM, Nienhuis PH, et al. Plasma Pyruvate kinase M2 as a marker of vascular inflammation in giant cell arteritis. *Rheumatology.* (2021). doi: 10.1093/rheumatology/keab814. [Epub ahead of print].
44. Johansen JS, Baslund B, Garbarsch C, Hansen M, Stoltenberg M, Lorenzen I, et al. YKL-40 in giant cells and macrophages from patients with giant cell arteritis. *Arthritis Rheum.* (1999) 42:2624–30. doi: 10.1002/1529-0131(199912)42:12<2624::AID-ANR17>3.0.CO;2-K
45. Watanabe R, Maeda T, Zhang H, Berry GJ, Zeisbrich M, Brockett R, et al. (matrix metalloprotease)-9-producing monocytes enable T cells to invade the vessel wall and cause vasculitis. *Circ Res.* (2018) 123:700–15. doi: 10.1161/CIRCRESAHA.118.313206
46. Rittner HL, Kaiser M, Brack A, Szweda LI, Goronzy JJ, Weyand CM. Tissue-destructive macrophages in giant cell arteritis. *Circ Res.* (1999) 84:1050–8. doi: 10.1161/01.RES.84.9.1050
47. Ciccia F, Alessandro R, Rizzo A, Raimondo S, Giardina AR, Raiata F, et al. IL-33 is overexpressed in the inflamed arteries of patients with giant cell arteritis. *Ann Rheum Dis.* (2013) 72:258–64. doi: 10.1136/annrheumdis-2012-201309
48. Weyand CM, Wagner AD, Björnsson J, Goronzy JJ. Correlation of the topographical arrangement and the functional pattern of tissue-infiltrating macrophages in giant cell arteritis. *J Clin Invest.* (1996) 98:1642–9. doi: 10.1172/JCI118959
49. Planas-Rigol E, Terrades-Garcia N, Corbera-Bellalta M, Lozano E, Alba MA, Segarra M, et al. Endothelin-1 promotes vascular smooth muscle cell migration across the artery wall: a mechanism contributing to vascular remodelling and intimal hyperplasia in giant-cell arteritis. *Ann Rheum Dis.* (2017) 76:1623–33. doi: 10.1136/annrheumdis-2016-210792
50. Parreau S, Vedrenne N, Regent A, Richard L, Sindou P, Mouthon L, et al. An immunohistochemical analysis of fibroblasts in giant cell arteritis. *Ann Diagn Pathol.* (2021) 52:151728. doi: 10.1016/j.anndiagpath.2021.151728
51. Akiyama M, Ohtsuki S, Berry GJ, Liang DH, Goronzy JJ, Weyand CM. Innate and adaptive immunity in giant cell arteritis. *Front Immunol.* (2020) 11:621098. doi: 10.3389/fimmu.2020.621098
52. Petursdottir V, Nordborg E, Nordborg C. Atrophy of the aortic media in giant cell arteritis. *APMIS.* (1996) 104:191–8. doi: 10.1111/j.1699-0463.1996.tb00707.x
53. Gordon I, Rennie AM, Branwood AW. Polymyalgia rheumatica: biopsy studies. *Ann Rheum Dis.* (1964) 23:447. doi: 10.1136/ard.23.6.447
54. Meliconi R, Pulsatelli L, Uguccioni M, Salvarani C, Macchioni P, Melchiorri C, et al. Leukocyte infiltration in synovial tissue from the shoulder of patients with polymyalgia rheumatica. Quantitative analysis and influence of corticosteroid treatment. *Arthritis Rheum.* (1996) 39:1199–207. doi: 10.1002/art.1780390719
55. Meliconi R, Pulsatelli L, Dolzani P, Boiardi L, Macchioni P, Salvarani C, et al. Vascular endothelial growth factor production in polymyalgia rheumatica. *Arthritis Rheum.* (2000) 43:2472–80. doi: 10.1002/1529-0131(200011)43:11<2472::AID-ANR14>3.0.CO;2-B
56. Reitsema R, Wekema L, Abdulahad W, Heeringa P, Huitema M, Sandovici M, et al. Characterization of synovial fluid T cells in polymyalgia rheumatica: implication of Th1 and Tc1 effector memory profiles [abstract]. *Arthrit Rheumatol.* (2021) 73:(suppl .10).
57. Zhu X, Lee CW, Xu H, Wang YF, Yung PSH, Jiang Y, et al. Phenotypic alteration of macrophages during osteoarthritis: a systematic review. *Arthritis Res Ther.* (2021) 23:1–13. doi: 10.1186/s13075-021-02457-3
58. Tardito S, Martinelli G, Soldano S, Paolino S, Pacini G, Patane M, et al. Macrophage M1/M2 polarization and rheumatoid arthritis: a systematic review. *Autoimmun Rev.* (2019) 18:102397. doi: 10.1016/j.autrev.2019.102397
59. Maleszewski JJ, Younge BR, Fritzlen JT, Hunder GG, Goronzy JJ, Warrington KJ, et al. Clinical and pathological evolution of giant cell arteritis: a prospective study of follow-up temporal artery biopsies in 40 treated patients. *Mod Pathol.* (2017) 30:788. doi: 10.1038/modpathol.2017.10
60. Jakobsson K, Jacobsson L, Mohammad AJ, Nilsson JÅ, Warrington K, Matteson EL, et al. The effect of clinical features and glucocorticoids on biopsy findings in giant cell arteritis. *BMC Musculoskelet Disord.* (2016) 17:363. doi: 10.1186/s12891-016-1225-2
61. Li HY, Xu JN, Shuai ZW. Cellular signaling pathways of T cells in giant cell arteritis. *J Geriatr Cardiol.* (2021) 18:768–78. doi: 10.11909/j.issn.1671-5411.2021.09.008
62. Di Gialleonardo V, Signore A, Willemsen ATM, Sijbesma JWA, Dierckx RAJO, De Vries EFJ. Pharmacokinetic modelling of N-(4-[(18)F]fluorobenzoyl)interleukin-2 binding to activated lymphocytes in an xenograft model of inflammation. *Eur J Nucl Med Mol Imaging.* (2012) 39:1551–60. doi: 10.1007/s00259-012-2176-y
63. van de Donk PP, Wind TT, Hooiveld-Noeken JS, van der Veen EL, Glaudemans AWJM, Diepstra A, et al. Interleukin-2 PET imaging in patients with metastatic melanoma before and during immune checkpoint inhibitor therapy. *Eur J Nucl Med Mol Imaging.* (2021) 48:4369–76. doi: 10.1007/s00259-021-05407-y
64. Di Gialleonardo V, Signore A, Glaudemans AWJM, Dierckx RAJO, De Vries EFJ. N-(4-18F-fluorobenzoyl)interleukin-2 for PET of human-activated T lymphocytes. *J Nucl Med.* (2012) 53:679–86. doi: 10.2967/jnumed.111.091306
65. Van der Veen EL, Suurs F V, Cleeren F, Bormans G, Elsinga PH, Hospers GAP, et al. Development and evaluation of interleukin-2–derived radiotracers for PET imaging of T cells in mice. *J Nucl Med.* (2020) 61:1355. doi: 10.2967/jnumed.119.238782
66. Traenkle B, Kaiser PD, Pezzana S, Richardson J, Gramlich M, Wagner TR, et al. Single-domain antibodies for targeting, detection, and *in vivo* imaging of human CD4+ cells. *Front Immunol.* (2021) 12:799910. doi: 10.3389/fimmu.2021.799910
67. Nagle VL, Hertz CAJ, Henry KE, Graham MS, Campos C, Pillarsetty N, et al.. Non-invasive imaging of CD4+ T cells in humanized mice. *Mol Cancer Ther.* (2022) 21:658–66. doi: 10.1158/1535-7163.MCT-21-0888

68. Maresca KP, Chen J, Mathur D, Giddabasappa A, Root A, Narula J, et al. Preclinical evaluation of 89 Zr-Df-IAB22M2C PET as an imaging biomarker for the development of the GUCY2C-CD3 bispecific PF-07062119 as a T cell engaging therapy. *Mol Imaging Biol.* (2021) 23:941–51. doi: 10.1007/s11307-021-01621-0
69. Griessinger CM, Olafsen T, Mascioni A, Jiang ZK, Zamilpa C, Jia F, et al. The PET-tracer 89 Zr-Df-IAB22M2C enables monitoring of intratumoral CD8 T-cell infiltrates in tumor-bearing humanized mice after T-cell bispecific antibody treatment. *Cancer Res.* (2020) 80:2903–13. doi: 10.1158/0008-5472.CAN-19-3269
70. Farwell MD, Gamache RF, Babazada H, Hellmann MD, Harding JJ, Korn R, et al. CD8-targeted PET imaging of tumor infiltrating T cells in patients with cancer: a phase I first-in-human study of 89 Zr-Df-IAB22M2C, a radiolabeled anti-CD8 minibody. *J Nucl Med.* (2021) 63:720–6. doi: 10.2967/jnumed.121.262485
71. Pandit-Taskar N, Postow MA, Hellmann MD, Harding JJ, Barker CA, O'Donoghue JA, et al. First-in-humans imaging with 89 Zr-Df-IAB22M2C anti-CD8 minibody in patients with solid malignancies: preliminary pharmacokinetics, biodistribution, and lesion targeting. *J Nucl Med.* (2020) 61:512–9. doi: 10.2967/jnumed.119.229781
72. Mitra S, Leonard WJ. Biology of IL-2 and its therapeutic modulation: mechanisms and strategies. *J Leukoc Biol.* (2018) 103:643–55. doi: 10.1002/JLB.2RI0717-278R
73. van der Geest KSM, Abdulahad WH, Teteloshvili N, Tete SM, Peters JH, Horst G, et al. Low-affinity TCR engagement drives IL-2-dependent post-thymic maintenance of naive CD4+ T cells in aged humans. *Aging Cell.* (2015) 14:744–53. doi: 10.1111/acel.12353
74. Chianelli M, Mather SJ, Grossman A, Sobnak R, Fritzberg A, Britton KE, et al. 99mTc-interleukin-2 scintigraphy in normal subjects and in patients with autoimmune thyroid diseases: a feasibility study. *Eur J Nucl Med Mol Imaging.* (2008) 35:2286–93. doi: 10.1007/s00259-008-0837-7
75. Telenga ED, van der Bij W, de Vries EFJ, Verschuuren EAM, Timens W, Luurtsema G, et al. 99m Tc-HYNIC-IL-2 scintigraphy to detect acute rejection in lung transplantation patients: a proof-of-concept study. *EJNMMI Res.* (2019) 9:41. doi: 10.1186/s13550-019-0511-z
76. Glaudemans AWJM, Bonanno E, Galli F, Zeebregts CJ, De Vries EFJ, Koole M, et al. *In vivo* and *in vitro* evidence that ^{99}mTc-HYNIC-interleukin-2 is able to detect T lymphocytes in vulnerable atherosclerotic plaques of the carotid artery. *Eur J Nucl Med Mol Imaging.* (2014) 41:1710–9. doi: 10.1007/s00259-014-2764-0
77. Lucia P, Parisella MG, Danese C, Bruno F, Manetti LL, Capriotti G, et al. Diagnosis and followup of Takayasu's arteritis by scintigraphy with radiolabelled interleukin 2. *J Rheumatol.* (2004) 31:1225–7.
78. Verhoeff SR, van den Heuvel MM, van Herpen CML, Piet B, Aarntzen EHJG, Heskamp S. Programmed cell death-1/ligand-1 PET imaging: a novel tool to optimize immunotherapy? *PET Clin.* (2020) 15:35–43. doi: 10.1016/j.cpet.2019.08.008
79. Cadena RH, Abdulahad WH, Hospers GAP, Wind TT, Boots AMH, Heeringa P, et al. Checks and balances in autoimmune vasculitis. *Front Immunol.* (2018) 9:315. doi: 10.3389/fimmu.2018.00315
80. Van Der Geest KSM, Sandovici M, Rutgers A, Hiltermann TJN, Oosting SF, Slart RHJA, et al. Imaging in immune checkpoint inhibitor-induced polymyalgia rheumatica. *Ann Rheum Dis.* (2020). doi: 10.1136/annrheumdis-2020-217381. [Epub ahead of print].
81. Grebinoski S, Vignali DA. Inhibitory receptor agonists: the future of autoimmune disease therapeutics? *Curr Opin Immunol.* (2020) 67:1–9. doi: 10.1016/j.coi.2020.06.001
82. Helou DG, Shafiei-Jahani P, Lo R, Howard E, Hurrell BP, Galle-Treger L, et al. PD-1 pathway regulates ILC2 metabolism and PD-1 agonist treatment ameliorates airway hyperreactivity. *Nat Commun.* (2020) 11:1–15. doi: 10.1038/s41467-020-17813-1
83. Bryan CM, Rocklin GJ, Bick MJ, Ford A, Majri-Morrison S, Kroll AV, et al. Computational design of a synthetic PD-1 agonist. *Proc Natl Acad Sci USA.* (2021) 118:e2102164118. doi: 10.1073/pnas.2102164118
84. Curnock AP, Bossi G, Kumaran J, Bawden LJ, Figueiredo R, Tawar R, et al. Cell-targeted PD-1 agonists that mimic PD-L1 are potent T cell inhibitors. *JCI Insight.* (2021) 6:e152468. doi: 10.1172/jci.insight.152468
85. Charbonneau P, Syrota A, Crouzel C, Valois JM, Prenant C. Peripheral-type benzodiazepine receptors in the living heart characterized by positron emission tomography. *Circulation.* (1986) 73:476–83. doi: 10.1161/01.CIR.73.3.476
86. Hashimoto K, Inoue O, Suzuki K, Yamasaki T, Kojima M. Synthesis and evaluation of 11C-PK 11195 for in vivo study of peripheral-type benzodiazepine receptors using positron emission tomography. *Ann Nucl Med.* (1989) 3:63–71. doi: 10.1007/BF03164587
87. Gerhard A, Neumaier B, Elitok E, Glatting G, Ries V, Tomczak R, et al. *In vivo* imaging of activated microglia using [11C]PK11195 and positron emission tomography in patients after ischemic stroke. *Neuroreport.* (2000) 11:2957–60. doi: 10.1097/00001756-200009110-00025
88. Gaemperli O, Shalhoub J, Owen DRJ, Lamare F, Johansson S, Fouladi N, et al. Imaging intraplaque inflammation in carotid atherosclerosis with 11C-PK11195 positron emission tomography/computed tomography. *Eur Heart J.* (2012) 33:1902–10. doi: 10.1093/eurheartj/ehr367
89. Ammirati E, Moroni F, Magnoni M, Busnardo E, Di Terlizzi S, Villa C, et al. Carotid artery plaque uptake of 11 C-PK11195 inversely correlates with circulating monocytes and classical CD14 ++ CD16 - monocytes expressing HLA-DR. *Int J Cardiol Hear Vasc.* (2018) 21:32–5. doi: 10.1016/j.ijcha.2018.09.005
90. van den Ameele J, Hong YT, Manavaki R, Kouli A, Biggs H, MacIntyre Z, et al. [11C]PK11195-PET brain imaging of the mitochondrial translocator protein in mitochondrial disease. *Neurology.* (2021) 96:e2761–73. doi: 10.1212/WNL.0000000000012033
91. Debruyne JC, Van Laere KJ, Versijpt J, De Vos F, Eng JK, Strijckmans K, et al. Semiquantification of the peripheral-type benzodiazepine ligand [11C]PK11195 in normal human brain and application in multiple sclerosis patients. *Acta Neurol Belg.* (2002) 102:127–35.
92. Groom GN, Junck L, Foster NL, Frey KA, Kuhl DE, PET. of peripheral benzodiazepine binding sites in the microgliosis of Alzheimer's disease. *J Nucl Med.* (1995) 36:2207–10.
93. Pappata S, Cornu P, Samson Y, Prenant C, Benavides J, Scatton B, et al. study of carbon-11-PK 11195 binding to peripheral type benzodiazepine sites in glioblastoma: a case report. *J Nucl Med.* (1991) 32:1608–10.
94. Pugliese F, Gaemperli O, Kinderlerer AR, Lamare F, Shalhoub J, Davies AH, et al. Imaging of vascular inflammation with [11C]-PK11195 and positron emission tomography/computed tomography angiography. *J Am Coll Cardiol.* (2010) 56:653–61. doi: 10.1016/j.jacc.2010.02.063
95. Shah F, Hume SP, Pike VW, Ashworth S, McDermott J. Synthesis of the enantiomers of [N-methyl-11C]PK 11195 and comparison of their behaviours as radioligands for PK binding sites in rats. *Nucl Med Biol.* (1994) 21:573–81. doi: 10.1016/0969-8051(94)90022-1
96. Banati RB, Goerres GW, Myers R, Gunn RN, Turkheimer FE, Kreutzberg GW, et al. [11C](R)-PK11195 positron emission tomography imaging of activated microglia *in vivo* in Rasmussen's encephalitis. *Neurology.* (1999) 53:2199–203. doi: 10.1212/WNL.53.9.2199
97. Pavese N, Gerhard A, Tai YF, Ho AK, Turkheimer F, Barker RA, et al. Microglial activation correlates with severity in Huntington disease: a clinical and PET study. *Neurology.* (2006) 66:1638–43. doi: 10.1212/01.wnl.0000222734.56412.17
98. Van Der Laken CJ, Elzinga EH, Kropholler MA, Molthoff CFM, Van Der Heijden JW, Maruyama K, et al. Noninvasive imaging of macrophages in rheumatoid synovitis using 11C-(R)-PK11195 and positron emission tomography. *Arthritis Rheum.* (2008) 58:3350–5. doi: 10.1002/art.23955
99. Kropholler MA, Boellaard R, Elzinga EH, Van Der Laken CJ, Maruyama K, Kloet RW, et al. Quantification of (R)-[11C]PK11195 binding in rheumatoid arthritis. *Eur J Nucl Med Mol Imaging.* (2009) 36:624–31. doi: 10.1007/s00259-008-0987-7
100. Gent YYJ, Voskuyl AE, Kloet RW, Van Schaardenburg D, Hoekstra OS, Dijkmans BAC, et al. Macrophage positron emission tomography imaging as a biomarker for preclinical rheumatoid arthritis: findings of a prospective pilot study. *Arthritis Rheum.* (2012) 64:62–6. doi: 10.1002/art.30655
101. Nakatomi Y, Mizuno K, Ishii A, Wada Y, Tanaka M, Tazawa S, et al. Neuroinflammation in patients with chronic fatigue syndrome/myalgic encephalomyelitis: an ^{11}C-(R)-PK11195 PET study. *J Nucl Med.* (2014) 55:945–50. doi: 10.2967/jnumed.113.131045

102. Haarman BCMB, Riemersma-Van der Lek RF, de Groot JC, Ruhé HGE, Klein HC, Zandstra TE, et al. Neuroinflammation in bipolar disorder - A [(11)C]-(R)-PK11195 positron emission tomography study. *Brain Behav Immun.* (2014) 40:219–25. doi: 10.1016/j.bbi.2014.03.016
103. Gent YYJ, ter Wee MM, Voskuyl AE, den Uyl D, Ahmadi N, Dowling C, et al. Subclinical synovitis detected by macrophage PET, but not MRI, is related to short-term flare of clinical disease activity in early RA patients: an exploratory study. *Arthritis Res Ther.* (2015) 17:266. doi: 10.1186/s13075-015-0770-7
104. Jeon SY, Seo S, Lee JS, Choi SH, Lee DH, Jung YH, et al. [11C]-(R)-PK11195 positron emission tomography in patients with complex regional pain syndrome: a pilot study. *Medicine.* (2017) 96:e5735. doi: 10.1097/MD.0000000000005735
105. Seo S, Jung YH, Lee D, Lee WJ, Jang JH, Lee JY, et al. Abnormal neuroinflammation in fibromyalgia and CRPS using [11C]-(R)-PK11195 PET. *PLoS ONE.* (2021) 16:0246152. doi: 10.1371/journal.pone.0246152
106. Lamare F, Hinz R, Gaemperli O, Pugliese F, Mason JC, Spinks T, et al. Detection and quantification of large-vessel inflammation with 11C-(R)-PK11195 PET/CT. *J Nucl Med.* (2011) 52:33–9. doi: 10.2967/jnumed.110.079038
107. Banati RB, Newcombe J, Gunn RN, Cagnin A, Turkheimer F, Heppner F, et al. The peripheral benzodiazepine binding site in the brain in multiple sclerosis: quantitative in vivo imaging of microglia as a measure of disease activity. *Brain.* (2000) 123:2321–37. doi: 10.1093/brain/123.11.2321
108. Cagnin A, Myers R, Gunn RN, Lawrence AD, Stevens T, Kreutzberg GW, et al. In vivo visualization of activated glia by [11C] (R)-PK11195-PET following herpes encephalitis reveals projected neuronal damage beyond the primary focal lesion. *Brain.* (2001) 124:2014–27. doi: 10.1093/brain/124.10.2014
109. Gerhard A, Banati RB, Goerres GB, Cagnin A, Myers R, Gunn RN, et al. [11C](R)-PK11195 PET imaging of microglial activation in multiple system atrophy. *Neurology.* (2003) 61:686–9. doi: 10.1212/01.WNL.0000078192.95645.E6
110. Turner MR, Cagnin A, Turkheimer FE, Miller CCJ, Shaw CE, Brooks DJ, et al. Evidence of widespread cerebral microglial activation in amyotrophic lateral sclerosis: an [11C](R)-PK11195 positron emission tomography study. *Neurobiol Dis.* (2004) 15:601–9. doi: 10.1016/j.nbd.2003.12.012
111. Gerhard A, Schwarz J, Myers R, Wise R, Banati RB. Evolution of microglial activation in patients after ischemic stroke: a [11C](R)-PK11195 PET study. *Neuroimage.* (2005) 24:591–5. doi: 10.1016/j.neuroimage.2004.09.034
112. Hammoud DA, Endres CJ, Chander AR, Guilarte TR, Wong DF, Sacktor NC, et al. Imaging glial cell activation with [11C]-R-PK11195 in patients with AIDS. *J Neurovirol.* (2005) 11:346–55. doi: 10.1080/13550280500187351
113. Gerhard A, Pavese N, Hotton G, Turkheimer F, Es M, Hammers A, et al. In vivo imaging of microglial activation with [11C](R)-PK11195 PET in idiopathic Parkinson's disease. *Neurobiol Dis.* (2006) 21:404–12. doi: 10.1016/j.nbd.2005.08.002
114. Cagnin A, Taylor-Robinson SD, Forton DM, Banati RB. *In vivo* imaging of cerebral "peripheral benzodiazepine binding sites" in patients with hepatic encephalopathy. *Gut.* (2006) 55:547–53. doi: 10.1136/gut.2005.075051
115. Brody AL, Gehlbach D, Garcia LY, Enoki R, Hoh C, Vera D, et al. Effect of overnight smoking abstinence on a marker for microglial activation: a [11C]DAA1106 positron emission tomography study. *Psychopharmacology.* (2018) 235:3525–34. doi: 10.1007/s00213-018-5077-3
116. Brody AL, Okita K, Shieh J, Liang L, Hubert R, Mamoun M, et al. Radiation dosimetry and biodistribution of the translocator protein radiotracer [(11)C]DAA1106 determined with PET/CT in healthy human volunteers. *Nucl Med Biol.* (2014) 41:871–5. doi: 10.1016/j.nucmedbio.2014.07.004
117. Yasuno F, Kosaka J, Ota M, Higuchi M, Ito H, Fujimura Y, et al. Increased binding of peripheral benzodiazepine receptor in mild cognitive impairment-dementia converters measured by positron emission tomography with [^{11}C]DAA1106. *Psychiatry Res.* (2012) 203:67–74. doi: 10.1016/j.pscychresns.2011.08.013
118. Takano A, Arakawa R, Ito H, Tateno A, Takahashi H, Matsumoto R, et al. Peripheral benzodiazepine receptors in patients with chronic schizophrenia: a PET study with [11C]DAA1106. *Int J Neuropsychopharmacol.* (2010) 13:943–50. doi: 10.1017/S1461145710000313
119. Yasuno F, Ota M, Kosaka J, Ito H, Higuchi M, Doronbekov TK, et al. Increased binding of peripheral benzodiazepine receptor in Alzheimer's disease measured by positron emission tomography with [11C]DAA1106. *Biol Psychiatry.* (2008) 64:835–41. doi: 10.1016/j.biopsych.2008.04.021
120. Ikoma Y, Yasuno F, Ito H, Suhara T, Ota M, Toyama H, et al. Quantitative analysis for estimating binding potential of the peripheral benzodiazepine receptor with [(11)C]DAA1106. *J Cereb Blood Flow Metab.* (2007) 27:173–84. doi: 10.1038/sj.jcbfm.9600325
121. Zhang MR Kida T, Noguchi J, Furutsuka K, Maeda J, Suhara T, Suzuki K. [(11)C]DAA1106: radiosynthesis and in vivo binding to peripheral benzodiazepine receptors in mouse brain. *Nucl Med Biol.* (2003) 30:513–9. doi: 10.1016/S0969-8051(03)00016-7
122. Schroeder DC, Popp E, Rohleder C, Vus S, de la Bethencourt DP, Finke SR, et al. Positron emission tomography imaging of long-term expression of the 18 kDa translocator protein after sudden cardiac arrest in rats. *Shock.* (2021) 55:620–9. doi: 10.1097/SHK.0000000000001546
123. Wang M, Gao M, Zheng QH. Fully automated synthesis of PET TSPO radioligands [11C]DAA1106 and [18F]FEDAA1106. *Appl Radiat Isot.* (2012) 70:965–73. doi: 10.1016/j.apradiso.2012.03.011
124. Kumata K, Zhang Y, Fujinaga M, Ohkubo T, Mori W, Yamasaki T, et al. [18 F]DAA1106: automated radiosynthesis using spirocyclic iodonium ylide and preclinical evaluation for positron emission tomography imaging of translocator protein (18 kDa). *Bioorg Med Chem.* (2018) 26:4817–22. doi: 10.1016/j.bmc.2018.08.017
125. Zhang MR, Maeda J, Furutsuka K, Yoshida Y, Ogawa M, Suhara T, et al. [18F]FMDAA1106 and [18F]FEDAA1106: two positron-emitter labeled ligands for peripheral benzodiazepine receptor (PBR). *Bioorg Med Chem Lett.* (2003) 13:201–4. doi: 10.1016/S0960-894X(02)00886-7
126. Fujimura Y, Ikoma Y, Yasuno F, Suhara T, Ota M, Matsumoto R, et al. Quantitative analyses of 18F-FEDAA1106 binding to peripheral benzodiazepine receptors in living human brain. *J Nucl Med.* (2006) 47:43–50.
127. Cuhlmann S, Gsell W, Van Der Heiden K, Habib J, Tremoleda JL, Khalil M, et al. *In vivo* mapping of vascular inflammation using the translocator protein tracer 18F-FEDAA1106. *Mol Imaging.* (2014) 13:1–11. doi: 10.2310/7290.2014.00014
128. Takano A, Piehl F, Hillert J, Varrone A, Nag S, Gulyás B, et al. *In vivo* TSPO imaging in patients with multiple sclerosis: a brain PET study with [18F]FEDAA1106. *EJNMMI Res.* (2013) 3:1–9. doi: 10.1186/2191-219X-3-30
129. Varrone A, Mattsson P, Forsberg A, Takano A, Nag S, Gulyàs B, et al. *In vivo* imaging of the 18-kDa translocator protein (TSPO) with [18F]FEDAA1106 and PET does not show increased binding in Alzheimer's disease patients. *Eur J Nucl Med Mol Imaging.* (2013) 40:921–31. doi: 10.1007/s00259-013-2359-1
130. Takano A, Gulyás B, Varrone A, Karlsson P, Sjoholm N, Larsson S, et al. Biodistribution and radiation dosimetry of the 18 kDa translocator protein (TSPO) radioligand [18F]FEDAA1106: a human whole-body PET study. *Eur J Nucl Med Mol Imaging.* (2011) 38:2058–65. doi: 10.1007/s00259-011-1864-3
131. Pascual B, Funk Q, Zanotti-Fregonara P, Cykowski MD, Veronese M, Rockers E, et al. Neuroinflammation is highest in areas of disease progression in semantic dementia. *Brain.* (2021) 144:1565–75. doi: 10.1093/brain/awab057
132. Klein J, Yan X, Johnson A, Tomljanovic Z, Zou J, Polly K, et al. Olfactory impairment is related to tau pathology and neuroinflammation in Alzheimer's disease. *J Alzheimers Dis.* (2021) 80:1051–65. doi: 10.3233/JAD-201149
133. Dimber R, Guo Q, Bishop C, Adonis A, Buckley A, Kocsis A, et al. Evidence of brain inflammation in patients with human T-lymphotropic virus type 1-associated myelopathy (HAM): a pilot, multimodal imaging study using 11C-PBR28 PET, MR T1-weighted, and diffusion-weighted imaging. *J Nucl Med.* (2016) 57:1905–12. doi: 10.2967/jnumed.116.175083
134. Park E, Gallezot JD, Delgadillo A, Liu S, Planeta B, Lin SF, et al. (11)C-PBR28 imaging in multiple sclerosis patients and healthy controls: test-retest reproducibility and focal visualization of active white matter areas. *Eur J Nucl Med Mol Imaging.* (2015) 42:1081–92. doi: 10.1007/s00259-015-3043-4

135. Fujita M, Imaizumi M, Zoghbi SS, Fujimura Y, Farris AG, Suhara T, et al. Kinetic analysis in healthy humans of a novel positron emission tomography radioligand to image the peripheral benzodiazepine receptor, a potential biomarker for inflammation. *Neuroimage.* (2008) 40:43–52. doi: 10.1016/j.neuroimage.2007.11.011
136. Brown AK, Fujita M, Fujimura Y, Liow JS, Stabin M, Ryu YH, et al. Radiation dosimetry and biodistribution in monkey and man of 11C-PBR28: a PET radioligand to image inflammation. *J Nucl Med.* (2007) 48:2072–9. doi: 10.2967/jnumed.107.044842
137. Imaizumi M, Kim HJ, Zoghbi SS, Briard E, Hong J, Musachio JL, et al. PET imaging with [11C]PBR28 can localize and quantify upregulated peripheral benzodiazepine receptors associated with cerebral ischemia in rat. *Neurosci Lett.* (2007) 411:200–5. doi: 10.1016/j.neulet.2006.09.093
138. Tran TT, Gallezot JD, Jilaveanu LB, Zito C, Turcu G, Lim K, et al. [11 C]Methionine and [11 C]PBR28 as PET imaging tracers to differentiate metastatic tumor recurrence or radiation necrosis. *Mol Imaging.* (2020) 19:1–9. doi: 10.1177/1536012120968669
139. Boerwinkle AH, Strain JF, Burdo T, Doyle J, Christensen J, Su Y, et al. Comparison of [11C]-PBR28 binding between persons living with HIV and HIV-uninfected individuals. *J Acquir Immune Defic Syndr.* (2020) 85:244–51. doi: 10.1097/QAI.0000000000002435
140. Dani M, Wood M, Mizoguchi R, Fan Z, Walker Z, Morgan R, et al. Microglial activation correlates in vivo with both tau and amyloid in Alzheimer's disease. *Brain.* (2018) 141:2740–54. doi: 10.1093/brain/awy188
141. Alshikho MJ, Zürcher NR, Loggia ML, Cernasov P, Reynolds B, Pijanowski O, et al. Integrated magnetic resonance imaging and [11 C]-PBR28 positron emission tomographic imaging in amyotrophic lateral sclerosis. *Ann Neurol.* (2018) 83:1186–97. doi: 10.1002/ana.25251
142. Lois C, González I, Izquierdo-García D, Zürcher NR, Wilkens P, Loggia ML, et al. Neuroinflammation in Huntington's disease: new insights with 11 C-PBR28 PET/MRI. *ACS Chem Neurosci.* (2018) 9:2563–71. doi: 10.1021/acschemneuro.8b00072
143. Paganoni S, Alshikho MJ, Zürcher NR, Cernasov P, Babu S, Loggia ML, et al. Imaging of glia activation in people with primary lateral sclerosis. *NeuroImage Clin.* (2017) 17:347–53. doi: 10.1016/j.nicl.2017.10.024
144. Ran C, Albrecht DS, Bredella MA, Yang J, Yang J, Liang SH, et al. Imaging of human brown adipose tissue with the TSPO Tracer [11 C]PBR28. *Mol Imaging Biol.* (2018) 20:188–93. doi: 10.1007/s11307-017-1129-z
145. Veronese M, Reis Marques T, Bloomfield PS, Rizzo G, Singh N, Jones D, et al. Kinetic modelling of [11 C]PBR28 for 18 kDa translocator protein PET data: a validation study of vascular modelling in the brain using XBD173 and tissue analysis. *J Cereb Blood Flow Metab.* (2018) 38:1227–42. doi: 10.1177/0271678X17712388
146. Singhal T, O'Connor K, Dubey S, Belanger AP, Hurwitz S, Chu R, et al. 18F-PBR06 versus 11C-PBR28 PET for assessing white matter translocator protein binding in multiple sclerosis. *Clin Nucl Med.* (2018) 43:e289–95. doi: 10.1097/RLU.0000000000002179
147. Wang M, Gao M, Miller KD, Zheng QH. Synthesis of [^{11}C]PBR06 and [^{18}F]PBR06 as agents for positron emission tomographic (PET) imaging of the translocator protein (TSPO). *Steroids.* (2011) 76:1331–40. doi: 10.1016/j.steroids.2011.06.012
148. Dickstein LP, Zoghbi SS, Fujimura Y, Imaizumi M, Zhang Y, Pike VW, et al. Comparison of 18F- and 11C-labeled aryloxyanilide analogs to measure translocator protein in human brain using positron emission tomography. *Eur J Nucl Med Mol Imaging.* (2011) 38:352–7. doi: 10.1007/s00259-010-1622-y
149. Fujimura Y, Kimura Y, Si?eon FG, Dickstein LP, Pike VW, Innis RB, et al. Biodistribution and radiation dosimetry in humans of a new PET ligand, (18)F-PBR06, to image translocator protein (18 kDa). *J Nucl Med.* (2010) 51:145–9. doi: 10.2967/jnumed.109.068064
150. Fujimura Y, Zoghbi SS, Simèon FG, Taku A, Pike VW, Innis RB, et al. Quantification of translocator protein (18 kDa) in the human brain with PET and a novel radioligand, (18)F-PBR06. *J Nucl Med.* (2009) 50:1047–53. doi: 10.2967/jnumed.108.060186
151. Imaizumi M, Briard E, Zoghbi SS, Gourley JP, Hong J, Musachio JL, et al. Kinetic evaluation in nonhuman primates of two new PET ligands for peripheral benzodiazepine receptors in brain. *Synapse.* (2007) 61:595–605. doi: 10.1002/syn.20394
152. Briard E, Zoghbi SS, Imaizumi M, Gourley JP, Shetty HU, Hong J, et al. Synthesis and evaluation in monkey of two sensitive 11C-labeled aryloxyanilide ligands for imaging brain peripheral benzodiazepine receptors *in vivo*. *J Med Chem.* (2008) 51:17–30. doi: 10.1021/jm0707370
153. Wilson AA, Garcia A, Parkes J, McCormick P, Stephenson KA, Houle S, et al. Radiosynthesis and initial evaluation of [18F]-FEPPA for PET imaging of peripheral benzodiazepine receptors. *Nucl Med Biol.* (2008) 35:305–14. doi: 10.1016/j.nucmedbio.2007.12.009
154. Rusjan PM, Wilson AA, Bloomfield PM, Vitcu I, Meyer JH, Houle S, et al. Quantitation of translocator protein binding in human brain with the novel radioligand [18F]-FEPPA and positron emission tomography. *J Cereb Blood Flow Metab.* (2011) 31:1807–16. doi: 10.1038/jcbfm.2011.55
155. Suridjan I, Rusjan PM, Kenk M, Verhoeff NPLG, Voineskos AN, Rotenberg D, et al. Quantitative imaging of neuroinflammation in human white matter: a positron emission tomography study with translocator protein 18 kDa radioligand, [18F]-FEPPA. *Synapse.* (2014) 68:536–47. doi: 10.1002/syn.21765
156. Mizrahi R, Rusjan PM, Vitcu I, Ng A, Wilson AA, Houle S, et al. Whole body biodistribution and radiation dosimetry in humans of a new PET ligand, [(18)F]-FEPPA, to image translocator protein (18 kDa). *Mol imaging Biol.* (2013) 15:353–9. doi: 10.1007/s11307-012-0589-4
157. Suridjan I, Rusjan PM, Voineskos AN, Selvanathan T, Setiawan E, Strafella AP, et al. Neuroinflammation in healthy aging: a PET study using a novel Translocator Protein 18kDa (TSPO) radioligand, [(18)F]-FEPPA. *Neuroimage.* (2014) 84:868–75. doi: 10.1016/j.neuroimage.2013.09.021
158. Kenk M, Selvanathan T, Rao N, Suridjan I, Rusjan P, Remington G, et al. Imaging neuroinflammation in gray and white matter in schizophrenia: an *in-vivo* PET study with [18F]-FEPPA. *Schizophr Bull.* (2015) 41:85–93. doi: 10.1093/schbul/sbu157
159. Suridjan I, Pollock BG, Verhoeff NPLG, Voineskos AN, Chow T, Rusjan PM, et al. *In-vivo* imaging of grey and white matter neuroinflammation in Alzheimer's disease: a positron emission tomography study with a novel radioligand, [18F]-FEPPA. *Mol Psychiatry.* (2015) 20:1579–87. doi: 10.1038/mp.2015.1
160. Koshimori Y, Ko JH, Mizrahi R, Rusjan P, Mabrouk R, Jacobs MF, et al. Imaging striatal microglial activation in patients with Parkinson's Disease. *PLoS ONE.* (2015) 10:138721. doi: 10.1371/journal.pone.0138721
161. Hafizi S, Tseng HH, Rao N, Selvanathan T, Kenk M, Bazinet RP, et al. Imaging microglial activation in untreated first-episode psychosis: a PET study with [18 F]FEPPA. *Am J Psychiatry.* (2017) 174:118–24. doi: 10.1176/appi.ajp.2016.16020171
162. Attwells S, Setiawan E, Wilson AA, Rusjan PM, Mizrahi R, Miler L, et al. Inflammation in the neurocircuitry of obsessive-compulsive disorder. *JAMA Psychiatry.* (2017) 74:833–40. doi: 10.1001/jamapsychiatry.2017.1567
163. Rathitharan G, Truong J, Tong J, McCluskey T, Meyer JH, Mizrahi R, et al. Microglia imaging in methamphetamine use disorder: a positron emission tomography study with the 18 kDa translocator protein radioligand [F-18]FEPPA. *Addict Biol.* (2021) 26:e12876. doi: 10.1111/adb.12876
164. Ottoy J, De Picker L, Verhaeghe J, Deleye S, Wyffels L, Kosten L, et al. 18 F-PBR111 PET imaging in healthy controls and schizophrenia: test-retest reproducibility and quantification of neuroinflammation. *J Nucl Med.* (2018) 59:1267–74. doi: 10.2967/jnumed.117.203315
165. Guo Q, Colasanti A, Owen DR, Onega M, Kamalakaran A, Bennacef I, et al. Quantification of the specific translocator protein signal of 18F-PBR111 in healthy humans: a genetic polymorphism effect on *in vivo* binding. *J Nucl Med.* (2013) 54:1915–23. doi: 10.2967/jnumed.113.121020
166. Bourdier T, Pham TQ, Henderson D, Jackson T, Lam P, Izard M, et al. Automated radiosynthesis of [18F]PBR111 and [18F]PBR102 using the Tracerlab FXFN and Tracerlab MXFDG module for imaging the peripheral benzodiazepine receptor with PET. *Appl Radiat Isot.* (2012) 70:176–83. doi: 10.1016/j.apradiso.2011.07.014
167. Van Camp N, Boisgard R, Kuhnast B, Thézé B, Viel T, Grégoire MC, et al. In vivo imaging of neuroinflammation: a comparative study between [(18)F]PBR111, [(11)C]CLINME and [(11)C]PK11195 in an acute rodent model. *Eur J Nucl Med Mol Imaging.* (2010) 37:962–72. doi: 10.1007/s00259-009-1353-0
168. Datta G, Colasanti A, Kalk N, Owen D, Scott G, Rabiner EA, et al. 11 C-PBR28 and 18 F-PBR111 detect white matter inflammatory

heterogeneity in multiple sclerosis. *J Nucl Med.* (2017) 58:1477–82. doi: 10.2967/jnumed.116.187161

169. Fookes CJR, Pham TQ, Mattner F, Greguric I, Loc'h C, Liu X, et al. Synthesis and biological evaluation of substituted [18F]imidazo[1,2-a]pyridines and [18F]pyrazolo[1,5-a]pyrimidines for the study of the peripheral benzodiazepine receptor using positron emission tomography. *J Med Chem.* (2008) 51:3700–12. doi: 10.1021/jm7014556
170. Verschuer JD, Towson J, Eberl S, Katsifis A, Henderson D, Lam P, et al. Radiation dosimetry of the translocator protein ligands [18F]PBR111 and [18F]PBR102. *Nucl Med Biol.* (2012) 39:742–53. doi: 10.1016/j.nucmedbio.2011.11.003
171. Ishibashi K, Miura Y, Imamura A, Toyohara J, Ishii K. Microglial activation on 11C-CB184 PET in a patient with cerebellar ataxia associated with HIV infection. *Clin Nucl Med.* (2018) 43:e82–4. doi: 10.1097/RLU.0000000000001936
172. Sakata M, Ishibashi K, Imai M, Wagatsuma K, Ishii K, Hatano K, et al. Assessment of safety, efficacy, and dosimetry of a novel 18-kDa translocator protein ligand, [11 C]CB184, in healthy human volunteers. *EJNMMI Res.* (2017) 7:26. doi: 10.1186/s13550-017-0271-6
173. Toyohara J, Sakata M, Hatano K, Yanai S, Endo S, Ishibashi K, et al. Preclinical and first-in-man studies of [(11)C]CB184 for imaging the 18-kDa translocator protein by positron emission tomography. *Ann Nucl Med.* (2016) 30:534–43. doi: 10.1007/s12149-016-1094-7
174. Hatano K, Sekimata K, Yamada T, Abe J, Ito K, Ogawa M, et al. Radiosynthesis and *in vivo* evaluation of two imidazopyridineacetamides, [(11)C]CB184 and [(11)C]CB190, as a PET tracer for 18 kDa translocator protein: direct comparison with [(11)C](R)-PK11195. *Ann Nucl Med.* (2015) 29:325–35. doi: 10.1007/s12149-015-0948-8
175. Boutin H, Chauveau F, Thominiaux C, Kuhnast B, Grégoire MC, Jan S, et al. In vivo imaging of brain lesions with [(11)C]CLINME, a new PET radioligand of peripheral benzodiazepine receptors. *Glia.* (2007) 55:1459–68. doi: 10.1002/glia.20562
176. Doorduin J, de Vries E, Dierckx R, Klein H, PET. imaging of the peripheral benzodiazepine receptor: monitoring disease progression and therapy response in neurodegenerative disorders. *Curr Pharm Des.* (2008) 14:3297–315. doi: 10.2174/138161208786549443
177. Perrone M, Moon BS, Park HS, Laquintana V, Jung JH, Cutrignelli A, et al. A novel PET imaging probe for the detection and monitoring of translocator protein 18 kDa expression in pathological disorders. *Sci Rep.* (2016) 6:20422. doi: 10.1038/srep20422
178. Kim GR, Paeng JC, Jung JH, Moon BS, Lopalco A, Denora N, Lee BC, Kim SE. Assessment of TSPO in a rat experimental autoimmune myocarditis model: a comparison study between [18 F]fluoromethyl-PBR28 and [18 F]CB251. *Int J Mol Sci.* (2018) 19:276. doi: 10.3390/ijms19010276
179. Kim K, Kim H, Bae SH, Lee SY, Kim YH, Na J, et al. [18 F]CB251 PET/MR imaging probe targeting translocator protein (TSPO) independent of its polymorphism in a neuroinflammation model. *Theranostics.* (2020) 10:9315–31. doi: 10.7150/thno.46875
180. Amitani M, Zhang MR, Noguchi J, Kumata K, Ito T, Takai N, et al. Blood flow dependence of the intratumoral distribution of peripheral benzodiazepine receptor binding in intact mouse fibrosarcoma. *Nucl Med Biol.* (2006) 33:971–5. doi: 10.1016/j.nucmedbio.2006.08.004
181. Yui J, Hatori A, Kawamura K, Yanamoto K, Yamasaki T, Ogawa M, et al. Visualization of early infarction in rat brain after ischemia using a translocator protein (18 kDa) PET ligand [11C]DAC with ultra-high specific activity. *Neuroimage.* (2011) 54:123–30. doi: 10.1016/j.neuroimage.2010.08.010
182. Yanamoto K, Yamasaki T, Kumata K, Yui J, Odawara C, Kawamura K, et al. Evaluation of N-benzyl-N-[11C]methyl-2- (7-methyl-8-oxo-2-phenyl-7,8-dihydro-9H-purin-9-yl)acetamide ([11C]DAC) as a novel translocator protein (18 kDa) radioligand in kainic acid-lesioned rat. *Synapse.* (2009) 63:961–71. doi: 10.1002/syn.20678
183. James ML, Fulton RR, Henderson DJ, Eberl S, Meikle SR, Thomson S, et al. Synthesis and *in vivo* evaluation of a novel peripheral benzodiazepine receptor PET radioligand. *Bioorg Med Chem.* (2005) 13:6188–94. doi: 10.1016/j.bmc.2005.06.030
184. Boutin H, Chauveau F, Thominiaux C, Grégoire MC, James ML, Trebossen R, et al. 11C-DPA-713: a novel peripheral benzodiazepine receptor PET ligand for *in vivo* imaging of neuroinflammation. *J Nucl Med.* (2007) 48:573–81. doi: 10.2967/jnumed.106.036764
185. Yaqub M, Verweij NJF, Pieplenbosch S, Boellaard R, Lammertsma AA, Van Der Laken CJ. Quantitative assessment of arthritis activity in rheumatoid arthritis patients using [11 C]DPA-713 positron emission tomography. *Int J Mol Sci.* (2020) 21:3137. doi: 10.3390/ijms21093137
186. Endres CJ, Pomper MG, James M, Uzuner O, Hammoud DA, Watkins CC, et al. Initial evaluation of 11C-DPA-713, a novel TSPO PET ligand, in humans. *J Nucl Med.* (2009) 50:1276–82. doi: 10.2967/jnumed.109.062265
187. Endres CJ, Coughlin JM, Gage KL, Watkins CC, Kassiou M, Pomper MG. Radiation dosimetry and biodistribution of the TSPO ligand 11C-DPA-713 in humans. *J Nucl Med.* (2012) 53:330–5. doi: 10.2967/jnumed.111.094565
188. Coughlin JM, Wang Y, Ma S, Yue C, Kim PK, Adams A V, et al. Regional brain distribution of translocator protein using [(11)C]DPA-713 PET in individuals infected with HIV. *J Neurovirol.* (2014) 20:219–32. doi: 10.1007/s13365-014-0239-5
189. Coughlin JM, Wang Y, Ambinder EB, Ward RE, Minn I, Vranesic M, et al. *In vivo* markers of inflammatory response in recent-onset schizophrenia: a combined study using [(11)C]DPA-713 PET and analysis of CSF and plasma. *Transl Psychiatry.* (2016) 6:1–8. doi: 10.1038/tp.2016.40
190. Wang Y, Coughlin JM, Ma S, Endres CJ, Kassiou M, Sawa A, et al. Neuroimaging of translocator protein in patients with systemic lupus erythematosus: a pilot study using [11 C]DPA-713 positron emission tomography. *Lupus.* (2017) 26:170–8. doi: 10.1177/0961203316657432
191. Rubin LH, Sacktor N, Creighton J, Du Y, Endres CJ, Pomper MG, et al. Microglial activation is inversely associated with cognition in individuals living with HIV on effective antiretroviral therapy. *AIDS.* (2018) 32:1661–7. doi: 10.1097/QAD.0000000000001858
192. Coughlin JM, Yang T, Rebman AW, Bechtold KT, Du Y, Mathews WB, et al. Imaging glial activation in patients with post-treatment Lyme disease symptoms: a pilot study using [11 C]DPA-713 PET. *J Neuroinflamm.* (2018) 82:29–36. doi: 10.1186/s12974-018-1381-4
193. Bruijnen STG, Verweij NJF, Gent YYJ, Huisman MC, Windhorst AD, Kassiou M, et al. Imaging disease activity of rheumatoid arthritis by macrophage targeting using second generation translocator protein positron emission tomography tracers. *PLoS ONE.* (2019) 14:222844. doi: 10.1371/journal.pone.0222844
194. Lavisse S, Goutal S, Wimberley C, Tonietto M, Bottlaender M, Gervais P, et al. Increased microglial activation in patients with Parkinson disease using [18 F]-DPA714 TSPO PET imaging. *Parkinsonism Relat Disord.* (2021) 82:29–36. doi: 10.1016/j.parkreldis.2020.11.011
195. James ML, Fulton RR, Vercoullie J, Henderson DJ, Garreau L, Chalon S, et al. DPA-714, a new translocator protein-specific ligand: synthesis, radiofluorination, and pharmacologic characterization. *J Nucl Med.* (2008) 49:814–22. doi: 10.2967/jnumed.107.046151
196. Médran-Navarrete V, Bernards N, Kuhnast B, Damont A, Pottier G, Peyronneau MA, et al. [18F]DPA-C5yne, a novel fluorine-18-labelled analogue of DPA-714: radiosynthesis and preliminary evaluation as a radiotracer for imaging neuroinflammation with PET. *J Labelled Comp Radiopharm.* (2014) 57:410–8. doi: 10.1002/jlcr.3199
197. López-Picón FR, Keller T, Bocancea D, Helin JS, Krzyczmonik A, Helin S, et al. Direct comparison of [18 F]F-DPA with [18 F]DPA-714 and [11 C]PBR28 for neuroinflammation imaging in the same Alzheimer's disease model mice and healthy controls. *Mol imaging Biol.* (2022) 24:157–66. doi: 10.1007/s11307-021-01646-5
198. Mou T, Tian J, Tian Y, Yun M, Li J, Dong W, et al. Automated synthesis and preliminary evaluation of [18 F]FDPA for cardiac inflammation imaging in rats after myocardial infarction. *Sci Rep.* (2020) 10:18685 doi: 10.1038/s41598-020-75705-2
199. Wang L, Cheng R, Fujinaga M, Yang J, Zhang Y, Hatori A, et al. A facile radiolabeling of [18 F]FDPA via spirocyclic iodonium ylides: preliminary PET imaging studies in preclinical models of neuroinflammation. *J Med Chem.* (2017) 60:5222–7. doi: 10.1021/acs.jmedchem.7b00432
200. Keller T, Krzyczmonik A, Forsback S, Picón FRL, Kirjavainen AK, Takkinen J, et al. Radiosynthesis and preclinical evaluation of [18 F]F-DPA, a novel pyrazolo[1,5a]pyrimidine acetamide TSPO radioligand, in healthy sprague dawley rats. *Mol imaging Biol.* (2017) 19:736–45. doi: 10.1007/s11307-016-1040-z

201. Tang D, Fujinaga M, Hatori A, Zhang Y, Yamasaki T, Xie L, et al. Evaluation of the novel TSPO radiotracer 2-(7-butyl-2-(4-(2-([18 F]fluoroethoxy)phenyl)-5-methylpyrazolo[1,5-a]pyrimidin-3-yl)-N,N-diethylacetamide in a preclinical model of neuroinflammation. *Eur J Med Chem.* (2018) 150:1–8. doi: 10.1016/j.ejmech.2018.02.076
202. Tang D, Li J, Nickels ML, Huang G, Cohen AS, Manning HC. Preclinical evaluation of a Novel TSPO PET Ligand 2-(7-Butyl-2-(4-(2-[18 F]Fluoroethoxy)phenyl)-5-Methylpyrazolo[1,5-a]Pyrimidin-3-yl)-N,N-Diethylacetamide (18 F-VUIIS1018A) to Image Glioma. *Mol imaging Biol.* (2019) 21:113–21. doi: 10.1007/s11307-018-1198-7
203. Yanamoto K, Kumata K, Yamasaki T, Odawara C, Kawamura K, Yui J, et al. [18F]FEAC and [18F]FEDAC: two novel positron emission tomography ligands for peripheral-type benzodiazepine receptor in the brain. *Bioorg Med Chem Lett.* (2009) 19:1707–10. doi: 10.1016/j.bmcl.2009.01.093
204. Maekawa K, Tsuji AB, Yamashita A, Sugyo A, Katoh C, Tang M, et al. Translocator protein imaging with 18 F-FEDAC-positron emission tomography in rabbit atherosclerosis and its presence in human coronary vulnerable plaques. *Atherosclerosis.* (2021) 337:7–17. doi: 10.1016/j.atherosclerosis.2021.10.003
205. Chung SJ, Yoon HJ, Youn H, Kim MJ, Lee YS, Jeong JM, et al. 18 F-FEDAC as a targeting agent for activated macrophages in DBA/1 mice with collagen-induced arthritis: comparison with 18 F-FDG. *J Nucl Med.* (2018) 59:839–45. doi: 10.2967/jnumed.117.200667
206. Chauveau F, Boutin H, Van Camp N, Thominiaux C, Hantraye P, Rivron L, et al. In vivo imaging of neuroinflammation in the rodent brain with [11C]SSR180575, a novel indoleacetamide radioligand of the translocator protein (18 kDa). *Eur J Nucl Med Mol Imaging.* (2011) 38:509–14. doi: 10.1007/s00259-010-1628-5
207. Damont A, Marguet F, Puech F, Dollé F. Synthesis and *in vitro* characterization of novel fluorinated derivatives of the TSPO 18 kDa ligand SSR180575. *Eur J Med Chem.* (2015) 101:736–45. doi: 10.1016/j.ejmech.2015.07.033
208. Khan W, Corben LA, Bilal H, Vivash L, Delatycki MB, Egan GF, et al. Neuroinflammation in the cerebellum and brainstem in Friedreich Ataxia: an [18F]-FEMPA PET Study. *Mov Disord.* (2022) 37:218–24. doi: 10.1002/mds.28825
209. Hellberg S, Silvola JMU, Kiugel M, Liljenbäck H, Savisto N, Li XG, et al. 18-kDa translocator protein ligand 18 F-FEMPA: biodistribution and uptake into atherosclerotic plaques in mice. *J Nucl Cardiol.* (2017) 24:862–71. doi: 10.1007/s12350-016-0527-y
210. Varrone A, Oikonen V, Forsberg A, Joutsa J, Takano A, Solin O, et al. Positron emission tomography imaging of the 18-kDa translocator protein (TSPO) with [18F]FEMPA in Alzheimer's disease patients and control subjects. *Eur J Nucl Med Mol Imaging.* (2015) 42:438–46. doi: 10.1007/s00259-014-2955-8
211. Fiorenza D, Nicolai E, Cavaliere C, Fiorino F, Esposito G, Salvatore M. Fully automated synthesis of novel TSPO PET imaging ligand [18 F]Fluoroethyltemazepam. *Molecules.* (2021) 26:2372. doi: 10.3390/molecules26082372
212. Ji B, Ono M, Yamasaki T, Fujinaga M, Zhang MR, Seki C, et al. Detection of Alzheimer's disease-related neuroinflammation by a PET ligand selective for glial versus vascular translocator protein. *J Cereb Blood Flow Metab.* (2021) 41:2076–89. doi: 10.1177/0271678X21992457
213. Tiwari AK Ji B, Yui J, Fujinaga M, Yamasaki T, Xie L, Luo R, et al. [18F]FEBMP: positron emission tomography imaging of TSPO in a model of neuroinflammation in rats, and *in vitro* autoradiograms of the human brain. *Theranostics.* (2015) 5:961–9. doi: 10.7150/thno.12027
214. Scott AP, Thomas P, Pattison DA, Francis L, Ridge P, Tey SK, Kennedy GA. [18 F]GE-180 PET/CT assessment of enterocytic translocator protein (TSPO) over-expression: a pilot study in gastrointestinal GVHD. *Bone Marrow Transplant.* (2022) 57:517–9. doi: 10.1038/s41409-022-01571-3
215. Hellberg S, Liljenbäck H, Eskola O, Morisson-Iveson V, Morrison M, Trigg W, et al. Positron emission tomography imaging of macrophages in atherosclerosis with 18 F-GE-180, a radiotracer for translocator protein (TSPO). *Contrast Media Mol Imaging.* (2018) 2018:9186902. doi: 10.1155/2018/9186902
216. Zanotti-Fregonara P, Pascual B, Rizzo G, Yu M, Pal N, Beers D, et al. Head-to-head comparison of 11 C-PBR28 and 18 F-GE180 for quantification of the translocator protein in the human brain. *J Nucl Med.* (2018) 59:1260–6. doi: 10.2967/jnumed.117.203109
217. Vomacka L, Albert NL, Lindner S, Unterrainer M, Mahler C, Brendel M, et al. TSPO imaging using the novel PET ligand [18 F]GE-180: quantification approaches in patients with multiple sclerosis. *EJNMMI Res.* (2017) 7:89. doi: 10.1186/s13550-017-0340-x
218. Fan Z, Calsolaro V, Atkinson RA, Femminella GD, Waldman A, Buckley C, et al. Flutriciclamide (18F-GE180) PET: first-in-human PET study of novel third-generation *in vivo* marker of human translocator protein. *J Nucl Med.* (2016) 57:1753–9. doi: 10.2967/jnumed.115.169078
219. Feeney C, Scott G, Raffel J, Roberts S, Coello C, Jolly A, et al. Kinetic analysis of the translocator protein positron emission tomography ligand [18 F]GE-180 in the human brain. *Eur J Nucl Med Mol Imaging.* (2016) 43:2201–10. doi: 10.1007/s00259-016-3444-z
220. Wadsworth H, Jones PA, Chau WF, Durrant C, Fouladi N, Passmore J, et al. [^{18}F]GE-180: a novel fluorine-18 labelled PET tracer for imaging Translocator protein 18 kDa (TSPO). *Bioorg Med Chem Lett.* (2012) 22:1308–13. doi: 10.1016/j.bmcl.2011.12.084
221. Vettermann FJ, Harris S, Schmitt J, Unterrainer M, Lindner S, Rauchmann BS, et al. Impact of TSPO receptor polymorphism on [18 F]GE-180 binding in healthy brain and pseudo-reference regions of neurooncological and neurodegenerative disorders. *Life.* (2021) 11:484. doi: 10.20944/preprints202104.0548.v1
222. Vainio SK, Dickens AM, Matilainen M, López-Picón FR, Aarnio R, Eskola O, et al. Dimethyl fumarate decreases short-term but not long-term inflammation in a focal EAE model of neuroinflammation. *EJNMMI Res.* (2022) 12:6. doi: 10.1186/s13550-022-00878-y
223. Qiao L, Fisher E, McMurray L, Milicevic Sephton S, Hird M, Kuzhuppilly-Ramakrishnan N, et al. Radiosynthesis of (R,S)-[18 F]GE387: a potential PET radiotracer for imaging translocator protein 18 kDa (TSPO) with low binding sensitivity to the human gene polymorphism rs6971. *ChemMedChem.* (2019) 14:982–93. doi: 10.1002/cmdc.201900023
224. Berroterán-Infante N, Kalina T, Fetty L, Janisch V, Velasco R, Vraka C, et al. (R)-[18 F]NEBIFQUINIDE: a promising new PET tracer for TSPO imaging. *Eur J Med Chem.* (2019) 176:410–8. doi: 10.1016/j.ejmech.2019.05.008
225. Rocha NP, Charron O, Latham LB, Colpo GD, Zanotti-Fregonara P, Yu M, et al. Microglia activation in basal ganglia is a late event in Huntington Disease pathophysiology. *Neurol Neuroimmunol Neuroinflamm.* (2021) 8:e984. doi: 10.1212/NXI.0000000000000984
226. Ikawa M, Lohith TG, Shrestha S, Telu S, Zoghbi SS, Castellano S, et al. 11C-ER176, a Radioligand for 18-kDa translocator protein, has adequate sensitivity to robustly image all three affinity genotypes in human brain. *J Nucl Med.* (2017) 58:320–5. doi: 10.2967/jnumed.116.178996
227. Fujita M, Kobayashi M, Ikawa M, Gunn RN, Rabiner EA, Owen DR, et al. Comparison of four 11 C-labeled PET ligands to quantify translocator protein 18 kDa (TSPO) in human brain: (R)-PK11195, PBR28, DPA-713, and ER176-based on recent publications that measured specific-to-non-displaceable ratios. *EJNMMI Res.* (2017) 7:84. doi: 10.1186/s13550-017-0334-8
228. Zanotti-Fregonara P, Pascual B, Veronese M, Yu M, Beers D, Appel SH, et al. Head-to-head comparison of 11 C-PBR28 and 11 C-ER176 for quantification of the translocator protein in the human brain. *Eur J Nucl Med Mol Imaging.* (2019) 46:1822–9. doi: 10.1007/s00259-019-04349-w
229. Siméon FG, Lee JH, Morse CL, Stukes I, Zoghbi SS, Manly LS, et al. Synthesis and screening in mice of fluorine-containing PET radioligands for TSPO: discovery of a promising 18 F-labeled ligand. *J Med Chem.* (2021) 64:16731–45. doi: 10.1021/acs.jmedchem.1c01562
230. Lee J-H, Simeon FG, Liow J-S, Morse CL, Gladding RL, Montero Santamaria JA, et al. *In vivo* evaluation of six analogs of 11 C-ER176 as candidate 18 F-labeled radioligands for translocator protein 18 kDa (TSPO). *J Nucl Med.* (2022). doi: 10.2967/jnumed.121.263168. [Epub ahead of print].
231. Ramakrishnan NK, Hird M, Thompson S, Williamson DJ, Qiao L, Owen DR, et al. Preclinical evaluation of (S)-[18 F]GE387, a novel 18-kDa translocator protein (TSPO) PET radioligand with low binding sensitivity to human polymorphism rs6971. *Eur J Nucl Med Mol Imaging.* (2021) 49:125–36. doi: 10.1007/s00259-021-05495-w
232. MacAskill MG, Wimberley C, Morgan TEF, Alcaide-Corral CJ, Newby DE, Lucatelli C, et al. Modelling [18 F]LW223 PET data using simplified

imaging protocols for quantification of TSPO expression in the rat heart and brain. *Eur J Nucl Med Mol Imaging.* (2021) 49:137–45. doi: 10.1007/s00259-021-05482-1

233. MacAskill MG, Stadulyte A, Williams L, Morgan TEF, Sloan NL, Alcaide-Corral CJ, et al. Quantification of macrophage-driven inflammation during myocardial infarction with 18 F-LW223, a novel TSPO radiotracer with binding independent of the rs6971 human polymorphism. *J Nucl Med.* (2021) 62:536–44. doi: 10.2967/jnumed.120.243600
234. Lee SH, Denora N, Laquintana V, Mangiatordi GF, Lopedota A, Lopalco A, et al. Radiosynthesis and characterization of [18 F]BS224: a next-generation TSPO PET ligand insensitive to the rs6971 polymorphism. *Eur J Nucl Med Mol Imaging.* (2021) 49:110–24. doi: 10.1007/s00259-021-05617-4
235. Locke LW, Mayo MW, Yoo AD, Williams MB, Berr SS. PET Imaging of tumor associated macrophages using mannose coated 64Cu liposomes. *Biomaterials.* (2012) 33:7785–93. doi: 10.1016/j.biomaterials.2012.07.022
236. Lee SP, Im HJ, Kang S, Chung SJ, Cho YS, Kang H, et al. Noninvasive imaging of myocardial inflammation in myocarditis using 68 Ga-tagged mannosylated human serum albumin positron emission tomography. *Theranostics.* (2017) 7:413–24. doi: 10.7150/thno.15712
237. Eo JS, Kim HK, Kim S, Lee YS, Jeong JM, Choi YH. Gallium-68 neomannosylated human serum albumin-based PET/CT lymphoscintigraphy for sentinel lymph node mapping in non-small cell lung cancer. *Ann Surg Oncol.* (2015) 22:636–41. doi: 10.1245/s10434-014-3986-x
238. Choi JY, Jeong JM, Yoo BC, Kim K, Kim Y, Yang BY, et al. Development of 68Ga-labeled mannosylated human serum albumin (MSA) as a lymph node imaging agent for positron emission tomography. *Nucl Med Biol.* (2011) 38:371–9. doi: 10.1016/j.nucmedbio.2010.09.010
239. Kim EJ, Kim S, Seo HS, Lee YJ, Eo JS, Jeong JM, et al. Novel PET Imaging of atherosclerosis with 68Ga-labeled NOTA-neomannosylated human serum albumin. *J Nucl Med.* (2016) 57:1792–7. doi: 10.2967/jnumed.116.172650
240. Fukuda H, Matsuzawa T, Abe Y, Endo S, Yamada K, Kubota K, et al. Experimental study for cancer diagnosis with positron-labeled fluorinated glucose analogs: [18F]-2-fluoro-2-deoxy-D-mannose: a new tracer for cancer detection. *Eur J Nucl Med.* (1982) 7:294–7. doi: 10.1007/BF00253423
241. Wienhard K, Pawlik G, Nebeling B, Rudolf J, Fink G, Hamacher K, et al. Estimation of local cerebral glucose utilization by positron emission tomography: comparison of [18F]2-fluoro-2-deoxy-D-glucose and [18F]2-fluoro-2-deoxy-D-mannose in patients with focal brain lesions. *J Cereb Blood Flow Metab.* (1991) 11:485–91. doi: 10.1038/jcbfm.1991.92
242. Qin Z, Hoh CK, Olson ES, Jahromi AH, Hall DJ, Barback C V, et al. Molecular Imaging of the Glomerulus via Mesangial Cell Uptake of Radiolabeled Tilmanocept. *J Nucl Med.* (2019) 60:1325–32. doi: 10.2967/jnumed.118.223727
243. Blykers A, Schoonooghe S, Xavier C, D'Hoe K, Laoui D, D'Huyvetter M, et al. PET imaging of macrophage mannose receptor-expressing macrophages in tumor stroma using 18F-radiolabeled camelid single-domain antibody fragments. *J Nucl Med.* (2015) 56:1265–71. doi: 10.2967/jnumed.115.156828
244. Senders ML, Hernot S, Carlucci G, van de Voort JC, Fay F, Calcagno C, et al. Nanobody-facilitated multiparametric PET/MRI phenotyping of atherosclerosis. *JACC Cardiovasc Imaging.* (2019) 12:2015. doi: 10.1016/j.jcmg.2018.07.027
245. Xavier C, Blykers A, Laoui D, Bolli E, Vaneyken I, Bridoux J, et al. Clinical translation of [68 Ga]Ga-NOTA-anti-MMR-sdAb for PET/CT imaging of protumorigenic macrophages. *Mol imaging Biol.* (2019) 21:898–906. doi: 10.1007/s11307-018-01302-5
246. Varasteh Z, Mohanta S, Li Y, López Armbruster N, Braeuer M, Nekolla SG, et al. Targeting mannose receptor expression on macrophages in atherosclerotic plaques of apolipoprotein E-knockout mice using 68 Ga-NOTA-anti-MMR nanobody: non-invasive imaging of atherosclerotic plaques. *EJNMMI Res.* (2019) 9:5. doi: 10.1186/s13550-019-0474-0
247. Bettio A, Honer M, Müller C, Brühlmeier M, Müller U, Schibli R, et al. Synthesis and preclinical evaluation of a folic acid derivative labeled with 18F for PET imaging of folate receptor-positive tumors. *J Nucl Med.* (2006) 47:1153–60.
248. Ross TL, Honer M, Lam PYH, Mindt TL, Groehn V, Schibli R, et al. Fluorine-18 click radiosynthesis and preclinical evaluation of a new 18F-labeled folic acid derivative. *Bioconjug Chem.* (2008) 19:2462–70. doi: 10.1021/bc800356r
249. Fani M, Wang X, Nicolas G, Medina C, Raynal I, Port M, et al. Development of new folate-based PET radiotracers: preclinical evaluation of ^{68}Ga-DOTA-folate conjugates. *Eur J Nucl Med Mol Imaging.* (2011) 38:108–19. doi: 10.1007/s00259-010-1597-8
250. Ross TL, Honer M, Müller C, Groehn V, Schibli R, Ametamey SM, et al. new 18F-labeled folic acid derivative with improved properties for the PET imaging of folate receptor-positive tumors. *J Nucl Med.* (2010) 51:1756–62. doi: 10.2967/jnumed.110.079756
251. Jammaz IA, Al-Otaibi B, Amer S, Okarvi SM. Rapid synthesis and in vitro and in vivo evaluation of folic acid derivatives labeled with fluorine-18 for PET imaging of folate receptor-positive tumors. *Nucl Med Biol.* (2011) 38:1019–28. doi: 10.1016/j.nucmedbio.2011.03.004
252. Fischer CR, Müller C, Reber J, Müller A, Krämer SD, Ametamey SM, et al. [18F]fluoro-deoxy-glucose folate: a novel PET radiotracer with improved *in vivo* properties for folate receptor targeting. *Bioconjug Chem.* (2012) 23:805–13. doi: 10.1021/bc200660z
253. Al Jammaz I, Al-Otaibi B, Amer S, Al-Hokbany N, Okarvi S. Novel synthesis and preclinical evaluation of folic acid derivatives labeled with (18)F-[FDG] for PET imaging of folate receptor-positive tumors. *Nucl Med Biol.* (2012) 39:864–70. doi: 10.1016/j.nucmedbio.2012.02.005
254. Fischer CR, Groehn V, Reber J, Schibli R, Ametamey SM, Müller C. Improved PET imaging of tumors in mice using a novel (18) F-folate conjugate with an albumin-binding entity. *Mol imaging Biol.* (2013) 15:649–54. doi: 10.1007/s11307-013-0651-x
255. Fani M, Tamma ML, Nicolas GP, Lasri E, Medina C, Raynal I, et al. *In vivo* imaging of folate receptor positive tumor xenografts using novel 68Ga-NODAGA-folate conjugates. *Mol Pharm.* (2012) 9:1136–45. doi: 10.1021/mp200418f
256. Kühle B, Müller C, Ross TL. A novel (68)Ga-labeled pteroic acid-based pet tracer for tumor imaging via the folate receptor. *Recent Results Cancer Res.* (2013) 194:257–67. doi: 10.1007/978-3-642-27994-2_13
257. Betzel T, Müller C, Groehn V, Müller A, Reber J, Fischer CR, et al. Radiosynthesis and preclinical evaluation of 3'-Aza-2'-[(18)F]fluorofolic acid: a novel PET radiotracer for folate receptor targeting. *Bioconjug Chem.* (2013) 24:205–14. doi: 10.1021/bc300483a
258. Gnesin S, Müller J, Burger IA, Meisel A, Siano M, Früh M, et al. Radiation dosimetry of 18 F-AzaFol: a first in-human use of a folate receptor PET tracer. *EJNMMI Res.* (2020) 10:32. doi: 10.1186/s13550-020-00624-2
259. Schniering J, Benešová M, Brunner M, Haller S, Cohrs S, Frauenfelder T, et al. 18 F-AzaFol for detection of folate receptor-β positive macrophages in experimental interstitial lung disease-a proof-of-concept study. *Front Immunol.* (2019) 10:2724. doi: 10.3389/fimmu.2019.02724
260. Gent YYJ, Weijers K, Molthoff CFM, Windhorst AD, Huisman MC, Smith DEC, et al. Evaluation of the novel folate receptor ligand [18F]fluoro-PEG-folate for macrophage targeting in a rat model of arthritis. *Arthritis Res Ther.* (2013) 15:R37. doi: 10.1186/ar4191
261. Chandrupatla DMSH, Molthoff CFM, Ritsema WIGR, Vos R, Elshof E, Matsuyama T, et al. Prophylactic and therapeutic activity of alkaline phosphatase in arthritic rats: single-agent effects of alkaline phosphatase and synergistic effects in combination with methotrexate. *Transl Res.* (2018) 199:24–38. doi: 10.1016/j.trsl.2018.04.001
262. Chandrupatla DMSH, Jansen G, Mantel E, Low PS, Matsuyama T, Musters RP, et al. Imaging and methotrexate response monitoring of systemic inflammation in arthritic rats employing the macrophage PET Tracer [18 F]Fluoro-PEG-Folate. *Contrast Media Mol Imaging.* (2018) 2018:8092781. doi: 10.1155/2018/8092781
263. Verweij NJF, Yaqub M, Bruijnen STG, Pieplenbosch S, ter Wee MM, Jansen G, et al. First in man study of [18 F]fluoro-PEG-folate PET: a novel macrophage imaging technique to visualize rheumatoid arthritis. *Sci Rep.* (2020) 10:1047. doi: 10.1038/s41598-020-57841-x
264. Kularatne SA, Bélanger MJ, Meng X, Connolly BM, Vanko A, Suresch DL, et al. Comparative analysis of folate derived PET imaging agents with [(18)F]-2-fluoro-2-deoxy-d-glucose using a rodent inflammatory paw model. *Mol Pharm.* (2013) 10:3103–11. doi: 10.1021/mp4001684
265. Aljammaz I, Al-Otaibi B, Al-Hokbany N, Amer S, Okarvi S. Development and pre-clinical evaluation of new 68Ga-NOTA-folate conjugates for PET imaging of folate receptor-positive tumors. *Anticancer Res.* (2014) 34:6547–56.

266. Brand C, Longo VA, Groaning M, Weber WA, Reiner T. Development of a new folate-derived Ga-68-based PET imaging agent. *Mol imaging Biol.* (2017) 19:754–61. doi: 10.1007/s11307-017-1049-y
267. Boss SD, Betzel T, Müller C, Fischer CR, Haller S, Reber J, et al. Comparative studies of three pairs of α- and γ-conjugated folic acid derivatives labeled with fluorine-18. *Bioconjug Chem.* (2016) 27:74–86. doi: 10.1021/acs.bioconjchem.5b00644
268. Chen Q, Meng X, McQuade P, Rubins D, Lin SA, Zeng Z, et al. Synthesis and preclinical evaluation of folate-NOTA-Al(18)F for PET imaging of folate-receptor-positive tumors. *Mol Pharm.* (2016) 13:1520–7. doi: 10.1021/acs.molpharmaceut.5b00989
269. Farkas R, Siwowska K, Ametamey SM, Schibli R, Van Der Meulen NP, Müller C. (64)Cu- and (68)Ga-based PET imaging of folate receptor-positive tumors: development and evaluation of an albumin-binding NODAGA-folate. *Mol Pharm.* (2016) 13:1979–87. doi: 10.1021/acs.molpharmaceut.6b00143
270. Zhang X, Yu Q, He Y, Zhang C, Zhu H, Yang Z, et al. Synthesis and biological evaluation of (68) Ga-labeled Pteroyl-Lys conjugates for folate receptor-targeted tumor imaging. *J Labelled Comp Radiopharm.* (2016) 59:346–53. doi: 10.1002/jlcr.3410
271. Jain A, Mathur A, Pandey U, Bhatt J, Mukherjee A, Ram R, et al. Synthesis and evaluation of a (68)Ga labeled folic acid derivative for targeting folate receptors. *Appl Radiat Isot.* (2016) 116:77–84. doi: 10.1016/j.apradiso.2016.07.024
272. Li N, Yu Z, Pham TT, Blower PJ, Yan R, A. generic 89 Zr labeling method to quantify the *in vivo* pharmacokinetics of liposomal nanoparticles with positron emission tomography. *Int J Nanomed.* (2017) 12:3281–94. doi: 10.2147/IJN.S134379
273. Choi PS, Lee JY, Park JH, Kim SW. Synthesis and evaluation of 68 Ga-HBED-CC-EDBE-folate for positron-emission tomography imaging of overexpressed folate receptors on CT26 tumor cells. *J Labelled Comp Radiopharm.* (2018) 61:4–10. doi: 10.1002/jlcr.3563
274. Chen Q, Meng X, McQuade P, Rubins D, Lin SA, Zeng Z, et al. Folate-PEG-NOTA-Al 18 F: a new folate based radiotracer for PET imaging of folate receptor-positive tumors. *Mol Pharm.* (2017) 14:4353–61. doi: 10.1021/acs.molpharmaceut.7b00415
275. Ma W, Fu F, Zhu J, Huang R, Zhu Y, Liu Z, et al. 64 Cu-Labeled multifunctional dendrimers for targeted tumor PET imaging. *Nanoscale.* (2018) 10:6113–24. doi: 10.1039/C7NR09269E
276. Kettenbach K, Reffert LM, Schieferstein H, Pektor S, Eckert R, Miederer M, et al. Comparison study of two differently clicked 18 F-folates-lipophilicity plays a key role. *Pharmaceuticals.* (2018) 11:30. doi: 10.3390/ph11010030
277. Silvola JMU, Li XG, Virta J, Marjamäki P, Liljenbäck H, Hytönen JP, et al. Aluminum fluoride-18 labeled folate enables in vivo detection of atherosclerotic plaque inflammation by positron emission tomography. *Sci Rep.* (2018) 8:9720. doi: 10.1038/s41598-018-27618-4
278. Jahandideh A, Uotila S, Ståhle M, Virta J, Li XG, Kytö V, et al. Folate receptor β-targeted PET imaging of macrophages in autoimmune myocarditis. *J Nucl Med.* (2020) 61:1643–9. doi: 10.2967/jnumed.119.241356
279. Körhegyi Z, Rózsa D, Hajdu I, Bodnár M, Kertész I, Kerekes K, et al. Synthesis of 68 Ga-labeled biopolymer-based nanoparticle imaging agents for positron-emission tomography. *Anticancer Res.* (2019) 39:2415–27. doi: 10.21873/anticanres.13359
280. Radford LL, Fernandez S, Beacham R, Sayed R El, Farkas R, Benešová M, et al. New 55 co-labeled albumin-binding folate derivatives as potential PET agents for folate receptor imaging. *Pharmaceuticals.* (2019) 12:166. doi: 10.3390/ph12040166
281. Larenkov A, Rakhimov M, Lunyova K, Klementyeva O, Maruk A, Machulkin A. Pharmacokinetic properties of 68 Ga-labelled folic acid conjugates: improvement using HEHE Tag. *Molecules.* (2020) 25:2712. doi: 10.3390/molecules25112712
282. Kim GG, Lee JY, Choi PS, Kim SW, Park JH. Tumor targeting effect of triphenylphosphonium cations and folic acid coated with Zr-89-labeled silica nanoparticles. *Molecules.* (2020) 25:2922. doi: 10.3390/molecules25122922
283. Moisio O, Palani S, Virta J, Elo P, Liljenbäck H, Tolvanen T, et al. Radiosynthesis and preclinical evaluation of [68 Ga]Ga-NOTA-folate for PET imaging of folate receptor β-positive macrophages. *Sci Rep.* (2020) 10:13593. doi: 10.1038/s41598-020-70394-3
284. Kim GG, Jang HM, Park SB, So JS, Kim SW. Synthesis of Zr-89-labeled folic acid-conjugated silica (SiO 2) microwire as a tumor diagnostics carrier for positron emission tomography. *Materials.* (2021) 14:3226. doi: 10.3390/ma14123226
285. Taddio MF, Castro Jaramillo CA, Runge P, Blanc A, Keller C, Talip Z, et al. *In vivo* imaging of local inflammation: monitoring LPS-induced CD80/CD86 upregulation by PET. *Mol imaging Biol.* (2021) 23:196–207. doi: 10.1007/s11307-020-01543-3
286. Zhang J, McCarthy TJ, Moore WM, Currie MG, Welch MJ. Synthesis and evaluation of two positron-labeled nitric oxide synthase inhibitors, S-[11C]methylisothiourea and S-(2-[18F]fluoroethyl)isothiourea, as potential positron emission tomography tracers. *J Med Chem.* (1996) 39:5110–8. doi: 10.1021/jm960481q
287. Tian H, Lee Z. Radiosynthesis of 8-Fluoro-3-(4-[18F]Fluorophenyl)-3,4-Dihydro-1-Isoquinolinamine ([18F]FFDI), a potential PET radiotracer for the inducible nitric oxide synthase. *Curr Radiopharm.* (2008) 1:49–53. doi: 10.2174/1874471010801020049
288. Zhou D, Lee H, Rothfuss JM, Chen DL, Ponde DE, Welch MJ, et al. Design and synthesis of 2-amino-4-methylpyridine analogues as inhibitors for inducible nitric oxide synthase and *in vivo* evaluation of [18F]6-(2-fluoropropyl)-4-methyl-pyridin-2-amine as a potential PET tracer for inducible nitric oxide synthase. *J Med Chem.* (2009) 52:2443–53. doi: 10.1021/jm801556h
289. Herrero P, Laforest R, Shoghi K, Zhou D, Ewald G, Pfeifer J, et al. Feasibility and dosimetry studies for 18F-NOS as a potential PET radiopharmaceutical for inducible nitric oxide synthase in humans. *J Nucl Med.* (2012) 53:994–1001. doi: 10.2967/jnumed.111.088518
290. Huang HJ, Isakow W, Byers DE, Engle JT, Griffin EA, Kemp D, et al. Imaging pulmonary inducible nitric oxide synthase expression with PET. *J Nucl Med.* (2015) 56:76–81. doi: 10.2967/jnumed.114.146381
291. Yeh SHH, Huang WS, Chiu CH, Chen CL, Chen HT, Chi DY, et al. Automated Synthesis and Initial Evaluation of (4'-Amino-5',8'-difluoro-1'H-spiro[piperidine-4,2'-quinazolin]-1-yl)(4-[18 F]fluorophenyl)methanone for PET/MR Imaging of Inducible Nitric Oxide Synthase. *Mol Imaging.* (2021) 2021:9996125. doi: 10.1155/2021/9996125
292. Liu Y, Gunsten SP, Sultan DH, Luehmann HP, Zhao Y, Blackwell TS, et al. PET-based Imaging of Chemokine Receptor 2 in experimental and disease-related lung inflammation. *Radiology.* (2017) 283:758–68. doi: 10.1148/radiol.2016161409
293. Liu Y, Li W, Luehmann HP, Zhao Y, Detering L, Sultan DH, et al. Noninvasive imaging of CCR2 + cells in ischemia-reperfusion injury after lung transplantation. *Am J Transplant.* (2016) 16:3016–23. doi: 10.1111/ajt.13907
294. Li W, Luehmann HP, Hsiao HM, Tanaka S, Higashikubo R, Gauthier JM, et al. Visualization of monocytic cells in regressing atherosclerotic plaques by intravital 2-photon and positron emission tomography-based imaging-brief report. *Arterioscler Thromb Vasc Biol.* (2018) 38:1030–6. doi: 10.1161/ATVBAHA.117.310517
295. Dobrucki LW, Sinusas AJ. Targeted imaging of abdominal aortic aneurysm: biology over structure. *Circ Cardiovasc Imaging.* (2020) 13:e010495. doi: 10.1161/CIRCIMAGING.120.010495
296. English SJ, Sastriques SE, Detering L, Sultan D, Luehmann H, Arif B, et al. CCR2 positron emission tomography for the assessment of abdominal aortic aneurysm inflammation and rupture prediction. *Circ Cardiovasc Imaging.* (2020) 13:e009889. doi: 10.1161/CIRCIMAGING.119.009889
297. Heo GS, Kopecky B, Sultan D, Ou M, Feng G, Bajpai G, et al. Molecular imaging visualizes recruitment of inflammatory monocytes and macrophages to the injured heart. *Circ Res.* (2019) 124:881–90. doi: 10.1161/CIRCRESAHA.118.314030
298. Brody SL, Gunsten SP, Luehmann HP, Sultan DH, Hoelscher M, Heo GS, et al. Chemokine receptor 2-targeted molecular imaging in pulmonary fibrosis. A clinical trial. *Am J Respir Crit Care Med.* (2021) 203:78–89. doi: 10.1164/rccm.202004-1132OC
299. Heo GS, Bajpai G, Li W, Luehmann HP, Sultan DH, Dun H, et al. Targeted PET imaging of chemokine receptor 2-positive monocytes and macrophages in the injured heart. *J Nucl Med.* (2021) 62:111–4. doi: 10.2967/jnumed.120.244673

300. Sultan D, Li W, Detering L, Heo GS, Luehmann HP, Kreisel D, Liu Y. Assessment of ultrasmall nanocluster for early and accurate detection of atherosclerosis using positron emission tomography/computed tomography. *Nanomedicine.* (2021) 36:102416. doi: 10.1016/j.nano.2021.102416
301. Zhang X, Detering L, Sultan D, Luehmann H, Li L, Heo GS, et al. CC Chemokine receptor 2-targeting copper nanoparticles for positron emission tomography-guided delivery of gemcitabine for pancreatic ductal adenocarcinoma. *ACS Nano.* (2021) 15:1186–98. doi: 10.1021/acsnano.0c08185
302. Wagner S, de Moura Gatti F, Silva DG, Ortiz Zacarias N V, Zweemer AJM, Hermann S, et al. Development of the first potential nonpeptidic positron emission tomography tracer for the imaging of CCR2 receptors. *ChemMedChem.* (2021) 16:640–5. doi: 10.1002/cmdc.202000728
303. Gao M, Wang M, Meyer JA, Peters JS, Zarrinmayeh H, Territo PR, et al. Synthesis and preliminary biological evaluation of [11 C]methyl (2-amino-5-(benzylthio)thiazolo[4,5-d]pyrimidin-7-yl)-d-leucinate for the fractalkine receptor (CX 3 CR1). *Bioorg Med Chem Lett.* (2017) 27:2727–30. doi: 10.1016/j.bmcl.2017.04.052
304. Jayson GC, Zweit J, Jackson A, Mulatero C, Julyan P, Ranson M, et al. Molecular imaging and biological evaluation of HuMV833 anti-VEGF antibody: implications for trial design of antiangiogenic antibodies. *J Natl Cancer Inst.* (2002) 94:1484–93. doi: 10.1093/jnci/94.19.1484
305. Collingridge DR, Carroll VA, Glaser M, Aboagye EO, Osman S, Hutchinson OC, et al. The development of [(124)I]iodinated-VG76e: a novel tracer for imaging vascular endothelial growth factor in vivo using positron emission tomography. *Cancer Res.* (2002) 62:5912–9.
306. Nagengast WB, De Vries EG, Hospers GA, Mulder NH, De Jong JR, Hollema H, et al. Lub-de Hooge MN. *In vivo* VEGF imaging with radiolabeled bevacizumab in a human ovarian tumor xenograft. *J Nucl Med.* (2007) 48:1313–9. doi: 10.2967/jnumed.107.041301
307. Nagengast WB, de Korte MA, Oude Munnink TH, Timmer-Bosscha H, den Dunnen WF, Hollema H, et al. 89Zr-bevacizumab PET of early antiangiogenic tumor response to treatment with HSP90 inhibitor NVP-AUY922. *J Nucl Med.* (2010) 51:761–7. doi: 10.2967/jnumed.109.071043
308. Van Es SC, Brouwers AH, Mahesh SVK, Leliveld-Kors AM, De Jong IJ, Lub-De Hooge MN, et al. 89 Zr-Bevacizumab PET: potential early indicator of everolimus efficacy in patients with metastatic renal cell carcinoma. *J Nucl Med.* (2017) 58:905–10. doi: 10.2967/jnumed.116.183475
309. Golestani R, Zeebregts CJ, Terwisscha van Scheltinga AGT, Lub-de Hooge MN, van Dam GM, Glaudemans AWJM, et al. Feasibility of vascular endothelial growth factor imaging in human atherosclerotic plaque using (89)Zr-bevacizumab positron emission tomography. *Mol Imaging.* (2013) 12:235–43. doi: 10.2310/7290.2012.00034
310. Van Der Bilt ARM, Terwisscha Van Scheltinga AGT, Timmer-Bosscha H, Schröder CP, Pot L, Kosterink JGW, et al. Measurement of tumor VEGF-A levels with 89Zr-bevacizumab PET as an early biomarker for the antiangiogenic effect of everolimus treatment in an ovarian cancer xenograft model. *Clin Cancer Res.* (2012) 18:6306–14. doi: 10.1158/1078-0432.CCR-12-0406
311. Gaykema SBM, Brouwers AH, Hooge MNL De, Pleijhuis RG, Timmer-Bosscha H, Pot L, et al. 89Zr-bevacizumab PET imaging in primary breast cancer. *J Nucl Med.* (2013) 54:1014–8. doi: 10.2967/jnumed.112.117218
312. Van Asselt SJ, Oosting SF, Brouwers AH, Bongaerts AHH, De Jong JR, Lub-de Hooge MN, et al. Everolimus reduces (89)Zr-bevacizumab tumor uptake in patients with neuroendocrine. *Tumors J Nucl Med.* (2014) 55:1087–92. doi: 10.2967/jnumed.113.129056
313. Van Scheltinga AG, Berghuis P, Nienhuis HH, Timmer-Bosscha H, Pot L, Gaykema SB, et al. Visualising dual downregulation of insulin-like growth factor receptor-1 and vascular endothelial growth factor-A by heat shock protein 90 inhibition effect in triple negative breast cancer. *Eur J Cancer.* (2014) 50:2508–16. doi: 10.1016/j.ejca.2014.06.008
314. Oosting SF, Brouwers AH, Van Es SC, Nagengast WB, Munnink THO, Lub-De Hooge MN, et al. 89Zr-bevacizumab PET visualizes heterogeneous tracer accumulation in tumor lesions of renal cell carcinoma patients and differential effects of antiangiogenic treatment. *J Nucl Med.* (2015) 56:63–9. doi: 10.2967/jnumed.114.144840
315. Oosting SF, Van Asselt SJ, Brouwers AH, Bongaerts AHH, Steinberg JDJ, De Jong JR, et al. 89Zr-Bevacizumab PET visualizes disease manifestations in patients with von Hippel-Lindau Disease. *J Nucl Med.* (2016) 57:1244–50. doi: 10.2967/jnumed.115.167643
316. Jansen MHA, Lagerweij T, Sewing ACP, Vugts DJ, Van Vuurden DG, Molthoff CFM, et al. Bevacizumab targeting diffuse intrinsic pontine glioma: results of 89Zr-bevacizumab PET imaging in brain tumor models. *Mol Cancer Ther.* (2016) 15:2166–74. doi: 10.1158/1535-7163.MCT-15-0558
317. Jansen MH, Van Zanten SEMV, Van Vuurden DG, Huisman MC, Vugts DJ, Hoekstra OS, et al. Molecular drug imaging: 89 Zr-Bevacizumab PET in children with diffuse intrinsic pontine glioma. *J Nucl Med.* (2017) 58:711–6. doi: 10.2967/jnumed.116.180216
318. Paudyal B, Paudyal P, Oriuchi N, Hanaoka H, Tominaga H, Endo K. Positron emission tomography imaging and biodistribution of vascular endothelial growth factor with 64Cu-labeled bevacizumab in colorectal cancer xenografts. *Cancer Sci.* (2011) 102:117–21. doi: 10.1111/j.1349-7006.2010.01763.x
319. Nagengast WB, Lub-de Hooge MN, Oosting SF, Den Dunnen WFA, Warnders FJ, Brouwers AH, et al. VEGF-PET imaging is a noninvasive biomarker showing differential changes in the tumor during sunitinib treatment. *Cancer Res.* (2011) 71:143–53. doi: 10.1158/0008-5472.CAN-10-1088
320. Zhang Y, Hong H, Engle JW, Yang Y, Barnhart TE, Cai W. Positron emission tomography and near-infrared fluorescence imaging of vascular endothelial growth factor with dual-labeled bevacizumab. *Am J Nucl Med Mol Imaging.* (2012) 2:1–13.
321. Christoforidis JB, Williams MM, Kothandaraman S, Kumar K, Epitropoulos FJ, Knopp M V. Pharmacokinetic properties of intravitreal I-124-aflibercept in a rabbit model using PET/CT. *Curr Eye Res.* (2012) 37:1171–4. doi: 10.3109/02713683.2012.727521
322. Chang AJ, Sohn R, Lu ZH, Arbeit JM, Lapi SE. Detection of rapalog-mediated therapeutic response in renal cancer xenografts using ^{64}Cu-bevacizumab immunoPET. *PLoS ONE.* (2013) 8:58949. doi: 10.1371/journal.pone.0058949
323. Marquez B V, Ikotun OF, Parry JJ, Rogers BE, Meares CF, Lapi SE. Development of a radiolabeled irreversible peptide ligand for PET imaging of vascular endothelial growth factor. *J Nucl Med.* (2014) 55:1029–34. doi: 10.2967/jnumed.113.130898
324. Owen DR, Yeo AJ, Gunn RN, Song K, Wadsworth G, Lewis A, et al. An 18-kDa translocator protein (TSPO) polymorphism explains differences in binding affinity of the PET radioligand PBR28. *J Cereb Blood Flow Metab.* (2012) 32:1–5. doi: 10.1038/jcbfm.2011.147
325. Owen DRJ, Gunn RN, Rabiner EA, Bennacef I, Fujita M, Kreisl WC, et al. Mixed-affinity binding in humans with 18-kDa translocator protein ligands. *J Nucl Med.* (2011) 52:24–32. doi: 10.2967/jnumed.110.079459
326. Turkheimer FE, Rizzo G, Bloomfield PS, Howes O, Zanotti-Fregonara P, Bertoldo A, et al. The methodology of TSPO imaging with positron emission tomography. *Biochem Soc Trans.* (2015) 43:586–92. doi: 10.1042/BST20150058
327. Schollhammer R, Lepreux S, Barthe N, Vimont D, Rullier A, Sibon I, et al. *In vitro* and pilot *in vivo* imaging of 18 kDa translocator protein (TSPO) in inflammatory vascular disease. *EJNMMI Res.* (2021) 11:45. doi: 10.1186/s13550-021-00786-7
328. Tahara N, Mukherjee J, De Haas HJ, Petrov AD, Tawakol A, Haider N, et al. 2-deoxy-2-[18F]fluoro-D-mannose positron emission tomography imaging in atherosclerosis. *Nat Med.* (2014) 20:215–9. doi: 10.1038/nm.3437
329. Mathias CJ, Wang S, Lee RJ, Waters DJ, Low PS, Green MA. Tumor-Selective Radiopharmaceutical targeting via receptor-mediated endocytosis of gallium-67-deferoxamine-folate. *J Nucl Med.* (1996) 37:1003–8.
330. Mathias CJ, Lewis MR, Reichert DE, Laforest R, Sharp TL, Lewis JS, et al. Preparation of 66Ga- and 68Ga-labeled Ga(III)-deferoxamine-folate as potential folate-receptor-targeted PET radiopharmaceuticals. *Nucl Med Biol.* (2003) 30:725–31. doi: 10.1016/S0969-8051(03)00080-5
331. Müller C, Zhernosekov K, Köster U, Johnston K, Dorrer H, Hohn A, et al. unique matched quadruplet of terbium radioisotopes for PET and SPECT and for α- and β- radionuclide therapy: an *in vivo* proof-of-concept study with a new receptor-targeted folate derivative. *J Nucl Med.* (2012) 53:1951–9. doi: 10.2967/jnumed.112.107540
332. AlJammaz I, Al-Otaibi B, Al-Rumayan F, Al-Yanbawi S, Amer S, Okarvi SM. Development and preclinical evaluation of new (124)I-folate conjugates

for PET imaging of folate receptor-positive tumors. *Nucl Med Biol.* (2014) 41:457–63. doi: 10.1016/j.nucmedbio.2014.03.013
333. Zhou M, Song S, Zhao J, Tian M, Li C. Theranostic CuS nanoparticles targeting folate receptors for PET image-guided photothermal therapy. *J Mater Chem B.* (2015) 3:8939–48. doi: 10.1039/C5TB01866H
334. Van Der Geest KSM, Wolfe K, Borg F, Sebastian A, Kayani A, Tomelleri A, et al. Ultrasonographic Halo Score in giant cell arteritis: association with intimal hyperplasia and ischaemic sight loss. *Rheumatology.* (2021) 60:4361–6. doi: 10.1093/rheumatology/keaa806
335. Langford CA, Cuthbertson D, Ytterberg SR, Khalidi N, Monach PA, Carette S, et al. A randomized, double-blind trial of abatacept (CTLA-4Ig) for the treatment of giant cell arteritis. *Arthritis Rheumatol.* (2017) 69:837–45. doi: 10.1002/art.40044
336. Toussirot E, Michaud M, Wendling D, Devauchelle V. Abatacept as adjunctive therapy in refractory polymyalgia rheumatica. *J Rheumatol.* (2021) 48:1888–9. doi: 10.3899/jrheum.210455
337. Goodfellow N, Morlet J, Singh S, Sabokbar A, Hutchings A, Sharma V, et al. Is vascular endothelial growth factor a useful biomarker in giant cell arteritis? *RMD Open.* (2017) 3:e000353. doi: 10.1136/rmdopen-2016-000353
338. Van Der Geest KSM, Abdulahad WH, Chalan P, Rutgers A, Horst G, Huitema MG, et al. Disturbed B cell homeostasis in newly diagnosed giant cell arteritis and polymyalgia rheumatica. *Arthritis Rheumatol.* (2014) 66:1927–38. doi: 10.1002/art.38625
339. Olafsen T, Betting D, Kenanova VE, Salazar FB, Clarke P, Said J, et al. Recombinant anti-CD20 antibody fragments for small-animal PET imaging of B-cell lymphomas. *J Nucl Med.* (2009) 50:1500–8. doi: 10.2967/jnumed.108.060426
340. Olafsen T, Sirk SJ, Betting DJ, Kenanova VE, Bauer KB, Ladno W, et al. ImmunoPET imaging of B-cell lymphoma using 124I-anti-CD20 scFv dimers (diabodies). *Protein Eng Des Sel.* (2010) 23:243–9. doi: 10.1093/protein/gzp081
341. Tran L, Huitema ADR, Van Rijswijk MH, Dinant HJ, Baars JW, Beijnen JH, et al. CD20 antigen imaging with ^{124}I-rituximab PET/CT in patients with rheumatoid arthritis. *Hum Antibodies.* (2011) 20:29–35. doi: 10.3233/HAB-2011-0239
342. Tran L, Vogel W V, Sinaasappel M, Muller S, Baars JW, Van Rijswijk M, et al. The pharmacokinetics of ^{124}I-rituximab in patients with rheumatoid arthritis. *Hum Antibodies.* (2011) 20:7–14. doi: 10.3233/HAB-2011-0237
343. Natarajan A, Habte F, Liu H, Sathirachinda A, Hu X, Cheng Z, et al. Evaluation of 89Zr-rituximab tracer by Cerenkov luminescence imaging and correlation with PET in a humanized transgenic mouse model to image NHL. *Mol Imaging Biol.* (2013) 15:468–75. doi: 10.1007/s11307-013-0624-0
344. Muylle K, Flamen P, Vugts DJ, Guiot T, Ghanem G, Meuleman N, et al. Tumour targeting and radiation dose of radioimmunotherapy with (90)Y-rituximab in CD20+ B-cell lymphoma as predicted by (89)Zr-rituximab immuno-PET: impact of preloading with unlabelled rituximab. *Eur J Nucl Med Mol Imaging.* (2015) 42:1304–14. doi: 10.1007/s00259-015-3025-6
345. de Jong A, Mous R, van Dongen GAMS, Hoekstra OS, Nievelstein RAJ, de Keizer B. (89) Zr-rituximab PET/CT to detect neurolymphomatosis. *Am J Hematol.* (2016) 91:649–50. doi: 10.1002/ajh.24328
346. Natarajan A, Gambhir SS. Radiation dosimetry study of [(89)Zr]rituximab tracer for clinical translation of B cell NHL imaging using positron emission tomography. *Mol Imaging Biol.* (2015) 17:539–47. doi: 10.1007/s11307-014-0810-8
347. Jauw YWS, Zijlstra JM, De Jong D, Vugts DJ, Zweegman S, Hoekstra OS, et al. Performance of 89Zr-labeled-rituximab-PET as an imaging biomarker to assess CD20 targeting: a pilot study in patients with relapsed/refractory diffuse large B cell lymphoma. *PLoS ONE.* (2017) 12:e0169828. doi: 10.1371/journal.pone.0169828
348. Bruijnen S, Tsang-A-Sjoe M, Raterman H, Ramwadhdoebe T, Vugts D, van Dongen G, et al. B-cell imaging with zirconium-89 labelled rituximab PET-CT at baseline is associated with therapeutic response 24weeks after initiation of rituximab treatment in rheumatoid arthritis patients. *Arthritis Res Ther.* (2016) 18:266. doi: 10.1186/s13075-016-1166-z
349. Natarajan A, Arksey N, Iagaru A, Chin FT, Gambhir SS. Validation of 64Cu-DOTA-rituximab injection preparation under good manufacturing practices: a PET tracer for imaging of B-cell non-Hodgkin lymphoma. *Mol Imaging.* (2015) 14:1–11. doi: 10.2310/7290.2014.00055
350. Natarajan A, Gowrishankar G, Nielsen CH, Wang S, Iagaru A, Goris ML, et al. Positron emission tomography of 64Cu-DOTA-Rituximab in a transgenic mouse model expressing human CD20 for clinical translation to image NHL. *Mol imaging Biol.* (2012) 14:608–16. doi: 10.1007/s11307-011-0537-8
351. Natarajan A, Hackel BJ, Gambhir SS. A novel engineered anti-CD20 tracer enables early time PET imaging in a humanized transgenic mouse model of B-cell non-Hodgkins lymphoma. *Clin Cancer Res.* (2013) 19:6820–9. doi: 10.1158/1078-0432.CCR-13-0626
352. Zettlitz KA, Tavaré R, Tsai WTK, Yamada RE, Ha NS, Collins J, et al. 18 F-labeled anti-human CD20 cys-diabody for same-day immunoPET in a model of aggressive B cell lymphoma in human CD20 transgenic mice. *Eur J Nucl Med Mol Imaging.* (2019) 46:489–500. doi: 10.1007/s00259-018-4214-x
353. Zettlitz KA, Tavaré R, Knowles SM, Steward KK, Timmerman JM, Wu AM. ImmunoPET of malignant and normal B cells with 89Zr- and 124I-labeled obinutuzumab antibody fragments reveals differential CD20 internalization *in vivo*. *Clin Cancer Res.* (2017) 23:7242. doi: 10.1158/1078-0432.CCR-17-0855
354. Bhatia A, Ell PJ, Edwards JCW. Anti-CD20 monoclonal antibody (rituximab) as an adjunct in the treatment of giant cell arteritis. *Ann Rheum Dis.* (2005) 64:1099–100. doi: 10.1136/ard.2005.036533
355. Li M, Younis MH, Zhang Y, Cai W, Lan X. Clinical summary of fibroblast activation protein inhibitor-based radiopharmaceuticals: cancer and beyond. *Eur J Nucl Med Mol Imaging.* (2022). doi: 10.1007/s00259-022-05706-y. [Epub ahead of print].
356. Meletta R, Herde AM, Chiotellis A, Isa M, Rancic Z, Borel N, et al. Evaluation of the radiolabeled boronic acid-based FAP inhibitor MIP-1232 for atherosclerotic plaque imaging. *Molecules.* (2015) 20:2081–99. doi: 10.3390/molecules20022081
357. Lindner T, Loktev A, Altmann A, Giesel F, Kratochwil C, Debus J, et al. Development of quinoline-based theranostic ligands for the targeting of fibroblast activation protein. *J Nucl Med.* (2018) 59:1415–22. doi: 10.2967/jnumed.118.210443
358. Moon ES, Elvas F, Vliegen G, De Lombaerde S, Vangestel C, De Bruycker S, et al. Targeting fibroblast activation protein (FAP): next generation PET radiotracers using squaramide coupled bifunctional DOTA and DATA 5m chelators. *EJNMMI Radiopharm Chem.* (2020) 5:19. doi: 10.1186/s41181-020-00102-z
359. Ballal S, Yadav MP, Moon ES, Kramer VS, Roesch F, Kumari S, et al. Biodistribution, pharmacokinetics, dosimetry of [68 Ga]Ga-DOTASAFAPi, and the head-to-head comparison with [18 F]F-FDG PET/CT in patients with various cancers. *Eur J Nucl Med Mol Imaging.* (2021) 48:1915–31. doi: 10.1007/s00259-020-05132-y
360. Wang G, Jin X, Zhu H, Wang S, Ding J, Zhang Y, et al. 68 Ga-NOTA-FAPI-04 PET/CT in a patient with primary gastric diffuse large B cell lymphoma: comparisons with [18 F] FDG PET/CT. *Eur J Nucl Med Mol Imaging.* (2021) 48:647–8. doi: 10.1007/s00259-020-04946-0
361. Loktev A, Lindner T, Burger EM, Altmann A, Giesel F, Kratochwil C, et al. Development of fibroblast activation protein-targeted radiotracers with improved tumor retention. *J Nucl Med.* (2019) 60:1421–9. doi: 10.2967/jnumed.118.224469
362. Xu M, Zhang P, Ding J, Chen J, Huo L, Liu Z. Albumin binder-conjugated fibroblast activation protein inhibitor radiopharmaceuticals for cancer therapy. *J Nucl Med.* (2021). doi: 10.2967/jnumed.121.262533
363. Zhang P, Xu M, Ding J, Chen J, Zhang T, Huo L, Liu Z. Fatty acid-conjugated radiopharmaceuticals for fibroblast activation protein-targeted radiotherapy. *Eur J Nucl Med Mol Imaging.* (2021). doi: 10.1007/s00259-021-05591-x. [Epub ahead of print].
364. Lin JJ, Chuang CP, Lin JY, Huang FT, Huang CW. Rational design, pharmacomodulation, and synthesis of [68 Ga]Ga-Alb-FAPtp-01, a selective tumor-associated fibroblast activation protein tracer for PET imaging of glioma. *ACS Sensors.* (2021) 6:3424–35. doi: 10.1021/acssensors.1c01316
365. Zhao L, Niu B, Fang J, Pang Y, Li S, Xie C, et al. Synthesis, preclinical evaluation, and a pilot clinical PET imaging study of 68 Ga-labeled FAPI dimer. *J Nucl Med.* (2021) 49:1985–96. doi: 10.2967/jnumed.121.263016
366. Toms J, Kogler J, Maschauer S, Daniel C, Schmidkonz C, Kuwert T, et al. Targeting fibroblast activation protein: radiosynthesis and preclinical evaluation of an 18 F-labeled FAP inhibitor. *J Nucl Med.* (2020) 61:1806–13. doi: 10.2967/jnumed.120.242958

367. Wang S, Zhou X, Xu X, Ding J, Liu S, Hou X, et al. Clinical translational evaluation of Al 18 F-NOTA-FAPI for fibroblast activation protein-targeted tumour imaging. *Eur J Nucl Med Mol Imaging.* (2021) 48:4259–71. doi: 10.1007/s00259-021-05470-5
368. Hicks RJ, Roselt PJ, Kallur KG, Tothill RW, Mileshkin L, FAPI. PET/CT: will it end the hegemony of 18F-FDG in oncology? *J Nucl Med.* (2021) 62:296–302. doi: 10.2967/jnumed.120.256271
369. Dorst DN, Rijpkema M, Buitinga M, Walgreen B, Helsen MMA, Brennan E, et al. Targeting of fibroblast activation protein in rheumatoid arthritis patients: imaging and *ex vivo* photodynamic therapy. *Rheumatology.* (2021). doi: 10.1093/rheumatology/keab664. [Epub ahead of print].
370. Nahrendorf M, Keliher E, Panizzi P, Zhang H, Hembrador S, Figueiredo JL, et al. 18F-4V for PET-CT imaging of VCAM-1 expression in atherosclerosis. *JACC Cardiovasc Imaging.* (2009) 2:1213–22. doi: 10.1016/j.jcmg.2009.04.016
371. Bala G, Blykers A, Xavier C, Descamps B, Broisat A, Ghezzi C, et al. Targeting of vascular cell adhesion molecule-1 by 18F-labelled nanobodies for PET/CT imaging of inflamed atherosclerotic plaques. *Eur Hear journal Cardiovasc Imaging.* (2016) 17:1001–8. doi: 10.1093/ehjci/jev346
372. Zhang X, Liu C, Hu F, Zhang Y, Wang J, Gao Y, et al. Imaging of VCAM-1 expression and monitoring therapy response in tumor with a 68 Ga-labeled single chain variable fragment. *Mol Pharm.* (2018) 15:609–18. doi: 10.1021/acs.molpharmaceut.7b00961
373. Pastorino S, Baldassari S, Ailuno G, Zuccari G, Drava G, Petretto A, et al. Two novel PET radiopharmaceuticals for endothelial vascular cell adhesion molecule-1 (VCAM-1) Targeting. *Pharmaceutics.* (2021) 13:1025. doi: 10.3390/pharmaceutics13071025
374. Golestani R, Mirfeizi L, Zeebregts CJ, Westra J, de Haas HJ, Glaudemans AWJM, et al. Feasibility of [18F]-RGD for ex vivo imaging of atherosclerosis in detection of αvβ3 integrin expression. *J Nucl Cardiol.* (2015) 22:1179–86. doi: 10.1007/s12350-014-0061-8
375. Ebenhan T, Kleynhans J, Zeevaart JR, Jeong JM, Sathekge M. Non-oncological applications of RGD-based single-photon emission tomography and positron emission tomography agents. *Eur J Nucl Med Mol Imaging.* (2021) 48:1414–33. doi: 10.1007/s00259-020-04975-9
376. Liolios C, Sachpekidis C, Kolocouris A, Dimitrakopoulou-Strauss A, Bouziotis P. PET diagnostic molecules utilizing multimeric cyclic RGD peptide analogs for imaging integrin αvβ3 receptors. *Molecules.* (2021) 26:1792. doi: 10.3390/molecules26061792
377. Hoshiga M, Alpers CE, Smith LL, Giachelli CM, Schwartz SM. αvβ3 integrin expression in normal and atherosclerotic artery. *Circ Res.* (1995) 77:1129–35. doi: 10.1161/01.RES.77.6.1129
378. Beer AJ, Pelisek J, Heider P, Saraste A, Reeps C, Metz S, et al. PET/CT imaging of integrin αvβ3 expression in human carotid atherosclerosis. *JACC Cardiovasc Imaging.* (2014) 7:178–87. doi: 10.1016/j.jcmg.2013.12.003
379. Steiger K, Quigley NG, Groll T, Richter F, Zierke MA, Beer AJ, et al. There is a world beyond αvβ3-integrin: Multimeric ligands for imaging of the integrin subtypes αvβ6, αvβ8, αvβ3, and α5β1 by positron emission tomography. *EJNMMI Res.* (2021) 11:106. doi: 10.1186/s13550-021-00842-2
380. Iqbal N, Iqbal N. Human epidermal growth factor receptor 2 (HER2) in cancers: overexpression and therapeutic implications. *Mol Biol Int.* (2014) 2014:1–9. doi: 10.1155/2014/852748
381. Tamura K, Kurihara H, Yonemori K, Tsuda H, Suzuki J, Kono Y, et al. 64Cu-DOTA-trastuzumab PET imaging in patients with HER2-positive breast cancer. *J Nucl Med.* (2013) 54:1869–75. doi: 10.2967/jnumed.112.118612
382. Baum RP, Prasad V, Müller D, Schuchardt C, Orlova A, Wennborg A, et al. Molecular imaging of HER2-expressing malignant tumors in breast cancer patients using synthetic 111In- or 68Ga-labeled affibody molecules. *J Nucl Med.* (2010) 51:892–7. doi: 10.2967/jnumed.109.073239
383. Dijkers EC, Oude Munnink TH, Kosterink JG, Brouwers AH, Jager PL, De Jong JR, et al. Biodistribution of 89Zr-trastuzumab and PET imaging of HER2-positive lesions in patients with metastatic breast cancer. *Clin Pharmacol Ther.* (2010) 87:586–92. doi: 10.1038/clpt.2010.12
384. Gebhart G, Lamberts LE, Wimana Z, Garcia C, Emonts P, Ameye L, et al. Molecular imaging as a tool to investigate heterogeneity of advanced HER2-positive breast cancer and to predict patient outcome under trastuzumab emtansine (T-DM1): the ZEPHIR trial. *Ann Oncol.* (2016) 27:619–24. doi: 10.1093/annonc/mdv577
385. Pereira PMR, Norfleet J, Lewis JS, Escorcia FE. Immuno-PET detects changes in multi-RTK tumor cell expression levels in response to targeted kinase inhibition. *J Nucl Med.* (2021) 62:366. doi: 10.2967/jnumed.120.244897
386. Veronese M, Santangelo B, Jauhar S, D'Ambrosio E, Demjaha A, Salimbeni H, et al. A potential biomarker for treatment stratification in psychosis: evaluation of an [18F] FDOPA PET imaging approach. *Neuropsychopharmacol.* (2020) 46:1122–32. doi: 10.1038/s41386-020-00866-7
387. van der Geest KSM, Sandovici M, van Sleen Y, Sanders JS, Bos NA, Abdulahad WH, et al. Review: what is the current evidence for disease subsets in giant cell arteritis? *Arthritis Rheumatol.* (2018) 70:1366. doi: 10.1002/art.40520
388. Signore A, Annovazzi A, Barone R, Bonanno E, D'Alessandria C, Chianelli M, et al. 99mTc-interleukin-2 scintigraphy as a potential tool for evaluating tumor-infiltrating lymphocytes in melanoma lesions: a validation study. *J Nucl Med.* (2004) 45:1647–52.
389. van Sleen Y, Sandovici M, Abdulahad WH, Bijzet J, van der Geest KSM, Boots AMH, et al. Markers of angiogenesis and macrophage products for predicting disease course and monitoring vascular inflammation in giant cell arteritis. *Rheumatology.* (2019) 58:1383–92. doi: 10.1093/rheumatology/kez034
390. Cid MC, Unizony SH, Blockmans D, Brouwer E, Dagna L, Dasgupta B, et al. Efficacy and safety of mavrilimumab in giant cell arteritis: a phase 2, randomised, double-blind, placebo-controlled trial. *Ann Rheum Dis.* (2022) 81:653–61. doi: 10.1136/annrheumdis-2021-221865
391. Eichendorff S, Svendsen P, Bender D, Keiding S, Christensen EI, Deleuran B, et al. Biodistribution and PET imaging of a novel [68Ga]-anti-CD163-antibody conjugate in rats with collagen-induced arthritis and in controls. *Mol Imaging Biol.* (2015) 17:87–93. doi: 10.1007/s11307-014-0768-6
392. Fu R, Carroll L, Yahioglu G, Aboagye EO, Miller PW. Antibody fragment and affibody immunoPET imaging agents: radiolabelling strategies and applications. *ChemMedChem.* (2018) 13:2466. doi: 10.1002/cmdc.201800624
393. Debie P, Devoogdt N, Hernot S. Targeted nanobody-based molecular tracers for nuclear imaging and image-guided surgery. *Antibodies.* (2019) 8:12. doi: 10.3390/antib8010012
394. Pascali G, Matesic L. How Far Are We from Dose On Demand of Short-Lived Radiopharmaceuticals? *Perspect Nucl Med Mol Diagnosis Integr Ther.* (2016) 79–92. doi: 10.1007/978-4-431-55894-1_6
395. Hansen SB, Bender D. Advancement in production of radiotracers. *Semin Nucl Med.* (2021) 52:266–75. doi: 10.1053/j.semnuclmed.2021.10.003

Conflict of Interest: KG has received a speaker fee from Roche paid to the UMCG. EB has received consultancy and speaker fees from Roche paid to the UMCG.

The remaining authors declare that the research was conducted in the absence of any commercial or financial relationships that could be construed as a potential conflict of interest.

Publisher's Note: All claims expressed in this article are solely those of the authors and do not necessarily represent those of their affiliated organizations, or those of the publisher, the editors and the reviewers. Any product that may be evaluated in this article, or claim that may be made by its manufacturer, is not guaranteed or endorsed by the publisher.

frontiers | Frontiers in Medicine

TYPE Brief Research Report
PUBLISHED 21 September 2022
DOI 10.3389/fmed.2022.1026944

OPEN ACCESS

EDITED BY
Giorgio Treglia,
Ente Ospedaliero Cantonale (EOC), Switzerland

REVIEWED BY
Xavier Palard-Novello,
University of Rennes 1, France
Annibale Versari,
IRCCS Local Health Authority of Reggio Emilia, Italy

*CORRESPONDENCE
Daniel Blockmans
Daniel.Blockmans@uzleuven.be

SPECIALTY SECTION
This article was submitted to Nuclear Medicine, a section of the journal Frontiers in Medicine

RECEIVED 24 August 2022
ACCEPTED 31 August 2022
PUBLISHED 21 September 2022

CITATION
Moreel L, Boeckxstaens L, Betrains A, Van Hemelen M, Vanderschueren S, Van Laere K and Blockmans D (2022) Diagnostic accuracy and validation of ^{18}F-fluorodeoxyglucose positron emission tomography scores in a large cohort of patients with polymyalgia rheumatica.
Front. Med. 9:1026944.
doi: 10.3389/fmed.2022.1026944

Diagnostic accuracy and validation of ^{18}F-fluorodeoxyglucose positron emission tomography scores in a large cohort of patients with polymyalgia rheumatica

Lien Moreel[1,2], Lennert Boeckxstaens[3], Albrecht Betrains[1,2], Maarten Van Hemelen[1], Steven Vanderschueren[1,2,4], Koen Van Laere[3,5] and Daniel Blockmans[1,2,4]*

[1]Department of General Internal Medicine, University Hospitals Leuven, Leuven, Belgium, [2]Department of Microbiology, Immunology, and Transplantation, KU Leuven, Leuven, Belgium, [3]Department of Nuclear Medicine, University Hospitals Leuven, Leuven, Belgium, [4]European Reference Network for Immunodeficiency, Autoinflammatory, Autoimmune and Pediatric Rheumatic Disease (ERN-RITA), Utrecht, Netherlands, [5]Department of Imaging and Pathology, Nuclear Medicine and Molecular Imaging, KU Leuven, Leuven, Belgium

Background: Several studies have shown that ^{18}F-FDG PET may contribute to the diagnosis of polymyalgia rheumatica (PMR). Previously, we developed a composite PET score called the Leuven score, which was recently adapted to the more concise Leuven/Groningen score by van der Geest et al. The aim of this study is to validate and compare the diagnostic accuracy and cut-off points of both scores in a large cohort of PMR patients.

Methods: Patients with a possible clinical diagnosis of PMR and a PET scan prior to the initiation of glucocorticoids between 2003 and 2020 were included retrospectively. The gold standard for the diagnosis of PMR was the judgment of two experienced clinicians after a follow-up of at least 6 months. FDG uptake was scored visually in 12 articular regions (scores 0–2) and a total skeletal score was calculated by summing the individual scores (maximum of 24 for the Leuven score and 14 for the Leuven/Groningen score). Receiver operating characteristic (ROC) analysis and the Youden index were used to determine the diagnostic accuracy and optimal cut-off points.

Results: A total of 162 patients with PMR and 83 control patients were included. Both PET scores showed high diagnostic accuracy in the ROC analysis (area under the curve 0.986 and 0.980, respectively). The Leuven Score provided a sensitivity of 91.4%, specificity of 97.6% and accuracy of 93.5% at its predefined cut-off point of 16. With the newly determined cut-off point of 12 the sensitivity was 98.8%, the specificity 95.2% and the accuracy 97.6%. The Leuven/Groningen score had a sensitivity, specificity and accuracy

of 93.2%, 95.2%, and 93.9%, respectively, with the pre-specified cut-off point of 8, and 96.9%, 92.8%, and 95.5% with the optimal cut-off point of 7.

Conclusion: The original Leuven score and the simplified Leuven/Groningen score both had excellent diagnostic accuracy. The latter may be easier to apply in clinical practice.

KEYWORDS

polymyalgia rheumatica (PMR), PET, diagnostic accuracy, validation, leuven score, Leuven/Groningen score

Introduction

Polymyalgia rheumatica (PMR) is a systemic inflammatory disease that affects elderly people. It is characterized by pain and morning stiffness in the neck, shoulders and pelvic girdle. It is commonly associated with constitutional symptoms and elevated inflammatory markers (1).

The diagnosis of PMR may be challenging, since there are no symptoms, laboratory abnormalities, or imaging findings specific for PMR. Other conditions, such as other musculoskeletal disorders, infectious disease and malignancy, should be ruled out. The 2012 EULAR/ACR criteria were developed for research and not for diagnostic purposes (2). In addition, the sensitivity and specificity of these criteria are quite low (68 and 78%, respectively).

Several studies have shown that ^{18}F-fluorodeoxyglucose (FDG) positron emission tomography (PET) may contribute to the diagnosis of PMR (3–6). FDG uptake is typically located at the shoulder and hip girdle, sternoclavicular joints, cervical and lumbar interspinous bursa, trochanteric bursa, and ischial tuberosities (4). Since individual sites do not provide sufficient diagnostic accuracy (7), several PET/CT algorithms (5, 8) and composite scores (4, 9–13) have been developed to determine when a PET/CT should be considered compatible with PMR. Direct comparison of 5 of these algorithms and composite scores (4, 5, 8, 11) showed that the Leuven Score, as reported by our group in 2018, had the best diagnostic accuracy with a sensitivity of 89.7% and specificity of 84.2% at the optimal cut-off point of 16 (14). Van der Geest et al. developed a more concise score, which is called the Leuven/Groningen score, based on the anatomic sites with an AUC $\geq$ 0.8 in ROC analysis (**Figure 1**) (14). This score provided a similar diagnostic accuracy with a sensitivity of 89.7% and specificity of 84.2% at the optimal cut-off point of 8.

In this study, we aim to validate and compare the diagnostic accuracy and cut-off points of the Leuven score and the Leuven/Groningen score in a large cohort of PMR patients.

Materials and methods

Patient population

We retrospectively included patients with a possible clinical diagnosis of PMR, who were evaluated by the Department of General Internal Medicine of the Leuven University Hospitals between 2003 and 2020 and had undergone PET imaging prior to the initiation of glucocorticoids. Patients with clinical symptoms of giant cell arteritis (GCA) or a positive temporal artery biopsy were excluded. Patients included in the study of Henckaerts et al., which were diagnosed between August 2012 and November 2015, were also excluded (4). The gold standard for the diagnosis of PMR was based on the judgment of two experienced clinicians (D.B. and S.V.) after at least 6 months of follow-up, considering all available information (clinical data, biochemical and radiological results, PET images, and evolution during follow-up).

The study was conducted in accordance with the Declaration of Helsinki and approved by the ethical committee of the University Hospitals Leuven. Informed consent was waived because of the retrospective nature of the study and the analysis used pseudonymized clinical data.

Data collection

We collected the following patient data from the electronic health record: age, sex, date of diagnosis, duration of symptoms until PET, clinical symptoms at diagnosis (fever [defined as temperature $\geq$38.3°C], anorexia, weight loss, morning stiffness, shoulder and pelvic girdle pain, neck and lower back pain, pain and swelling of peripheral joints), laboratory values (erythrocyte sedimentation rate [ESR; mm/h], C-reactive protein [CRP; mg/L], hemoglobin [g/dL] and alkaline phosphatase [U/L]), and final diagnosis.

Positron emission tomography imaging and analysis

Patients were required to fast for at least 6 h before intravenous injection of 4.5 MBq/kg of ^{18}F-FDG, and glycemia levels were determined in all patients (<140 mg/dl). A whole-body PET scan was performed 45–60 min after tracer administration. PET scans were performed between 2003 and 2020, consecutively acquired on a ECAT HR + PET camera, Hirez Biograph 16 PET/CT or Truepoint Biograph 40 PET/CT (Siemens, Knoxville, TN, USA). Because of scan duration, HR + data were not corrected for attenuation using transmission scanning. On the PET/CT systems, either a low-dose non-diagnostic CT scan or a diagnostic CT scan with oral and intravenous contrast was performed immediately before PET acquisition.

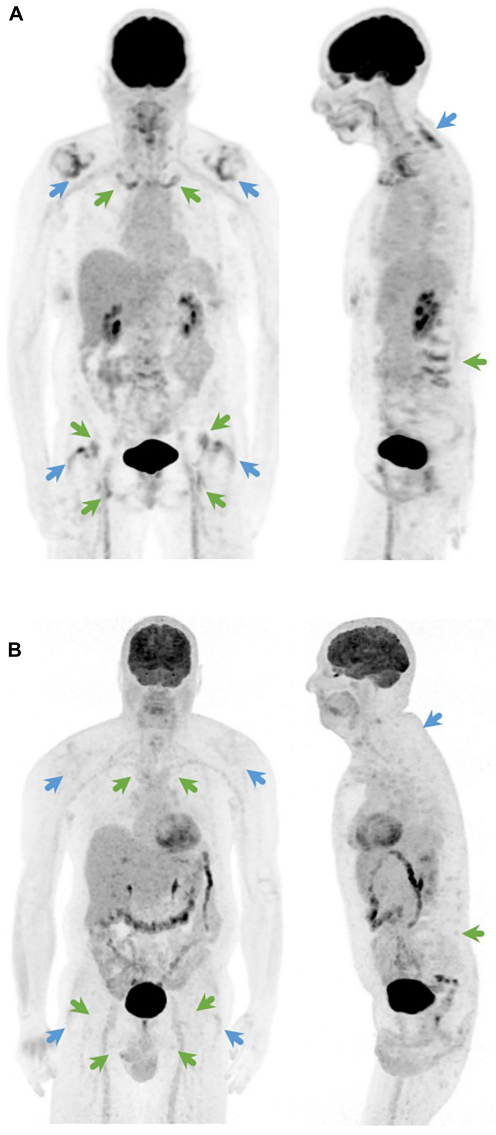

FIGURE 1
Coronal (left) and sagittal (right) ^{18}F-FDG-PET image of **(A)** a PMR patient with a Leuven score of 24 and a Leuven/Groningen score of 14 and **(B)** a patient with fibromyalgia as final diagnosis with a Leuven score of 3 and a Leuven/Groningen score of 1. The Leuven score is the sum of joints indicated by green and blue arrows. The Leuven/Groningen score is the sum of joints indicated only by green arrows.

Non-attenuation corrected (non-AC) PET images were available for all included patients and attenuation-corrected (AC) PET images were only available for the patients who were scanned with a PET/CT system (n = 119/245). PET data were corrected for scatter and randoms. Data were reconstructed using iterative OSEM reconstruction, with parameters optimized over the years (FWHM HR + 6–7 mm, for the Truepoint 5 mm).

Reconstructed PET images were re-evaluated visually by two independent specialists in nuclear medicine (K.V.L., L.B.), who were blinded for all other patient information. Both the non-AC PET images and the AC PET images were evaluated independently when available. To assess inter-reader reliability, PET images for the first 20 patients were evaluated by both specialists. The interrater agreement was assessed *via* the intra-class correlation coefficient (ICC) with a two-way mixed effects model. All other PET images were randomized and scored by one of both specialists only as interrater agreement was high in the sample set.

FDG PET uptake was visually assessed for 12 predefined skeletal regions (cervical spinous processes, lumbar spinous processes, left and right sternoclavicular joint, left and right ischial tuberosity, left and right greater trochanter, left and right hip, and left and right shoulder), and scored using a three-point scoring system: 0 (no elevated FDG uptake), 1 (moderately elevated FDG uptake, but less than mean liver uptake) or 2 (intense FDG uptake, equal or more than average liver uptake). The mean liver uptake is harder to assess in non-AC images as a radial non-linear gradient is present in the liver due to attenuation. The skeletal scores of the non-AC PET images and the AC PET images were compared if they were both available. The Leuven score was calculated for every patient, by summing the individual scores at the 12 different skeletal sites (total score of 0–24) (Figure 1). For the Leuven/Groningen score the scores for the lumbar spinous processes, sternoclavicular joints, ischial tuberosities and hips were summed with a total score ranging from 0 to 14.

Statistical analysis

Categorical and continuous variables were expressed as count (percentage) and median ± interquartile range (IQR), respectively. Chi square tests or Mann-Whitney *U*-tests were used to compare characteristics between PMR patients and patients in whom PMR was initially suspected, but who

TABLE 1 Baseline characteristics for the entire population.

Characteristics	Total (n = 245)	PMR (n = 162)	Non-PMR (n = 83)	P-value
Age at inclusion, years, median (IQR)	70 (60–76)	71 (63–77)	63 (56–75)	**0.001**
Sex, no. of females, n (%)	131 (53)	89 (55)	42 (51)	0.52
Symptom duration until PET/CT, weeks, median (IQR)	11.5 (5–25.75)[28]	10 (4.5–19)[16]	15 (6–41.5)[12]	**0.02**
Symptoms, n (%)				
○ Fever	34 (14)	21 (13)	13 (16)	0.56
○ Anorexia	73 (30)	46 (28)	27 (33)	0.50
○ Weight loss	85 (35)	61 (38)	24 (29)	0.17
• Amount of weight loss, kg, median (IQR)	6 (4–8)[9]	6 (4–8)[7]	6 (5–7)[2]	0.80
○ Morning stiffness	136 (83)[81]	102 (89)[47]	34 (69)[34]	**0.003**
• Duration, minutes, median (IQR)	60 (30–120)[59]	60 (30–120)[44]	60 (30–60)[15]	0.24
○ Shoulder pain	212 (87)	150 (93)	62 (75)	**0.0001**
○ Neck pain	63 (26)	45 (28)	18 (22)	0.30
○ Lower back pain	55 (22)	35 (22)	20 (24)	0.66
○ Pelvic girdle pain	188 (77)	133 (82)	55 (66)	**0.006**
○ Pain in peripheral joints	108 (44)	73 (45)	35 (42)	0.67
○ Swelling of peripheral joints	39 (16)	30 (19)	9 (11)	0.11
Laboratory values				
○ ESR, mm/h, median (IQR)	46 (29.75–66.25)[37]	47 (35.5–66.25)[14]	30.5 (14.75–66.25)[23]	**0.007**
○ CRP, mg/L, median (IQR	31.0 (9.325–67.975)[1]	36.0 (14.4–73.7)[1]	15.8 (2.55–60.95)	**0.0003**
○ Hemoglobin, g/dL, median (IQR)	12.65 (11.4–13.68)[7]	12.4 (11.3–13.5)[5]	13.0 (11.9–14.1)[2]	**0.03**
Alkaline phosphatase, U/L, median (IQR)	100.5 (76.25–184.75)[31]	134 (81.25–210.25)[28]	85.5 (69.75–119.25)[3]	<**0.0001**

CRP, C-reactive protein; ESR, erythrocyte sedimentation rate; IQR, interquartile range; n, number; no., number; PET/CT, positron emission tomography/computed tomography; PMR, polymyalgia rheumatica. Number of missing values are reported in superscript. The bolded p-values are the p-values that are significant.

received an alternative diagnosis after further tests and follow-up (further called "non-PMR patients"). The Leuven and Leuven/Groningen score were compared via the Mann-Whitney U-test. The sensitivity, specificity, accuracy, positive and negative likelihood ratio (LR) of the Leuven score and the Leuven/Groningen score were calculated for different cut-off values and plotted in a receiver operating characteristic (ROC) curve. The optimal cut-off value was determined by the Youden index (formula sensitivity + specificity–1). We did a sensitivity analysis excluding patients with only non-AC PET images. All statistical tests were performed using 2-tailed tests with significance set at the $p < 0.05$ level. Statistical analysis was performed in R Studio (version 2022.03.10, The R Foundation for Statistical Computing) with inclusion of the *psych*, *epiR*, *ggplot*, and p*ROC* packages.

Results

A total of 245 patients were included in this study, of which 162 had a diagnosis of PMR and 83 received an alternative diagnosis (**Supplementary Table 1**). PET contributed to the alternative diagnosis in 8 non-PMR patients (9.6%): a paraneoplastic syndrome in 4 patients and dermatomyositis, polyarteritis nodosa, cholangitis and a liver abscess in one patient each.

The baseline characteristics are presented in **Table 1**. PMR patients were older compared to non-PMR patients (71 vs. 63 years, $p = 0.001$), but had a similar female to male ratio (55 vs. 51% female patients, $p = 0.52$). The symptom duration was significantly shorter in PMR patients (10 vs. 15 weeks, $p = 0.02$). PMR patients more frequently reported morning stiffness (89 vs. 69%, $p = 0.003$) and pelvic (82 vs. 66%, $p = 0.006$) and shoulder girdle pain (93 vs. 75%, $p = 0.0001$). There were no significant differences in neck and lower back pain, in pain and swelling of peripheral joints and in constitutional symptoms. ESR (47 vs. 31 mm/h, $p = 0.007$), CRP (36.0 vs. 15.8 mg/L, $p = 0.0003$) and alkaline phosphatase (134 vs. 86 U/L, $p < 0.0001$) were significantly higher in PMR patients compared to non-PMR patients. Hemoglobin was significantly lower (12.4 vs. 13.0 g/dL, $p = 0.03$).

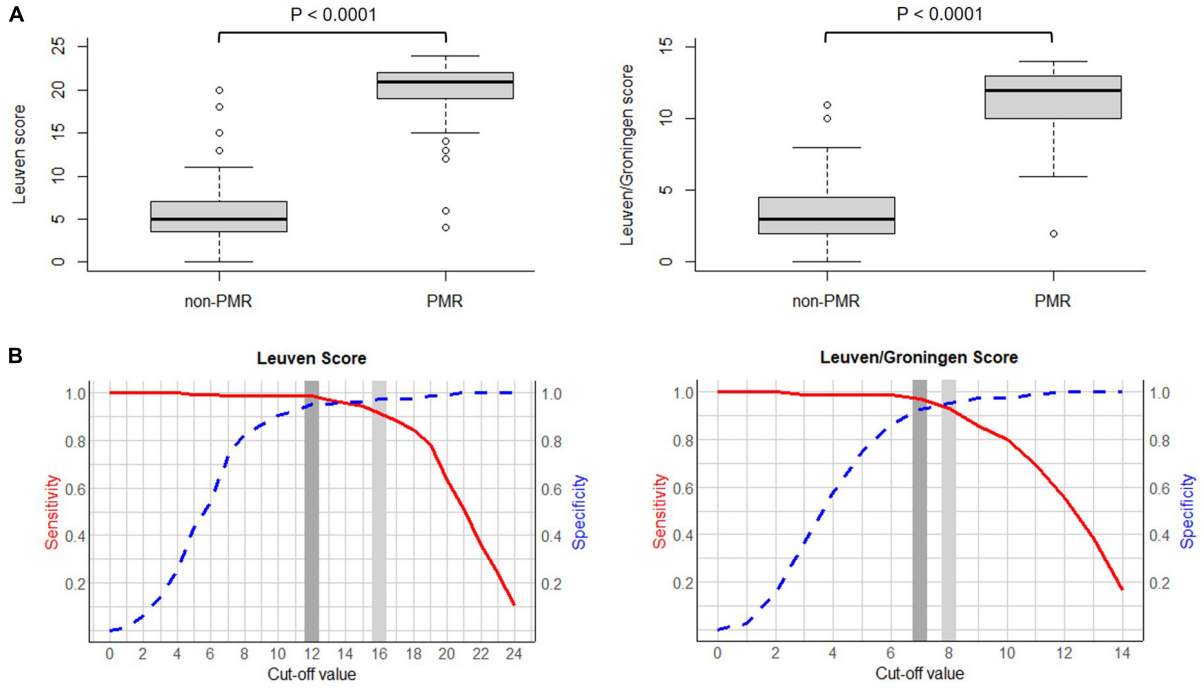

FIGURE 2
(A) Boxplot of the Leuven score (left) and the Leuven/Groningen score (right) in PMR patients vs. non-PMR patients. **(B)** Curve of the sensitivity and specificity of the Leuven score (left) and the Leuven/Groningen score (right) with variable cut-offs. Legend: light gray, predetermined cut-off value; dark gray, optimal cut-off value determined by the Youden index. Abbreviations: PMR, polymyalgia rheumatica.

When considering all joints involved, FDG uptake was more frequently symmetrical in PMR patients compared to non-PMR patients (43.8 vs. 14.5%, $p < 0.0001$) (**Supplementary Table 2**). Also in each joint separately the FDG uptake was significantly more often symmetrical.

The Leuven and Leuven/Groningen scores showed excellent interrater agreement (ICC 0.90 and 0.88, respectively). Both the Leuven and the Leuven/Groningen scores were significantly higher in PMR patients compared to non-PMR patients (21 [IQR 19–22] vs. 5 [IQR 3.5–7], $p < 0.0001$ and 12 [IQR 10–13] vs. 3 [IQR 2–4.5], $p < 0.0001$, respectively) (**Figure 2**). Both scores had an excellent and comparable diagnostic accuracy in the ROC analysis (AUC 0.986 [95% CI 0.971–1.000] and 0.980 [95% CI 0.963–0.997], respectively) (**Table 2** and **Figure 2** and **Supplementary Figure 1**). The *Leuven score* provided a sensitivity of 91.4% [95% CI 85.9–95.2%], a specificity of 97.6% [95% CI 91.6–99.7%] and an accuracy of 93.5% [95% CI 89.6–96.2%] at its predefined cut-off point of 16 with a positive LR of 37.9 [95% CI 9.6–149.2] and a negative LR of 0.09 [95% CI 0.05–0.15]. Based on the current cohort, the optimal cut-off point determined by the Youden index was 12. With this cut-off point, the sensitivity, specificity, accuracy, positive and negative LR were 98.8% [95% CI 95.6–99.9%], 95.2% [95% CI 88.1–98.7%], 97.6% [95% CI 95% CI 94.7–99.1%], 20.5 [95% CI 7.9–53.3], and 0.01 [95% CI 0.003–0.05], respectively. Four non-PMR patients had a Leuven score above the cut-off of 12: rotator cuff tendinopathy, rotator cuff tendinopathy combined with osteoarthritis of the lower back, systemic lupus erythematosus and Whipple's disease in one patient each. The *Leuven/Groningen* score had a sensitivity of 93.2% [95% CI 88.2–96.6%], specificity of 95.2% [95% CI 88.1–98.7%], and accuracy of 93.9% [95% CI 90.1–96.5%] at its pre-specified cut-off point of 8 with a positive LR of 19.3 [95% CI 7.4–50.4] and a negative LR of 0.07 [95% CI 0.04–0.13]. The optimal cut-off point determined by the Youden index was 7 in the current cohort. With this cut-off point, the sensitivity, specificity, accuracy, positive and negative LR were 96.9% [95% CI 92.9–99.0%], 92.8% [95% CI 84.9–97.3%], 95.5% [95% CI 92.1–97.7%], 13.4 [95% CI 6.2–29.0], and 0.03 [95% CI 0.01–0.08]. Six non-PMR patients had a score of 7 or more with the following diagnoses: rotator cuff tendinopathy, systemic lupus erythematosus, Whipple's disease, osteoarthritis, fibromyalgia and infection-related arthralgia in one patient each. A sensitivity analysis excluding patients with only non-AC images yielded similar results (**Supplementary Table 3**).

Discussion

This is the first study to compare and validate the diagnostic accuracy of the Leuven score and the Leuven/Groningen score

TABLE 2 Diagnostic accuracy of Leuven and Leuven/Groningen score.

Score	Sensitivity (95% CI)	Specificity (95% CI)	Accuracy (95% CI)	LR + (95% CI)	LR- (95% CI)	AUC (95% CI)
Leuven score						
Cut-off 16	91.4% (85.9–95.2%)	97.6% (91.6–99.7%)	93.5% (89.6–96.2%)	37.9 (9.6–149.2)	0.09 (0.05–0.15)	0.986 (0.971–1.000)
Cut-off 12	98.8% (95.6–99.9%)	95.2% (88.1–98.7%)	97.6% (94.7–99.1%)	20.5 (7.9–53.3)	0.01 (0.003–0.05)	
Leuven/Groningen score						
Cut-off 8	93.2% (88.2–96.6%)	95.2% (88.1–98.7%)	93.9% (90.1–96.5%)	19.3 (7.4–50.4)	0.07 (0.04–0.13)	0.980 (0.963–0.997)
Cut-off 7	96.9% (92.9–99.0%)	92.8% (84.9–97.3%)	95.5% (92.1–97.7%)	13.4 (6.2–29.0)	0.03 (0.01–0.08)	

95% CI, 95% confidence interval. AUC, area under the curve; LR, likelihood ratio.

for the diagnosis of PMR in a large real-life cohort. Our group developed the Leuven score in 2018 and found a sensitivity of 85.1% and specificity of 87.5% at a cut-off point of 16 (4). The retrospective study of van der Geest et al., in which several PET algorithms and scores were compared, yielded a comparable diagnostic accuracy of the Leuven score with a sensitivity of 89.7% and a specificity of 84.2% at the same cut-off point (14). In this study, we observed a higher diagnostic accuracy with a sensitivity of 91.4% and a specificity of 97.6%. Van der Geest et al. adapted the Leuven score to a more concise score, which provided a sensitivity of 89.7% and a specificity of 84.2% at the optimal cut-off point of 8 (14). This study confirms these findings with a sensitivity of 93.2% and a specificity of 95.2% for the Leuven/Groningen score. Thus, we found an excellent and comparable diagnostic accuracy for both scores with AUC 0.986 and 0.980, respectively, which are the best diagnostic accuracy results for a PET algorithm or score for PMR reported to date. However, we mainly want to emphasize the comparable performance of the Leuven and the Leuven/Groningen score. Since the Leuven/Groningen score only requires evaluation of 7 anatomic sites instead of 12, it may be easier to implement and apply in routine clinical practice.

Since this cohort is much larger than the studies in which the Leuven score and the Leuven/Groningen score were developed (99 and 58 patients, respectively) (4, 14), we determined the optimal cut-off points in the current cohort. We found an optimal cut-off point of 12 and 7, respectively, which were both lower than the initial cut-off points. This resulted in a sensitivity and specificity of 98.8% and 95.2% for the Leuven score and 96.9% and 92.8% for the Leuven/Groningen score, respectively. The predefined and newly determined cut-off points should ideally be compared in a large prospective cohort to determine the definitive cut-off. Several cut-off points may be applied depending on the preference for a higher sensitivity or specificity. All cut-off points between 10 and 16 for the Leuven score and a cut-off point of 7 or 8 for the Leuven/Groningen score had a sensitivity and specificity for PMR over 90%.

In this study, PMR patients were significantly older and had a more pronounced inflammatory response. The symptom duration was longer in non-PMR patients probably due to a considerable amount of patients with a mechanical cause in this group. PMR patients more frequently reported shoulder and pelvic girdle pain and morning stiffness. In addition, we observed more frequently a symmetrical articular and periarticular FDG uptake in PMR patients compared to non-PMR patients. Since the diagnostic accuracy of the Leuven and Leuven/Groningen score is already excellent, consideration of the symmetry would make the scores more complex without a large increase in diagnostic yield.

This study confirms that FDG-PET may be an excellent diagnostic tool for PMR. Additionally, FDG-PET may contribute to the diagnosis of common mimics of PMR. In our cohort, PET revealed an alternative diagnosis in 8 of the 83 (9.6%) non-PMR patients.

Strengths of our study include the large cohort, a control group consisting of patients with PMR-like disorders who had a similar clinical presentation, the fact that PET imaging was performed prior to the initiation of glucocorticoids and the assessment of interrater agreement. This study also has several limitations. First, part of the FDG-PET scans were performed on a stand-alone PET system with lower resolution and sensitivity compared with current PET-CT systems. In addition, PET images without CT-scan preclude attenuation correction, so the mean liver uptake is an assessment by the reader. However, sensitivity analysis excluding these PET scans found similar results. Second, the interrater agreement was only assessed in the first 20 patients. Third, we did not assess PET images quantitatively as we aimed to validate the Leuven and the Leuven/Groningen score. These scores used a semi-quantitative method with visual scores intended for application in clinical practice. Compared to quantitative methods, they require less experience and are less time-consuming. In addition, selection bias due to the retrospective design could have potentially influenced the results. Fifth, the clinicians responsible for the diagnosis of PMR had access to the PET images, since it was performed as part of routine clinical practice. This could result in circular reasoning and increased diagnostic accuracy. However, PMR-PET scores were not specified in the PET report and the final diagnosis was based on all available diagnostic information. In addition, the two nuclear specialists who re-evaluated the PET images, were blinded for all patient information. Finally, since all patients were diagnosed and

followed in a general internal medicine department, the non-PMR group contained only a limited number of patients with rheumatic diseases, which could explain the high specificity of the Leuven and Leuven/Groningen score.

In conclusion, the Leuven score and the Leuven/Groningen score provided an excellent and comparable diagnostic accuracy in a real-life cohort. Due to the lower number of anatomic sites that needs to be evaluated, the Leuven/Groningen score may be easier to apply in clinical practice. The optimal cut-off points were 12 for the Leuven score and 7 for the Leuven/Groningen score, but require further validation in a large prospective cohort. Further imaging studies should address if these scores can be used for disease monitoring.

Data availability statement

The raw data supporting the conclusions of this article will be made available by the authors, without undue reservation.

Ethics statement

The studies involving human participants were reviewed and approved by the Ethical Committee of the University Hospitals Leuven. Written informed consent for participation was not required for this study in accordance with the national legislation and the institutional requirements.

Author contributions

LM: conceptualization, methodology, validation, investigation, formal analysis, writing – original draft, writing – review and editing, and visualization. LB: conceptualization, methodology, validation, investigation, and writing – review and editing. AB and KV: conceptualization, methodology, investigation, and writing – review and editing. MV: investigation and writing – review and editing. SV and DB: conceptualization, writing – review and editing, and supervision. All authors contributed to the article and approved the submitted version.

Conflict of interest

The authors declare that the research was conducted in the absence of any commercial or financial relationships that could be construed as a potential conflict of interest.

Publisher's note

All claims expressed in this article are solely those of the authors and do not necessarily represent those of their affiliated organizations, or those of the publisher, the editors and the reviewers. Any product that may be evaluated in this article, or claim that may be made by its manufacturer, is not guaranteed or endorsed by the publisher.

Supplementary material

The Supplementary Material for this article can be found online at: https://www.frontiersin.org/articles/10.3389/fmed.2022.1026944/full#supplementary-material

References

1. Buttgereit F, Dejaco C, Matteson EL, Dasgupta B. Polymyalgia rheumatica and giant cell arteritis: a systematic review. *JAMA*. (2016) 315:2442–58. doi: 10.1001/jama.2016.5444

2. Dasgupta B, Cimmino MA, Kremers HM, Schmidt WA, Schirmer M, Salvarani C, et al. 2012 Provisional classification criteria for polymyalgia rheumatica: a European league against rheumatism/American college of rheumatology collaborative initiative. *Arthritis Rheum.* (2012) 64:943–54. doi: 10.1002/art.34356

3. Camellino D, Paparo F, Morbelli S, Cutolo M, Sambuceti G, Cimmino MA. Interspinous bursitis is common in polymyalgia rheumatica, but is not associated with spinal pain. *Arthritis Res Ther.* (2014) 16:492. doi: 10.1186/s13075-015-0620-7

4. Henckaerts L, Gheysens O, Vanderschueren S, Goffin K, Blockmans D. Use of 18f-fluorodeoxyglucose positron emission tomography in the diagnosis of polymyalgia rheumatica — A prospective study of 99 patients. *Rheumatology.* (2018) 57:1908–16. doi: 10.1093/rheumatology/kex376

5. Owen CE, Poon AMT, Yang V, McMaster C, Lee ST, Liew DFL, et al. Abnormalities at three musculoskeletal sites on whole-body positron emission tomography/computed tomography can diagnose polymyalgia rheumatica with high sensitivity and specificity. *Eur J Nucl Med Mol Imaging.* (2020) 47:2461–8. doi: 10.1007/s00259-020-04731-z

6. Palard-Novello X, Querellou S, Gouillou M, Saraux A, Marhadour T, Garrigues F, et al. Value of 18F-FDG PET/CT for therapeutic assessment of patients with polymyalgia rheumatica receiving tocilizumab as first-line treatment. *Eur J Nucl Med Mol Imaging.* (2016) 43:773–9. doi: 10.1007/s00259-015-3287-z

7. van der Geest KSM, Treglia G, Glaudemans AWJM, Brouwer E, Jamar F, Slart RHJA, et al. Diagnostic value of [18F]FDG-PET/CT in polymyalgia rheumatica: a systematic review and meta-analysis. *Eur J Nucl Med Mol Imaging.* (2021) 48:1876–89. doi: 10.1007/s00259-020-05162-6

8. Flaus A, Amat J, Prevot N, Olagne L, Descamps L, Bouvet C, et al. Decision tree with only two musculoskeletal sites to diagnose polymyalgia rheumatica using [18F]FDG PET-CT. *Front Med.* (2021) 8:646974. doi: 10.3389/fmed.2021.646974

9. Yamashita H, Kubota K, Takahashi Y, Minaminoto R, Morooka M, Ito K, et al. Whole-body fluorodeoxyglucose positron emission tomography/computed tomography in patients with active polymyalgia rheumatica: evidence for distinctive bursitis and large-vessel vasculitis. *Mod Rheumatol.* (2012) 22:705–11.

10. Takahashi H, Yamashita H, Kubota K, Miyata Y, Okasaki M, Morooka M, et al. Differences in fluorodeoxyglucose positron emission tomography/computed tomography findings between elderly onset rheumatoid arthritis and polymyalgia rheumatica. *Mod Rheumatol.* (2015) 25:546–51. doi: 10.3109/14397595.2014.978936

11. Sondag M, Guillot X, Verhoeven F, Blagosklonov O, Prati C, Boulahdour H, et al. Utility of 18F-fluoro-dexoxyglucose positron emission tomography for the diagnosis of polymyalgia rheumatica: a controlled study. *Rheumatology.* (2016) 55:1452–7. doi: 10.1093/rheumatology/kew202

12. Wakura D, Kotani T, Takeuchi T, Komori T, Yoshida S, Makino S, et al. Differentiation between polymyalgia rheumatica (PMR) and elderly-onset rheumatoid arthritis using 18F-fluorodeoxyglucose positron emission tomography/computed tomography: is enthesitis a new pathological lesion in PMR? *PLoS One.* (2016) 11:e0158509. doi: 10.1371/journal.pone.0158509

13. Emamifar A, Ellingsen T, Hess S, Gerke O, Hviid Larsen R, Ahangarani Farahani Z, et al. The utility of 18F-FDG PET/CT in patients with clinical suspicion of polymyalgia rheumatica and giant cell arteritis: a prospective, observational, and cross-sectional study. *ACR Open Rheumatol.* (2020) 2:478–90. doi: 10.1002/acr2.11163

14. van der Geest KSM, van Sleen Y, Nienhuis P, Sandovici M, Westerdijk N, Glaudemans AWJM, et al. Comparison and validation of FDG-PET/CT scores for polymyalgia rheumatica. *Rheumatology.* (2021) 61:1072–82. doi: 10.1093/rheumatology/keab483

frontiers | Frontiers in Medicine

TYPE Mini Review
PUBLISHED 28 September 2022
DOI 10.3389/fmed.2022.1026060

OPEN ACCESS

EDITED BY
Giorgio Treglia,
Ente Ospedaliero Cantonale (EOC), Switzerland

REVIEWED BY
Edel Noriega-Álvarez,
Hospital General Universitario de Ciudad Real, Spain
Sharjeel Usmani,
Kuwait Cancer Control Center, Kuwait

*CORRESPONDENCE
Michael Schirmer
michael.schirmer@i-med.ac.at

SPECIALTY SECTION
This article was submitted to Nuclear Medicine, a section of the journal Frontiers in Medicine

RECEIVED 23 August 2022
ACCEPTED 07 September 2022
PUBLISHED 28 September 2022

CITATION
Wenger M and Schirmer M (2022) Indications for diagnostic use of nuclear medicine in rheumatology: A mini-review. *Front. Med.* 9:1026060. doi: 10.3389/fmed.2022.1026060

Indications for diagnostic use of nuclear medicine in rheumatology: A mini-review

Martin Wenger[1] and Michael Schirmer[2]*

[1]Department of Nuclear Medicine, Klinikum Bad Hersfeld, Bad Hersfeld, Germany, [2]Clinic II, Department of Internal Medicine, Medical University of Innsbruck, Innsbruck, Austria

Nuclear medicine techniques allow important insights not only into oncologic, neurologic, and infectious conditions, but also for the assessment of rheumatic diseases. This review provides a brief, update on the potential role of nuclear imaging in rheumatology, especially on ^{18}F-fluorodeoxyglucose (FDG) positron emission tomography for the diagnosis of giant cell arteritis and other large vessel arteritis according to international recommendations. Besides, the potential role of this and other nuclear imaging techniques for the rheumatologic practice are summarized. With ^{18}F-fluoride as tracer for positron emission tomography, a new option for bone scintigraphy comes up, whereas the use of a semiquantitative sialoscintigraphy is no more supported for classification of Sjögren's syndrome according to current recommendations. Other techniques are used for different organ manifestations in systemic rheumatic diseases like for myocardial infarction and apoplectic insult.

KEYWORDS

imaging, scintigraphy, tomography, magnetic resonance, fluorodeoxyglucose, Technetium-99m, fluoride, giant cell arteritis

Introduction

The application of nuclear medicine techniques allows diagnostic insights not only into most oncologic, neurologic and infectious conditions, but also into selected rheumatic diseases. In rheumatology, ^{18}F-fluorodeoxyglucose (FDG)-positron emission tomography (PET) can be considered as the nuclear medicine techniques most often requested by rheumatologists. According to a recent survey for diagnostic purposes, large vessel vasculitis, fever or increased erythrocyte sedimentation rate of unknown origin are the most common indications to request FDG-PET, while sarcoidosis, immunoglobulin G4-related disease, total joint replacement, constitutional symptoms, suspicion of malignancy, polymyalgia rheumatica (PMR) and suspicion of osteomyelitis are rare indications (1). Bone scintigraphy, and semiquantitative sialoscintigraphy have been established in rheumatology, but today are less frequently needed in rheumatology as compared to orthopedics and oncology, respectively.

The combined use of nuclear medicine techniques together with computerized topography (CT) or magnetic resonance imaging (MRI) provides a combination of functional data of increased cellular metabolism together with exact localization and description of the affected anatomic structures. Amongst experts including 80% rheumatologists with ≥5 years of experience in FDG-PET, 95% already utilize PET–CT, 9% PET–MRI and only 12% standalone PET (respondents were allowed to indicate more than one option) (1). For the future, the increasing availability of total body imaging will certainly have a revolutionary impact on day-to-day practice of medicine (2).

This narrative mini-review summarizes the most important clinical aspects of nuclear medicine techniques—from the rheumatologist's and a nuclear medicine specialist's perspectives.

Established nuclear medicine techniques for indications in rheumatology

FDG-PET in large vessel vasculitis

General considerations

According to the 2012 Revised International Chapel Hill Consensus Conference Nomenclature of Vasculitides, inflammation of large vessels are typical for giant cell arteritis (GCA) and Takayasu arteritis (TAK), but may also present in variable vessel vasculitis like Behçet's disease and in isolated aortitis as single organ vasculitis (3). This consensus stated that "primarily because there are no specific biomarkers for TAK and GCA, it is not possible to know if any or all examples of single organ vasculitis aortitis are limited expressions of TAK or GCA." This aspect has important implications on therapeutic decision-making, as controlled interventional studies are not available so far.

For the differentiation between isolated aortitis and TAK or GCA, imaging using FDG-PET with or without CT or MRI is helpful. Since about 20 years, FDG-PET has been introduced into clinical practice (4), and for diagnosis of non-cranial large vessel arteritis, first successful cases were reported back in 2003 (5), with more and more studies coming up in the following years. The most important milestones in the field were achieved in 2017 and in 2018 as outlined below.

FDG-PET for classification of giant cell arteritis in 2017

Since 1990, the American College of Rheumatology (ACR)-criteria GCA have been successfully applied (6). At this time, the focus on GCA was on temporal arteritis as the cranial form of GCA. Only later, the non-cranial forms of GCA were more and more realized, especially by using imaging tools for examining the aorta and its major branches.

In 2017, the diagnostic delay of non-cranial GCA was still reported with 17.6 weeks and thus supported the need of fast-track diagnostic pathways (7). In the same year, however, a large interventional trial was published reporting not only the effects of tocilizumab as an inhibitor of interleukin-6 receptor alpha in GCA, but also used PET as an imaging option for identifying patients with non-cranial GCA (8). In this trial, "diagnosis of GCA was based either on results of a temporal-artery biopsy showing features of GCA or on evidence of large-vessel vasculitis on angiography, CT or magnetic resonance angiography, or PET" (8).

Since then, FDG- PET/CT is accepted as an imaging technique to be included into considerations for both diagnosing and classifying GCA. Such use of imaging tools like the F-FDG-PET for the non-cranial forms of GCA without involvement of the temporal arteries had never been formally validated in combination with other parameters for their potential accuracy as classification tool. As this trial further led to the approval of tocilizumab for the indication of GCA by national and international authorities, the study can be considered both as a milestone for classification of GCA and introduction of a new treatment also for GCA in general including the non-cranial form of GCA (9).

2018 recommendations for use of FDG-PET

In 2018, both a joint procedural recommendation of the European Association of Nuclear Medicine (EANM), the Society of Nuclear Medicine & Molecular Imaging (SNMMI) and the PET Interest Group (PIG) endorsed by the American Society of Nuclear Cardiology (ASNC), and a study group of the European Alliance of Associations For Rheumatology (EULAR) made recommendations for FDG-PET/CT imaging in large vessel vasculitis and polymyalgia rheumatica (PMR) (10, 11). These two recommendations are summarized in Table 1. Today, the use of FDG-PET/CT with or without angiography [FDG-PET/CT(A)] is well-established for diagnosing the non-cranial form of GCA, TAK and isolated aortitis. The consensus of experts in the field include the aspects of patient preparation, FDG-PET/CT(A) acquisition and interpretation for the diagnosis and follow-up of patients with suspected or diagnosed large vessel vasculitis and/or PMR.

At this time in 2018, FDG-PET/CT was still considered as not disease-specific and primarily developed to diagnose malignant and infectious/inflammatory diseases (10). The main limitation of FDG-PET/CT with or without angiography (A) to becoming a standardized diagnostic tool for large vessel arteritis was still the lack of an internationally accepted definition of vascular inflammation, based on the intensity and pattern of the glucose analog uptake (10).

TABLE 1 Summary of 2018 recommendations for FDG-PET/CT(A) imaging in large vessel vasculitis and polymyalgia rheumatica by (a) the EANM, SNMMI, and the PET Interest Group (PIG), endorsed by the ASNC (10) and (b) a EULAR study group (11).

Topic	EANM, SNMMI, and PET interest group	EULAR study group
PET/CT	Low-Dose non-contrast CT for attenuation correction and anatomical reference	Hybrid PET with low-dose CT
Dietary preparation	Fasting for at least 6 h prior to FDG administration, intake of non-caloric beverages allowed. In case of FUO or suspected cardiac involvement: Consider fat-enriched diet lacking carbohydrates for 12–24, 12–18 h fast, and/or use of i.v. unfractionated heparin ∼15 min prior to FDG injection	
Blood glucose level	Normal blood glucose levels desirable, but glucose levels <7 mmol/L (126 mg/dL) preferable	Preferably <7 mmol/L (126 mg/dL) Acceptable <10 mmol/L (180 mg/dL)
Glucocorticoids	Withdraw or delay GC therapy until after PET, unless there is risk of ischemic complications, as in case of GCA with temporal artery involvement. FDG-PET within 3 days after start of GC is optional as possible alternative	
Dose of FDG injection	3D: 2–3 MBq/kg (0.054–0.081 mCi/kg) body weight (depending on vendor suggestion of camera system)	
Interval between FDG administration and imaging	Minimum interval of 60 min between FDG administration and acquisition for adequate biodistribution	≥60 min, preferably 90 min
Position of patient	Supine, arms next to the body	Supine, arms should be down
Body parts to include	Head down to feet	From top to head to at least midthigh, preferably to below the knees
Scan duration	3D: 2–3 min/bed position (depending on vendor suggestion of camera system)	
Scoring FDG uptake	Use of standardized grading system proposed: 0 = no uptake (≤mediastinum); 1 = low-grade uptake (<liver); 2 = intermediate-grade uptake (= liver), 3 = high-grade uptake (>liver), with grade 2 considered possibly positive and grade 3 positive for active LVV. Typical FDG joint uptake patterns* should be reported if present. Normalization of arterial wall uptake to background activity of venous blood pool provides good reference for assessing vascular inflammation. Grading of arterial inflammation against liver background is established method	Qualitative visual grading; if result is unclear, compare it with liver background (grading 0–3)
Diagnostic performance for LVV and PMR	Based on available evidence, FDG-PET imaging exhibits high diagnostic performance CTA and FDG-PET have complementary roles in diagnosis of LVV	
Diagnostic performance for LVV and PMR	FDG-PET/CT(A) may be ofvalue for evaluating response to treatment by monitoring functional metabolic information and detecting structural vascular changes (evidence level III, grade C), but additional prospective FDG-PET/CT(A) studies are warranted	

CT, computerized tomography; CTA, CT angiography; FDG, ^{18}F-Fluorodeoxyglucose; FUO, fever of unknown origin; GC, glucocorticoids; LVV, large vessel vasculitis; PET, positron emission tomography; PMR, polymysalgia rheumatic.
*Including scapular and pelvic girdles, interspinous regions of cervical and lumbar vertebrae, or knees.

According to the 2018 EULAR recommendation, PET was not recommended for the assessment of inflammation of cranial arteries, but may be used for detection of mural inflammation and/or luminal changes in extracranial arteries to support the diagnosis of large vessel GCA and as alternative imaging modality in patients with suspected TAK (11). A limitation to both of these recommendations is that in the clinical setting FDG-PET/CT imaging is certainly not routinely applied for diagnosing PMR because of its availability and the priority of sonography which was already introduced in the 2012 provisional classification criteria for PMR (12).

Bone scintigraphy in current rheumatology

Since decades, bone scintigraphy with the radioactive tracer Technetium-99m pertechnetate (99mTc-pertechnetate) has been used for the diagnosis and follow-up of metabolic bone diseases, although diffuse scintigraphic changes are generally of little diagnostic value (13). Because of its high sensitivity and the easily acquired image of the whole body, its most common use was the detection of fractures in osteoporosis, pseudofractures in osteomalacia and the evaluation of Paget's disease (14).

Today, ^{18}F-fluoride as tracer for PET/CT has shown to be more sensitive and specific than traditional bone scintigraphy, and the addition of CT further increases specificity in detecting bone metastasis (15). With 15–30 min vs. 3–4 h, uptake times are shorter than for conventional bone scintigraphy, and imaging times are shorter but the radiation exposure is approximately double with Fluoride PET/CT compared to standard bone scintigraphy (16). The main indications for ^{18}F-fluoride PET/CT are bone metastases, only limited data are available for metabolic bone diseases.

Despite the limited value of bone scintigraphy in the primary diagnostic procedure, bone scintigraphy is of value in the preparation and follow up of radiosynoviorthesis. The method then allows direct comparisons before and after radiosynoviorthesis. Almost all national procedure guidelines include bone scintigraphy or other imaging techniques as mandatory before and 6 months after radiosynoviorthesis.

Semiquantitative sialoscintigraphy and Sjögren's disease

According to the revised version of the European criteria proposed by the American-European Consensus Group for the classification of primary Sjögren's syndrome in 2002, a positive scintigraphy was defined as delayed uptake, reduced concentration, and/or delayed excretion of the radioactive tracer Technetium-99m pertechnetate (99mTc-pertechnetate) (17).

Already in 2007, it was foreseeable that the role of sialoscintigraphy will be reduced when applying the American-European criteria (AECG) (18). Since then, two separate arguments support this assumption: First, according to a meta-analysis with pooled sensitivity of 80% and specificity of 89%, the diagnostic accuracy of salivary sonography is comparable with sialography in patients with Sjögren's disease (19). Thus, the sonographic finding of major salivary gland involvement was proposed to replace sialoscintigraphy in the AECG criteria for diagnosis of primary Sjögren's syndrome (20). Second, due to the low specificity and the inability to differentiate uptake failure from secretory failure, specialists proposed that scintigraphic examination should focus on the degree of salivary gland dysfunction rather than the diagnosis or classification of primary Sjögren's syndrome (21). In 2016 then, new criteria were designed and validated by the ACR and EULAR, without using sialography at all (22).

Although in the cohort at the National Institutes of Health, USA, the older AECG set and the new 2016 ACR-EULAR set were found to be equivalent (23), sialoscintigraphy is currently not recommended for the classification of Sjögren's syndrome and may only remain a possible, but rarely indicated technique for the assessment of salivary gland dysfunction in clinical and research settings.

Nuclear medicine techniques for rare rheumatological conditions

Musculoskeletal indications

In rheumatology, nuclear medicine techniques are not recommended for the routine assessment of arthritis, enthesitis, dactylitis or spondyloarthritis. Only in rare cases, it may be exceptionally indicated.

Spondyloarthritis and rheumatoid arthritis

Scintigraphy of the sacroiliac joints is of limited value for the diagnosis of axial Spondyloarthritis, but unilateral compared to bilateral sacroiliitis is slightly superior despite low sensitivity (with sensitivities of scintigraphy for unilateral or bilateral, bilateral and isolated unilateral sacroiliitis of 64.9, 40.2, and 24.7%, and specificities of 50.5, 57.7, and 92.8%, respectively) (24). Therefore, scintigraphy is used only very rare in case of a contraindication for MRI.

Concerning FDG-PET in rheumatoid arthritis, a recent study finds even more harm than benefit for the patients (25). This unblinded study showed that FDG-PET/CT allowed incidental detection of extra-articular abnormalities in 57% of the patients, resulting in additional diagnostic procedures in 26.6% of them. Most important, 7.4% of the patients were suspected with a malignancy, but none turned out to be malignant—but as many as six clinical malignancies developed during follow-up, who were all negative on baseline FDG-PET/CT.

Adult-onset Still's disease

Several groups propose FDG-PET for the diagnosis and assessment of disease activity in adult-onset Still's disease (AOSD). Indeed, the glucose metabolism of liver, spleen and bone marrow were correlated with laboratory inflammatory markers, and FDG uptake in the spleen was proposed as a potential biomarker for predicting clinical prognosis of AOSD patients (26).

Polymyalgia rheumatica

According to the 2012 provisional EULAR/ACR classification criteria for PMR, sonography has been implemented as additional imaging option to support the classification (12). This consensus was based on data from a prospective cohort using clinical characteristics and laboratory data, together with sonography at least in several of the participating centers, but not FDG-PET.

A recent systematic review and meta-analysis now concludes that significant FDG uptake at a combination of anatomic sites is informative for diagnosis of PMR (27). According to a recent

study significant FDG-uptake at least in three sites identified PMR with a sensitivity of 86% and a specificity of 85.5% in inflammatory rheumatic patients (28), whereas others showed that presence of optimal ordered combination of two sites already had a sensitivity and specificity to diagnose PMR of 73.2 and 87.5% in the training cohort and 78.6 and 80.1% in the validation cohort, respectively (29). When comparing these results with data from rheumatologists trained in sonography, both sensitivity (with 92.6%) and specificity (with 91.3%) were much higher than using FDG-PET (30). Thus, PMR can be helpful but is not considered as typical indication for FDG-PET.

Only in rare cases of "untypical" PMR, other diseases like large vessel arteritis, malignancies or infections may be detected using FDG-PET (31).

Non-musculoskeletal indications

The most frequent non-musculoskeletal indications for FDG-PET are fever and elevated erythrocyte sedimentation rate of unknown origin. Besides, if nuclear medicine imaging has been applied for non-rheumatological indications it may occasionally provide additional information useful for the rheumatologist. Non-musculoskeletal indications include all assessments of organs involved in systemic rheumatic diseases, including the central nervous system (e.g., for apoplectic insult), the heart (e.g., for myocardial infarction) and the lungs (e.g., for pulmonary embolism).

Fever or elevated erythrocyte sedimentation rate of unknown origin

In 2017, from a systematic review with meta-analysis of the literature until 2015 together with a DELPHI exercise to evaluate the diagnostic yield of combined FDG-PET/CT in fever of unknown origin it was concluded, that the pooled diagnostic yield was 56%, with an estimated yield beyond conventional CT of 32%, —which was considered as insufficient evidence to support the value of FDG-PET/CT in investigative algorithms of fever of unknown origin (32).

In 2018 then, using FDG-PET in a cohort of 240 patients with fever or inflammation of unknown origin, diagnosis could be established in 79.2% of the patients (33). AOSD was diagnosed in 15.3% of patients with fever of unknown origin, large vessel vasculitis and PMR in 21.1 and 18.3% of the patients with inflammation of unknown origin, respectively, and IgG4-related disease in 15.4 of the patients after fever or inflammation of unknown origin.

Sarcoidosis

FDG-PET is usually not indicated for the assessment of musculoskeletal manifestations, as sonography and other imaging techniques are available. As FDG-PET, however, has a role for functional imaging in sarcoidosis, and positive pulmonary FDG-PET findings were shown to occur in two-thirds of patients with radiographic stage II and III sarcoidosis, occasional findings of arthritis may lead the patient to a rheumatologist. Negative pulmonary FDG-PET findings were common in patients with radiographic stage 0, I, and IV sarcoidosis, but do not exclude inflammatory findings in the musculoskeletal system (34).

Idiopathic retroperitoneal fibrosis

Diagnosis of idiopathic retroperitoneal fibrosis (iRPF) may be difficult, but important to be differentiated from malignant diseases. Therefore, FDG-PET was validated to distinguish between iRPF and malignancies, and indeed iRPF displayed a lower frequency of high-FDG-uptake retroperitoneal lesions and a lower mean maximum standardized FDG-uptake value (35). When combining the FDG-PET findings with the location of specific lymph nodes at axillary, retroperitoneal, supraclavicular, inguinal, or peritoneal sites, the area under the curve for the logistic regression model combining the lesions above renal arteries, a sensitivity of 90.5% and a specificity of 98.6% was reached for the maximum standardized uptake value. The authors concluded that FDG PET/CT can help to distinguish iRPF from retroperitoneal lymphoma and metastatic malignancy. During follow-up, persistent FDG uptake may help to better stratify the risk of relapse and target therapy (36).

Conclusions

Nuclear medicine techniques are routinely used for the assessment of large vessel vasculitis like GCA and TAK, for diagnosis of rare metabolic bone diseases like Paget's disease and the assessment of salivary gland dysfunction in primary Sjögren's syndrome.

At present, FDG-PET is the nuclear medicine technique most often used in rheumatology. Combined with CT, MRI or angiography, it provides both functional and structural insights, which can be important for diagnostic or follow-up purposes. Also the use of FDG-PET in patients with fever or elevated erythrocyte sedimentation rate of unknown origin may lead to otherwise overseen rheumatologic diagnoses. Only rarely, FDG-PET is applied for diagnosis of adult Still's disease, sarcoidosis and idiopathic retroperitoneal fibrosis. Other nuclear medicine techniques may be more appropriate for assessment of specific organ involvements in systemic rheumatic diseases.

Indeed, there are several research gaps for use of nuclear medicine in rheumatology. First, sensitivity and specificity of different nuclear medicine techniques are not always well-established for each indication, especially for the rarest of the rheumatic diagnoses. Therefore, larger,

controlled, and investigator-blinded studies are needed for further validation of existing tracers and development of more specific new markers.

Author contributions

MW and MS contributed equally to the design, concept, and finishing of this article. All authors contributed to the article and approved the submitted version.

Funding

The work was partly funded by the Verein zur Förderung der Hämatologie, Onkologie und Immunologie, Innsbruck, Austria.

Conflict of interest

The authors declare that the research was conducted in the absence of any commercial or financial relationships that could be construed as a potential conflict of interest.

Publisher's note

References

1. Mandl P, Ciechomska A, Terslev L, Baraliakos X, Conaghan PG, D'Agostino MA, et al. Implementation and role of modern musculoskeletal imaging in rheumatological practice in member countries of EULAR. *RMD Open.* (2019) 5:e000950. doi: 10.1136/rmdopen-2019-000950

2. Alavi A, Saboury B, Nardo L, Zhang V, Wang M, Li H, et al. Potential and most relevant applications of total body PET/CT imaging. *Clin Nucl Med.* (2022) 47:43–55. doi: 10.1097/RLU.0000000000003962

3. Jennette JC, Falk RJ, Bacon PA, Basu N, Cid MC, Ferrario F, et al. 2012 Revised international chapel hill consensus conference nomenclature of vasculitides. *Arthritis Rheum.* (2013) 65:1–11. doi: 10.1002/art.37715

4. Schirmer M, Calamia KTT, Wenger M, Klauser A, Salvarani C, Moncayo R. 18F-fluorodeoxyglucose-positron emission tomography: a new explorative perspective. *Exp Gerontol.* (2003) 38:463–70. doi: 10.1016/S0531-5565(02)00267-X

5. Wenger M, Gasser R, Donnemiller E, Erler H, Glossmann H, Patsch JRJR, et al. Images in cardiovascular medicine. Generalized large vessel arteritis visualized by 18fluorodeoxyglucose-positron emission tomography. *Circulation.* (2003) 107:923. doi: 10.1161/01.CIR.0000050689.89407.87

6. Hunder GG, Bloch DA, Michel BA, Stevens MB, Arend WP, Calabrese LH, et al. The American college of rheumatology 1990 criteria for the classification of giant cell arteritis. *Arthritis Rheum.* (1990) 33:1122–8. doi: 10.1002/art.1780330810

7. Prior JA, Ranjbar H, Belcher J, Mackie SL, Helliwell T, Liddle J, et al. Diagnostic delay for giant cell arteritis - a systematic review and meta-analysis. *BMC Med.* (2017) 15:120. doi: 10.1186/s12916-017-0871-z

8. Stone JH, Tuckwell K, Dimonaco S, Klearman M, Aringer M, Blockmans D, et al. Trial of tocilizumab in giant-cell arteritis. *N Engl J Med.* (2017) 377:317–28. doi: 10.1056/NEJMoa1613849

9. Schirmer M, Muratore F, Salvarani C. Tocilizumab for the treatment of giant cell arteritis. *Expert Rev Clin Immunol.* (2018) 14:339–49. doi: 10.1080/1744666X.2018.1468251

10. Slart RHJA, Glaudemans AWJM, Chareonthaitawee P, Treglia G, Besson FL, Bley TA, et al. FDG-PET/CT(A) imaging in large vessel vasculitis and polymyalgia rheumatica: joint procedural recommendation of the EANM, SNMMI, and the PET interest group (PIG), and endorsed by the ASNC. *Eur J Nucl Med Mol Imaging.* (2018) 45:1250–69. doi: 10.1007/s00259-018-3973-8

11. Dejaco C, Ramiro S, Duftner C, Besson FL, Bley TA, Blockmans D, et al. EULAR recommendations for the use of imaging in large vessel vasculitis in clinical practice. *Ann Rheum Dis.* (2018) 77:636–43. doi: 10.1136/annrheumdis-2017-212649

12. Dasgupta B, Cimmino MA, Maradit-Kremers H, Schmidt WA, Schirmer M, Salvarani C, et al. 2012 Provisional classification criteria for polymyalgia rheumatica: a European league against rheumatism/American college of rheumatology collaborative initiative. *Arthritis Rheum.* (2012) 64:943–54. doi: 10.1002/art.34356

13. Mikosch P. [Bone scintigraphy for the diagnosis of metabolic bone diseases]. *Wien Med Wochenschr.* (2004) 154:119–26. doi: 10.1007/s10354-004-0053-4

14. Medijainen K, Pääsuke M, Lukmann A, Taba P. Versatile guideline-based physiotherapy intervention in groups to improve gait speed in Parkinson's disease patients. *NeuroRehabilitation.* (2019) 44:579–86. doi: 10.3233/NRE-192723

15. Liu Y, Sheng J, Dong Z, Xu Y, Huang Q, Pan D, et al. The diagnostic performance of 18F-fluoride PET/CT in bone metastases detection: a meta-analysis. *Clin Radiol.* (2019) 74:196–206. doi: 10.1016/j.crad.2018.12.011

16. Scarsbrook AF, Barrington SF. PET-CT in the UK: current status and future directions. *Clin Radiol.* (2016) 71:673–90. doi: 10.1016/j.crad.2016.02.023

17. Vitali C, Bombardieri S, Jonsson R, Moutsopoulos HM, Alexander EL, Carsons SE, et al. Classification criteria for Sjögren's syndrome: a revised version of the European criteria proposed by the American-European consensus group. *Ann Rheum Dis.* (2002) 61:554–8. doi: 10.1136/ard.61.6.554

18. Langegger C, Wenger M, Duftner C, Dejaco C, Baldissera I, Moncayo R, et al. Use of the European preliminary criteria, the Breiman-classification tree and the American-European criteria for diagnosis of primary Sj??gren's Syndrome in daily practice: a retrospective analysis. *Rheumatol Int.* (2007) 27:699–702. doi: 10.1007/s00296-006-0291-4

19. Song GG, Lee YH. Diagnostic accuracies of sialography and salivary ultrasonography in Sjögren's syndrome patients: a meta-analysis. *Clin Exp Rheumatol.* (2014) 32:516–22.

20. Milic V, Petrovic R, Boricic I, Radunovic G, Marinkovic-Eric J, Jeremic P, et al. Ultrasonography of major salivary glands could be an alternative tool to sialoscintigraphy in the American-European classification criteria for primary Sjogren's syndrome. *Rheumatology.* (2012) 51:1081–5. doi: 10.1093/rheumatology/ker431

21. van Ginkel MS, Glaudemans AWJM, van der Vegt B, Mossel E, Kroese FGM, Bootsma H, et al. Imaging in primary Sjögren's Syndrome. *J Clin Med.* (2020) 9:2492. doi: 10.3390/jcm9082492

22. Shiboski CH, Shiboski SC, Seror R, Criswell LA, Labetoulle M, Lietman TM, et al. 2016 American college of rheumatology/European league against rheumatism classification criteria for primary sjögren's syndrome: a consensus and data-driven methodology involving three international patient cohorts. *Arthritis Rheumatol.* (2017) 69:35–45. doi: 10.1002/art.39859

23. Billings M, Amin Hadavand M, Alevizos I. Comparative analysis of the 2016 ACR-EULAR and the 2002 AECG classification criteria for Sjögren's syndrome: findings from the NIH cohort. *Oral Dis.* (2018) 24:184–90. doi: 10.1111/odi.12772

24. Song I-H, Brandt H, Rudwaleit M, Sieper J. Limited diagnostic value of unilateral sacroiliitis in scintigraphy in assessing axial spondyloarthritis. *J Rheumatol.* (2010) 37:1200–2. doi: 10.3899/jrheum.091216

25. Ulijn E, den Broeder AA, Boers N, Gotthardt M, Bouman CAM, Landewé R, et al. Extra-articular findings with FDG-PET/CT in rheumatoid arthritis patients: more harm than benefit. *Rheumatol Adv Pract.* (2022) 6:rkac014. doi: 10.1093/rap/rkac014

26. Li X, Dong C, Ma X, Wang Y. 18F-FDG PET/CT associates with disease activity and clinical recurrence of AOSD patients. *Front Med.* (2021) 8:668323. doi: 10.3389/fmed.2021.668323

27. van der Geest KSM, Treglia G, Glaudemans AWJM, Brouwer E, Jamar F, Slart RHJA, et al. Diagnostic value of [18F]FDG-PET/CT in polymyalgia rheumatica: a systematic review and meta-analysis. *Eur J Nucl Med Mol Imaging.* (2021) 48:1876–89. doi: 10.1007/s00259-020-05162-6

28. Amat J, Chanchou M, Olagne L, Descamps L, Flaus A, Bouvet C, et al. Utility of 18F-fluorodeoxyglucose positron emission tomography in inflammatory rheumatism, particularly polymyalgia rheumatica: a retrospective study of 222 PET/CT. *Front Med.* (2020) 7:394. doi: 10.3389/fmed.2020.00394

29. Flaus A, Amat J, Prevot N, Olagne L, Descamps L, Bouvet C, et al. Decision tree with only two musculoskeletal sites to diagnose polymyalgia rheumatica using [18F]FDG PET-CT. *Front Med.* (2021) 8:148. doi: 10.3389/fmed.2021.646974

30. Macchioni P, Boiardi L, Catanoso M, Pazzola G, Salvarani C. Performance of the new 2012 EULAR/ACR classification criteria for polymyalgia rheumatica: comparison with the previous criteria in a single-centre study. *Ann Rheum Dis.* (2014) 73:1190–3. doi: 10.1136/annrheumdis-2013-204167

31. Wenger M, Gasser R, Donnemiller E, Klauser A, Moncayo R, Schirmer M. [Lymph node tuberculosis in a patient with polymyalgic symptoms: value of 18F-fluorodeoxyglucose positron emission tomography (18F-FDG-PET)]. *Z Rheumatol.* (2003) 62:294–5. doi: 10.1007/s00393-003-0521-z

32. Bharucha T, Rutherford A, Skeoch S, Alavi A, Brown M, Galloway J, et al. Diagnostic yield of FDG-PET/CT in fever of unknown origin: a systematic review, meta-analysis, and Delphi exercise. *Clin Radiol.* (2017) 72:764–71. doi: 10.1016/j.crad.2017.04.014

33. Schönau V, Vogel K, Englbrecht M, Wacker J, Schmidt D, Manger B, et al. The value of 18F-FDG-PET/CT in identifying the cause of fever of unknown origin (FUO) and inflammation of unknown origin (IUO): data from a prospective study. *Ann Rheum Dis.* (2018) 77:70–7. doi: 10.1136/annrheumdis-2017-211687

34. Teirstein AS, Machac J, Almeida O, Lu P, Padilla ML, Iannuzzi MC. Results of 188 whole-body fluorodeoxyglucose positron emission tomography scans in 137 patients with sarcoidosis. *Chest.* (2007) 132:1949–53. doi: 10.1378/chest.07-1178

35. Wang Y, Guan Z, Gao D, Luo G, Li K, Zhao Y, et al. The value of 18F-FDG PET/CT in the distinction between retroperitoneal fibrosis and its malignant mimics. *Semin Arthritis Rheum.* (2018) 47:593–600. doi: 10.1016/j.semarthrit.2017.07.011

36. Morin G, Mageau A, Benali K, Bertinchamp R, Piekarski E, Raimbourg Q, et al. Persistent FDG/PET CT uptake in idiopathic retroperitoneal fibrosis helps identifying patients at a higher risk for relapse. *Eur J Intern Med.* (2019) 62:67–71. doi: 10.1016/j.ejim.2019.01.019

frontiers | Frontiers in Medicine

TYPE Study Protocol
PUBLISHED 12 October 2022
DOI 10.3389/fmed.2022.993151

OPEN ACCESS

EDITED BY
Giorgio Treglia,
Ente Ospedaliero Cantonale (EOC), Switzerland

REVIEWED BY
Edel Noriega-Álvarez,
Hospital General Universitario de Ciudad Real, Spain
Chentian Shen,
Shanghai Jiao Tong University, China
Salvatore Annunziata,
Fondazione Policlinico Universitario A. Gemelli IRCCS, Italy

*CORRESPONDENCE
Emilie Thivat
emilie.thivat@clermont.unicancer.fr

†These authors share first authorship

SPECIALTY SECTION
This article was submitted to Nuclear Medicine, a section of the journal Frontiers in Medicine

RECEIVED 13 July 2022
ACCEPTED 11 August 2022
PUBLISHED 12 October 2022

CITATION
Thivat E, Chanchou M, Mathieu S, Levesque S, Billoux T, Auzeloux P, Sas N, Molnar I, Jouberton E, Rouanet J, Fois G, Maigne L, Galmier M-J, Penault-Llorca F, Miot-Noirault E, Durando X and Cachin F (2022) Assessment of ^{99m}Tc-NTP 15-5 uptake on cartilage, a new proteoglycan tracer: Study protocol for a phase I trial (CARSPECT). *Front. Med.* 9:993151. doi: 10.3389/fmed.2022.993151

Assessment of ^{99m}Tc-NTP 15-5 uptake on cartilage, a new proteoglycan tracer: Study protocol for a phase I trial (CARSPECT)

Emilie Thivat[1,2,3*†], Marion Chanchou[1,4†], Sylvain Mathieu[5], Sophie Levesque[1,2,6], Tommy Billoux[1,7], Philippe Auzeloux[1], Nicolas Sas[1,7], Ioana Molnar[1,2,3], Elodie Jouberton[1,4], Jacques Rouanet[1,8], Giovanna Fois[9], Lydia Maigne[9], Marie-Josephe Galmier[1], Frédérique Penault-Llorca[1,3,10], Elisabeth Miot-Noirault[1], Xavier Durando[1,2,3,11] and Florent Cachin[1,3,4]

[1]Institut National de la Santé et de la Recherche Médicale (INSERM) U1240 Imagerie Moléculaire et Stratégies Theranostiques (IMoST), Université Clermont Auvergne, Clermont-Ferrand, France, [2]Département de Recherche Clinique, Centre Jean PERRIN, Clermont-Ferrand, France, [3]Centre d'Investigation Clinique UMR501, Clermont-Ferrand, France, [4]Service de Médecine Nucléaire, Centre Jean PERRIN, Clermont-Ferrand, France, [5]Service de Rhumatologie, Centre Hospitalier Universitaire (CHU) Gabriel Montpied, Université Clermont-Auvergne, Clermont-Ferrand, France, [6]Unité de Radiopharmacie, Centre Jean PERRIN, Clermont-Ferrand, France, [7]Service de Physique Médicale, Centre Jean PERRIN, Clermont-Ferrand, France, [8]Service de Dermatologie et d'Oncologie Cutanée, Centre Hospitalier Universitaire (CHU) Clermont-Ferrand, Clermont-Ferrand, France, [9]Laboratoire de Physique de Clermont, UMR6533, Centre National de la Recherche Scientifique (CNRS)/Institut National de Physique Nucléaire et de Physique des Particules (IN2P3), Université Clermont Auvergne, Clermont-Ferrand, France, [10]Département de Biopathologie, Centre Jean PERRIN, Clermont-Ferrand, France, [11]Département d'oncologie Médicale, Centre Jean PERRIN, Clermont-Ferrand, France

Background: ^{99m}Tc-NTP 15-5 is a SPECT radiotracer targeting proteoglycans (PG), components of the cartilaginous extracellular matrix. Imaging of PGs would be useful for the early detection of cartilage disorders (osteoarthritis, arthritis and chondrosarcoma, Aromatase Inhibitor associated arthralgia (AIA) in breast cancer), and the follow-up of patients under treatment. According to preclinical study results, ^{99m}Tc-NTP 15-5, is a good candidate for a specific functional molecular imaging of joints. We intend to initiate a first in-human study to confirm and quantify ^{99m}Tc-NTP 15-5 uptake in healthy joints.

Methods: As the clinical development of this radiotracer would be oriented toward the functional imaging of joint pathologies, we have chosen to include patients with healthy joints (unilateral osteoarthritis of the knee or breast cancer with indication of AI treatment). This phase I study will be an open-label, multicenter, dose-escalation trial of a radiopharmaceutical orientation to determine the recommended level of activity of ^{99m}Tc-NTP 15-5 to obtain the best joint tracer contrasts on images, without dose limiting toxicity (DLT). The secondary objectives will include the study of the pharmacology, biodistribution (using planar whole body and SPECT-CT acquisitions), toxicity, and dosimetry of this radiotracer. The dose escalation with 3 activity levels (5, 10, and 15 MBq/kg), will be conditioned by the absence at the previous level

of DLT and of a visualized tracer accumulation on more than 80% of healthy joints as observed on scintigraphy performed at ≤ 2 h post-injection.

Discussion: This first in-human phase I trial will be proof-of-concept of the relevance of ^{99m}Tc-NTP 15-5 as a cartilage tracer, with the determination of the optimal methodology (dose and acquisition time) to obtain the best contrast to provide a functional image of joints with SPECT-CT.

Trial registration number: Clinicaltrials.gov: NCT04481230. Identifier in French National Agency for the Safety of Medicines and Health Products (ANSM): N°EudraCT 2020-000495-37.

KEYWORDS

radiopharmaceutical-diagnostic use, cartilage, proteoglycan targeting, SPECT imaging, phase I

Introduction

Biomechanical joint function depends on cartilage integrity. For many years UMR 1240 INSERM has developed a nuclear medicine imaging strategy targeting cartilage proteoglycans *in vivo*, such as ^{99m}Tc-NTP 15-5. This radiotracer is a bifunctional agent which contains in its structure a polyazamacrocycle to complex ^{99m}Tc and a positively charged quaternary ammonium (QA) function for binding to glycosaminoglycans of proteoglycans, components of the cartilaginous extracellular matrix (1). This radiotracer has emerged as a promising candidate for single-photon emission computed tomography (SPECT) imaging in nuclear medicine for specific, relevant, and functional molecular imaging of cartilage (2, 3). When intravenously administered to healthy rodents or lagomorph animals, ^{99m}Tc-NTP 15-5 has been observed to accumulate markedly within articular cartilage with high *in vivo* stability (4, 5). The potential of the radiotracer to bind to cartilage has also been confirmed *ex vivo* on human knee specimens (3). A selective, intense accumulation was confirmed in cartilaginous tissue. In addition, areas of deficit in tracer uptake were clearly localized in anatomical areas of altered and eroded cartilage as seen in osteoarthritis specimens (3). Numerous preclinical studies have shown its relevance in molecular imaging of cartilaginous pathologies such as osteoarthritis (2, 4), inflammatory disease (6), and chondrosarcoma (7). ^{99m}Tc-NTP 15-5 nuclear imaging was recently used in the murine destabilization of medial meniscus models, to monitor *in vivo* cartilage remodeling in response to disease-modifying osteoarthritis drugs (DMOAD) (8). Diagnosis of cartilaginous biochemical alterations could enable *in vivo* studies of joint functionality (9), which cannot be evaluated by conventional imaging techniques such as CT and MRI (10, 11). In addition, these conventional imaging techniques have poor diagnostic performances in early-stage osteoarthritis, which is a real public health problem (12–15). Functional articular cartilage imaging is of interest in joint treatment-related toxicities, such as Aromatase Inhibitor-Arthralgia (AIA). Aromatase inhibitors (AIs) are standard care for the adjuvant treatment of early hormone-sensitive breast cancer. However from 20% to 50% of women experience joint pain under AI treatment, with up to 20% treatment discontinuation for this toxicity which can compromise the effectiveness of these therapies (16, 17).

As the clinical development of this radiotracer would be oriented toward the functional imaging of cartilage in degenerative cartilage pathologies, we intend to carry out this first clinical proof-of-concept study on this radiotracer among patients (osteoarthritis and breast cancer) rather than among healthy volunteers. The evaluation of this radiotracer in this population (patients with unilateral osteoarthritis or patients with breast cancer with an indication for adjuvant AI treatment) will make it possible to verify: i) its binding to healthy joints, and ii) specific conditions enabling an initial evaluation of osteoarthritic joints.

This CARSPECT trial is thus a first in-human clinical study designed to confirm tracer accumulation in healthy cartilage joints. The main objective is to determine the recommended dose (activity in MBq/kg) of ^{99m}Tc-NTP 15-5 to optimize joint fixation contrast on scintigraphy acquisitions, avoiding

Abbreviations: AD, absorbed dose; AIA, Aromatase inhibitor arthralgia; AI, Aromatase inhibitors; ALP, Alkaline phosphatase; ALT, Alanine aminotransferase; ANSM, French Agency for the Safety of Medicines and Health Products; AST, Aspartate aminotransferase; CTCAE, Common Terminology Criteria for Adverse Events; DMOAD, disease-modifying osteoarthritis drugs; DLT, dose-limiting toxicity; ECG, Electrocardiogram; fT3, free triiodothyronine; fT4, free thyroxine; GGT, Gamma-glutamyl transferase; IDMC, Independent Data Monitoring Committee; MIRD, Medical Internal Radiation Dose Committee; NSAIDs, Non-steroidal anti-inflammatory drugs; PG, Proteoglycans; QA, quaternary ammonium; SPECT-CT, Single Photon Emission Computed Tomography/Computed Tomography; TRT, Targeted radionuclide therapy; TSH, Thyroid-stimulating hormone; WBDC, Web-Based Data Capture.

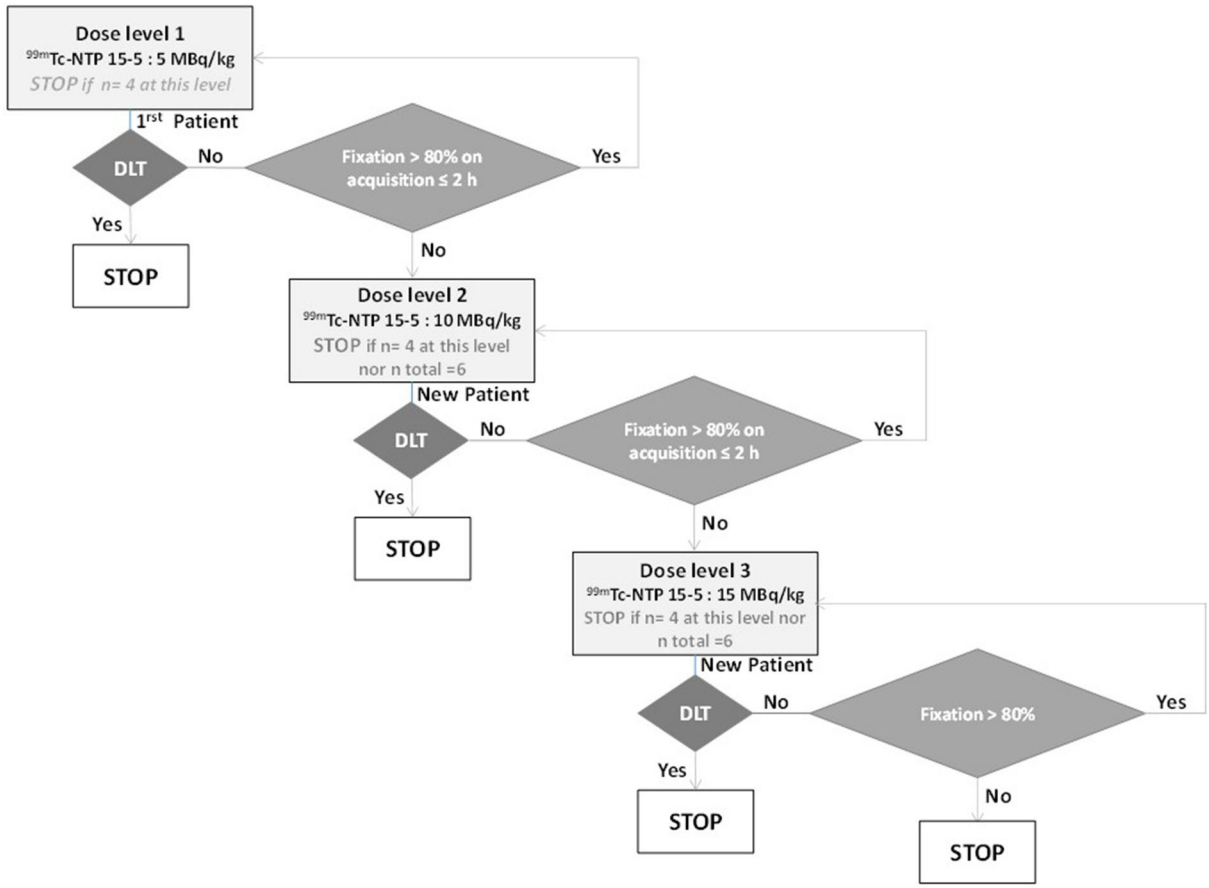

FIGURE 1
Dose escalation plan of CARSPECT study.

any toxicity. The secondary objectives relate to pharmacology, biodistribution, toxicity, and dosimetry evaluation. Differences in tracer accumulation between healthy and degenerative joints will also be assessed visually and quantitatively.

Methods and analysis

Study design

This "first in-human" phase I study is an open-label, multicenter, dose-escalation trial on a radiopharmaceutical tracer. The main objective is to identify, among three levels of ^{99m}Tc-NTP 15-5 activity, the *recommended* (accurate) dose to detect tracer accumulation in a sufficient number of healthy joints, avoiding any toxicity.

Dose escalation will include 3 activity levels: 5, 10, and 15 MBq/kg. The initial dose of 5 MBq/kg will be used as the first level. The dose escalation scheme will allow dose escalations of one level conditioned by the absence, at the previous level, of dose-limiting toxicity (DLT) and the presence of tracer accumulation in healthy joints appearing on scintigraphy performed at $\leq$ 2 h post-injection (Figure 1). With a semi-quantitative visual scale, a score of 3 for at least 80% of healthy joints was chosen because it corresponds to a sensitivity of 80%, considered sufficient for diagnostic imaging.

A maximum of 6 patients will be included in the study. A maximum of 4 patients will be included per dose level. The rule for termination will be that at least 2 patients have received the recommended dose level, with one patient from each group in the selected dose level. Recruitment will be carried out alternately in each of the 2 groups (breast cancer patients/osteoarthritis patients) as far as possible.

The recruitment period will be 24 months, with a follow-up period of 1 week, for a total duration of 25 months.

Coordination and participating institutions

The sponsor and body responsible for the coordination of the trial, data management, monitoring, and statistical analyses will be the Center Jean Perrin, Clermont-Ferrand.

The multicenter study is currently based at 2 sites in France: The University Hospital of Clermont-Ferrand and Center Jean Perrin. Patients with osteoarthritis will be recruited from the Rheumatology Department of the University Hospital of Clermont-Ferrand and patients with breast cancer will be recruited at the Jean Perrin Cancer Center. For all patients, radiopharmaceutical injections will be performed at the Nuclear Medicine Department of the Jean Perrin Cancer Center.

Study objectives and endpoints

Primary objective and endpoint

The objective of this phase I trial is to determine the recommended dose (activity in MBq/kg) of ^{99m}Tc-NTP 15-5 corresponding to an optimal joint tracer contrast, analyzed on a semi-quantitative visual scale.

The tracer accumulation observed (whole body imaging) on healthy joints (according to clinical evaluation by rheumatologist) ($n = 31$) of the wrists, elbows, shoulders, lumbar, and spine joints, C6-C7, hips, knees, and ankles will be scored on a semi-quantitative visual scale using three levels:

1. Lower level of fixation than the adjacent diaphyseal uptake,
2. Fixation level equal to the adjacent diaphyseal uptake,
3. Fixation level higher than the adjacent diaphyseal uptake.

The visual analysis will be performed by 2 nuclear physicians with reconciliation of the results. In case of disagreement, consensus will be reached *via* a joint reassessment.

For each patient, the ratio of the number of healthy joints scored at level 3 to the total number of healthy joints studied will be calculated.

The recommended dose will be defined as the dose at which 100% of patients present a score of 3 in at least 80% of healthy joints as seen on scintigraphy performed at 2 h post-injection or less, and without DLT. DLT is defined as any grade 3–4 toxicity occurring in the week following the injection.

Secondary objectives and endpoints

The secondary objectives and the corresponding endpoints are:

- Analysis of the impact of activity level and acquisition time on tracer accumulation assessed by visual and quantitative analysis. A 3D quantification will complete the semi-quantitative visual analysis. SPECT Volumetric Regions of Interest will be centered on 7 cartilaginous zones (three lumbar discs, two hips, two knees) then on the corresponding bony diaphyses or vertebral body or the adjacent muscles. The articular uptake of ^{99m}Tc-NTP 15-5 will thus be normalized to bone or muscle uptake.
- Analysis of pharmacokinetics (including excretion), biodistribution, and dosimetry of ^{99m}Tc-NTP 15-5; the evolution of tracer activity/mL (AUC, Tmax and Cmax) will also be measured on whole blood and on plasma in the first 8 hours. Tracer urinary elimination over 8 h will be measured by counting.

Whole body planar (2D) and SPECT (3D) acquisitions will be performed for bio-distribution analysis and quantification of absorbed doses of tracer in target and non-target organs using a Monte-Carlo simulation and MIRD formalism (18). The analysis of ^{99m}Tc-NTP 15-5 uptake intensity between osteoarthritis joints and normal joints will be carried out using visual methods and quantitative 3D analysis.

- The tolerance of ^{99m}Tc-NTP 15-5 will be evaluated according to NCI-CTCAE (version 4.03). Tolerance assessments will include clinical examination, recording vital signs (heart rate, blood pressure, temperature, respiratory rate), weight, height, and OMS performance status; electrocardiogram (ECG); blood tests including full blood counts, prothrombin time, sodium, potassium, chloride, calcium, phosphorus, bicarbonate, serum total protein, serum albumin, fasting blood glucose levels, Thyroid-stimulating hormone (TSH), free thyroxine (fT4), free triiodothyronine (fT3), creatinine, urea, Alkaline phosphatase (ALP), Gamma-glutamyl transferase (GGT), Aspartate amino transferase (AST), Alanine amino transferase (ALT); 24-h urine collection tests: glucose, urea, creatinine, albumin, sodium, potassium, magnesium, calcium, and protein electrophoresis. Reporting of serious adverse events and suspected unexpected serious adverse reactions will be carried out according to the local regulations.

Patients

Inclusion criteria

Inclusion criteria specific to group 1:

- Patients with painful unilateral osteoarthritis of the knee, such as femorotibial pattern defined by a radiographic score of 0/1 (Kellgren/Lawrence), and an average WOMAC score of 4 or more and by minor disorders on MRI (MOCART 2.0 score > 70).

Inclusion criteria specific to group 2:

- Patients with non-metastatic breast cancer, hormone receptor-positive, HER2-negative, with indication for adjuvant therapy with AI; treatment not yet started.
- Age < 60 years.

Common inclusion criteria:

- Patients with at least 31 healthy joints (based on clinical assessment).
- Signed written informed consent.
- Affiliation to a health insurance plan.
- For women of childbearing age (fertile, from menarche and to post-menopause unless sterile subsequent to surgery) including patients under GnRH agonist for ovarian suppression: negative serum pregnancy test at inclusion (fewer than 7 days before injection of ^{99m}Tc-NTP 15-5). Menopause is defined as amenorrhea for at least 12 consecutive months without other cause and a level of FSH and estradiol consistent with levels of the post-menopausal period.
- Willing and able to comply with study visits, treatment, examinations, and the protocol.

Non-inclusion criteria

- Patients < 18 years of age.
- Pregnant or lactating patient.
- BMI > 30.
- History of known allergy to excipients present in the solution of ^{99m}Tc-NTP 15-5.
- Chronic inflammatory rheumatism (rheumatoid arthritis, spondyloarthropathy, psoriatic arthritis, etc.) diffuse arthritis (at least 3 joints affected), autoimmune connectivitis, fibromyalgia.
- Known chronic joint pathology: osteoarthritis affecting at least 3 joints, autoimmune disease, inflammatory rheumatism (except unilateral knee arthritis).
- Individuals deprived of their freedom, under guardianship/curatorship, or under legal protection measures.
- Treatment with NSAIDs or cessation under 48 h previously.
- Inability to comply with medical requirements/follow-up of the trial for geographic, family, social, or psychological reasons. These conditions should be discussed with the patient before registration in the study.

Intervention

Study drug and administration

^{99m}Tc-NTP 15-5 is synthesized by radioactive labeling with ^{99m}Tc of the chemical precursor NTP 15-5, N-[(3-triethylammonio)propyl]- 1,4,7,10,13-pentaazacyclopentadecane, in presence of sodium pertechnetate (19). The synthesis of the pharmaceutical grade NTP 15-5 cold precursor is manufactured in accordance with GMP (Eras Laboratoire). The cold kit is manufactured in the experimental radiopharmacy unit in the Jean Perrin Center, in the form of a single-dose sterile kit.

The experimental drug is an injectable solution of ^{99m}Tc-NTP 15-5with a molar activity greater than 2.5 GBq/μmol and radiochemical purity required to be over 90%.

According to the dose escalation plan, a single injection of 5, or 10, or 15 MBq/kg of ^{99m}Tc-NTP 15-5 will be administered by slow intravenous injection on D0 in the presence of a nuclear medicine physician, without any premedication. Any treatment with NSAIDs will be discontinued at least 48 h before injection and can be resumed 24 h after injection. Prior and concomitant treatments will be collected at baseline and throughout the study.

Study procedures and participant timeline

Before any study-related assessment starts, written informed consent will be obtained from each patient. At screening/baseline (within 15 days before administration of ^{99m}Tc-NTP 15-5), the patients will have a clinical evaluation noting vital signs, ECG, a specialized consultation with a rheumatologist, blood and urine tests, and a pregnancy test (for women of childbearing age), and for patients with osteoarthritis, an evaluation of osteoarthritis by MRI and X-ray dating from less than 2 months prior.

After checking the eligibility criteria, a dose allocation request will be performed using an eCRF.

The ^{99m}Tc-NTP 15-5 dose at an activity level of 5, or 10, or 15 MBq/kg (according to the dose escalation plan), will be injected on D0 with a follow-up of vital signs: before, and 5 min, 10 min, 15 min, 30 min, 1 h, 2 h, 4 h, and 6–8 h after the end of infusion.

e In vivo biodistribution of ^{99m}Tc-NTP 15-5 will be assessed using:

- Whole-body planar scintigraphy acquisition 30 min, 2 h, 4 h, and 6–8 h after injection on D0; SPECT acquisitions at 1 h, 2.5 h, 4.5 h, and 6–8 h after injection on D0; Computed Tomography will be carried out before the injection or at the time of SPECT acquisition.
- Blood samples for the pharmacokinetic study will be collected at 5 min, 10 min, 15 min, 30 min, 1 h, 2 h, 4 h, and 6–8 h post injection on D0. An 8-h urine collection will be performed for excretion evaluation.

Patients will be followed for 1 week with a visit on D8 for safety evaluation with clinical examination, vital signs, blood and urine analyses, and ECG.

Statistical considerations

A maximum of 6 patients should be included.

The number of subjects to be included takes into account the population selected and makes it possible to validate the hypothesis that healthy cartilage will present a significantly higher fixation than the adjacent diaphyseal fixation. For each patient, 31 observations (healthy joints) at 4 different times will be available for the evaluation of the main objective.

The optimal level of activity will be chosen using the dose escalation algorithm (Figure 1). The recommended dose will be defined as the dose from which 100% of patients present a score of 3 in at least 80% of healthy joints as observed on scintigraphy performed 2 h post-injection or less, and without DLT. If more than one time period (30 min or 2 h) meets these conditions, to choose the optimal time, we will perform a McNemar test where the number (minimum 2 patients, providing $n \geq 62$ healthy joints) provides a power of 0.8, with an average effect size of 0.3 and an alpha risk of 0.05. For the moment, we do not have any element enabling estimation of the correlation with each patient.

Due to the nature and the design of the study, statistical analyses will be mainly descriptive. Missing data will not be replaced. The statistical significance threshold is set at 5%. Statistical analyses will be performed using R software.

Data management and monitoring

An eCRF based on the Web-Based Data Capture (WBDC) system "Ennov Clinical" will be used for data collection, data management, and monitoring. Health-related personal data captured in the course of this study is strictly confidential and accessible only by investigators and authorized personnel. The investigator ensures the accuracy, completeness, and relevance of the data recorded (pseudonymized patient data) and of the provision of answers to data queries.

Compliance with the study protocol and the procedures therein, and the quality of the data collected (accuracy, missing data, consistency with the source documents) will be regularly reviewed by on-site monitoring and central data monitoring. Monitoring reports will ensure traceability.

Independent data monitoring committee

The IDMC will review all safety problems or other issues identified during the medical review and seek advice as needed. Experts in the IDMC performing this review will be selected for their relevant clinical trial/medical expertise. The committee will include a nuclear physician, a rheumatologist, and an oncologist. Given the very small number of DLTs expected, the committee will meet for each severe toxicity observed (grade ≥ 3).

Trial status

The CARSPECT trial is currently recruiting. Participant recruitment began in November 2020 with a 24-month enrollment period and an estimated completion in December 2022. The approved protocol is version 5, 15 March 2022.

Discussion

The CARSPECT trial is the first in-human evaluation of ^{99m}Tc-NTP 15-5 as a cartilage imaging radiotracer. This proof-of-concept study aims to confirm ^{99m}Tc-NTP 15-5 uptake in healthy joints and to determine the recommended dose (activity in MBq/kg) of ^{99m}Tc-NTP 15-5 to obtain the best joint fixation contrast on scintigraphy acquisitions, avoiding toxicity.

As observed in preclinical studies, ^{99m}Tc-NTP 15-5 uptake in healthy joints is expected to be intense, with high contrast compared to adjacent diaphyseal uptake or adjacent vertebral body. Our hypothesis is that at least 80% of the healthy joints of a patient will significantly bind ^{99m}Tc-NTP 15-5 (taking into account the resolution limits of the cameras).

Once this phase I trial is completed and the optimal injected activity of ^{99m}Tc-NTP 15-5 validated, phase II clinical trial will be designed to address clinical questions in both degenerative/inflammatory and tumoral diseases. Clinical development of a functional articular cartilage imaging radiotracer such as ^{99m}Tc-NTP 15-5 should be of interest in presence of pathological joints: osteoarthritis, arthritis, and chondrosarcoma, and in clinical situations where drugs induce severe articular cartilage toxicity, as with AI treatment in breast cancer.

Functional imaging such as proteoglycan tracer scintigraphy could be used to identify patient subgroups with PG altered cartilage, for which joint prosthesis is expected to really improve articular function and mobility. A recent preclinical study in a murine destabilization of medial meniscus model, highlights the potential of ^{99m}Tc-NTP 15-5 as an imaging-based companion to monitor cartilage remodeling in osteoarthritis and response to the disease-modifying osteoarthritis drug, sprifermin (rhFGF-18), one of the most promising anabolic agents that have demonstrated cartilage repair properties in patients (8).

Further to this, in hormone-responsive early breast cancer, arthralgia has been reported for up to 50% of women treated with aromatase inhibitors, and this affects compliance and thus the response to treatment (16, 17). Functional imaging using ^{99m}Tc-NTP 15-5 could provide a better understanding of the pathogenic mechanisms of arthralgia under AI and could identify patients at risk and improve their management.

Given the affinity of QA for cartilage, QA derivatives offer the possibility of an approach targeting cartilage in

imaging, and also for therapies in joint diseases, serving as carriers able to selectively deliver drugs. Preclinical studies have demonstrated the possibility of using QA as vector for D-glucosamine, and DMOAD (20), or anti-inflammatory drugs (21) in arthritis treatment. Another targeted therapy developed for chondrosarcoma uses QA as a targeting strategy by addressing selectively to chondrosarcoma cytotoxic drugs such as melphalan, an alkylating agent (7). An interesting application of ^{99m}Tc-NTP 15-5 imaging is as a "methodology companion" for innovative therapeutic approaches to degenerative and tumoral pathologies of the cartilage, using a proteoglycan targeting strategy.

Ethics statement

The studies involving human participants were reviewed and approved by Comité de Protection des Personnes Sud-Ouest et Outre-Mer II. The patients/participants provided their written informed consent to participate in this study.

Author contributions

Conception and design: FC, ET, and IM. Investigators of the study: FC, MC, SM, and XD. Review of study design and protocol: SL, PA, TB, NS, GF, LM, EJ, IM, ET, FC, JR, XD, FP-L, and EM-N. Study coordination: FC and ET. Data management and statistical analysis: IM. Obtaining funding and supervision: FC and EM-N. Drafting ^{99m}Tc-NTP 15-5 IMPD: PA, M-JG, SL, EM-N, and FC. Drafting the manuscript: ET and MC. All authors contributed to revision, adaptation, and final approval of the manuscript and accountable for all aspects of the work.

Funding

The trial will be funded by the French government IDEX-ISITE initiative 16-IDEX-0001-CAP 20-25 (Challenge 3: mobility-2017) of the University of Clermont Auvergne. The toxicology regulatory studies needed for the IMPD of 99mTc-NTP 15-5 were supported by the French National Research Agency (ANR 15-CE18-003). The funding parties were not involved in the design or conduct of the study, nor in the collection, management, analysis, and interpretation of the data. They were not involved in the writing of the manuscript.

Acknowledgments

We are grateful to all the patients and their caregivers, the members of the Independent Data Monitoring Committee and the investigators.

Conflict of interest

The authors declare that the research was conducted in the absence of any commercial or financial relationships that could be construed as a potential conflict of interest.

Publisher's note

References

1. Maurizis JC, Rapp M, Nicolas C, Ollier M, Verny M, Madelmont JC. Disposition in rats of N-pyridinium-propyl-cyclam, N-triethylammonium-propyl-cyclam, and N-[Triethylammonium]-3-propyl-[15]ane-N5, potential cartilage imaging agents. *Drug Metab Dispos Biol Fate Chem*. (2000) 28:418–22. doi: 10.1021/bc990128+

2. Miot-Noirault E, Guicheux J, Vidal A, Gauthier O, Auzeloux P, Lesoeur J, et al. In vivo experimental imaging of osteochondral defects and their healing using (99m)Tc-NTP 15-5 radiotracer. *Eur J Nucl Med Mol Imaging*. (2012) 39:1169–72. doi: 10.1007/s00259-012-2081-4

3. Cachin F, Boisgard S, Vidal A, Filaire M, Auzeloux P, Culot D, et al. First ex vivo study demonstrating that 99mTc-NTP 15-5 radiotracer binds to human articular cartilage. *Eur J Nucl Med Mol Imaging*. (2011) 38:2077–82. doi: 10.1007/s00259-011-1890-1

4. Miot-Noirault E, Vidal A, Pastoureau P, Bonafous J, Chomel A, Sarry L, et al. Early detection and monitoring of cartilage alteration in the experimental meniscectomised guinea pig model of osteoarthritis by 99mTc-NTP 15-5 scintigraphy. *Eur J Nucl Med Mol Imaging*. (2007) 34:1280–90. doi: 10.1007/s00259-006-0320-2

5. Miot-Noirault E, Vidal A, Auzeloux P, Madelmont JC, Maublant J, Moins N. First In Vivo SPECT Imaging of Mouse Femorotibial Cartilage Using 99mTc-NTP 15-5. *Mol Imaging*. (2008) 7:263–71. doi: 10.2310/7290.2008.00026

6. Khairnar A, Marchand F, Vidal A, Etienne M, Miladi I, Auzeloux P, et al. 99mTc-NTP 15-5 imaging for cartilage involvement in experimental rheumatoid arthritis: comparison with routinely used molecular imaging methods and sensitivity to chronic nonsteroidal antiinflammatory drug treatment. *J Nucl Med Off Publ Soc Nucl Med*. (2015) 56:798-804. doi: 10.2967/jnumed.114.151415

7. Peyrode C, Weber V, Voissière A, Maisonial-Besset A, Vidal A, Auzeloux P, et al. Proteoglycans as target for an innovative therapeutic approach in chondrosarcoma: preclinical proof of concept. *Mol Cancer Ther*. (2016) 15:2575–85. doi: 10.1158/1535-7163.MCT-16-0003

8. Briat A, Jacques C, Malige M, Sudre L, Nourissat G, Auzeloux P, et al. 99mTc-NTP 15-5 is a companion radiotracer for assessing joint functional response to sprifermin (rhFGF-18) in a murine osteoarthritis model. *Sci Rep*. (2022) 12:8146. doi: 10.1038/s41598-022-11080-4

9. Wilmot A, Gieschler S, Behera D, Gade TP, Reumann MK, Biswal S, et al. Molecular imaging: an innovative force in musculoskeletal radiology. *AJR Am J Roentgenol*. (2013) 201:264–77. doi: 10.2214/AJR.13.10713

10. Alizai H, Walter W, Khodarahmi I, Burke CJ. Cartilage Imaging in Osteoarthritis. *Semin Musculoskelet Radiol*. (2019) 23:569–78. doi: 10.1055/s-0039-1695720

11. Kijowski R, Demehri S, Roemer F, Guermazi A. Osteoarthritis year in review 2019: imaging. *Osteoarthritis Cartilage.* (2020) 28:285–95. doi: 10.1016/j.joca.2019.11.009

12. Ding C, Zhang Y, Hunter D. Use of imaging techniques to predict progression in osteoarthritis. *Curr Opin Rheumatol.* (2013) 25:127–35. doi: 10.1097/BOR.0b013e32835a0fe1

13. van der Kraan PM, Berenbaum F, Blanco FJ, Cosimo de B, Lafeber F, Hauge E, et al. Translation of clinical problems in osteoarthritis into pathophysiological research goals. *RMD Open.* (2016) 2:e000224. doi: 10.1136/rmdopen-2015-000224

14. Katz JN, Arant KR, Loeser RF. Diagnosis and Treatment of Hip and Knee Osteoarthritis: A Review. *JAMA*. (2021) 325:568–78. doi: 10.1001/jama.2020.22171

15. Berenbaum F, Kloppenburg M. Osteoarthritis: Research in motion. *Best Pract Res Clin Rheumatol.* (2017) 31:611–2. doi: 10.1016/j.berh.2018.07.001

16. Din OS, Dodwell D, Wakefield RJ, Coleman RE. Aromatase inhibitor-induced arthralgia in early breast cancer: what do we know and how can we find out more? *Breast Cancer Res Treat.* (2010) 120:525–38. doi: 10.1007/s10549-010-0757-7

17. Niravath P. Aromatase inhibitor-induced arthralgia: a review. *Ann Oncol Off J Eur Soc Med Oncol.* (2013) 24:1443–9. doi: 10.1093/annonc/mdt037

18. Fois GR, Valla C, Jouberton E, Sas N, Billoux T, Auzeloux P, et al. Internal dosimetry of [99m Tc]NTP15-5 radiotracer for cartilage imaging in preclinical and clinical models using the GATE Monte Carlo platform. *Med Phys.* (2021) 48:477–87. doi: 10.1002/mp.14603

19. Vidal A, Gaumet V, Galmier MJ, Besse S, Leal F, Gachon F, et al. Development of a freeze-dried kit formulation for the preparation of 99mTc-NTP 15-5, a radiotracer for scintigraphic imaging of proteoglycans. *Appl Radiat Isot Data Instrum Methods Use Agric Ind Med.* (2015) 101:1–9. doi: 10.1016/j.apradiso.2015.03.010

20. Giraud I, Rapp M, Maurizis JC, Madelmont JC. Application to a cartilage targeting strategy: synthesis and in vivo biodistribution of (14)C-labeled quaternary ammonium-glucosamine conjugates. *Bioconjug Chem.* (2000) 11:212–8. doi: 10.1021/bc990128+

21. Vidal A, Chezal JM, Mounetou E. New quaternary ammonium oxicam derivatives: synthesis and in vitro antiosteoarthritis evaluation. *Eur J Med Chem.* (2010) 45:405–10. doi: 10.1016/j.ejmech.2009.09.026

frontiers | Frontiers in Medicine

TYPE Brief Research Report
PUBLISHED 16 November 2022
DOI 10.3389/fmed.2022.1042620

OPEN ACCESS

EDITED BY
Giorgio Treglia,
Ente Ospedaliero Cantonale (EOC), Switzerland

REVIEWED BY
Francesco Dondi,
Università degli Studi di Brescia, Italy
Lucia Leccisotti,
Agostino Gemelli University Polyclinic (IRCCS), Italy

*CORRESPONDENCE
Michele Colaci
michele.colaci@unict.it

SPECIALTY SECTION
This article was submitted to Nuclear Medicine, a section of the journal Frontiers in Medicine

RECEIVED 12 September 2022
ACCEPTED 31 October 2022
PUBLISHED 16 November 2022

CITATION
Colaci M, Dichiara J, Aprile ML, Ippolito M, Schinocca C, Guggino G and Malatino L (2022) Use of 18F-fluorodeoxyglucose positron emission tomography-computed tomography in patients affected by polymyalgia rheumatica and persistent increase of acute phase reactants.
Front. Med. 9:1042620.
doi: 10.3389/fmed.2022.1042620

Use of 18F-fluorodeoxyglucose positron emission tomography-computed tomography in patients affected by polymyalgia rheumatica and persistent increase of acute phase reactants

Michele Colaci[1]*, Jessika Dichiara[1], Maria Letizia Aprile[1], Massimo Ippolito[2], Claudia Schinocca[3], Giuliana Guggino[3] and Lorenzo Malatino[1]

[1]Rheumatology Clinic, Internal Medicine Unit, Azienda Ospedaliera per l'Emergenza (AOE) Cannizzaro, University of Catania, Catania, Italy, [2]Nuclear Medicine Unit, Azienda Ospedaliera per l'Emergenza (AOE) Cannizzaro, Catania, Italy, [3]Rheumatology Unit, Policlinico "P. Giaccone", University of Palermo, Palermo, Italy

Polymyalgia rheumatica (PMR) is an inflammatory disease affecting older adults characterized by aching pain and morning stiffness of the shoulder and pelvic girdles. Moreover, PMR can be associated with giant cell arteritis (GCA). Generally, PMR is highly responsive to steroids, reaching complete remission in the majority of cases. However, the possibility of occult diseases, including extra-cranial GCA, should be excluded. 18F-fluorodeoxyglucose positron emission tomography (^{18}F-FDG-PET) is able to detect the presence of peri-/articular or vascular inflammation, which may be both present in PMR, thus representing a useful diagnostic tool, mainly in presence of extra-cranial GCA. We retrospectively evaluated all consecutive patients who received the diagnosis of PMR in our rheumatology clinic, classified according to the 2012 American College of Rheumatology/European League Against Rheumatism (ACR/EULAR) criteria, in the period between April 2020 and May 2022. Among this case series, we selected the patients who underwent ^{18}F-FDG-positron emission tomography (PET) because of the persistent increase of acute phase reactants (APR) besides the steroid therapy. Eighty patients were diagnosed with PMR. Nine out of them also presented arthritis of the wrists during the follow-up, whereas none showed signs of cranial GCA at the diagnosis. Seventeen out of eighty subjects (mean age 71.5 ± 7.5 years; M/F 2/15) presented persistent increase of erythrocyte sedimentation rate (mean ESR 44.2 ± 20.8 mm/h) and/or C-reactive protein (mean CRP 25.1 ± 17 mg/l), thus they underwent total body ^{18}F-FDG-PET/CT. Large vessel ^{18}F-FDG uptake indicating an occult GCA was found in 5/17 (29.4%) cases. Twelve out of seventeen (70.6%) patients showed persistence of peri-/articular

inflammation, suggesting a scarce control of PMR or the presence of chronic arthritis. Finally, in 2 cases, other inflammatory disorders were found, namely an acute thyroiditis and a hip prosthesis occult infection. ^{18}F-FDG-PET/CT in PMR patients with persistent increase of APR is a useful diagnostic technique in order to detect occult GCA, persistence of active PMR or other misdiagnosed inflammatory diseases.

KEYWORDS

polymyalgia rheumatica, PET, giant cell arteritis, arthritis, inflammation

Introduction

Polymyalgia rheumatica (PMR) is an inflammatory disease affecting adults older than 50 years characterized by aching pain and morning stiffness of the shoulder and pelvic girdles. The presence of elevated inflammatory markers is typical, but non-specific for diagnosis; moreover no specific autoantibodies have been found and rheumatoid factor is generally absent (1, 2).

Polymyalgia rheumatica is associated with tenosynovitis, bursitis and, in a minority of cases, synovitis of proximal large joints, that may be easily evidenced by means of ultrasounds. For this reason, the 2012 European League Against Rheumatism/American College of Rheumatology Classification Criteria for PMR included the role of ultrasounds in identifying subdeltoid or trochanteric bursitis, biceps tenosynovitis and/or hip or glenohumeral synovitis (3).

Polymyalgia rheumatica may overlap with giant cell arteritis (GCA) in about 20% of patients (4). The diagnosis of vasculitis is easy in the case of cranial GCA, whereas the coexistence of an extra-cranial GCA involving aorta and its main branches could be frequently misdiagnosed because of the absence of typical clinical features. In this case, the eventual presence of large vessel inflammation requires the use of diagnostic techniques such as the magnetic resonance imaging or, more appropriately, the 18F-fluorodeoxyglucose positron emission tomography-computed tomography (^{18}F-FDG-PET/CT) (5, 6). These imaging techniques are not included in the first line check-up of PMR patients because of their high costs and frequent logistic issues.

Generally, PMR is highly responsive to steroids, reaching complete remission in the majority of cases. In clinical practice, patients' symptoms and the serum levels of acute phase reactants (i.e., erythrocyte sedimentation rate, ESR, and C-reactive protein, CRP) are considered to decide diagnostics and treatment, including the possibility to investigate the presence of an occult extra-cranial GCA (5–7). In this purpose, the persistent elevation of ESR and/or CRP, besides the apparent patients' clinical response to steroid therapy, could justify the indication to carry out second level diagnostic exams, such as total body ^{18}F-FDG-PET/CT, in order to identify an extra-cranial GCA or to exclude other inflammatory occult disorders, i.e., infectious diseases or neoplasms (6–9).

In this study, we aimed to analyze the clinical histories of a cohort of PMR patients, dwelling on cases who carried out total body ^{18}F-FDG-PET/CT and focusing on the diagnostic findings.

Methods

We retrospectively evaluated the clinical records of all consecutive patients affected by PMR, satisfying the 2012 EULAR/ACR classification criteria for this disease (3), who referred our rheumatology clinics at the Azienda ospedaliera per l'Emergenza "Cannizzaro," Catania, and at the Policlinico Universitario "P. Giaccone," Palermo, Italy, in the period between January 2020 and January 2022. Patients with PMR associated with GCA at baseline were excluded.

The patients were treated with steroids, according to the 2015 EULAR/ACR recommendations for the management of PMR (5). The starting dose of prednisone was within the range of 12.5–25 mg/day that was tapered to 10 mg/day within 4–8 weeks and then by 1 mg every 4 weeks until the end, if remission was achieved.

All patients gave their informed consent to the study, which was carried out in accordance with the ethical standards of 1964 Helsinki Declaration and its later amendments, and approved by the local Ethical Committee.

Patients' records included their complete clinical histories, with demographic data, rheumatologic work-up and treatments, in particular ESR and CRP results during the follow-up and the findings of second level diagnostic exams (i.e., total body PET), if performed.

In the purpose of this study, we selected only the cases who underwent the total body PET because of the persistent increase of ESR and/or CRP, despite the apparent favorable clinical course using steroid therapy. In all subjects, the PET was planned after 1 year of treatment, while the patients were treated with low dose of steroids ($\leq$6.25 mg of prednisone), discontinuing its intake in the 3 days prior to the exam.

TABLE 1 The polymyalgia rheumatica (PMR) patients (Pts) with increased acute phase reactants (APR), besides steroid therapy, who underwent total body 18F-fluorodeoxyglucose positron emission tomography-computed tomography (^{18}F-FDG-PET/CT).

Pts	APR		^{18}F-FDG uptake at PET/CT			
Age/ sex	ESR mm/h	CRP mg/l	Vascular sites	Peri-/articular sites	Other sites	Follow-up
74F	40	15		Shoulders and coxofemorals, wrists		RA diagnosis; successful treatment with baricitinib 27 months long
72F	70	9	Thoracic aorta	Right shoulder		MTX 10 mg/week, plus TCZ 12 months later for persistence of ^{18}F-FDG aortic uptake at 2nd PET
64M	30	27		Shoulders and right knee		MTX 15–20 mg/week, reaching clinical control (no 2nd PET)
80F	79	23		Right shoulder		MTX 7.5 mg/week, reaching clinical control (no 2nd PET)
66F	16	10	Femoral aa.	Shoulders and coxofemorals		TCZ from 14 months, clinical control (no 2nd PET)
61F	38	18		Shoulders and coxofemorals, cervical and lumbar spinous processes		MTX 10 mg/week, reaching clinical control (no 2nd PET)
71F	44	28		Wrists		MTX not tolerated; the patient is paucisymptomatic and she refused other treatments
71M	73	10	Femoral aa.			MTX 15 mg/week: asymptomatic but persistent increase of APR; candidate to TCZ
78F	56	19	Femoral aa.	Shoulders, knees, ankles		MTX 15–20 mg/week, reaching clinical control (no 2nd PET)
68F	12	24		Shoulders, ankles		MTX 10 mg/week, reaching clinical control (no 2nd PET)
56F	73	41			Thyroid	Treated for acute thyroiditis
72F	33	18		Ischiatic tuberosities		MTX 10 mg/week, reaching clinical control (no 2nd PET)
76F	41	12	Subclavian, axillary, and carotid aa.			MTX 15 mg/week, reaching clinical control (no 2nd PET)
87F	55	19			Hip prosthesis	Hip prosthesis infection, refuse of the replacement, death after few months
78F	18	67		Shoulders and right coxofemoral		Increase of steroid, refuse of other treatments
67F	44	24		Shoulders, ischiatic tuberosities		Since MTX failure, TCZ prescription reaching clinical control (no 2nd PET)
74F	29	63				Confirmation of MTX 15 mg/week

The table illustrates the sites with ^{18}F-FDG uptake. Therapies and follow-up after positron emission tomography (PET) performance are also indicated for each patient. RA, rheumatoid arthritis; MTX, methotrexate; TCZ, tocilizumab; aa., arteries.

Positron emission tomography findings were reported in the clinical records, while the images were available using the hospital software for instrumental diagnostics.

The PETs/CTs were performed using the tracer ^{18}F-FDG and a dedicated, commercially available PET/CT scanner (Biograph Horizon 16, Siemens Healthcare GmbH, Erlangen, Germany).

In each patient, 3.7 MBq/Kg of FDG was intravenously administered after fasting for at least 4 h. Scans were conducted from the middle of the thigh to the top of the skull 60 min after FDG administration. ^{18}F-FDG-PET/CT images were obtained by integrated PET/CT scanner (Discovery ST; GE Medical Systems, Milwaukee, WI, USA) or Biograph mCT (Siemens Medical Solutions, Erlangen, Germany). All emission scans were performed in three-dimensional mode and acquisition time per bed position was 2.5 min for Discovery ST and 2 min for Biograph mCT.

The PET reconstruction settings were subjected to CT-based attenuation correction, using an ordered subset expectation maximization (OSEM) algorithm.

The full-width at half-maximum values of the Discovery ST and Biograph mCT were 5.2 and 4.4 mm, respectively. A low-dose 16-slice CT (tube voltage 120 kV; effective tube current 30–250 mA, Discovery ST) and a low-dose 16-slice CT (tube voltage 120 kV; use of angular and longitudinal dose modulation, CAREDose4D®, Biograph mCT) from the skull

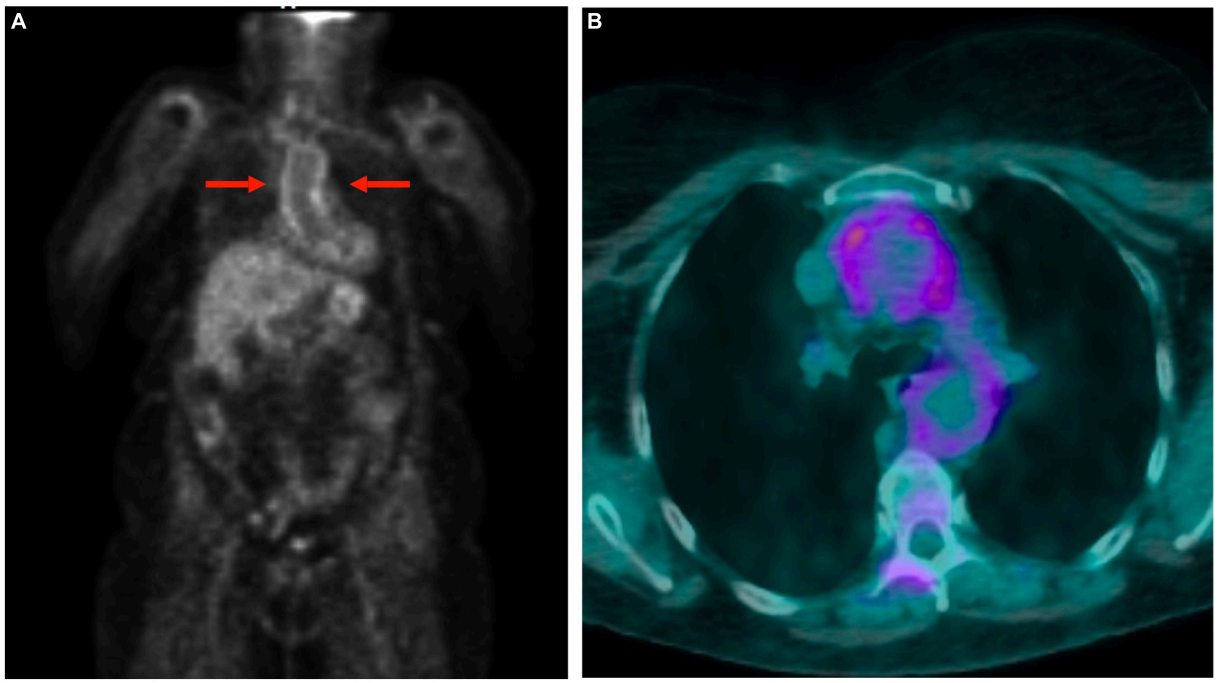

FIGURE 1
Total body 18F-fluorodeoxyglucose positron emission tomography-computed tomography (^{18}F-FDG-PET/CT) in a polymyalgia rheumatica (PMR) patient with giant cell arteritis. The images show the involvement of the aorta: uptake of the thoracic aortic wall in maximum intensity projection image **(A)** and transverse fused (PET and CT) slice **(B)**.

base to the proximal thigh were performed for attenuation correction, and for determining the precise anatomic location of lesions before acquisition of PET images. CT scans were reconstructed by filtered back projection into 512 × 512 pixel images with slice thickness of 5 mm to match the PET scan.

Overall, the ^{18}F-FDG-PET/CT study was conducted according to the international procedural recommendations for the study of patients affected by PMR and GCA (9).

All continuous variables are presented as mean ± standard deviation (SD), after confirming their normal distribution by means of the Kolmogorov–Smirnov test; categorical variables are presented as a percentage value. The variables were compared using the appropriate tests, in particular subgroup proportions were compared by Fisher's exact test. *P*-values < 0.05 were considered statistically significant.

The statistical analysis was performed using NCSS 2007 and PASS 11 software (Gerry Hintze, Kaysville, UT, USA).

Results

We retrospectively evaluated the clinical records of 80 consecutive PMR patients. None showed signs of cranial GCA at the diagnosis or during the follow-up. Moreover, 9 out of 80 also presented arthritis of the wrists during the follow-up, but not satisfying the classification criteria for rheumatoid arthritis.

Seventeen out of eighty (21.2%) PMR patients (mean age 71.5 ± 7.5 years; M/F 2/15) presented a persistent increase of ESR (mean ESR 44.2 ± 20.8 mm/h) and/or CRP (mean CRP 25.1 ± 17 mg/l), thus they underwent total body ^{18}F-FDG-PET/CT (Table 1). These 17 cases were considered for this study.

Large vessel ^{18}F-FDG uptake indicating an occult GCA was found in 5/17 (29.4%) cases (Figure 1), 6.2% of the entire cohort. Twelve out of seventeen (70.6%) patients showed persistence of peri-/articular inflammation (Figure 2), suggesting a scarce control of PMR and the coexistence of chronic arthritis.

In 2 cases, other inflammatory disorders were found, namely an acute thyroiditis in a 56 years old woman and a hip prosthesis occult infection, with a subcutaneous abscess, in an 87 years old woman unable to walk. Finally, in the last case, a woman 74 years old, PET/CT did not show significant ^{18}F-FDG uptake anywhere.

The presence of vasculitis did not correlate with age, sex, ESR or CPR serum levels, or clinical PMR presentation at the onset. Of interest, 3 out of 5 patients with GCA showed a prevalent involvement of the femoral arteries (Figure 2).

Among the 12 patients with persistent peri-arthritis or arthritis, the main pattern was the involvement of one or more girdles: namely, both shoulders and both hips in 4 cases, only shoulders in other 4 cases, just one shoulder in other 2 patients. The remaining cases showed ^{18}F-FDG uptake at the cervical

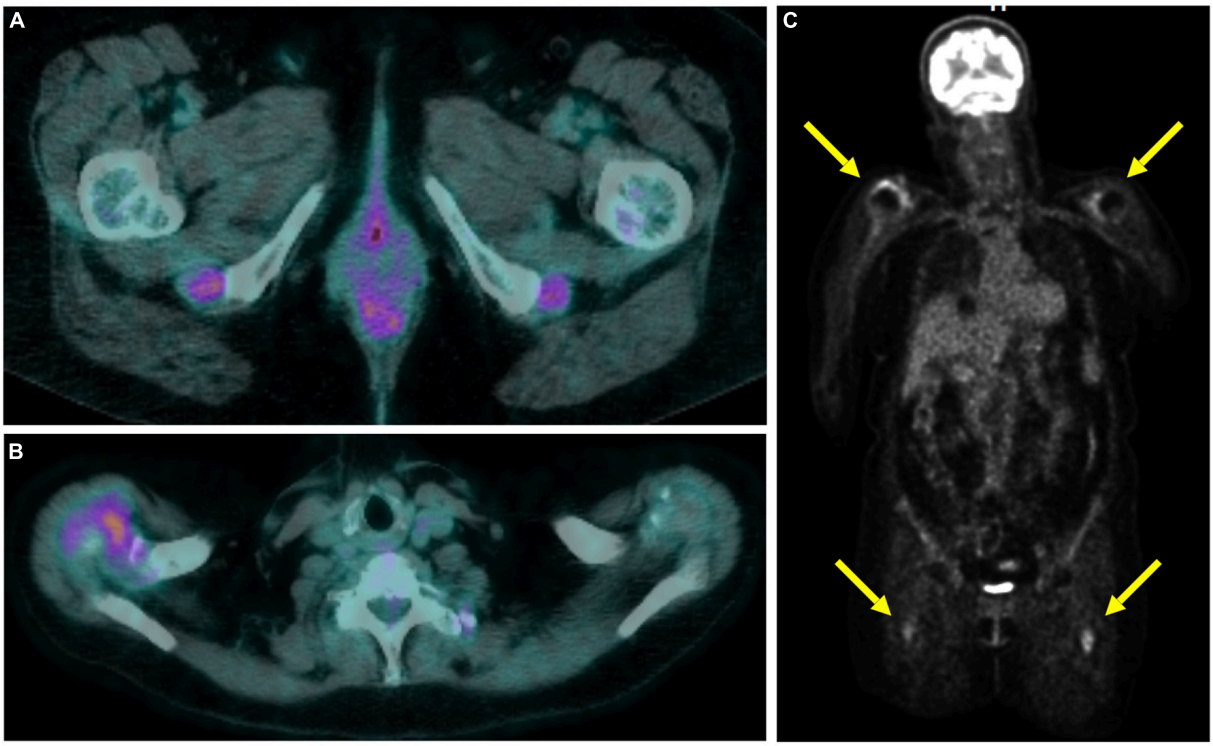

FIGURE 2
Total body 18F-fluorodeoxyglucose positron emission tomography-computed tomography (^{18}F-FDG-PET/CT) in a polymyalgia rheumatica (PMR) patient with persistent articular inflammation in the ischial tuberosities **(A)** and right shoulder **(B)**. Coronal slice in maximum intensity projection showing the uptake at the shoulders and subtrochanteric bursae **(C)**.

spinous processes in one subject, of the ischial bursae in another one, and of the wrists in the last one.

In the majority of these cases (8/12), a modest level of pain or joint limitation at the movement of the girdles were reported in the clinical records, but these symptoms were not considered clinically significant for active PMR. The other 4 subjects were described as totally asymptomatic.

The low number of cases did not permit finding eventual associations between the starting dose of steroids and the persistence of peri-/articular inflammation.

In the follow-up, the 5 patients with new diagnosis of GCA underwent treatment with tocilizumab. Instead, the 12 cases with persistent active PMR or arthritis were treated with methotrexate, as steroid-sparing agent.

Discussion

In this retrospective study, about a fifth of PMR patients treated with steroid therapy showed persistent increase of acute phase reactants during the follow-up. After the ^{18}F-FDG/CT evaluation, a misdiagnosed GCA was diagnosed in about 6% of cases, other occult inflammatory disorders in two cases, while the majority of PET-positive patients showed the persistence of peri-/articular inflammation associated with PMR. According to these findings, PMR patients with persistent increase of acute phase reactants should be considered resistant to steroid therapy first, even though the patient's feedback would indicate clinical remission and despite the use of recommended dosages of prednisone (5).

At the retrospective view of the clinical records, we found that 8 out of 12 PMR patients who showed ^{18}F-FDG uptake at peri-/articular sites were not totally asymptomatic. However, the modest entity of symptoms and the knowledge of confounders, such as concomitant osteoarthritis, made it difficult to attribute clinical relevance to those clinical signs. For this reason, the persistent increase of acute phase reactants represented the main cause to perform the total body ^{18}F-FDG-PET/CT for differential diagnosis. In the totally asymptomatic patients, ^{18}F-FDG-PET was considered an even more useful diagnostic exam, in order to find eventual occult inflammatory disorders; this is the case of extracranial GCA (6, 8, 9).

Furthermore, we could not find any correlation between clinical features, lab tests and standardized uptake value (SUV) values of ^{18}F-FDG-PET. Indeed, we did not find significant differences between patients as regards their symptoms or ESR/CRP serum levels. However, it would be possible that the small patient sample did not permit to evidence

significant correlations between ^{18}F-FDG-PET/CT findings and clinical parameters.

Recent meta-analysis (10, 11) focused on the prevalence of GCA in subjects who received the diagnosis of PMR. Besides the relevant frequency of coexistence of these two diseases, the authors underlined the high methodological heterogeneity of the studies that evaluated GCA onset in patients diagnosed with only PMR at baseline (as in the present study). The main issue was that the clinical screening for later development of GCA in PMR patients' follow-up was not performed systematically, leading to the risk of underdiagnosis for extra-cranial GCA. The latter, involving aorta and its main branches but not the superficial temporal arteries, usually remains asymptomatic, with the exception of the sign of systemic inflammation (i.e., fatigue, body weight loss, anemia), which are highly non-specific. In fact, it is hard to diagnose GCA without appropriate diagnostic techniques, such as ^{18}F-FDG-PET/CT. Therefore, clinical awareness should be raised in the management of PMR patients, in order to select subjects suitable for second level diagnostics. In this purpose, the persistent increase of acute phase reactants without any other plausible reason could represent a useful clue to lead selected patients to second level instrumental investigations.

Non-specific signs of systemic inflammation may be part of the clinical presentation of a number of other diseases, including cancer. PMR itself is considered a paraneoplastic syndrome, especially when its onset and clinical course is atypical, such as less or not responsive to steroids, asymmetrical, or with inappropriately high acute phase reactants (12, 13). Therefore, PMR diagnosis did not exclude *a priori* the coexistence of occult neoplasms. Considering this possibility, total body ^{18}F-FDG-PET/CT represents a good diagnostic approach, permitting to investigate in several directions contemporarily (14).

Systemic inflammation may be the expected consequence of infections that should be excluded virtually whenever serum levels of acute phase reactants were found increased. However, the differential diagnosis is often hard to make, in absence of clear signs of respiratory, intestinal or genitourinary infections, even after the main microbiological tests. In selected cases, total body ^{18}F-FDG-PET/CT represents a useful method of investigation (15), as it happened in our case with occult infection of the hip prosthesis. In particular, in our patient, the pain at the passive hip external-rotation did not allow to distinguish between PMR and other pathological causes, therefore the ^{18}F-FDG-PET/CT proved to be decisive in addressing the diagnosis.

Up to date, glucocorticoids are the cornerstone of PMR therapy (1–5), generally sufficient to obtain clinical remission. However, several studies described PMR patients steroids-resistant or that experienced a flare upon glucocorticoid tapering (16, 17). In these cases, additional use of traditional disease modifying drugs (DMARDs) to enforce the treatment and as steroid-sparing therapy is generally considered. In the case of GCA, the administration of tocilizumab, anti-IL6 agent, may be indicated.

Recently, Marsman et al. (18) announced a multicenter double-blind placebo controlled trial in order to investigate the therapeutic role of methotrexate in PMR patients, as well as its timing, dose and steroid-sparing capability. At first, in our case series, all patients were not considered resistant to steroid therapy, however, 8 out of 17 subjects with persistent increase of acute phase reactants showed mild symptoms presumably compatible with PMR. In these cases, we decided to carry out total body ^{18}F-FDG-PET/CT in order to exclude extra-cranial GCA, before enforcing therapy with methotrexate in the case of persistent peri-/articular inflammation.

Our study has some limitations. It is a retrospective study including a limited case series, thus it did not have the statistical strength to give us indications as regards the actual proportions of the phenomena described. However, the study represented a real life experience of second level rheumatology clinics. Moreover, our findings are suggestive in order to raise relevant clinical issues and to trace future lines of research.

In conclusion, the diagnosis of PMR could appear relatively simple in everyday clinical practice. However, this rheumatic condition could hide more severe diseases, particularly GCA. In the absence of specific clinical signs, the diagnosis of this vasculitis or other occult inflammatory disorders (i.e., infections or cancer) cannot be formulated without second level instrumental investigations, such as using total body ^{18}F-FDG-PET/CT. For this reason, physicians should be aware of the potential significance of persistent high levels of acute phase reactants in PMR patients, besides steroid therapy. In our opinion, it would be necessary to design multicenter large-cohort studies in order to focus on the opportunity to carry out total body ^{18}F-FDG-PET/CT in selected PMR patients, by means of new tools such as a clinical score (11).

The response of PMR to steroids is classically considered brilliant, thus medium-low doses of prednisone are recommended. Nonetheless, clinical remission could not be so easily achievable in every patient. Therefore, the possibility of persistence of inflammation, however, subclinical, should be considered and verified in the case of persistent high levels of acute phase reactants.

Data availability statement

The raw data supporting the conclusions of this article will be made available by the authors, without undue reservation.

Ethics statement

The studies involving human participants were reviewed and approved by the Ethical Committee of Catania 1. The patients/participants provided their written informed consent to participate in this study.

Author contributions

MC: study design. JD, MA, and CS: data collection. MI: data analysis. MC and MI: manuscript writing. GG and LM: manuscript editing. LM: study supervision. All authors contributed to the article and approved the submitted version.

Conflict of interest

The authors declare that the research was conducted in the absence of any commercial or financial relationships that could be construed as a potential conflict of interest.

Publisher's note

All claims expressed in this article are solely those of the authors and do not necessarily represent those of their affiliated organizations, or those of the publisher, the editors and the reviewers. Any product that may be evaluated in this article, or claim that may be made by its manufacturer, is not guaranteed or endorsed by the publisher.

References

1. Matteson EL, Dejaco C. Polymyalgia rheumatica. *Ann Intern Med.* (2017) 166:ITC65–80. doi: 10.7326/AITC201705020

2. González-Gay MA, Matteson EL, Castañeda S. Polymyalgia rheumatica. *Lancet.* (2017) 390:1700–12. doi: 10.1016/S0140-6736(17)31825-1

3. Dasgupta B, Cimmino MA, Maradit-Kremers H, Schmidt WA, Schirmer M, Salvarani C, et al. 2012 provisional classification criteria for polymyalgia rheumatica: a European league against rheumatism/American college of rheumatology collaborative initiative. *Ann Rheum Dis.* (2012) 71:484–92. doi: 10.1002/art.34356

4. Buttgereit F, Dejaco C, Matteson EL, Dasgupta B. Polymyalgia rheumatica and giant cell arteritis: a systematic review. *JAMA.* (2016) 315:2442–58. doi: 10.1001/jama.2016.5444

5. Dejaco C, Singh YP, Perel P, Hutchings A, Camellino D, Mackie S, et al. European league against rheumatism; American college of rheumatology. 2015 recommendations for the management of polymyalgia rheumatica: a European league against rheumatism/American college of rheumatology collaborative initiative. *Ann Rheum Dis.* (2015) 74:1799–807. doi: 10.1136/annrheumdis-2015-207492

6. van der Geest KSM, Treglia G, Glaudemans AWJM, Brouwer E, Jamar F, Slart RHJA, et al. Diagnostic value of [18F]FDG-PET/CT in polymyalgia rheumatica: a systematic review and meta-analysis. *Eur J Nucl Med Mol Imaging.* (2021) 48:1876–89. doi: 10.1007/s00259-020-05162-6

7. Camellino D, Matteson EL, Buttgereit F, Dejaco C. . Monitoring and long-term management of giant cell arteritis and polymyalgia rheumatica. *Nat Rev Rheumatol.* (2020) 16:481–95. doi: 10.1038/s41584-020-0458-5

8. Rehak Z, Sprlakova-Pukova A, Kazda T, Fojtik Z, Vargova L, Nemec P. 18F-FDG PET/CT in polymyalgia rheumatica-a pictorial review. *Br J Radiol.* (2017) 90:20170198. doi: 10.1259/bjr.20170198

9. Slart RHJA, Writing group, Reviewer group; Members of Eanm Cardiovascular, Members of Eanm Infection & Inflammation, Members of Committees, Snmmi Cardiovascular, Members of Council, Pet Interest Group, et al. FDG-PET/CT(A) imaging in large vessel vasculitis and polymyalgia rheumatica: joint procedural recommendation of the EANM, SNMMI, and the PET interest group (PIG), and endorsed by the ASNC. *Eur J Nucl Med Mol Imaging.* (2018) 45:1250–69. doi: 10.1007/s00259-018-3973-8

10. Nielsen AW, Frølund LL, Våben C, Bonde AR, Gormsen LC, de Thurah AL, et al. Concurrent baseline diagnosis of giant cell arteritis and polymyalgia rheumatica – A systematic review and meta-analysis. *Semin Arthritis Rheum.* (2022) 56:152069. doi: 10.1016/j.semarthrit.2022.152069

11. Hemmig AK, Gozzoli D, Werlen L, Ewald H, Aschwanden M, Blockmans D, et al. Subclinical giant cell arteritis in new onset polymyalgia rheumatica A systematic review and meta-analysis of individual patient data. *Semin Arthritis Rheum.* (2022) 55:152017. doi: 10.1016/j.semarthrit.2022.152017

12. Muller S, Hider S, Helliwell T, Partington R, Mallen C. The real evidence for polymyalgia rheumatica as a paraneoplastic syndrome. *Reumatismo.* (2018) 70:23–34. doi: 10.4081/reumatismo.2018.1031

13. Manzini CU, Colaci M, Ferri C, Manzini E. Paraneoplastic rheumatic disorders: a narrative review. *Reumatismo.* (2018) 70:199–211. doi: 10.4081/reumatismo.2018.1069

14. Muoio B, Albano D, Dondi F, Bertagna F, Annunziata S, Fiz F, et al. The role of [18F]FDG PET/CT in paraneoplastic autoimmune disorders: an umbrella review. *Q J Nucl Med Mol Imaging.* (2022) 66:229–33. doi: 10.23736/S1824-4785.22.03456-2

15. Casali M, Lauri C, Altini C, Bertagna F, Cassarino G, Cistaro A, et al. State of the art of 18F-FDG PET/CT application in inflammation and infection: a guide for image acquisition and interpretation. *Clin Transl Imaging.* (2021) 9:299–339. doi: 10.1007/s40336-021-00445-w

16. Mori S, Koga Y. Glucocorticoid-resistant polymyalgia rheumatica: pretreatment characteristics and tocilizumab therapy. *Clin Rheumatol.* (2016) 35:1367–75. doi: 10.1007/s10067-014-2650-y

17. Partington RJ, Muller S, Helliwell T, Mallen CD, Abdul SA. Incidence, prevalence and treatment burden of polymyalgia rheumatica in the UK over two decades: a population-based study. *Ann Rheum Dis.* (2018) 77:1750–6. doi: 10.1136/annrheumdis-2018-213883

18. Marsman DE, Bolhuis TE, den Broeder N, den Broeder AA, van der Maas A. PolyMyalgia rheumatica treatment with methotrexate in optimal dose in an early disease phase (PMR MODE): study protocol for a multicenter double-blind placebo controlled trial. *Trials.* (2022) 23:318. doi: 10.1186/s13063-022-06263-3

frontiers | Frontiers in Medicine

TYPE Original Research
PUBLISHED 25 November 2022
DOI 10.3389/fmed.2022.1050854

OPEN ACCESS

EDITED BY
Giorgio Treglia,
Ente Ospedaliero Cantonale (EOC), Switzerland

REVIEWED BY
Edel Noriega-Álvarez,
Hospital General Universitario de Ciudad Real, Spain
Sharjeel Usmani,
Kuwait Cancer Control Center, Kuwait

*CORRESPONDENCE
Marie Nicod Lalonde
marie.nicod-lalonde@chuv.ch

SPECIALTY SECTION
This article was submitted to Nuclear Medicine, a section of the journal Frontiers in Medicine

RECEIVED 22 September 2022
ACCEPTED 07 November 2022
PUBLISHED 25 November 2022

CITATION
Jreige M, Hall N, Becce F, Aubry-Rozier B, Gonzalez Rodriguez E, Schaefer N, Prior JO and Nicod Lalonde M (2022) A novel approach for fibrous dysplasia assessment using combined planar and quantitative SPECT/CT analysis of Tc-99m-diphosphonate bone scan in correlation with biological bone turnover markers of disease activity. *Front. Med.* 9:1050854. doi: 10.3389/fmed.2022.1050854

A novel approach for fibrous dysplasia assessment using combined planar and quantitative SPECT/CT analysis of Tc-99m-diphosphonate bone scan in correlation with biological bone turnover markers of disease activity

Mario Jreige[1], Nicolas Hall[2], Fabio Becce[3], Bérengère Aubry-Rozier[2], Elena Gonzalez Rodriguez[2], Niklaus Schaefer[1], John O. Prior[1] and Marie Nicod Lalonde[1]*

[1]Department of Nuclear Medicine and Molecular Imaging, Lausanne University Hospital and University of Lausanne, Lausanne, Switzerland, [2]Interdisciplinary Centre for Bone Diseases, Service of Rheumatology, Lausanne University Hospital and University of Lausanne, Lausanne, Switzerland, [3]Department of Diagnostic and Interventional Radiology, Lausanne University Hospital and University of Lausanne, Lausanne, Switzerland

Purpose: To investigate the emerging role of Tc-99m-labeled diphosphonate (Tc-99m-DPD) uptake quantification by SPECT/CT in fibrous dysplasia (FD) bone lesions and its correlation with biological bone turnover markers (BTMs) of disease activity.

Materials and methods: Seven patients (49 ± 16 years) with a confirmed diagnosis of FD were included in this retrospective study. Bone scans with Tc-99m-DPD and quantitative SPECT/CT (xSPECT/CT) were performed. SUV_{max} (maximum standard unit value) and SUV_{mean} (mean standard unit value) were measured in all FD bone lesions. The skeletal burden score (SBS) was assessed on planar scintigraphy and multiplied by mean SUV_{max} and SUV_{mean} to generate two new parameters, SBS_SUV_{max} and SBS_SUV_{mean}, respectively. Planar and xSPECT/CT quantitative measures were correlated with biological BTMs of disease activity, including fibroblast growth factor 23 (FGF-23), alkaline phosphatase (ALP), procollagen 1 intact N-terminal propeptide (P1NP) and C-terminal telopeptide (CTX), as well as scoliosis angle measured on radiographs. Statistical significance was evaluated with Spearman's correlations.

Results: A total of 76 FD bone lesions were analyzed, showing an average SUV_{max} and SUV_{mean} (g/mL) of 13 ± 7.3 and 8 ± 4.5, respectively. SBS, SBS_SUV_{max} and SBS_SUV_{mean} values were 30.8 ± 25.6, 358 ± 267 and

220.1 ± 164.5, respectively. Mean measured values of FGF-23 (pg/mL), ALP (U/L), P1NP (μg/L) and CTX (pg/mL) were 98.4 (22–175), 283.5 (46–735), 283.1 (31–1,161) and 494 (360–609), respectively. Mean scoliosis angle was 15.7 (7–22) degrees. We found a very strong positive correlation between planar-derived SBS and CTX (r = 0.96, p = 0.010), but no significant correlation between SUV_{max} or SUV_{mean} and biological BTMs. SBS_SUV_{max} showed a strong to very strong positive correlation with CTX (ρ = 0.99, p = 0.002), FGF-23 (ρ = 0.91, p = 0.010), ALP (ρ = 0.82, p = 0.020), and P1NP (ρ = 0.78, p = 0.039), respectively.

Conclusion: This study showed that biological BTMs are significantly correlated with diphosphonate uptake on bone scan, quantified by a new parameter combining information from both planar and quantitative SPECT/CT. Further analysis of bone scan quantitative SPECT/CT data in a larger patient population might help better characterize the skeletal disease burden in FD, and guide treatment and follow-up.

KEYWORDS

fibrous dysplasia, SPECT/CT, scintigraphy, bone scan, quantitative imaging, bone turnover markers

Introduction

Fibrous dysplasia (FD) is a benign, non-hereditary congenital bone disorder caused by impaired osteogenesis secondary to an activating somatic mutation in the GNAS gene, leading to mutations in the alpha subunit of the Gs protein (1, 2). FD is characterized by intramedullary fibro-osseous proliferative lesions and may present in a monostotic (single bone) or polyostotic (multiple bones) form, or as a feature of two rare syndromes, namely the McCune-Albright syndrome or the Mazabraud syndrome (1, 3). Symptoms of FD include bone pain, fractures, bone deformities and neurological deficits (4). Bone turnover markers (BTMs), namely alkaline phosphatase (ALP), procollagen 1 intact N-terminal propeptide (P1NP) and C-terminal telopeptide (CTX), have been used as markers of disease activity, but serum levels may be influenced by age, comorbidities and treatments, including bisphosphonates and denosumab (2, 5, 6). FGF-23 is a phosphate-regulating hormone overproduced in FD lesions which levels correlate with the disease burden and can also be used as a biomarker of disease activity (7). The skeletal burden score (SBS) derived from planar ^{99}Tc-methylene diphosphonate (^{99}Tc-MDP) bone scan evaluation has been validated as a reliable instrument for measuring the global skeletal burden of FD, based on estimation of the percentage of affected skeleton area on whole-body images. However, SBS derived from ^{99}Tc-MDP is limited as it is a semiquantitative method based on two-dimensional imaging (8). To overcome these limitations, Van der Bruggen et al. proposed to quantify the skeletal burden in FD using sodium fluoride PET/CT (9). Their study showed a strong correlation of Na^{18}F-PET/CT FD burden measurements with biological BTMs and suggested a possible role of this technique in treatment follow-up. The major limitation of Na^{18}F-PET/CT is its low availability and high cost, as opposed to bone scintigraphy. Recently, technological advances enabled to quantify ^{99m}Tc-DPD uptake in single-photon emission computed tomography (SPECT) coupled with computed tomography (CT) (xSPECT/CT, Symbia Intevo, Siemens Healthineers, Erlangen, Germany). The xSPECT showed an accurate activity recovery within 10% of the expected value for objects > 10 mL, which is similar to PET/CT (10).

The aim of our study was to investigate the correlation between Tc-99m-DPD xSPECT/CT uptake quantification of FD bone lesions and biological BTMs and scoliosis, as a complication of FD.

Materials and methods

Patient selection

Between 2016 and 2021, 17 patients with a confirmed diagnosis of FD were treated in our Interdisciplinary Centre for Bone Diseases at Lausanne University Hospital. Of these, 2 patients were excluded from this retrospective analysis because they did not have bone scintigraphy and 8 because they did not undergo quantitative SPECT/CT. Hence, our final study population consisted of 7 patients: 2 males and

5 females, with a median age of 59 years (range, 26–72 years), with confirmed diagnosis of FD based on histopathology or as part of a clinical syndrome (Mazabraud or McCune-Albright syndromes), available BTMs values and Tc-99m-DPD xSPECT/CT images. We retrospectively collected clinical, biological and radiological data from the patients' hospital medical records. The local Ethics Research Committee of the State of Vaud approved the research protocol (CER-VD #2018-01513). All patients participating in this study had signed an institutional general consent for retrospective use of their data in clinical research.

Biological bone turnover markers measurements

Dosage of biological markers were performed on early morning fasting blood samples. Results of the most recent BTMs dosage in respect to bone imaging were used. ALP, P1NP and CTX were measured in the central clinical routine laboratory of the Lausanne University Hospital; intact FGF-23 was measured by ELISA (Kainos, Tokyo, Japan) at the Inselspital (Bern, Switzerland). For P1NP and CTX premenopausal women normal ranges are used as reference (P1NP: < 58.6 µg/L; CTX: < 573 ng/L). Normal values are 36–120 UI/L for ALP, and 10–50 pg/mL for FGF-23.

Tc-99m-labeled diphosphonate single-photon emission computed tomography/computed tomography acquisition and analysis

All patients underwent whole-body planar imaging with low-energy high-resolution collimators, and a scanning speed of 12 cm/min, followed by quantitative SPECT/CT (Symbia Intevo, Siemens Healthineers, Erlangen, Germany) on regions with high uptake on planar scintigraphy. The xSPECT was acquired in average at 3 h and 22 min ± 31 min after intravenous injection of 10 MBq/kg of 99mTc-DPD with a mean patient dose of 798 ± 58 MBq. Images were acquired with 3 degrees rotation/step and 12 s/projection with a 256 × 256 matrix. Reduced-dose CT was acquired using 120 kV and 25 reference mAs modulation (Siemens Care Dose, Symbia Intevo, Erlangen, Germany). Images were reconstructed to generate xSPECT data allowing SUVbw quantification on post-processed images and measurement of SUV_{max} and SUV_{mean} (g/mL) using xSPECT reconstruction algorithm.

For each patient, the SUV_{max} and SUV_{mean} of all FD bone lesions visible on xSPECT and CT were measured with a 42% thresholding and classified according to their location in the axial or appendicular skeleton (**Figure 1**). All FD bone lesions were visually assessed based on pathological high uptake, excluding uptake due to degenerative changes. The SBS was assessed on planar scintigraphy for all patients in consensus by two nuclear medicine specialists (MJ and MNL) as described by Collins et al., and SBS_SUV_{max} and SBS_SUV_{mean} were generated by multiplying SBS by mean SUV_{max} and SUV_{mean} of all lesions for each patient, respectively (8).

Scoliosis Cobb angles were measured using the Carestream Vue PACS's orthopedics workflow tool by a musculoskeletal radiologist.

Statistical analysis

Continuous variables are reported as mean ± standard deviation (SD) and range.

Categorical data were analyzed using Fisher's exact test or chi-squared test, as appropriate. For comparison of two groups, the Student's *t*-test was used when assumptions for parametric tests were met; otherwise, the Mann-Whitney *U*-test was used.

Planar SBS and all xSPECT/CT quantitative measures were correlated with biological BTMs of disease activity, including FGF-23, ALP, P1NP and CTX, as well as with scoliosis angle using Spearman's correlation. Statistical analysis was performed using STATA (version 14.0; STATA Corp., College Station, Texas, USA). *P*-values less than 0.05 were considered as statistically significant.

Results

Study population

Seven patients with confirmed FD, quantitative SPECT/CT and BTMs dosage were retrospectively identified and included in this study. They had been referred for evaluation of FD confirmed on histopathological analysis ($n = 6$) and/or within the spectrum of a known syndrome ($n = 3$, 1 McCune-Albright syndrome and 2 Mazabraud syndromes). One patient with McCune-Albright syndrome did not have histopathological confirmation (**Table 1**). FD lesions were assessed on Tc-99m-DPD xSPECT/CT in all 7 patients. All seven included patients had a polyostotic form of FD. Four out of seven (57%) patients had previously been treated with bisphosphonates. A total number of 76 lesions for all patients were measured on xSPECT/CT with a mean number of lesions per patient of 10.9 ± 9.6. No difference was observed in terms of distribution of the 76 lesions between the axial ($n = 50$) and appendicular ($n = 26$) skeleton ($p = 0.273$).

Biological bone turnover markers

Mean measured values of biological BTMs were: FGF-23, 98.4 ± 56.3 pg/mL (22–175); ALP, 283.5 ± 243.6 U/L (46–735);

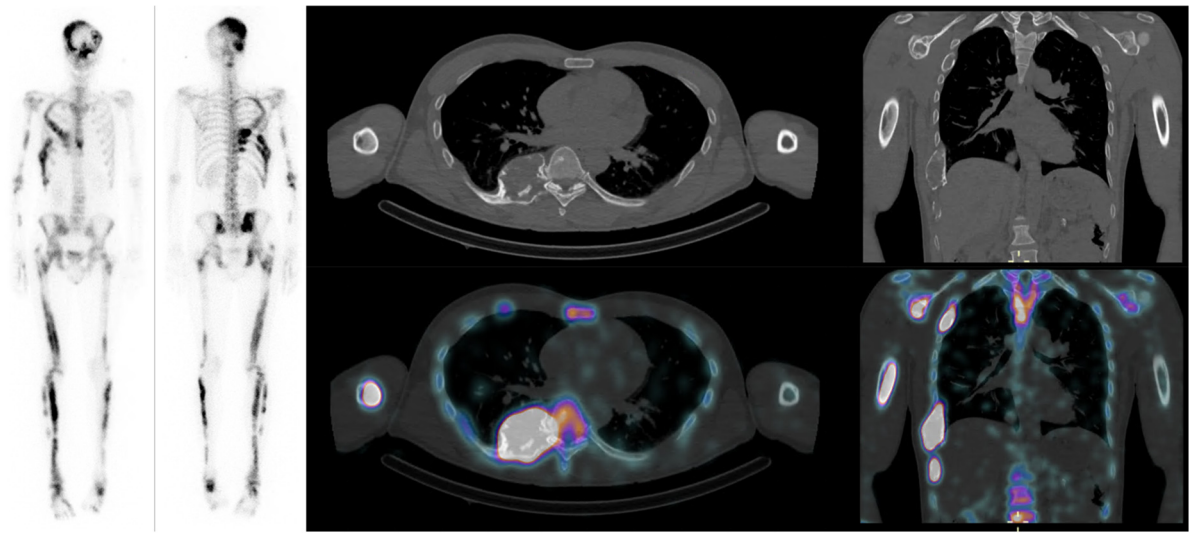

FIGURE 1
Forty-year-old male patient with Mazabraud syndrome: Mean SUV_{max} and SUV_{mean} of 11 and 6.7 g/mL, respectively. SBS: 46.3, FGF-23: 175 (10–50 pg/mL), CTX: 531 pg/mL, P1NP: 383 (15–78 μg/L), ALP: 277 (36–108) U/L, scoliosis angle: 11 degrees.

TABLE 1 Patient characteristics.

Patient number	Age (years)	Sex	Syndrome	Lesion location	Number of analyzed lesions	Scoliosis angle (degree)	Previous fractures	Treatment
1	48	Female	McCune-Albright	Axial and appendicular	10	22	Right 3rd, 6th, and 7th ribs	Bisphosphonate followed by denosumab
2	34	Female	–	Appendicular	1	7	–	–
3	26	Female	–	Axial and appendicular	4	11	–	Bisphosphonate
4	39	Male	Mazabraud	Axial and appendicular	13	11	–	–
5	62	Female	Mazabraud	Appendicular	5	21	–	Bisphosphonate
6	72	Male	–	Axial and appendicular	30	19	Right femoral diaphysis	–
7	55	Female	–	Axial and appendicular	13	19	–	Bisphosphonates

P1NP, 283.1 ± 406.7μg/L (31–1,161); and CTX, 494 ± 90.5 pg/mL (360–609). Scoliosis was reported in all patients with a mean angle of 15.7 ± 5.9 (7–22) degrees.

Quantitative Tc-99m-labeled diphosphonate single-photon emission computed tomography/computed tomography

A total number of 76 FD bone lesions were analyzed, showing a mean SUV_{max} and SUVmean of 13 ± 7.3 and 8 ± 4.5 g/mL, respectively. Mean SBS score was 30.8 ± 25.6. Mean SBS_SUV_{max} and SBS_SUV_{mean} were 358 ± 267 and 220 ± 165 g/mL, respectively. We found significantly higher values of SUV_{max} and SUV_{mean} in axial skeleton lesions (14.5 ± 1.1 and 8.9 ± 0.6 g/mL, respectively) compared to appendicular skeleton lesions (10 ± 1.2 and 6.2 ± 0.8 g/mL, respectively) ($p = 0.010$ and $p = 0.013$, respectively).

Correlations between bone turnover markers and imaging quantification

Spearman correlations results are shown in Table 2. We found a very strong positive correlation between planar-derived SBS and CTX ($\rho = 0.96$, $p = 0.01$), a statistical trend for a positive correlation with FGF-23 ($\rho = 0.81$, $p = 0.053$) and ALP ($\rho = 0.79$,

TABLE 2 Correlations between bone scintigraphy quantitative measures and biological bone turnover markers of disease activity and scoliosis angle.

Spearman correlations (ρ, CI, *p*-value)	SUV_{max}	SUV_{mean}	SBS	SBS_SUV_{max}	SBS_SUV_{mean}
FGF-23	(0.28, −0.69–0.89, 0.585)	(0.29, −0.68–0.89, 0.581)	(0.81, −0.02–0.98, 0.053)	**(0.91, 0.40–0.99, 0.010)**	**(0.91, 0.36–0.99, 0.013)**
ALP	(0.01, −0.81–0.81, 0.994)	(0.01, −0.81–0.81, 0.997)	(0.79, −0.05–0.98, 0.060)	**(0.82, 0.25–0.99, 0.020)**	**(0.88, 0.26–0.99, 0.019)**
P1NP	(0.04, −0.73–0.77, 0.928)	(0.06, −0.73–0.77, 0.901)	(0.69, −0.14–0.95, 0.089)	**(0.78, 0.06–0.97, 0.039)**	**(0.78, 0.07–0.97, 0.028)**
CTX	(0.13, −0.85–0.91, 0.837)	(0.18, −0.84–0.92, 0.772)	**(0.96, 0.50– 0.99, 0.010)**	**(0.99, 0.83–0.99, 0.002)**	**(0.99, 0.85–0.99, 0.001)**
Scoliosis angle	(0.33, −0.56–0.87, 0.472)	(0.36, −0.52–0.88, 0.432)	(0.58, −0.31–0.93, 0.168)	(0.62, −0.25–0.94, 0.137)	(0.63, −0.24–0.94, 0.133)

CI, Confidence interval; SUV, Standard uptake value; SUVmax, maxium Standard Uptake Value; SUVmean, mean Standard Uptake Value; SBS, Skeletal Burden Score; SBS_SUVmax, SBS score multiplied by SUVmax; SBS_SUVmean, SBS score multiplied by SUVmean; FGF-23, Fibroblast growth factor 23; ALP, Alkaline phosphatase; P1NP, Procollagen 1 intact N-terminal propeptide; CTX, C-terminal telopeptide.

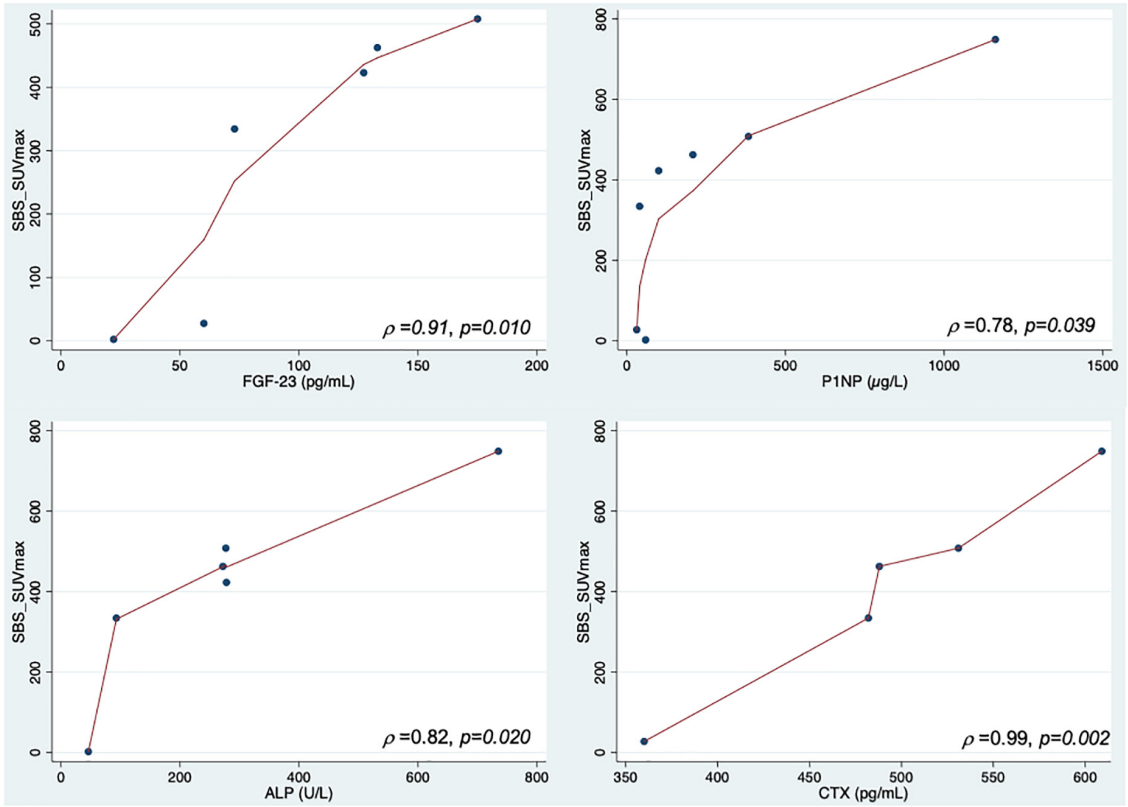

FIGURE 2
Correlations between SBS_SUV_{max} and FGF-23, ALP, P1NP and CTX.

$p = 0.060$) but no correlation with P1NP (ρ = 0.69, $p = 0.089$). No significant correlation was found between SUV_{max} or SUV_{mean} and biological BTMs. Combining both SBS and SUV increased the strength of the correlations: SBS_SUV_{max} and SBS_SUV_{mean} showed a strong to very strong positive correlation with CTX (ρ = 0.99, $p = 0.002$ and ρ = 0.99, $p = 0.001$), FGF-23 (ρ = 0.91, $p = 0.010$ and ρ = 0.91, $p = 0.013$), ALP (ρ = 0.82, $p = 0.020$ and ρ = 0.88, $p = 0.019$), and P1NP (ρ = 0.78, $p = 0.039$ and ρ = 0.78, $p = 0.028$), as shown in Figure 2. There was no correlation between bone scan quantitative measures and scoliosis angle. No significant correlation was found between SUV_{max} or SUV_{mean} of axial skeleton FD lesions with scoliosis angle (ρ = 0.33, $p = 0.472$ and ρ = 0.36, $p = 0.432$, respectively).

Discussion

In this study, we propose a novel approach to quantify the FD disease burden on Tc-99m-DPD bone scan using a combination of planar and absolute SPECT/CT

quantification by multiplying the well-known SBS score by the average SUV_{max} and SUV_{mean} values of the patient's FD lesions, leading to a disease-extension-corrected SUV value, which we termed SBS_SUV_{max} and SBS_SUV_{mean}, respectively. We showed that SBS_SUV_{max} and SBS_SUV_{mean} improved the correlation of bone imaging with disease activity as compared to SBS and SUV values alone: correlations between the results of this combined quantitative bone scan approach and biological activity as assessed by BTMs were strong to very strong and highly statistically significant.

To differentiate monostotic from polyostotic forms of FD and to evaluate the disease extent, patients with FD routinely undergo a Tc-99m-diphosphonate bone scan as recommended by current guidelines (11). Collins et al. have developed and validated the SBS, which is derived from a weighted score based on the estimation of the amount of FD lesions in anatomical segments on bone scintigraphy (8). The SBS correlated positively with BTMs, such as ALP, bone-specific ALP, osteocalcin, pyridinium cross-links, deoxypyridinoline cross-links, and N-telopeptide (8). However, this score has its limitations as it remains semiquantitative and is unable to quantify bone turnover activity within individual FD lesions, which may be of clinical relevance. ^{18}F-NaF-PET/CT overcomes this limitation by allowing single lesion bone turnover quantification (12). Van der Bruggen et al. demonstrated that 18F-NaF-PET/CT SUV thresholds could discriminate healthy bone from FD lesions (9). In addition, their study showed a strong relationship between serum markers of bone formation and measurements of FD burden by ^{18}F-NaF-PET/CT. Whereas SBS is not influenced by medical treatment, total lesion fluorination was higher in patients at baseline than in patients treated with biphosphonates, implying a potential role for $Na^{18}F$-PET/CT in treatment response assessment (9). Papadakis et al. also investigated the role of ^{18}F-NaF-PET/CT in FD skeletal burden assessment, and showed that BTMs, including ALP, N-telopeptides, and osteocalcin, were strongly correlated with total volume of all ^{18}F-NaF-positive FD lesions. These authors also found a very strong correlation between SBS derived from ^{18}F-NaF PET/CT and ^{99m}Tc-MDP scintigraphy (13). The drawback of ^{18}F-NaF PET/CT is that it is not reimbursed in many countries and/or not readily available, constituting an obstacle to its use in routine clinical practice.

Recently, absolute quantification of bone scintigraphy has become available and has been the subject of several studies. For example, Yamane et al. showed in a pediatric population that SUV was higher at the epiphyseal plates of children under 15 years of age compared to older subjects, consistent with higher osteoblastic activity (14). Another study in an adult population showed a significant difference in quantitative ^{99m}Tc-DPD uptake on bone xSPECT/CT between prostate cancer bone metastases and spinal and pelvic osteoarthritic changes, with higher SUV_{max} and SUV_{mean} in metastases (15). Therefore, the quantification of radiotracer uptake on bone scan might help differentiating between benign and malignant pathologies or other rheumatological disorders with high bone turnover, which needs to be confirmed by prospective studies.

To the best of our knowledge, our study is the first to report the absolute quantification of ^{99m}Tc-DPD uptake on xSPECT/CT in FD. We introduced new quantitative parameters, SBS_SUV_{max} and SBS_SUV_{mean}, to evaluate the disease burden. The main motivation for this quantitative model was to optimize the information extracted from bone scintigraphy combining both the overall disease activity assessed by SBS on a whole-body basis and the degree of tracer uptake assessed by mean SUV measurements of lesions in the xSPECT/CT field of view, as xSPECT/CT was not acquired on the whole body.

In our study, SBS alone correlated only with CTX, with a statistical trend toward a positive association with FGF-23 and ALP, while SUV_{max} and SUV_{mean} did not correlate with any BTMs. In contrast, SBS_SUV_{max} and SBS_SUV_{mean} correlated with all four BTMs. Multiplying mean SUV_{max} and SUV_{mean} of all lesions on xSPECT/CT by SBS could allow a more accurate characterization of bone turnover and disease activity in FD. The advantage of this quantification method is that bone scan is widely available and SPECT/CT quantification methods are increasingly implemented with new gamma cameras.

Finally, ^{18}F-FDG PET/CT has also been studied in FD and has shown a significant role in detecting malignant transformation of FD and optimizing patient management strategies in a complementary manner to ^{99m}Tc-MDP SPECT/CT (16). Therefore, quantification of bone scintigraphy may increase the accuracy of SPECT/CT in predicting disease activity, allowing this modality to remain competitive in the era of novel multimodal imaging, with particular potential as a biomarker for assessing disease activity and for monitoring treatment response.

This is a preliminary retrospective study, and thus its main limitation is the small number of patients included. However, the relatively large number of FD lesions analyzed increased the accuracy of the bone scan scores calculated for each patient. Further analyses of larger patient populations are needed to confirm the observed correlation between bone scintigraphy quantification and biological BTMs. In this study, SUV thresholding was used with a standard level of 42%, limiting reproducibility issues. However, an optimized approach to lesion delineation should be evaluated in larger future studies and compared with a standard fixed-level thresholding approach. In our study, the values of the scintigraphic quantitative measures did not correlate with the scoliosis angle. Interpretation of this observation remains limited as the range of scoliosis angles measured in our population was low.

Conclusion

This preliminary study showed a significant correlation between biological BTMs of disease activity and diphosphonate uptake on bone scan, quantified by a new parameter combining information from both planar and quantitative SPECT/CT. This approach could become the routine technique for clinical assessment of skeletal burden in FD due to its widespread availability. Further analysis of bone scan quantitative SPECT/CT data might help better characterize the skeletal disease burden in FD, and its role in guiding treatment and follow-up.

Data availability statement

The raw data supporting the conclusions of this article will be made available by the authors, without undue reservation.

Ethics statement

The studies involving human participants were reviewed and approved by the Ethics Research Committee of the State of Vaud. Written informed consent for participation was not required for this study in accordance with the national legislation and the institutional requirements.

Author contributions

MJ and MN designed the work, performed and interpreted the data analysis, and drafted and revised the work. NH participated to data collection. FB performed the radiologic measurements and revised the work. BA-R, EG, NS, and JP critically revised the work. All authors contributed to the article and approved the submitted version.

Conflict of interest

The authors declare that the research was conducted in the absence of any commercial or financial relationships that could be construed as a potential conflict of interest.

Publisher's note

All claims expressed in this article are solely those of the authors and do not necessarily represent those of their affiliated organizations, or those of the publisher, the editors and the reviewers. Any product that may be evaluated in this article, or claim that may be made by its manufacturer, is not guaranteed or endorsed by the publisher.

References

1. Schoenau E, Rauch F. Fibrous dysplasia. *Horm Res.* (2002) 57:79–82. doi: 10.1159/000058106

2. Boyce AM, Collins MT. Fibrous dysplasia/mccune-albright syndrome: a rare, mosaic disease of gαs activation. *Endocr Rev.* (2019) 41:345–70. doi: 10.1210/endrev/bnz011

3. Munksgaard PS, Salkus G, Iyer VV, Fisker RV. Mazabraud's syndrome: case report and literature review. *Acta Radiol Short Rep.* (2013) 2:2047981613492532. doi: 10.1177/2047981613492532

4. DiCaprio MR, Enneking WF. Fibrous dysplasia. Pathophysiology, evaluation, and treatment. *J Bone Joint Surg Am.* (2005) 87:1848–64. doi: 10.2106/JBJS.D.02942

5. Majoor BC, Appelman-Dijkstra NM, Fiocco M, van de Sande MA, Dijkstra PS, Hamdy NA. Outcome of long-term bisphosphonate therapy in mccune-albright syndrome and polyostotic fibrous dysplasia. *J Bone Miner Res.* (2017) 32:264–76. doi: 10.1002/jbmr.2999

6. Florenzano P, Pan KS, Brown SM, Paul SM, Kushner H, Guthrie LC, et al. Age-related changes and effects of bisphosphonates on bone turnover and disease progression in fibrous dysplasia of bone. *J Bone Miner Res.* (2019) 34:653–60. doi: 10.1002/jbmr.3649

7. Riminucci M, Collins MT, Fedarko NS, Cherman N, Corsi A, White KE, et al. FGF-23 in fibrous dysplasia of bone and its relationship to renal phosphate wasting. *J Clin Invest.* (2003) 112:683–92. doi: 10.1172/JCI18399

8. Collins MT, Kushner H, Reynolds JC, Chebli C, Kelly MH, Gupta A, et al. An instrument to measure skeletal burden and predict functional outcome in fibrous dysplasia of bone. *J Bone Miner Res.* (2005) 20:219–26. doi: 10.1359/JBMR.041111

9. van der Bruggen W, Hagelstein-Rotman M, de Geus-Oei L-F, Smit F, Dijkstra PDS, Appelman-Dijkstra NM, et al. Quantifying skeletal burden in fibrous dysplasia using sodium fluoride PET/CT. *Eur J Nucl Med Mol Imaging.* (2020) 47:1527–37. doi: 10.1007/s00259-019-04657-1

10. Gnesin S, Leite Ferreira P, Malterre J, Laub P, Prior JO, Verdun FR. Phantom validation of Tc-99m absolute quantification in a SPECT/CT commercial device. *Comput Math Methods Med.* (2016) 2016:4360371. doi: 10.1155/2016/4360371

11. Javaid MK, Boyce A, Appelman-Dijkstra N, Ong J, Defabianis P, Offiah A, et al. Best practice management guidelines for fibrous dysplasia/McCune-albright syndrome: a consensus statement from the FD/MAS international consortium. *Orphanet J Rare Dis.* (2019) 14:139. doi: 10.1186/s13023-019-1102-9

12. Czernin J, Satyamurthy N, Schiepers C. Molecular mechanisms of bone 18F-NaF deposition. *J Nucl Med.* (2010) 51:1826–9. doi: 10.2967/jnumed.110.077933

13. Papadakis GZ, Manikis GC, Karantanas AH, Florenzano P, Bagci U, Marias K, et al. 18F-NaF PET/CT imaging in fibrous dysplasia of bone. *J Bone Miner Res.* (2019) 34:1619–31. doi: 10.1002/jbmr.3738

14. Yamane T, Kuji I, Seto A, Matsunari I. Quantification of osteoblastic activity in epiphyseal growth plates by quantitative bone SPECT/CT. *Skeletal Radiol.* (2018) 47:805–10. doi: 10.1007/s00256-017-2861-9

15. Tabotta F, Jreige M, Schaefer N, Becce F, Prior JO, Nicod Lalonde M. Quantitative bone SPECT/CT: high specificity for identification of prostate cancer bone metastases. *BMC Muscul Dis.* (2019) 20:619. doi: 10.1186/s12891-019-3001-6

16. Wei W-J, Sun Z-K, Shen C-T, Zhang X-Y, Tang J, Song H-J, et al. Value of 99mTc-MDP SPECT/CT and 18F-FDG PET/CT scanning in the evaluation of malignantly transformed fibrous dysplasia. *Am J Nucl Med Mol Imaging.* (2017) 7:92–104.

frontiers | Frontiers in Medicine

TYPE Mini Review
PUBLISHED 30 November 2022
DOI 10.3389/fmed.2022.1070445

OPEN ACCESS

EDITED BY
Giorgio Treglia,
Ente Ospedaliero Cantonale (EOC), Switzerland

REVIEWED BY
Ryogo Minamimoto,
National Center For Global Health and Medicine, Japan

*CORRESPONDENCE
Gaetane Nocturne
gaetane.nocturne@aphp.fr
Florent L. Besson
florent.besson@aphp.fr

†These authors share last authorship

SPECIALTY SECTION
This article was submitted to Nuclear Medicine, a section of the journal Frontiers in Medicine

RECEIVED 14 October 2022
ACCEPTED 15 November 2022
PUBLISHED 30 November 2022

CITATION
Pean De Ponfilly – Sotier M, Seror R, Nocturne G and Besson FL (2022) ^{18}F-FDG PET molecular imaging: A relevant tool to investigate chronic inflammatory rheumatisms in clinical practice?
Front. Med. 9:1070445.
doi: 10.3389/fmed.2022.1070445

^{18}F-FDG PET molecular imaging: A relevant tool to investigate chronic inflammatory rheumatisms in clinical practice?

Marie Pean De Ponfilly – Sotier[1], Raphaële Seror[1,2,3], Gaetane Nocturne[1,2,3]*† and Florent L. Besson[2,4,5]*†

[1]Rheumatology, AP-HP. Université Paris-Saclay, Hôpital Bicêtre, Le Kremlin-Bicêtre, France, [2]Faculté de Médecine, Université Paris-Saclay, Le Kremlin-Bicêtre, France, [3]Université Paris-Saclay, INSERM, CEA, Centre de Recherche en Immunologie des Infections Virales et des Maladies Auto-immunes, Le Kremlin-Bicêtre, France, [4]Biophysics and Nuclear Medicine-Molecular Imaging, AP-HP. Université Paris-Saclay, Hôpital Bicêtre, Le Kremlin-Bicêtre, France, [5]Université Paris-Saclay, CEA, CNRS, Inserm, BioMaps, Orsay, France

^{18}F-Labeled Fluorodeoxyglucose-Positron Emission Tomography (^{18}F-FDG PET) is a molecular imaging tool commonly used in practice for the assessment of many cancers. Thanks to its properties, its use has been progressively extended to numerous inflammatory conditions, including chronic inflammatory rheumatism (CIR) such as rheumatoid arthritis (RA), spondylarthritis (SpAs) and polymyalgia rheumatica (PMR). ^{18}F-FDG PET is currently not recommended for the diagnostic of CIRs. However, this whole-body imaging tool has emerged in clinical practice, providing a general overview of systemic involvement occurring in CIRs. Numerous studies have highlighted the capacity of ^{18}F-FDG PET to detect articular and extra articular involvements in RA and PMR. However, the lack of specificity of ^{18}F-FDG limits its use for diagnosis purpose. Finally, the key question is the definition of the best way to integrate this whole-body imaging tool in the patient's management workflow.

KEYWORDS

^{18}F-FDG, PET, rheumatoid arthritis, spondylarthropathy, polymyalgia rheumatica

Introduction

Positron Emission Tomography (PET) is a whole-body, non-invasive, and highly sensitive imaging modality based on the detection of radiolabeled vectors of interest. During the last 20 years, PET using ^{18}F-fluoro-deoxy-glucose (^{18}F-FDG), an analog of glucose radiolabeled with Fluor 18 (^{18}F), has become a key imaging tool to diagnose, stage, and monitor many cancers in practice. Exploiting the metabolic properties of activated cells, the use of ^{18}F-FDG has been progressively extended to numerous inflammation and infection disorders (1). A recent report from the European league Against Rheumatisms (EULAR) highlighted the heterogeneity of the availability to PET

imaging for rheumatologic purpose across 25 European countries (2), which is currently dominated for the diagnosis of large vessel vasculitis (LVV) (3, 4) or to investigate fever of unknown origin (5). EULAR has provided official recommendations for the use of imaging in LVV, rheumatoid arthritis (RA) and spondylarthritis (SpAs) in clinical practice (2, 3, 6). While the use of PET modality is clearly defined only for LVV (3), ^{18}F-FDG PET applied to chronic inflammatory rheumatisms (CIR) has concretely emerged in clinical practice (7, 8) (**Figure 1** and **Table 1**). In this context, the choice of the best imaging modalities in patients with suspected CIRs – and the place of PET-CT in this strategy - arises at several stages of the management: to establish a positive diagnosis, to eliminate a differential diagnosis and in particular an infectious or para-neoplastic cause and finally to monitor the response to treatment.

The aim of this short review is to summarize the evidence-based literature on the benefits of ^{18}F-FDG PET imaging in patients with CIR, focusing on rheumatoid arthritis (RA), spondyloarthritis (SpA) and polymyalgia rheumatica (PMR). Promising other radiotracers of interest in this field will also be discussed.

^{18}F-FDG PET in rheumatoid arthritis

Rheumatoid arthritis is the most frequent CIR affecting 0.3–0.5% of the general population (9, 10). RA is characterized by an inflammation of synovial membrane (synovitis) resulting in bone erosion. The frequency of systemic manifestations seems to be decreasing apart from pulmonary involvement which affects about 20% of patients (11). According to the ACR/EULAR 2010 classification criteria (12), the diagnosis is based on clinical presentation and biological criteria [Acute-phase reactants, anti – cyclic citrullinated peptide2 antibodies (ACPA2) and/or rheumatoid factor (RF)]. Imaging by X-ray is required to look for structural damage (joint erosions).

Abbreviations: ^{18}F-FDG PET-CT, ^{18}F-labeled fluorodeoxyglucose-positron emission tomography/computed tomography; CIR, chronic inflammatory rheumatism; RA, rheumatoid arthritis; SpAs, spondylarthris; PMR, polymyalgia rheumatica; ACPA2, anti – cyclic citrullinated peptide2 antibodies; RF, rheumatoid factor; SUVmax, maximum standardized uptake value; DAS28 CRP, Disease activity score 28 C – Reactive Protein; SJC, Swollen joint count; TJC, Tender Joint Count; CVD, cardiovascular diseases; RLDA, Remission or low disease activity; MHDA, Moderate or high disease activity; AS, ankylosing spondylitis; SAPHO, Synovitis – Arthritis – Palmoplantar pustulosis - Hyperostosis – Osteitis syndrome; SIJ, sacroiliac joint; MLBP, mechanical low back pain; BASDAI, Bath Ankylosing Spondylitis Disease Activity Index; BASFI, Bath ankylosing spondylitis functional index; ROC, Receiver Operating Characteristic Curve; MRI, Magnetic resonance imaging; AUC, Area Under the Curve; SpA, Spondylarthritis; TNFi, TNF inhibitors; PMR, Polymyalgia rheumatic; GCA, giant cell arteritis; LVV, Live vessel vasculitis; RS3PE, remittive symmetrical seronegative synovitis with pitting edema; ICIs, immune check point inhibitors; irAes, immune-related adverse events; RMDs, Rheumatologic and Musculo-skeletal Disorders.

Although ^{18}F-FDG PET is not currently validated in this case, PET molecular imaging has demonstrated its diagnostic value in atypical and challenging cases. Bhattarai et al. (13) reported good performance of ^{18}F-FDG PET combined with computed tomography (PET-CT) to discriminate 18 RA from 17 non-RA patients (SAPHO syndrome, IgG4 arthritis, psoriatic arthritis and non-specific arthritis). Compared to non-RA patients, RA patients had significantly higher metabolic visual score defined by the sum of the maximum standardized uptake value of each joint (shoulders, elbow, wrist, hip, knee, and ankle). In the same way, Yamashita et al. (14) demonstrated significant differences of ^{18}F-FDG uptake on ischial tuberosity, great trochanter, spinous process, vertebral body and sacroiliac joint between RA, PMR, and SpA patients. Recently, Wang et al. (15) demonstrated that ^{18}F-FDG PET could discriminate 54 suspected RA (n = 23) from PMR (n = 31) patient, based on interspinous uptake combined with rheumatoid factor (AUC = 0.892).

Concerning the assessment of disease activity, Lee et al. investigated 91 active and mainly treatment-naïve RA with a mean Disease activity score of 28, C – Reactive Protein (DAS28 CRP) of 6.4. While univariate analyses showed correlations between PET-positive joint and clinic-biological symptoms (the swollen joint and Tender Joint Counts, DAS28 CRP and Erythrocyte sedimentation rate), multivariate analyses confirmed a positive correlation between PET positive joint and DAS28 ESR and patient's global disease score. Beckers et al. (16) supported these result and further demonstrated relationship between ^{18}F-FDG PET and ultrasonography to detect inflamed joints. However, the use of PET-CT for this purpose of monitoring response to therapy in RA patients is not sound in clinical practice. The gold standard should be clinico-biological follow-up by DAS28 score and structural follow-up by X-ray.

As a prognosis marker in RA, few ^{18}F-FDG PET studies have shown positive results. Roivainen et al. (17) have assessed the early predictive value of ^{18}F-FDG PET in RA patients treated by Methotrexate/Salazopyrine/Hydroxychloroquine tri-therapy. In 17 RA patients, ^{18}F-FDG-PET was performed at baseline, 2 and 4 weeks after the initiation of treatment. Interestingly, a decrease of disease activity on PET after 2 and 4 weeks of treatment correlated with DAS28 and CRP at 12 weeks. Elzinga et al. (18) supported these preliminary results with Infliximab, a monoclonal inhibitor of TNF, by showing a correlation between the early PET changes at 2 weeks and DAS28 at 14 and 22 weeks. Same performance was also reported with Tocilizumab, an interleukine – 6 inhibitor (19). To note, Bouman et al. did not supported this prognosis value in RA patients with low disease activity treated by TNF inhibitors (20). Again, the clinical usefulness arises. It would be useful to evaluate the economic cost and benefit-risk balance of performing 2 PET scans a few weeks apart in patients versus conventional clinical-biological monitoring.

10.3389/fmed.2022.1070445

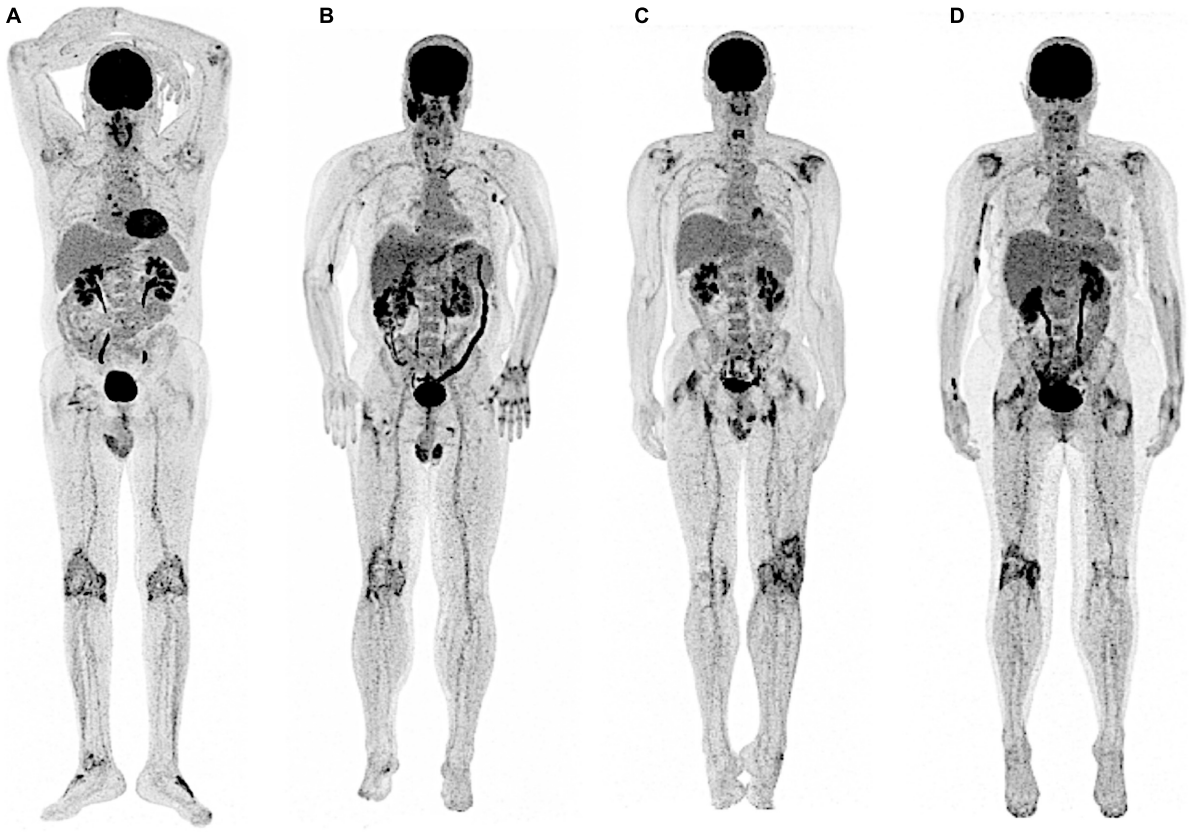

FIGURE 1
SpA and PMR: typical but non-specific periarticular patterns of ^{18}F-FDG uptake at the individual whole-body level. In both SpA **(A,B)** and PMR **(C,D)**, typical increase of ^{18}F-FDG uptake is frequently observed in the scapular and pelvic girdles as illustrated here, but also at sterno-clavicular joints and interspinous processes. In both CIR, peripheric articular involvement (knees) may also be observed. Typical ^{18}F-FDG PET findings are thus non-specific at the patient level.

Finally, the holistic nature of ^{18}F-FDG as a biomarker of cellular metabolic activity makes ^{18}F-FDG PET an intrinsic "swiss-knife" to evaluate multidimensional aspects of the same disease, even at a subclinical level. Due to vascular wall and/or systemic chronic inflammation condition, RA patients had an increased risk of cardiovascular diseases (CVD) (21, 22), up to 2–3-fold excess of mortality in comparison with general population (23). In their recent study, Geraldino-Pardilla et al. (22) showed in 91 RA patients without clinical evidence of CVD a significant relationship between ^{18}F-FDG PET vascular uptake of the aortic wall and both CVD risk factors (arterial hypertension and body mass index) and RA disease features (rheumatoid nodules and Disease activity score) (22). In the same way, Trang et al. (24) showed in 64 RA patients increased ^{18}F-FDG uptake of the aortic wall after 6 months of biologic therapies (TNF inhibitors, IL6 blockers and Ig CTLA4), even in RA patients with low disease activity or in clinical remission. Moreover, Amigues et al. reported subclinical myocardial ^{18}F-FDG uptake in 39% of their 119 RA patients without known CVD (25). For 8 patients requiring an step-up of their treatment, the longitudinal follow-up showed substantial decrease of myocardial ^{18}F-FDG uptake over 6 months, together with the clinical disease activity index. In a controlled study including 33 RA and age/gender matched controls with neither RA nor CVD, a significant correlation between synovial (acromioclavicular and acetabulo-femoral joints) and aortic ^{18}F-FDG uptake was observed only in the RA group (26). These results are interesting. Nevertheless, it would be necessary to define the pathological value of vascular abnormalities in RA patients and to be able to determine whether their detection should result in therapeutic intervention.

In summary, there are abnormalities specific to RA on PET CT. However, it is not clear whether this examination has a place in the diagnostic or follow-up strategy of patients.

^{18}F-FDG PET in spondylarthritis

Spondylarthritis is a composite spectrum of rheumatism disorders sharing common clinical and genetic features, including ankylosing spondylitis (AS), reactional arthritis,

TABLE 1 Characteristics of ^{18}F-FDG PET-CT in RA, SpAs, and PMR.

	Rheumatoid arthritis	Spondylarthritis	Polymyalgia rheumatica
Positive diagnosis	^{18}F-FDG uptake on peripheral joint (shoulder, elbow, wrist, hip, knee, ankle)	Specific but rare ^{18}F-FDG uptake on sacro iliitis.	Bilateral and symmetric ^{18}F-FDG uptake on gleno humeral, great trochanter, ischial tuberosities, sterno-clavicular joint and spinous process Similar FDG uptake for PMR-like irAEs
Differential diagnosis	Good discriminative performance for other RMDs;	Good discriminative performance for malignancies, infectious and mechanical back pain. Similarities between SpA and PMR requiring a composite score to discriminate both entities.	Good discriminative performance for certains RMDs, malignancies, paraneoplastic PMR-like syndrome and infectious. Similarities between SpA and PMR requiring a composite score to discriminate both entities.
Associated diseases	• Inflammation of the aortic wall Possibly correlated with CVD risk factors. Non-clear effect of the treatment and disease activity on the outcome of the inflammation. • Detection of subclinical myocardial inflammation Correlated with disease activity		LVV: • Official recommendation for suspicion of GCA isolated or associated with PMR • Good performance for the detection of subclinical GCA in patients with isolated symptoms of PMR
Treatment outcome	Good correlation between ^{18}F-FDG PET-CT and disease activity (DAS28, acute phase reactant, patient's global assessment, ultrasound)	One study: No correlation between clinical report disease activity (BASDAI, BASFI) and ^{18}F-FDG PET-CT. Require more data.	Not relevant neither for monitoring treatment response nor disease activity.
Other tracers	Zirconium-89 (B-cell target) [11C](R)PK11195 (macrophages target)	^{18}F-Na, ^{18}F-fluoride PET (osteoblastic activity)	

RMD, Rheumatic Musculo-skeletal diseases; AS, ankylosing spondylarthritis; BASDAI, Bath Ankylosing Spondylitis Disease Activity Index; BASFI, Bath ankylosing spondylitis functional index; irAEs, immune related adverses events.

arthritis associated to bowel inflammatory diseases, psoriatic arthritis, undifferentiated SpA and Synovitis – Arthritis – Palmoplantar pustulosis - Hyperostosis – Osteitis syndrome (SAPHO). SpA affects 0.2 to 0.3% of the general population and typically concerns young males below 40 years old. Musculoskeletal manifestations include pelvic and axial inflammatory pain, peripheral joint involvement and enthesis (27). SpA had no specific biologic marker contrary to RA. Conventional radiography and ultrasonography typically lack of sensitivity (28). Magnetic resonance imaging (MRI) remains the gold standard to assess spine and sacroiliac joint (SIJ), SIJ involvement being critical according to the diagnostic criteria of the 2009 Assessment of Spondyloarthritis international Society classification (29).

Despite the lack of clinical validation, ^{18}F-FDG PET-CT showed interesting results as a diagnostic tool in SpA (**Figure 2**). In a challenging clinical context mixing 21 SpA, 16 RA and 16 PMR patients, Yamashita et al. found higher ^{18}F-FDG uptake in sacroiliac joint of SpA patients compared to other CIR (14). To note, only 60% of the sacroiliitis diagnosed with MRI were identified on PET-CT, and no inter-groups difference of ^{18}F-FDG uptake was observed for the other joints (ischiatic tuberosity, greater trochanter, spinous process, and vertebral body). These data are supported by Strobel et al. (30) who found moderate diagnostic performance of ^{18}F-FDG PET-CT to detect sacroiliitis in 28 patients with active AS (n = 15) or mechanical low back pain (MLBP, n = 13), especially for grades II (localized erosions or scleroses, no alteration in the joint width, Se = 40%) and IV (ankylosis, Sen = 50%). Recently, Pean de Ponfilly-Sotier et al. (31) evaluated ^{18}F-FDG PET-CT in a particular population of 27 atypical SpA mixing late onset SpA patients, patients refractory to TNF inhibitors and/or with general manifestations. In this specific challenging population, ^{18}F-FDG PET-CT showed rare but higher ^{18}F-FDG uptake in SIJ compared to PMR patients. Other ^{18}F-FDG uptake locations (ischial tuberosity, great trochanter, hips, shoulders, interspinous process) were significantly associated with PMR. At the patient level, ^{18}F-FDG PET could not discriminate PMR from atypical SpA (**Figure 1**). In another study by Toussirot et al. (32), ^{18}F-FDG PET-CT demonstrated a good concordance with MRI to detect sacroiliitis and spinal inflammatory lesions in AS. However, in non-radiographic axial SpA patient, ^{18}F-FDG-PET-CT showed no metabolic activity and did not seem to be helpful in this specific population, suggesting ^{18}F-FDG PET-CT to be relevant in patients with active SpA. In summary, PET CT may have value in the diagnostic approach to atypical presentations in patients with suspected SpA.

Monitoring the disease independently from the self-reported clinical score Bath Ankylosing Spondylitis Disease Activity Index (BASDAI) and Bath ankylosing spondylitis functional index (BASFI) remains an important issue in SpA. In this perspective, Wendling et al. evaluated three AS patients with ^{18}F-FDG PET-CT at baseline and after 6–8 weeks of TNF inhibitors (33). No decrease in ^{18}F-FDG uptake was observed

10.3389/fmed.2022.1070445

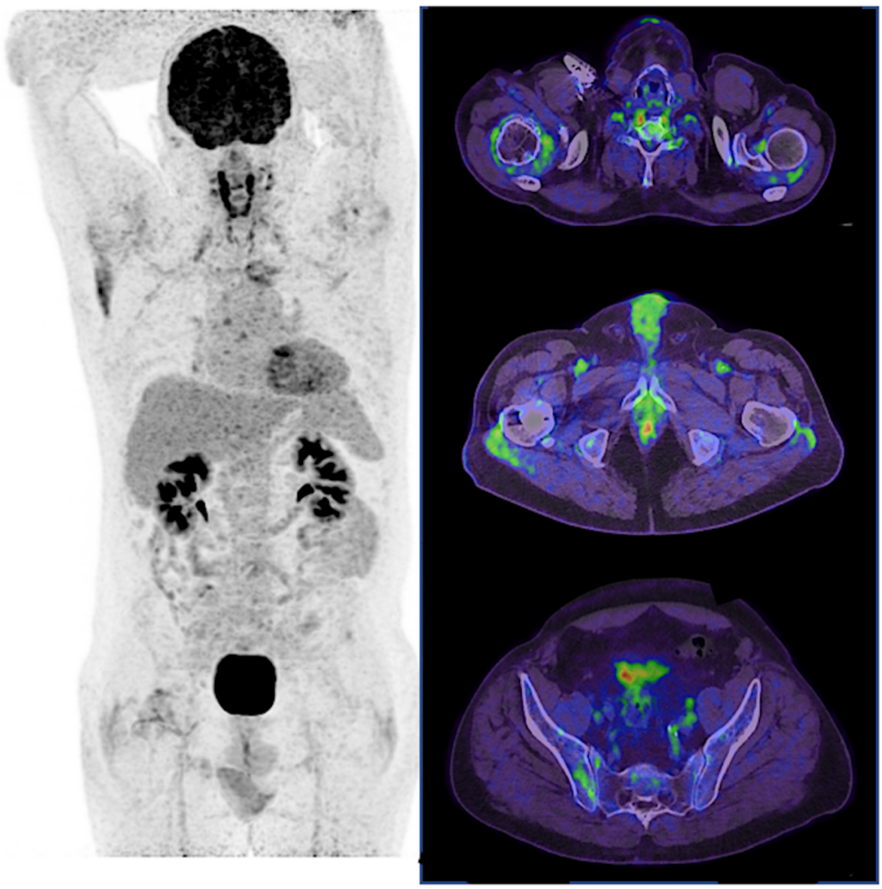

FIGURE 2
^{18}F-FDG PET of SpA. In SpA, sacro-iliitis is a highly specific pattern of ^{18}F-FDG uptake, as illustrated here in the right sacro-iliac joint, but is rarely observed in practice. As for PMR, ^{18}F-FDG uptake of the sterno-clavicular joints, scapular and pelvic girdles is also observed.

under treatment, highlighting the need of further large cohort investigations in this particular field.

^{18}F-FDG PET in polymyalgia rheumatica

Polymyalgia rheumatic (PMR) is an inflammatory disease of unknown origin affecting patients over 50 years old, causing arthromyalgia of the pelvic and/or scapular girdle, systemic manifestations and sometimes peripheral arthritis (34, 35). A biologic inflammatory syndrome is classical. As well as SpA, PMR has no specific biomarkers. The diagnosis is based on clinical and laboratory evidence and the exclusion of the numerous differential diagnosis (e.g., late onset SpA, rheumatoid arthritis with rhizomelic presentation, remittive symmetrical seronegative synovitis with pitting edema (RS3PE), inflammatory myositis ….) with plain radiography and exhaustive biologic tests. In 15 to 20% of cases, PMR is associated with giant cell arteritis (GCA), an inflammatory disease of the vascular wall of large arteries (**Figure 3**). Corticosteroids are the cornerstone of treatment both for GCA and PMR.

Although ^{18}F-FDG-PET-CT is not recommended to diagnose isolated PMR, ^{18}F-FDG PET-CT is now indicated as a first line imaging procedure in the case of suspected GCA (3). Historically, Blockmans et al. were the first to apply ^{18}F-FDG PET on isolated PMR patients (36). In their seminal paper, the authors reported the currently well-known reference pattern of ^{18}F-FDG uptake in this RIC: a bilateral and symmetrical increase of ^{18}F-FDG uptake in the shoulders and pelvic girdles, frequently associated with multi-tiered increase of ^{18}F-FDG uptake of spinous process. During the last 15 years, several studies reported these typical ^{18}F-FDG uptake, but also sternoclavicular joints (14, 31, 37). At the population level, the intensity of ^{18}F-FDG uptake in these locations appears higher in PMR patients compared to RA, SpA and other inflammatory condition (38). A recent meta-analysis by van der Geest et al. showed that combining these targeted anatomic sites of ^{18}F-FDG uptake improved the diagnosis

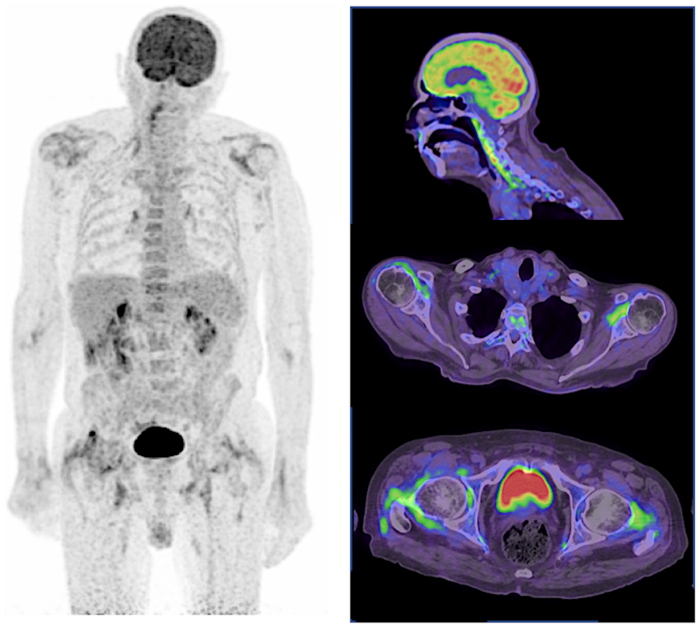

FIGURE 3
^{18}F-FDG PET of PMR. In PMR, active LVV frequently overlaps, as illustrated here with the long linear and smooth 18F-FDG uptake of the right vertebral artery in this corticosteroid resistant PMR patient. As for SpA, ^{18}F-FDG uptake of the sterno-clavicular joints, scapular, and pelvic girdles is also typically observed.

performance of PET in PMR (37). These data were later confirmed by other studies (31, 39), highlighting the fact that ^{18}F-FDG-PET-CT could be a relevant tool to discriminate PMR from other inflammatory rheumatisms, even in challenging case-mix populations. Steroid treatment prior to PET-CT reduces the scan's ability to demonstrate inflammation in PMR patients. This should be kept in mind when interpreting PET-CT in patients already exposed to steroids (40). PMR-like syndrome have been reported in patients receiving immune check point inhibitors (ICIs) for cancers (41, 42). Rheumatic and Musculo-skeletal immune-related adverse events (irAes) often do not fulfill to the traditional classification criteria (42). Compared with classical PMR, PMR-like syndromes showed higher prevalence of peripheral arthritis and the biologic inflammation can be lacking (43). Previous report (44) and van der Geest et al. (45) assessed the role of ^{18}F-FDG PET-CT before the initiation of corticosteroid in 6 patients with PMR – like syndrome. He found the same symmetric ^{18}F-FDG uptake locations than those in classical PMR, without LVV associated. One third exhibited peripheral ^{18}F-FDG uptake. These results were confirmed recently by Ponce et al. (44). To note, patients experienced irAEs induced by ICI had a better cancer prognosis than those in non – irAEs patients (46).

Monitoring the response to treatment with ^{18}F-FDG PET-CT may be tempting (**Figure 4**). However, standard clinical and biological biomarkers are currently sufficient in most practical cases. Nevertheless, Palard-Novello et al. assessed the value of ^{18}F-FDG PET-CT to monitor 18 PMR patients receiving Tocilizumab as first line treatment (TENOR trial) (47). The PET-CT were performed at baseline, two and 12 weeks. Between baseline and 12 weeks, the authors observed significant improvement of the PMR activity score and biological markers, together with a decrease of ^{18}F-FDG uptake in targeted joints (hips, ischial tuberosity, lumbar spinous process). During follow-up, no correlation was found between PET, clinical and biological biomarkers. Devauchelle-Pensec et al. confirmed these results in a cohort of 20 glucocorticoid-free PMR onset receiving Tocilizumab as first line treatment (48). Thus ^{18}F-FDG PET-CT may not appear relevant neither for monitoring treatment response nor disease activity in PMR patients.

Whether ^{18}F-FDG-PET-CT could be a relevant tool or not to predict response to treatment is poorly evaluated. In 2007, the seminal paper by Blockman et al. (36) found no difference of ^{18}F-FDG uptake between relapsers and non-relapsers at 3 and 6 months, and ^{18}F-FDG PET uptake was not correlated with the risk of relapse. In a recent study, Prieto-Peña et al. (49) identified predictive factor of ^{18}F-FDG PET positivity for LVV in a population of 84 isolated PMR patient with persistent of classical PMR symptoms and/or unusual symptoms (inflammatory low back pain, diffuse lower limb pain). Among 84 patients, 51 (61%) patients had evidence of LVV on ^{18}F-FDG PET. In multivariate analysis, diffuse lower limb pain, pelvic girdle pain and inflammatory low back pain were the best set of predictors of PET positivity for LVV in patients with initially isolated

10.3389/fmed.2022.1070445

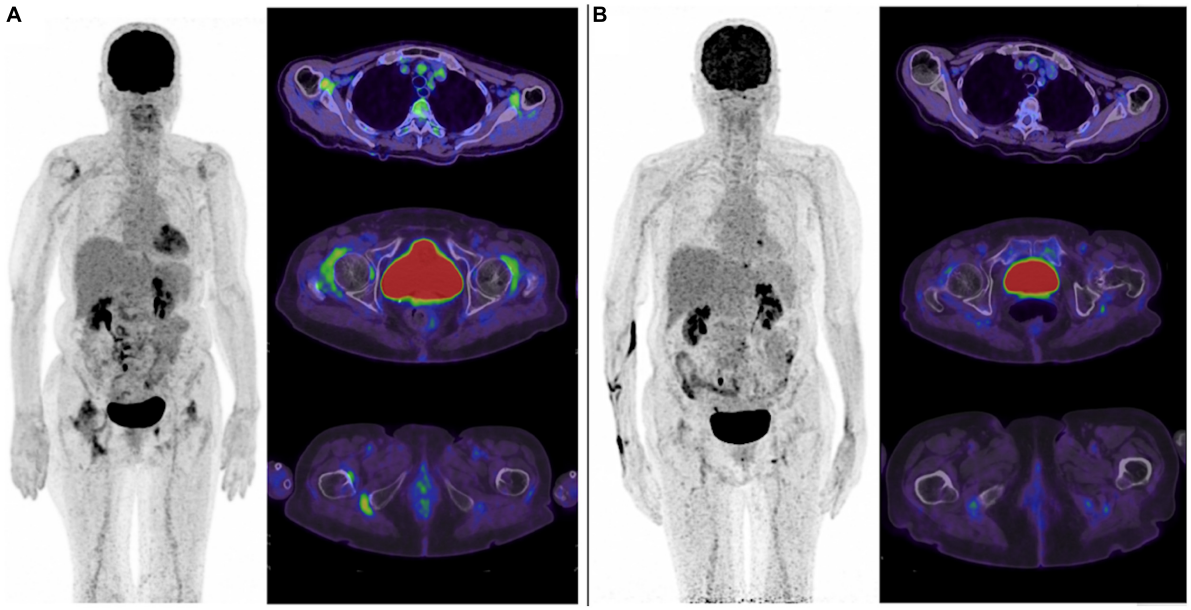

FIGURE 4
^{18}F-FDG PET changes under treatment: typical but no current benefit over standard biomarkers. In this case of PMR, significant decrease of ^{18}F-FDG uptake is observed in the targeted joints (here the scapular and pelvic girdles, ischial tuberosities) under treatment **(A)** baseline scan, and **(B)** after several lines of treatment). Although metabolic changes assessed with ^{18}F-FDG are frequently observed, the clinical benefit of such imaging biomarker over standard clinical and biological biomarkers for disease monitoring remains to be defined.

PMR. Finally, a take home message of this study is the potential existence of LVV signs in PMR patients in whom GCA was not clinically suspected. The presence of predictive signs could raise the question of systematically searching for GCA by PET CT given the therapeutic and prognostic impact. This work will therefore need to be confirmed in a new cohort. As mentioned previously, caution should be made in patients already exposed to glucocorticoids. Because glucocorticoids rapidly reduce the ^{18}F-FDG uptake of the vascular wall in LVV patients, withdraw or delay therapy until after ^{18}F-FDG PET when possible (i.e., no risk of ischemic complications) or ^{18}F-FDG PET acquisition within the first days of therapy are currently recommended to reduce the risk of false negative results (4).

Finally, ^{18}F-FDG PET could be used for differential diagnosis including cancers revealed by musculoskeletal manifestations including PMR-like symptoms. In this perspective, Moya-Alvarado et al. (50) assessed the added value of ^{18}F-FDG PET-CT to diagnose other underlying conditions in a cohort of 103 onset and steroid resistant PMR patients. The final diagnosis of PMR, LVV, malignancies and other (small vessel vasculitis, osteoarthritis, elderly onset of RA, Sjögren's syndrome) were retained in 73, 16, 5, and 9 patients, respectively. In the case of bio-clinical flare after glucocorticoid tapering in GCA patients with or without PMR, Camellino et al. promote the use of ^{18}F-FDG PET-CT to rule-out cancer and detect subclinical LVV (35).

Time for new tracers?

PET imaging is characterized by its vectorized imaging capabilities. Beyond ^{18}F-FDG we have focused on here, other tracers have been investigated in CIRs (51). In SpA, several studies reported the relevance of ^{18}F-Na (^{18}F-fluoride PET) to evaluate osteoblastic activity in chronic AS, and diagnose new bone formation in spine and SIJ which were misjudged by MRI and delayed by plain radiography (52–54). Son et al. (55) evaluated ^{18}F-Na in a retrospective cohort of 68 patients with suspected AS. Among 68 patients, 72% reach ASAS criteria for SpA. Eighty percent in AS group exhibited higher frequency of ^{18}F-Na uptake (enthesopathy, syndesmophyte, symmetric sacroiliitis), in comparison with the control group. In 2018, in a pilot study, Bruijnen et al. (53) suggested that AS activity was better reflected by bone activity assessed by ^{18}F-Na than inflammation assessed by ^{18}F-FDG and [11C](R)PK11195, a radiotracer of inflammation targeting the mitochondrial outer membrane translocator protein of activated macrophages (TSPO PET). In RA, TSPO PET radiotracers have also been assessed (56, 57). In their study including 29 RA patients without clinical arthritis, Gent et al. showed increased TSPO PET uptake in metacarpophalangeal, proximal interphalangeal, and wrist joints in 55% of cases, of whom 69% developed a flare within the 3-years of follow-up (56). More recently, the baseline PET assessment of B-cell load by using radiolabeled Rituximab (Zirconium-89) showed independent value of PET

to prognose therapeutic response, with positive and negative predictive values for clinical response at 24 weeks of 90 and 75%, respectively (58).

To conclude, the place of ^{18}F-PET-CT in the management of patients with RA, SpA and PMR remains to be defined. In classical presentations, ^{18}F-FDG PET does not appear useful in the diagnostic process. It should be reserved for atypical presentations or in case of poor response to treatment in order to ensure the absence of a differential diagnosis. Its relevance for the assessment of associated manifestations - cardiovascular complications of RA - GCA associated with PMR appears promising, deserving dedicated lines of research. Finally, the use of new tracers is to be followed to improve the diagnostic and prognostic performance of this whole-body imaging modality.

Author contributions

All authors contributed to design and acquisition analysis, revising for intellectual content, final approval, and agreement to be accountable for all aspects of this work (accuracy and integrity of any part of the work).

Conflict of interest

The authors declare that the research was conducted in the absence of any commercial or financial relationships that could be construed as a potential conflict of interest.

Publisher's note

All claims expressed in this article are solely those of the authors and do not necessarily represent those of their affiliated organizations, or those of the publisher, the editors and the reviewers. Any product that may be evaluated in this article, or claim that may be made by its manufacturer, is not guaranteed or endorsed by the publisher.

References

1. Manhas NS, Salehi S, Joyce P, Guermazi A, Ahmadzadehfar H, Gholamrezanezhad A. PET/computed tomography scans and PET/MR imaging in the diagnosis and management of musculoskeletal diseases. *PET Clin.* (2020) 15:535–45. doi: 10.1016/j.cpet.2020.06.005

2. Mandl P, Ciechomska A, Terslev L, Baraliakos X, Conaghan PG, D'Agostino MA, et al. Implementation and role of modern musculoskeletal imaging in rheumatological practice in member countries of EULAR. *RMD Open.* (2019) 5:e000950. doi: 10.1136/rmdopen-2019-000950

3. Dejaco C, Ramiro S, Duftner C, Besson FL, Bley TA, Blockmans D, et al. EULAR recommendations for the use of imaging in large vessel vasculitis in clinical practice. *Ann Rheum Dis.* (2018) 77:636–43. doi: 10.1136/annrheumdis-2017-212649

4. Slart RHJA, Writing group, Reviewer group, Members of EANM Cardiovascular, Members of EANM Infection & Inflammation, Members of Committees, et al. FDG-PET/CT(A) imaging in large vessel vasculitis and polymyalgia rheumatica: joint procedural recommendation of the EANM, SNMMI, and the PET Interest Group (PIG), and endorsed by the ASNC. *Eur J Nucl Med Mol Imaging.* (2018) 45:1250–69. doi: 10.1007/s00259-018-3973-8

5. Besson FL, Chaumet-Riffaud P, Playe M, Noel N, Lambotte O, Goujard C, et al. Contribution of (18)F-FDG PET in the diagnostic assessment of fever of unknown origin (FUO): a stratification-based meta-analysis. *Eur J Nucl Med Mol Imaging.* (2016) 43:1887–95. doi: 10.1007/s00259-016-3377-6

6. Colebatch AN, Edwards CJ, Østergaard M, van der Heijde D, Balint PV, D'Agostino MA, et al. EULAR recommendations for the use of imaging of the joints in the clinical management of rheumatoid arthritis. *Ann Rheum Dis.* (2013) 72:804–14. doi: 10.1136/annrheumdis-2012-203158

7. Yamashita H, Kubota K, Mimori A. Clinical value of whole-body PET/CT in patients with active rheumatic diseases. *Arthritis Res Ther.* (2014) 16:423. doi: 10.1186/s13075-014-0423-2

8. Kubota K, Yamashita H, Mimori A. Clinical value of FDG-PET/CT for the evaluation of rheumatic diseases: rheumatoid arthritis, polymyalgia rheumatica, and relapsing polychondritis. *Semin Nucl Med.* (2017) 47:408–24. doi: 10.1053/j.semnuclmed.2017.02.005

9. Smolen JS, Aletaha D, McInnes IB. Rheumatoid arthritis. *Lancet.* (2016) 388:2023–38. doi: 10.1016/S0140-6736(16)30173-8

10. Roux CH, Saraux A, Le Bihan E, Fardellone P, Guggenbuhl P, Fautrel B, et al. Rheumatoid arthritis and spondyloarthropathies: geographical variations in prevalence in France. *J Rheumatol.* (2007) 34:117–22.

11. Juge PA, Granger B, Debray MP, Ebstein E, Louis-Sidney F, Kedra J, et al. A risk score to detect subclinical rheumatoid arthritis-associated interstitial lung disease. *Arthritis Rheumatol.* (2022) 74:1755–65. doi: 10.1002/art.42162

12. Aletaha D, Neogi T, Silman AJ, Funovits J, Felson DT, Bingham CO, et al. 2010 Rheumatoid arthritis classification criteria: an American college of rheumatology/European league against rheumatism collaborative initiative. *Arthritis Rheum.* (2010) 62:2569–81. doi: 10.1002/art.27584

13. Bhattarai A, Nakajima T, Sapkota S, Arisaka Y, Tokue A, Yonemoto Y, et al. Diagnostic value of 18F-fluorodeoxyglucose uptake parameters to differentiate rheumatoid arthritis from other types of arthritis. *Medicine.* (2017) 96:e7130. doi: 10.1097/MD.0000000000007130

14. Yamashita H, Kubota K, Takahashi Y, Minamimoto R, Morooka M, Kaneko H, et al. Similarities and differences in fluorodeoxyglucose positron emission tomography/computed tomography findings in spondyloarthropathy, polymyalgia rheumatica and rheumatoid arthritis. *Joint Bone Spine.* (2013) 80:171–7. doi: 10.1016/j.jbspin.2012.04.006

15. Wang G, Liu X, Chen J, Zhang F, Xu X, Wang Y, et al. The combination of 18F-fluorodeoxyglucose positron emission tomography metabolic and clinical parameters can effectively distinguish rheumatoid arthritis and polymyalgia rheumatic. *Contrast Media Mol Imaging.* (2022) 2022:9614678. doi: 10.1155/2022/9614678

16. Beckers C, Ribbens C, André B, Marcelis S, Kaye O, Mathy L, et al. Assessment of disease activity in rheumatoid arthritis with (18)F-FDG PET. *J Nucl Med.* (2004) 45:956–64.

17. Roivainen A, Hautaniemi S, Möttönen T, Nuutila P, Oikonen V, Parkkola R, et al. Correlation of 18F-FDG PET/CT assessments with disease activity and markers of inflammation in patients with early rheumatoid arthritis following the initiation of combination therapy with triple oral antirheumatic drugs. *Eur J Nucl Med Mol Imaging.* (2013) 40:403–10. doi: 10.1007/s00259-012-2282-x

18. Elzinga EH, van der Laken CJ, Comans EFI, Boellaard R, Hoekstra OS, Dijkmans BAC, et al. 18F-FDG PET as a tool to predict the clinical outcome of infliximab treatment of rheumatoid arthritis: an explorative study. *J Nucl Med.* (2011) 52:77–80. doi: 10.2967/jnumed.110.076711

19. Okamura K, Yonemoto Y, Okura C, Higuchi T, Tsushima Y, Takagishi K. Evaluation of tocilizumab therapy in patients with rheumatoid arthritis based on FDG-PET/CT. *BMC Musculoskelet Disord.* (2014) 15:393. doi: 10.1186/1471-2474-15-393

20. Bouman CAM, van Herwaarden N, Blanken AB, Van der Laken CJ, Gotthardt M, Oyen WJG, et al. 18F-FDG PET-CT in rheumatoid arthritis patients tapering

TNFi: reliability, validity and predictive value. *Rheumatology.* (2022) 61:SI6–13. doi: 10.1093/rheumatology/keab842

21. Alavi A, Saboury B, Nardo L, Zhang V, Wang M, Li H, et al. Potential and most relevant applications of total body PET/CT imaging. *Clin Nucl Med.* (2022) 47:43–55. doi: 10.1097/RLU.0000000000003962

22. Geraldino-Pardilla L, Zartoshti A, Bag Ozbek A, Giles JT, Weinberg R, Kinkhabwala M, et al. Arterial inflammation detected with 18 F-fluorodeoxyglucose-positron emission tomography in rheumatoid arthritis. *Arthritis Rheumatol.* (2018) 70:30–9. doi: 10.1002/art.40345

23. Avina-Zubieta JA, Thomas J, Sadatsafavi M, Lehman AJ, Lacaille D. Risk of incident cardiovascular events in patients with rheumatoid arthritis: a meta-analysis of observational studies. *Ann Rheum Dis.* (2012) 71:1524–9. doi: 10.1136/annrheumdis-2011-200726

24. Trang DAMT, Okamura K, Suto T, Sakane H, Yonemoto Y, Nakajima T, et al. Do biologic therapies reduce aortic inflammation in rheumatoid arthritis patients? *Arthritis Res Ther.* (2021) 23:206. doi: 10.1186/s13075-021-02585-w

25. Amigues I, Tugcu A, Russo C, Giles JT, Morgenstein R, Zartoshti A, et al. Myocardial inflammation, measured using 18-fluorodeoxyglucose positron emission tomography with computed tomography, is associated with disease activity in rheumatoid arthritis. *Arthritis Rheumatol.* (2019) 71:496–506. doi: 10.1002/art.40771

26. Emami H, Vijayakumar J, Subramanian S, Vucic E, Singh P, MacNabb MH, et al. Arterial 18F-FDG uptake in rheumatoid arthritis correlates with synovial activity. *JACC Cardiovasc Imaging.* (2014) 7:959–60. doi: 10.1016/j.jcmg.2014.03.018

27. Taurog JD, Chhabra A, Colbert RA. Ankylosing spondylitis and axial spondyloarthritis. *N Engl J Med.* (2016) 374:2563–74. doi: 10.1056/NEJMra1406182

28. van Tubergen AM, Landewé RBM. Tools for monitoring spondyloarthritis in clinical practice. *Nat Rev Rheumatol.* (2009) 5:608–15. doi: 10.1038/nrrheum.2009.207

29. Rudwaleit M, van der Heijde D, Landewé R, Akkoc N, Brandt J, Chou CT, et al. The assessment of spondyloarthritis international society classification criteria for peripheral spondyloarthritis and for spondyloarthritis in general. *Ann Rheum Dis.* (2011) 70:25–31. doi: 10.1136/ard.2010.133645

30. Strobel K, Fischer DR, Tamborrini G, Kyburz D, Stumpe KDM, Hesselmann RGX, et al. 18F-fluoride PET/CT for detection of sacroiliitis in ankylosing spondylitis. *Eur J Nucl Med Mol Imaging.* (2010) 37:1760–5. doi: 10.1007/s00259-010-1464-7

31. Pean de Ponfilly-Sotier M, Besson FL, Gomez L, Ottaviani S, Dieudé P, Pavy S, et al. Use of 18F FDG PET-CT to discriminate polymyalgia rheumatica and atypical spondylarthritis in clinical practice. *Joint Bone Spine.* (2022) 89:105325.

32. Toussirot E, Caoduro C, Ungureanu C, Michel F, Runge M, Boulahdour H. 18F- fluoride PET/CT assessment in patients fulfilling the clinical arm of the ASAS criteria for axial spondyloarthritis. A comparative study with ankylosing spondylitis. *Clin Exp Rheumatol.* (2015) 33:588.

33. Wendling D, Blagosklonov O, Streit G, Lehuédé G, Toussirot E, Cardot JC. FDG-PET/CT scan of inflammatory spondylodiscitis lesions in ankylosing spondylitis, and short term evolution during anti-tumour necrosis factor treatment. *Ann Rheum Dis.* (2005) 64:1663–5. doi: 10.1136/ard.2005.040345

34. Salvarani C, Cantini F, Boiardi L, Hunder GG. Polymyalgia rheumatica and giant-cell arteritis. *N Engl J Med.* (2002) 347:261–71. doi: 10.1056/NEJMra011913

35. Camellino D, Matteson EL, Buttgereit F, Dejaco C. Monitoring and long-term management of giant cell arteritis and polymyalgia rheumatica. *Nat Rev Rheumatol.* (2020) 16:481–95. doi: 10.1038/s41584-020-0458-5

36. Blockmans D, De Ceuninck L, Vanderschueren S, Knockaert D, Mortelmans L, Bobbaers H. Repetitive 18-fluorodeoxyglucose positron emission tomography in isolated polymyalgia rheumatica: a prospective study in 35 patients. *Rheumatology.* (2007) 46:672–7. doi: 10.1093/rheumatology/kel376

37. van der Geest KSM, Treglia G, Glaudemans AWJM, Brouwer E, Jamar F, Slart RHJA, et al. Diagnostic value of [18F]FDG-PET/CT in polymyalgia rheumatica: a systematic review and meta-analysis. *Eur J Nucl Med Mol Imaging.* (2021) 48:1876–89. doi: 10.1007/s00259-020-05162-6

38. Yuge S, Nakatani K, Yoshino K, Koyama T. Diagnosing polymyalgia rheumatica on 18F-FDG PET/CT: typical uptake patterns. *Ann Nucl Med.* (2018) 32:573–7. doi: 10.1007/s12149-018-1269-5

39. van der Geest KSM, van Sleen Y, Nienhuis P, Sandovici M, Westerdijk N, Glaudemans AWJM, et al. Comparison and validation of FDG-PET/CT scores for polymyalgia rheumatica. *Rheumatology.* (2022) 61:1072–82. doi: 10.1093/rheumatology/keab483

40. Lund Petersen A, Voss A, Laustrup H. PET-CT findings in patients with polymylagia rheumatica without symptoms of cranial ischaemia. *Dan Med J.* (2017) 64:A5410.

41. Braaten TJ, Brahmer JR, Forde PM, Le D, Lipson EJ, Naidoo J, et al. Immune checkpoint inhibitor-induced inflammatory arthritis persists after immunotherapy cessation. *Ann Rheum Dis.* (2020) 79:332–8. doi: 10.1136/annrheumdis-2019-216109

42. Kostine M, Finckh A, Bingham CO, Visser K, Leipe J, Schulze-Koops H, et al. EULAR points to consider for the diagnosis and management of rheumatic immune-related adverse events due to cancer immunotherapy with checkpoint inhibitors. *Ann Rheum Dis.* (2021) 80:36–48. doi: 10.1136/annrheumdis-2020-217139

43. Martin de Fremont G, Belkhir R, Henry J, Voisin AL, Lambotte O, Besson FL, et al. Features of polymyalgia rheumatica-like syndrome after immune checkpoint inhibitor therapy. *Ann Rheum Dis.* (2022) 81:e52. doi: 10.1136/annrheumdis-2020-217225

44. Ponce A, Frade-Sosa B, Sarmiento-Monroy JC, Sapena N, Ramírez J, Azuaga AB, et al. Imaging findings in patients with immune checkpoint inhibitor-induced arthritis. *Diagnostics.* (2022) 12:1961. doi: 10.3390/diagnostics12081961

45. van der Geest, KSM, Sandovici M, Rutgers A, Hiltermann TJN, Oosting SF, Slart RHJA, et al. Management of immune checkpoint inhibitor-induced polymyalgia rheumatica. *Ann Rheum Dis.* (2020) 81:e263. doi: 10.1136/annrheumdis-2020-218276

46. Zhong L, Wu Q, Chen F, Liu J, Xie X. Immune-related adverse events: promising predictors for efficacy of immune checkpoint inhibitors. *Cancer Immunol Immunother.* (2021) 70:2559–76. doi: 10.1007/s00262-020-02803-5

47. Palard-Novello X, Querellou S, Gouillou M, Saraux A, Marhadour T, Garrigues F, et al. Value of (18)F-FDG PET/CT for therapeutic assessment of patients with polymyalgia rheumatica receiving tocilizumab as first-line treatment. *Eur J Nucl Med Mol Imaging.* (2016) 43:773–9. doi: 10.1007/s00259-015-3287-z

48. Devauchelle-Pensec V, Berthelot JM, Cornec D, Renaudineau Y, Marhadour T, Jousse-Joulin S, et al. Efficacy of first-line tocilizumab therapy in early polymyalgia rheumatica: a prospective longitudinal study. *Ann Rheum Dis.* (2016) 75:1506–10. doi: 10.1136/annrheumdis-2015-208742

49. Prieto-Peña D, Martínez-Rodríguez I, Loricera J, Banzo I, Calderón-Goercke M, Calvo-Río V, et al. Predictors of positive 18F-FDG PET/CT-scan for large vessel vasculitis in patients with persistent polymyalgia rheumatica. *Semin Arthritis Rheum.* (2019) 48:720–7. doi: 10.1016/j.semarthrit.2018.05.007

50. Moya-Alvarado P, Fernandez Leon A, Corica ME, Camacho Marti V, López-Mora DA, Castellví I, et al. The added value of 18f-FDG PET/CT in the assessment of onset and steroid resistant polimyalgia rheumatica. *PLoS One.* (2021) 16:e0255131. doi: 10.1371/journal.pone.0255131

51. van der Krogt JMA, van Binsbergen WH, van der Laken CJ, Tas SW. Novel positron emission tomography tracers for imaging of rheumatoid arthritis. *Autoimmun Rev.* (2021) 20:102764. doi: 10.1016/j.autrev.2021.102764

52. Idolazzi L, Salgarello M, Gatti D, Viapiana O, Vantaggiato E, Fassio A, et al. 18F-fluoride PET/CT for detection of axial involvement in ankylosing spondylitis: correlation with disease activity. *Ann Nucl Med.* (2016) 30:430–4. doi: 10.1007/s12149-016-1080-0

53. Bruijnen STG, van der Weijden MAC, Klein JP, Hoekstra OS, Boellaard R, van Denderen JC, et al. Bone formation rather than inflammation reflects ankylosing spondylitis activity on PET-CT: a pilot study. *Arthritis Res Ther.* (2012) 14:R71. doi: 10.1186/ar3792

54. Raynal M, Bouderraoui F, Ouichka R, Melchior J, Morel O, Blum A, et al. Performance of 18F-sodium fluoride positron emission tomography with computed tomography to assess inflammatory and structural sacroiliitis on magnetic resonance imaging and computed tomography, respectively, in axial spondyloarthritis. *Arthritis Res Ther.* (2019) 21:119. doi: 10.1186/s13075-019-1903-1

55. Son SM, Kim K, Pak K, Kim SJ, Goh TS, Lee JS. Evaluation of the diagnostic performance of 18F-NaF positron emission tomography/computed tomography in patients with suspected ankylosing spondylitis according to the assessment of spondyloarthritis international society criteria. *Spine J.* (2020) 20:1471–9. doi: 10.1016/j.spinee.2020.03.011

56. Gent YYJ, Ahmadi N, Voskuyl AE, Hoetjes N, van Kuijk C, Britsemmer K, et al. Detection of subclinical synovitis with macrophage targeting and positron emission tomography in patients with rheumatoid arthritis without clinical arthritis. *J Rheumatol.* (2014) 41:2145–52. doi: 10.3899/jrheum.140059

57. Bruijnen STG, Verweij NJF, Gent YYJ, Huisman MC, Windhorst AD, Kassiou M, et al. Imaging disease activity of rheumatoid arthritis by macrophage targeting using second generation translocator protein positron emission tomography tracers. *PLoS One.* (2019) 14:e0222844. doi: 10.1371/journal.pone.0222844

58. Bruijnen S, Tsang-A-Sjoe M, Raterman H, Ramwadhdoebe T, Vugts D, van Dongen G, et al. B-cell imaging with zirconium-89 labelled rituximab PET-CT at baseline is associated with therapeutic response 24 weeks after initiation of rituximab treatment in rheumatoid arthritis patients. *Arthritis Res Ther.* (2016) 18:266. doi: 10.1186/s13075-016-1166-z

frontiers | Frontiers in Medicine

TYPE Mini Review
PUBLISHED 19 January 2023
DOI 10.3389/fmed.2023.1103752

OPEN ACCESS

EDITED BY
Clément Bailly,
Centre Hospitalier Universitaire (CHU) de Nantes, France

REVIEWED BY
Bastien Jamet,
Centre Hospitalier Universitaire (CHU) de Nantes, France

*CORRESPONDENCE
Cloé Comarmond
✉ chloe.comarmondortoli@aphp.fr

SPECIALTY SECTION
This article was submitted to Nuclear Medicine, a section of the journal Frontiers in Medicine

RECEIVED 20 November 2022
ACCEPTED 04 January 2023
PUBLISHED 19 January 2023

CITATION
Nassarmadji K, Vanjak A, Bourdin V, Champion K, Burlacu R, Mouly S, Sène D and Comarmond C (2023) 18-Fluorodeoxyglucose positron emission tomography/computed tomography for large vessel vasculitis in clinical practice.
Front. Med. 10:1103752.
doi: 10.3389/fmed.2023.1103752

18-Fluorodeoxyglucose positron emission tomography/computed tomography for large vessel vasculitis in clinical practice

Kladoum Nassarmadji, Anthony Vanjak, Venceslas Bourdin, Karine Champion, Ruxandra Burlacu, Stéphane Mouly, Damien Sène and Cloé Comarmond*

Department of Internal Medicine and Clinical Immunology, Lariboisière Hospital, Université Paris Cité, Paris, France

Diagnosis, prognostic assessment, and monitoring disease activity in patients with large vessel vasculitis (LVV) can be challenging. Early recognition of LVV and treatment adaptation is essential because vascular complications (aneurysm, dilatations, ischemic complications) or treatment related side effects can occur frequently in these patients. 18-fluorodeoxyglucose positron emission tomography/computed tomography (2-[18F]FDG-PET/CT) is increasingly used to diagnose, follow, and evaluate treatment response in LVV. In this review, we aimed to summarize the current evidence on the value of 2-[18F]FDG-PET/CT for diagnosis, follow, and treatment monitoring in LVV.

KEYWORDS

2-[18F]FDG-PET/CT, giant cell arteritis, takayasu arteritis, large vessel vasculitis, large vessel arteritis

Introduction

Giant cell arteritis (GCA) and Takayasu arteritis (TA) are two vasculitis predominantly affecting large vessels: aorta and its major branches (1). They differ by their clinical presentation, prognosis, and treatment. Imaging modalities such as ultrasound (US), computed tomography (CT) and 18-Fluorodeoxyglucose positron emission tomography (2-[18F]FDG-PET/CT) are more frequently used, have replaced angiography and have modified management of these diseases (2).

18-Fluorodeoxyglucose positron emission tomography/computed tomography is a functional imaging modality of fundamental utility in oncology that has progressively been used in rheumatic diseases. Indeed, 2-[18F]FDG-PET/CT has shown in preclinical models the ability to detect glucose intake in inflammatory and endothelial cells (3, 4). In this review, we aim to illustrate the usefulness of 2-[18F]FDG-PET/CT in management of LVV.

2-[18F]FDG-PET/CT and giant cell arteritis

2-[18F]FDG-PET/CT in GCA diagnosis

Giant cell arteritis is the most frequent large vessel vasculitis affecting patients older than 50 years with a prevalence of 9/100,000 in a prospective study of a German population and up

to 25/100,000 in patients older than 50 years (5). Diagnosis of GCA is based on the presence of clinical signs of vasculitis, proof of vessel inflammation, eliminating alternate diagnosis and dramatic response to steroids in patients older than 50 years.

Giant cell arteritis encompass cranial and extracranial manifestations. Constitutional symptoms and elevated inflammatory markers are present in >90% of cases and patients may present with fever of unknown origin as the initial symptom in 15% of cases (6, 7). Cranial manifestations such as headaches may present in two third of patients (8). The most severe acute complication, visual loss, is described in around 20% of cases but this has been reduced with early recognition of disease and usage of temporal artery ultrasound (9, 10). Pseudomyalgia rheumatica (PMR) is the most common extra cranial manifestation in GCA and occur in 45–50% of GCA patients (11). Clinical manifestations of large vessel involvement (limb claudication, thoracic pain) may develop in one fifth of GCA patients (12).

Temporal artery biopsy (TAB) was initially recommended in every case of suspected GCA and was considered the gold standard (13). However, results are delayed and biopsy may be negative in up to 42% of patients with predominantly large vessel GCA (LV GCA) (12). Temporal artery ultrasound has shown very good performance with a pooled sensitivity of 77% and a pooled specificity of 96% as compared with the clinical diagnosis of GCA (2). It is also cost effective compared to TAB but remains limited for the exploration of aorta and visceral arteries (14). Thus, it is the first line recommended imaging technique for suspected predominantly cranial GCA (2). Nevertheless, TAB remains strongly recommended over imaging in ACR 2021 guidelines (15). Recently, the 2022 American College of Rheumatology/EULAR GCA classification criteria emphasized the use of 2-[18F]FDG-PET/CT, as well as other investigative methods: Ultrasound, MRI, for use in clinical practice (16). PET, MRI, and CT are equally proposed to detect large vessel inflammation in GCA in recommendations from different scientific societies: ACR, EULAR, the British Society for Rheumatology and the French study Group for Large Vessel Vasculitis (2, 15, 17, 18).

18-Fluorodeoxyglucose positron emission tomography/computed tomography has overall good performance for the diagnosis of GCA. Specific patterns of PET/CT uptake show that patients with GCA and positive 2-[18F]FDG-PET/CT are more likely to have a diffuse disease with thoracic and abdominal aorta, bilateral subclavian and axillary arteries involvement (19). Ascending aorta is the most affected zone (72%) followed by the brachiocephalic trunk (62%), aortic arch (60%), and descending aorta (60%) (20).

Blockmans et al. (21) have compared PET versus TAB performance and found a sensitivity of 77% and a specificity of 66%. Subsequently, three meta-analysis including studies of GCA patients comparing PET alone or with CT vs. different gold standard (clinical diagnosis or TAB) found sensitivity of 80–89% and specificity of 89–98% (22–24). The main limitations of these meta-analysis are the inclusion of predominantly retrospective studies and the usage of different reference standard between included studies. More recently, a longitudinal prospective study comparing 2-[18F]FDG-PET/CT with clinical diagnosis at 6 months found a sensitivity of 67%, a specificity of 100%, a negative predictive value of 64% and a positive predictive value of 100% (25).

18-Fluorodeoxyglucose positron emission tomography/computed tomography is also a useful imaging technique to assess large vessel involvement in patients with suspected GCA and negative TAB. In a retrospective study of 63 patients with suspected GCA and negative TAB, large vessel involvement with 2-[18F]FDG-PET/CT was observed in 14 patients (22%). The final diagnosis of GCA was based on the presence of clinical symptoms, laboratory results, imaging data compatible with GCA, and good response to corticosteroid therapy (26).

Moreover, new generations of 2-[18F]FDG-PET/CT provide improved image resolution and can detect arteritis in smaller cranial arteries (temporal, maxillary, vertebral and occipital arteries) (**Figure 1**). Diagnosis of cranial artery inflammation with head, neck and chest PET/CT before or within 72 h after glucocorticoids intake showed a sensitivity of 82–92% and a specificity of 85–100% for diagnosis of GCA (27–29).

Finally, 2-[18F]FDG-PET/CT can be helpful in patients presenting with extracranial manifestation of GCA. In patients presenting with fever of unknown origin (FUO), abnormal 2-[18F]FDG-PET/CT increase the diagnosis rate to 83% among whom one-third have inflammatory diseases, such as vasculitis (30). In patients with suspicion of PMR, prospective studies using 2-[18F]FDG-PET/CT revealed the presence of LVV involvement in 31–60% of patients (31, 32).

The main differential diagnosis of FDG vessel uptake in vasculitis is atherosclerosis. Based on qualitative and quantitative vascular 18 FDG uptake, vascular site involved and disappearance upon steroid treatment, some differences can be noted (33): In atherosclerotic disease, uptake is usually low to moderate (Grade 0–1), has a patchy pattern and is predominantly located on iliofemoral sites and aortic bifurcations. In vasculitis however, FDG uptake is usually intense: a grade 3 uptake is found in aortitis only and semi quantitative analysis of FDG uptake are significantly higher in aortitis compared to atherosclerotic disease (mean SUVm 4.6 vs. 2.7) (34). Furthermore, FDG uptake in aortitis has a concentric, smooth linear pattern and may affect whole aorta. Also, CT images show non-concentric calcifications in atherosclerotic disease versus circumferential aortic wall thickness of more than 2–3 mm in vasculitis (35; **Table 1**).

2-[18F]FDG-PET/CT in GCA prognosis

The prognosis in GCA is dominated by irreversible vision during short term course and vascular complications (dilatation, dissection, aneurysm, atherosclerosis) during long term follow-up (36).

Positron emission tomography/computed tomography is not adequate to evaluate the risk of vision loss because if ocular involvement is suspected, glucocorticoids must be started immediately and no imaging should delay the treatment (2). Moreover, ciliary arteries and central retinal arteries which are involved in ocular retinal damages are too small to be evaluated by PET/CT. Patients with GCA have a 2-fold increased risk of aortic aneurysm than control in a large UK cohort (37). Approximatively 20% of patients with GCA may develop aortic structural damage (aneurysm, dissection) (38, 39), mainly after 5 years from diagnosis (40).

Some risk factors for aortic damage in GCA have been identified and include male sex, smoking, hypertension and diabetes (37).

In two prospective studies by Blockmans et al. (31) and Galli et al. (41) assessing FDG uptake at diagnosis and during follow up, respectively up to 6 months and with a mean 97 months, vascular uptake at diagnosis did not predict subsequent relapse. However, an increased FDG uptake in the aorta at the diagnosis of GCA was associated with development of thoracic aorta dilatation (42)

10.3389/fmed.2023.1103752

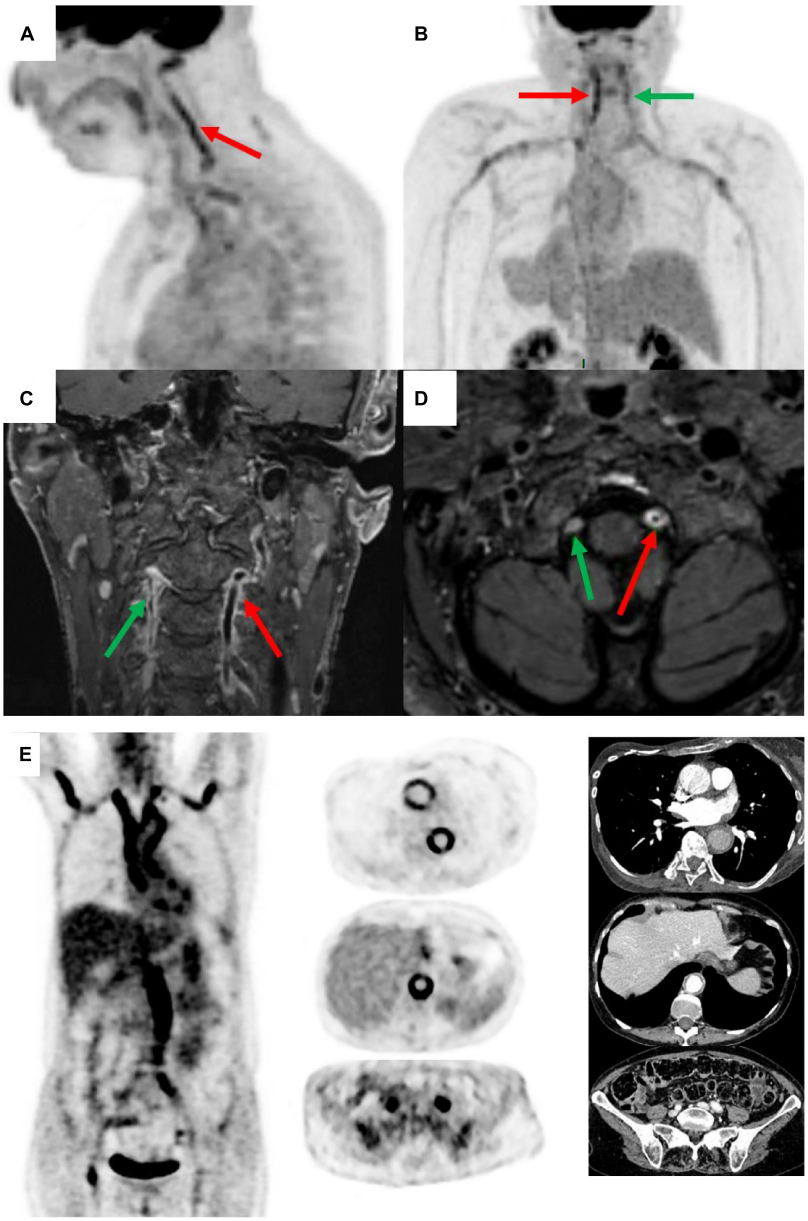

FIGURE 1
Positron emission tomography (PET) and magnetic resonance angiography (MRA) in a patient with giant cell arteritis (GCA) (man of 73 years old, CRP 17 mg/L, TAB positive). PET shows an inflammatory pattern with clear uptake (>liver uptake, grade 3) in vertebral arteries (left = red arrow and right = green arrow), sub-clavicular arteries, aortic arch, and thoracic aorta [panels **(A,B)** posterior image]. MRA shows vertebral arterial wall thickening, occlusion, and parietal enhancement [panels **(C,D)**]. PET and compute tomography angiography (CTA) illustrating aortitis at diagnosis in GCA patient, woman of 64 years old, CRP 84 mg/L, TAB negative [panel **(E)**].

TABLE 1 Differences in the pattern of fluorodeoxyglucose (FDG) uptake between vasculitis and atherosclerosis.

	Large-vessel vasculitis		Atherosclerosis
Intensity of FDG uptake	Grade 2–3		Grade 0–1
Pattern of uptake	Concentric, smooth, and linear		Patchy
Sites	GCA: Diffuse, disease, ascending aorta >brachiocephalic trunk and vertebral arteries >aortic arch = descending aorta	TAK: Axillar, subclavian, and common carotid arteries, abdominal aorta and renal, mesenteric arteries	Iliofemoral arteries, aortic bifurcations.
Calcifications on CT images	No		Yes
Response to steroids	Usually, disappear		Doesn't change

Source Liozon et al. (19), Slart et al. (35), Gribbons et al. (79).

and in a prospective study including both GCA and TAK, future clinical relapses were more frequent in patients with a high PETVAS (≥20) than in patients with a low PETVAS (55 vs. 11%; $P = 0.03$) over a median follow-up of 15 months (43). More recently, the presence of FDG-PET activity at baseline in arterial territories of patients with LVV (TA or GCA) preceded angiographic progression and change (44). An arterial territory with baseline PET activity had 20 times increased odds for angiographic change compared to a paired arterial territory without PET activity. Concomitant edema and wall thickness further increased risk for angiographic change (44).

2-[18F]FDG-PET/CT in monitoring GCA activity

Therapeutic options for GCA comprise glucocorticoids (GC), tocilizumab (TCZ) and methotrexate (MTX). The optimal length of therapy is not well-known but treatment is usually maintained at least 2 years (15, 45). Indeed, relapses have been reported in around 30% of cases in prospective studies, mainly during the first 2 years following diagnosis (46, 47).

18-Fluorodeoxyglucose positron emission tomography/computed tomography in GCA can detect active aortitis and localize inflammation for extra-cranial arterial territories and peripheral arthritis (bilateral shoulder/hip pain and morning stiffness compatible with polymyalgia rheumatica–PMR) (2, 7). An activity score has been proposed to compare uptake evolution and is based on the sum of visual scores in different arterial regions: the Total Vascular Score (TVS). This visual score uses a standardized 0–3 grading system: 0 = no uptake (≤mediastinum); 1 = low-grade uptake (<liver); 2 = intermediate-grade uptake (=liver), 3 = high-grade uptake (>liver). Grade 2 is considered possibly indicative and grade 3 is considered positive for active LVV. The total score can be determined at seven different vascular regions (thoracic aorta, abdominal aorta, subclavian arteries, axillary arteries, carotid arteries, iliac arteries, and femoral arteries) and ranges from 0 to 21 (35). An increased number of vascular region can be chosen in a similar score: PET vascular activity score (PETVAS) by including four segments of the aorta (ascending, arch, descending thoracic, and abdominal) and five branch arteries (carotids, brachiocephalic trunk, subclavian/axillary arteries) with a maximum score of 27 (43).

In a prospective study of 29 patients with biopsy proven GCA and initially positive 2-[18F]FDG-PET/CT, TVS decreased from baseline to 3 months after treatment but remained unchanged at 6 months (31). Furthermore, there was no significant correlation between PET activity and clinical score (BVAS) or biological markers of activity (CRP, ESR) in patients with vascular complications or persistent inflammatory markers despite treatment (48). The persistence of FDG uptake despite clinical and biological remission is poorly understood (vascular remodeling vs. persistent mural inflammation) and its role in further vessel damage is unknown and is among the future research agenda (2).

The role of 2-[18F]FDG-PET/CT for treatment monitoring in LVV has been recently reviewed by van der Geest et al. (49). Longitudinal studies showed a decrease of baseline arterial FDG uptake after treatment induced remission. Investigation of early changes upon glucocorticoid treatment showed the persistence of FDG uptake after 3 days but its disappearance in 64% of cases after 10 days (50). The meta-analysis of four cross-sectional showed a moderate diagnostic accuracy for detecting active disease with a pooled sensitivity of 77% (95% CI 57–90%) and specificity of 71% [95% CI (47–87%)] (49). In a subsequent study comparing treatment effect on vascular inflammation, MTX and TCZ were associated with a higher decreased PETVAS than corticosteroids alone (51). The PET vascular activity score is useful to differentiate active and inactive disease and to predict relapse. However, PET/CT seems less accurate to evaluate clinically active disease in GCA compared to TAK probably explained by a younger age and less atherosclerosis in TAK, and a spectrum of cranial and articular clinical manifestations less frequently the expression of the LVV inflammation in GCA population.

There are no studies available using 2-[18F]FDG-PET/CT alone to guide treatment adaptation. 2-[18F]FDG-PET/CT provides information about vascular inflammation that is complementary from clinical assessment in LVV. A prospective imaging study in patients with GCA treated with tocilizumab shows that 2-[18F]FDG-PET/CT activity is significantly reduced in response to treatment with tocilizumab and repeat 2-[18F]FDG-PET/CT after tocilizumab discontinuation reveal worsening vascular PET activity in most patients (52). Therefore, treatment adaptation is guided by multimodal assessment with clinical, biological and imaging parameters. The 2-[18F]FDG-PET/CT place remains to be specified but 2-[18F]FDG-PET/CT persistent uptake despite clinical remission could be associated with future clinical relapse.

2-[18F]FDG-PET/CT versus other imaging

Comparison of extended vascular US and 2-[18F]FDG-PET/CT showed comparable diagnostic accuracy in a cohort of suspected GCA (53). However, US was more sensible for temporal arteries vasculitis and popliteal vasculitis and 2-[18F]FDG-PET/CT was more performant for thoracic and abdominal aorta vasculitis. Thus, these two imaging modalities may be complementary. The advantages of US over 2-[18F]FDG-PET/CT are its availability, the absence of irradiation and a lower-cost imaging. However, it is operator dependent and does not detect alternate diagnosis such as neoplasia.

Multiple studies have shown comparable diagnostic accuracy between CT angiography (CTA) and PET/CT (25, 54–56). A higher correlation of PET with inflammatory markers was found (25, 55). The main advantages of CT over PET alone were the better evaluation of parietal damage and its availability. However, combination of PET with CT allows better evaluation of parietal damage even if reconstructed slice thickness remains superior to CT alone (∼3.5 mm vs. ∼2 mm) (**Figure 1E**).

In a prospective study comparing early diagnosis performance of MRI and 2-[18F]FDG-PET/CT, their diagnosis accuracy were comparable, however, 2-[18F]FDG-PET/CT detected more vascular regions involved than MRI (57). It should be noted that both are poorly correlate with clinical disease activity in patients with preexisting immunosuppressive therapy (48, 58). We summarize diagnostic performances of different imaging modalities for baseline evaluation in **Table 2**.

Conclusion 2-[18F]FDG-PET/CT and GCA

To sum up, 2-[18F]FDG-PET/CT is a useful diagnosis to assess diagnosis and prognosis of GCA.

TABLE 2 Study characteristics and main findings on the diagnostic accuracy by angiography, ultrasound, CTA, magnetic resonance angiography (MRA) and 18-fluorodeoxyglucose positron emission tomography/computed tomography (2-[18F]FDG-PET/CT) at baseline in giant cell arteritis (GCA) and Takayasu arteritis.

	Angiography	US	CTA	MRA	2-[18F]FDG-PET/CT
Stenosis	+++	+++	+++	++	-
Artery wall thickness	-	+++	+++	++	-
Aneurysm	+++	+++	+++	+++	-
Parietal inflammation	-	+	++	++	+++
Flow	+	+++	-	+++	-

GCA	References	Design	Population	Reference standard	Index test	Performance	Risk of bias based on EULAR evaluation (66)
US	Luqmani et al. (14)	Prospective	381	Clinical diagnosis at 6 months (6m) or positive TAB	Halo/stenosis/occlusion (cranial arteries)	Se 54%, Sp 81% PPV 73% NPV 69%	Moderate
	Rinagel et al. (80)	Meta analysis	1,062 (20 studies)	Positive TAB	Halo/stenosis/occlusion (cranial arteries)	Se 78% Sp 79% PLR 3.80 NLR 0.29	Moderate
	Nielsen et al. (81)	Prospective	46	Clinical diagnosis and positive PET	Halo/compression sign (cranial and extra cranial arteries)	Se 97% Sp 100%	Low
	Hop et al. (82)	Retrospective	113	Clinical diagnosis 6 months	Halo/occlusion (cranial and extra cranial arteries)	Se 71% Sp 93%	Low
	Skoog et al. (83)	Restrospective	201	Clinical diagnosis at 6 months	Halo/compression sign (cranial and extra cranial arteries)	Se 95% Sp 98%	Moderate
CTA	Lariviere et al. (25)	Prospective	24	Clinical diagnosis at 6 months	Wall thickening+contrast enhancement score (1–4)	Se 73% Sp 84% PPV 84 NPV 64%	Low
MRA (cranial arteries)	Bley et al. (84)	Prospective	32	ACR criteria or positive TAB	Wall thickening+contrast enhancement score (0–3)	Se 80.6% Sp 97%	Low
	Siemonsen et al. (80)	Retrospective	28	ACR criteria or positive TAB	Wall thickening+contrast enhancement score (0–3)	Se 80% Sp 80%	Moderate
	Rhéaume et al. (85)	Prospective	171	ACR criteria or positive TAB	Wall thickening+contrast enhancement score (0–3)	Se 93.6% Sp 77.9% PPV 48.3% NPV 98.2%	Moderate
PET/CT	Blockmans et al. (21)	Retrospective	69	Clinical criteria and positive TAB	Visual intensity of FDG uptake	Se 56% Sp 98% PPV 93% NPV 80%	Moderate
	Soussan et al. (24)	Meta analysis	127 (8 studies)	ACR criteria or positive TAB	Visual or semiquantitative analysis of FDG uptake	Se 90% Sp 98% PLR 28.7 NLR 0.15	Moderate
	Lariviere et al. (25)	Prospective	24	Positive TAB	Visual intensity of FDG uptake	Se 66% Sp 100% PPV 100% NPV 64%	Low
	Sammel et al. (28)	Prospective	64	Positive TAB	Visual intensity of FDG uptake	Se 92% Sp 85% PPV 61% NPV 98% AUC 88%	Low
TA	**References**	**Design**	**Population**	**Reference standard**	**Index test**	**Performance**	**Risk of bias based on EULAR evaluation (66)**
US	Barra et al. (72)	Meta analysis	63	ACR Criteria and/or angiography	Carotid Intima-media thickness >1 mm	Se 81% Sp 100%	Moderate
CTA	Yamada et al. (81)	Retrospective	25	Conventional angiography	Luminal changes: stenosis, occlusion, dilatation	Se 67% Sp 100%	Low

(Continued)

Table 2 (Continued)

TA	References	Design	Population	Reference standard	Index test	Performance	Risk of bias based on EULAR evaluation (66)
MRA	Kumar et al. (86)	Retrospective	16	Conventional angiography	Luminal changes: stenosis, occlusion, dilatation	Se 91% Sp 88%	High
	Yamada et al. (87)	Retrospective	30	Conventional angiography	Luminal changes: stenosis, occlusion, dilatation	Se 100% Sp 100%	Low
	Barra et al. (72)	Meta analysis	182	Conventional angiography	Luminal changes: stenosis, occlusion, dilatation	Se 92% Sp 92%	Moderate
PET/CT	Santhosh et al. (65)	Retrospective	51	ACR criteria	Intensity of FDG uptake	Se 83% Sp 90%	Moderate. Evaluated all together performance for both diagnosis and disease activity

Se, sensibility; Sp, specificity; PPV, positive predictive value; NPV, negative predictive value; PLR, positive likehood ratio; NLR, negative likehood ratio; AUC, area under the curve; TAB, temporal artery biopsy.

It can be used in two situations: first, GCA is confirmed or highly probable, for example a high pretest probability and positive US or TAB. In this clinical situation the role of 2-[18F]FDG-PET/CT is to early detect large vessel involvement and to predict vessel damage, particularly thoracic aortitis which is associated with an increased risk of developing thoracic aorta dilatation (42, 44).

Secondly, GCA is suspected but uncertain. For example in patients presenting with constitutional symptoms, FUO, suspected LV involvement or signs of PMR with an intermediate or low pretest probability. In this clinical situation, 2-[18F]FDG-PET/CT is useful to detect signs of vasculitis and search for an alternate diagnosis: signs of PMR, neoplasia, other inflammatory diseases (sarcoidosis) or infection.

Its role in the follow-up of patients with GCA is not well-established. We propose to use 2-[18F]FDG-PET/CT during follow-up of GCA patients depending on clinical and biological parameters evolution to aid in therapeutic decisions: If patient present with clinical symptoms (extracephalic) but without inflammatory markers, a negative TEP may help in deciding to stop or not restart treatment. Also, in a patient with increased biological markers without clinical signs, a positive TEP may detect preclinical lesions and help in deciding to restart or increase anti-inflammatory treatment.

2-[18F]FDG-PET/CT and takayasu arteritis

Takayasu arteritis (TA) is the second primitive vasculitis affecting predominantly large vessels (1). It is ubiquitous but the highest incidence is found in Asia (59). Contrary to GCA it affects mainly patients under 40 years, has a higher F/M sex ratio and differs by clinical presentation and disease course (60).

2-[18F]FDG-PET/CT and TA diagnosis

There is no gold standard for diagnosis of TA and artery biopsy is not routinely available. Diagnosis is mainly based on the presence of characteristic imaging of large arteries in young patients under 50 years with clinical signs and/or elevated inflammatory markers (61).

Patients with TA may present with vascular symptoms attributable to arteritis but also systemic symptoms or "non-vascular" symptoms. Systemic symptoms may precede the vascular phase and are non-specific. They encompass fever, skin manifestations, arthralgia, episcleritis. Also, TA may be associated with other inflammatory diseases, such as sarcoidosis, spondylarthritis, or Crohn disease (62).

TA predominantly affect subclavian and common carotid arteries but aorta and all its branches may be involved (60). The disease is often diagnosed during the vascular phase which results from vascular complications: stenosis in >90% of cases, aneurysm in 20% of cases (63).

Appropriate imaging is the mainstay for the diagnosis of TA (**Table 2**). Based on its performance to investigate mural inflammation and/or luminal changes and the young age of the patients, European guidelines recommend angio-MRI as the first line imaging option replacing angiography (2). Moreover, to assess peripheral artery disease, French guidelines propose vascular doppler ultrasound to evaluate vessel wall morphology and blood flow (61).

We did not find study evaluating the accuracy of 2-[18F]FDG-PET/CT as a diagnostic tool only in TA. However, based on current clinical practice, recent 2022 ACR/EULAR classification criteria for Takayasu arteritis fully integrate evidence of vasculitis in the aorta or branch arteries confirmed by vascular imaging: CT/catheter-based/magnetic resonance angiography (MRA), ultrasound and PET (58, 64). One study by Santhosh et al. (65) studied 2-[18F]FDG-PET/CT as diagnostic tool but also included activity evaluation. Other studies or meta-analysis focused on 2-[18F]FDG-PET/CT as a measurement of the disease activity or included both GCA and TA. Similarly, there was no study on 2-[18F]FDG-PET/CT as diagnostic tool in TA included in the meta-analysis informing the EULAR guidelines on imaging (66).

2-[18F]FDG-PET/CT and TA prognosis

In a multicentric retrospective study of TA patients, relapse were observed in 43% of patients and vascular complications occurred in

38% of patients after a median follow up of 6.1 years (67). Main vascular complications in TA are: neurovascular disease (stroke, transitory ischemic attack), ischemic retinopathy, cardiovascular complications ranging from aortic regurgitation to pulmonary hypertension including coronaropathy and microvascular ischemia, renovascular disease, and peripheral artery disease. Risk factors for relapse were male sex, high CRP and carotidynia at diagnosis. Progressive disease, thoracic aorta involvement and retinopathy were associated with vascular complications (67).

One retrospective study evaluated the predictive value of 2-[18F]FDG-PET/CT in 32 patients with baseline 2-[18F]FDG-PET/CT and a median follow up of 83.5 months. Maximal standardized uptake value (SUVmax) in arteries ≥1.3 seemed to be associated with disease relapse [Odds ratio (OR): 5.667; 95% confidence interval (95 CI): (1.067–30.085)] and the need to change therapy [OR: 7.933; 95 CI: (1.478–42.581)]. Interpretation of these results must be cautious because of potential bias due to study design and very large 95% confidence interval of ORs. Also, there was no association between SUVmax intensity at baseline and the development of ischemic events, new angiographic lesions or sustained remission (68). In a recent prospective cohort to assess whether vascular 2-[18F]FDG-PET/CT activity is associated with angiographic change in LVV including 38 TA patients, lack of 2-[18F]FDG-PET/CT activity was strongly associated with stable angiographic disease, $P < 0.01$ (44). An arterial territory with baseline 2-[18F]FDG-PET/CT activity had 20 times increased odds for angiographic change compared to a paired arterial territory without PET activity. Angiographic progression with arterial damage was preceded by the presence of 2-[18F]FDG-PET/CT activity (44).

2-[18F]FDG-PET/CT and monitoring TA activity

Treatment of TA is based on glucocorticoids often associated with methotrexate or anti-TNFα in severe disease or in case of steroids dependence (15, 45, 61). There are no consensual criteria for assessing TA activity. Inflammatory markers are poorly correlated with angiographic progression and may remain negative in 30% of patients with clinically active disease (69). Two tools are commonly used : First the NIH criteria and more recently, the ITAS2010 criteria which is increasingly being used (70, 71).

A meta-analysis including 131 patients with TA evaluated 2-[18F]FDG-PET/CT performance for assessing activity of disease based on NIH and showed a sensitivity and specificity of 84% (24). All four included studies had a retrospective design. These results were confirmed in a second meta-analysis including 57 studies, mainly cross-sectional and of low methodological quality. The pooled sensitivity was 81% and specificity 74% (72). A recent longitudinal study included 126 patients with LVV (GCA = 50; TAK = 76) with 2-[18F]FDG-PET/CT at enrollment and follow up. Global arterial FDG uptake was quantified with PETVAS. After a median follow up of 2.6 years, there was no significant decrease in PETVAS in TA patients. Also, there was no direct correlation between PETVAS during follow up and clinical and biological activity (73).

One case report suggested that 2-[18F]FDG-PET/CT may not detect pulmonary artery (PA) involvement in TA) (74). This was infirmed in a study Gao et al. (75) which compared performance of 2-[18F]FDG-PET/CT versus CTPA or AMR in TA patients with PA involvement. 2-[18F]FDG-PET/CT was as sensible as radiological imaging (71.4 vs. 92.9%, $P = 0.250$) and seemed to have higher specificity (91.7 vs. 37.5%, $P = 0.001$).

Finally, a multimodal assessment of TA activity was proposed by amalgamating the sum of mean SUV, ESR and soluble interleukin-2 receptor (IL-2Rs) which seemed concordant with NIH and ITAS2010 criteria (76). However, the population included had different disease course and treatment. This model needs further validation using prospective studies and homogenous population.

Conclusion PET/CT and TA

The place of 2-[18F]FDG-PET/CT in TA management remains poorly defined. Diagnosis and disease activity assessment in TA can be challenging as patients may not have overt clinical symptoms or elevated CRP at diagnosis or during periods of active disease. Combination of non-invasive vascular imaging such as doppler ultrasound, MRA, CTA, and 2-[18F]FDG-PET/CT remains the first line modality for diagnosis of TA and is essential to monitor vascular disease in patients with TA. During follow up, new areas of arterial damage can develop despite apparent clinical and biological remission in TA. 2-[18F]FDG-PET/CT cannot be systematically recommended for follow up but incorporate the use of 2-[18F]FDG-PET/CT with non-invasive vascular imaging may complete multimodal imaging assessment of disease activity and risk of vascular damage.

Prospects

Novel PET imaging techniques are progressively used or under research.

Positron emission tomography/MRI has been evaluated in large vessel vasculitis and allow analysis of different pattern: fibrous vs. inflammatory pattern (77). Its place in LVV, TA particularly, remains to be specified.

Van der Geest et al. (49) recently reviewed novel PET imaging techniques using novel cell targets and novel tracers. These techniques could improve imaging accuracy by using a more specific cell uptake of FDG with less background activity. Also, it could enhance activity evaluation after treatment (78). Some of these novel targets are: T cells targeted radio tracers (IL2-R, CD4, CD8), macrophages [Translocator protein (TSPO), mannose receptor (CD206), folate receptor and others], B cells, activated fibroblasts (Fibroblast activation protein alpha pathway), endothelial cells (VCAM-1).

Some drawbacks have been underlined by Van der Geest et al. (49): the risk of high irradiation dose, the complexity and cost of radiotracers development and the need of clinical study to confirm their utility.

Conclusion

This review illustrates that 2-[18F]FDG-PET/CT is a powerful metabolic imaging tool that may help improving early diagnosis, current classification, and prognostic assessment in LVV. In patients with a clinical suspicion for LVV, 2-[18F]FDG-PET/CT can help

to diagnose LVV especially at the early onset of disease or in case of non-specific signs. Early recognition of LVV is essential because irreversible ischemic complication (e.g., stroke, vision loss, myocardial infarction) almost always occur early, prior to steroids therapy. Moreover, the presence of vascular 2-[18F]FDG-PET/CT activity can precede angiographic change and progression in LVV. Conversely, the disappearance of 2-[18F]FDG-PET/CT uptake after effective therapy is possible. Thus, 2-[18F]FDG-PET/CT may be useful to evaluate treatment efficiency as well as for detection of LVV relapse and vascular complication at an early stage. Persistent activity however, is difficult to interpret, and its impact on disease treatment modifications is not well-known yet and needs further research. 2-[18F]FDG-PET/CT may help clinician to determine patients with more active, diffuse, and severe LVV requiring a more intensive treatment and close monitoring.

Author contributions

KN and CC collected the data and wrote the manuscript. AV, VB, KC, RB, SM, and DS made imaging analysis. KN and CC were responsible for verification of all the underlying data and took full responsibility for the integrity of the work. All authors critically reviewed and approved the final version of the manuscript.

Conflict of interest

The authors declare that the research was conducted in the absence of any commercial or financial relationships that could be construed as a potential conflict of interest.

Publisher's note

References

1. Jennette J, Falk R, Bacon P, Basu N, Cid M, Ferrario F, et al. 2012 Revised international chapel hill consensus conference nomenclature of vasculitides. *Arthritis Rheum.* (2013) 65:1–11. doi: 10.1002/art.37715

2. Dejaco C, Ramiro S, Duftner C, Besson F, Bley T, Blockmans D, et al. EULAR recommendations for the use of imaging in large vessel vasculitis in clinical practice. *Ann Rheum Dis.* (2018) 77:636–43. doi: 10.1136/annrheumdis-2017-212649

3. Kubota R, Yamada S, Kubota K, Ishiwata K, Tamahashi N, Ido T. Intratumoral distribution of fluorine-18-fluorodeoxyglucose in vivo: high accumulation in macrophages and granulation tissues studied by microautoradiography. *J Nucl Med.* (1992) 33:1972–80.

4. Yamada S, Kubota K, Kubota R, Ido T, Tamahashi N. High accumulation of fluorine-18-fluorodeoxyglucose in turpentine-induced inflammatory tissue. *J Nucl Med.* (1995) 36:1301–6.

5. Reinhold-Keller E, Zeidler A, Gutfleisch J, Peter H, Raspe H, Gross W. Giant cell arteritis is more prevalent in urban than in rural populations: results of an epidemiological study of primary systemic vasculitides in Germany. *Rheumatol Oxf Engl.* (2000) 39:1396–402. doi: 10.1093/rheumatology/39.12.1396

6. Calamia K, Hunder G. Giant cell arteritis (Temporal Arteritis) presenting as fever of undetermined origin. *Arthritis Rheum.* (1981) 24:1414–8.

7. Buttgereit F, Dejaco C, Matteson E, Dasgupta B. Polymyalgia rheumatica and giant cell arteritis: A systematic review. *JAMA.* (2016) 315:2442–58.

8. Salvarani C, Macchioni P, Tartoni P, Rossi F, Baricchi R, Castri C, et al. Polymyalgia rheumatica and giant cell arteritis: a 5-year epidemiologic and clinical study in Reggio Emilia. Italy. *Clin Exp Rheumatol.* (1987) 5:205–15.

9. Patil P, Williams M, Maw W, Achilleos K, Elsideeg S, Dejaco C, et al. Fast track pathway reduces sight loss in giant cell arteritis: results of a longitudinal observational cohort study. *Clin Exp Rheumatol.* (2015) 33(2 Suppl 89):103–6.

10. Diamantopoulos A, Haugeberg G, Lindland A, Myklebust G. The fast-track ultrasound clinic for early diagnosis of giant cell arteritis significantly reduces permanent visual impairment: towards a more effective strategy to improve clinical outcome in giant cell arteritis? *Rheumatol Oxf Engl.* (2016) 55:66–70. doi: 10.1093/rheumatology/kev289

11. Schmidt W, Seifert A, Gromnica-Ihle E, Krause A, Natusch A. Ultrasound of proximal upper extremity arteries to increase the diagnostic yield in large-vessel giant cell arteritis. *Rheumatol Oxf Engl.* (2008) 47:96–101. doi: 10.1093/rheumatology/kem322

12. Brack A, Martinez-Taboada V, Stanson A, Goronzy J, Weyand C. Disease pattern in cranial and large-vessel giant cell arteritis. *Arthritis Rheum.* (1999) 42:311–7.

13. Mukhtyar C, Guillevin L, Cid M, Dasgupta B, Groot de K, Gross W, et al. EULAR recommendations for the management of large vessel vasculitis. *Ann Rheum Dis.* (2009) 68:318–23. doi: 10.1136/ard.2008.088351

14. Luqmani R, Lee E, Singh S, Gillett M, Schmidt W, Bradburn M, et al. The Role of Ultrasound Compared to Biopsy of Temporal Arteries in the Diagnosis and Treatment of Giant Cell Arteritis (TABUL): a diagnostic accuracy and cost-effectiveness study. *Health Technol Assess Winch Engl.* (2016) 20:1–238. doi: 10.3310/hta20900

15. Maz M, Chung S, Abril A, Langford C, Gorelik M, Guyatt G, et al. 2021 American college of rheumatology/vasculitis foundation guideline for the management of giant cell arteritis and takayasu arteritis. *Arthritis Rheumatol.* (2021) 73:1349–65.

16. Ponte C, Grayson P, Robson J, Suppiah R, Gribbons K, Judge A, et al. 2022 American College of Rheumatology/EULAR classification criteria for giant cell arteritis. *Ann Rheum Dis.* (2022) 81:1647–53.

17. Bienvenu B, Ly K, Lambert M, Agard C, André M, Benhamou Y, et al. Management of giant cell arteritis: Recommendations of the French Study Group for Large Vessel Vasculitis (GEFA). *Rev Med Interne.* (2016) 37:154–65. doi: 10.1016/j.revmed.2015.12.015

18. Mackie S, Dejaco C, Appenzeller S, Camellino D, Duftner C, Gonzalez-Chiappe S, et al. British Society for Rheumatology guideline on diagnosis and treatment of giant cell arteritis: executive summary. *Rheumatology.* (2020) 59:487–94. doi: 10.1093/rheumatology/kez664

19. Gribbons K, Ponte C, Carette S, Craven A, Cuthbertson D, Hoffman G, et al. Patterns of arterial disease in takayasu's arteritis and giant cell arteritis. *Arthritis Care Res.* (2020) 72:1615–24. doi: 10.1002/acr.24055

20. Malich L, Gühne F, Hoffmann T, Malich A, Weise T, Oelzner P, et al. Distribution patterns of arterial affection and the influence of glucocorticoids on 18F-fluorodeoxyglucose positron emission tomography/CT in patients with giant cell arteritis. *RMD Open.* (2022) 8:e002464. doi: 10.1136/rmdopen-2022-002464

21. Blockmans D, Stroobants S, Maes A, Mortelmans L. Positron emission tomography in giant cell arteritis and polymyalgia rheumatica: evidence for inflammation of the aortic arch. *Am J Med.* (2000) 108:246–9. doi: 10.1016/s0002-9343(99)00424-6

22. Besson F, Parienti J, Bienvenu B, Prior J, Costo S, Bouvard G, et al. Diagnostic performance of 18F-fluorodeoxyglucose positron emission tomography in giant cell arteritis: a systematic review and meta-analysis. *Eur J Nucl Med Mol Imaging.* (2011) 38:1764–72. doi: 10.1007/s00259-011-1830-0

23. Lee Y, Choi S, Ji J, Song G. Diagnostic accuracy of 18F-FDG PET or PET/CT for large vessel vasculitis: A meta-analysis. *Z Rheumatol.* (2016) 75:924–31.

24. Soussan M, Nicolas P, Schramm C, Katsahian S, Pop G, Fain O, et al. Management of large-vessel vasculitis with FDG-PET: A systematic literature review and meta-analysis. *Medicine (Baltimore).* (2015) 94:e622. doi: 10.1097/MD.0000000000000622

25. Lariviere D, Benali K, Coustet B, Pasi N, Hyafil F, Klein I, et al. Positron emission tomography and computed tomography angiography for the diagnosis of giant cell arteritis: A real-life prospective study. *Medicine (Baltimore).* (2016) 95:e4146. doi: 10.1097/MD.0000000000004146

26. Hay B, Mariano-Goulart D, Bourdon A, Benkiran M, Vauchot F, De Verbizier D, et al. Diagnostic performance of 18F-FDG PET-CT for large vessel involvement assessment in patients with suspected giant cell arteritis and negative temporal artery biopsy. *Ann Nucl Med.* (2019) 33:512–20. doi: 10.1007/s12149-019-01358-5

27. Nielsen B, Hansen I, Kramer S, Haraldsen A, Hjorthaug K, Bogsrud T, et al. Simple dichotomous assessment of cranial artery inflammation by conventional 18F-FDG PET/CT shows high accuracy for the diagnosis of giant cell arteritis: a case-control study. *Eur J Nucl Med Mol Imaging.* (2019) 46:184–93. doi: 10.1007/s00259-018-4106-0

28. Sammel A, Hsiao E, Schembri G, Nguyen K, Brewer J, Schrieber L, et al. Diagnostic accuracy of positron emission tomography/computed tomography of the head, neck, and chest for giant cell arteritis: A prospective, double-blind, cross-sectional study. *Arthritis Rheumatol.* (2019) 71:1319–28. doi: 10.1002/art.40864

29. Nienhuis P, Sandovici M, Glaudemans A, Slart R, Brouwer E. Visual and semiquantitative assessment of cranial artery inflammation with FDG-PET/CT in giant cell arteritis. *Semin Arthritis Rheum.* (2020) 50:616–23. doi: 10.1016/j.semarthrit.2020.04.002

30. Besson F, Chaumet-Riffaud P, Playe M, Noel N, Lambotte O, Goujard C, et al. Contribution of (18)F-FDG PET in the diagnostic assessment of fever of unknown origin (FUO): a stratification-based meta-analysis. *Eur J Nucl Med Mol Imaging.* (2016) 43:1887–95. doi: 10.1007/s00259-016-3377-6

31. Blockmans D, De Ceuninck L, Vanderschueren S, Knockaert D, Mortelmans L, Bobbaers H. Repetitive 18-fluorodeoxyglucose positron emission tomography in isolated polymyalgia rheumatica: a prospective study in 35 patients. *Rheumatol Oxf Engl.* (2007) 46:672–7. doi: 10.1093/rheumatology/kel376

32. Lavado-Pérez C, Martínez-Rodríguez I, Martínez-Amador N, Banzo I, Quirce R, Jiménez-Bonilla J, et al. (18)F-FDG PET/CT for the detection of large vessel vasculitis in patients with polymyalgia rheumatica. *Rev Esp Med Nucl Imagen Mol.* (2015) 34:275–81.

33. Belhocine T, Blockmans D, Hustinx R, Vandevivere J, Mortelmans L. Imaging of large vessel vasculitis with (18)FDG PET: illusion or reality? A critical review of the literature data. *Eur J Nucl Med Mol Imaging.* (2003) 30:1305–13.

34. Espitia O, Schanus J, Agard C, Kraeber-Bodéré F, Hersant J, Serfaty J, et al. Specific features to differentiate Giant cell arteritis aortitis from aortic atheroma using FDG-PET/CT. *Sci Rep*. (2021) 11:17389. doi: 10.1038/s41598-021-96923-2

35. Slart R. FDG-PET/CT(A) imaging in large vessel vasculitis and polymyalgia rheumatica: joint procedural recommendation of the EANM, SNMMI, and the PET Interest Group (PIG), and endorsed by the ASNC. *Eur J Nucl Med Mol Imaging.* (2018) 45:1250–69. doi: 10.1007/s00259-018-3973-8

36. Pugh D, Karabayas M, Basu N, Cid M, Goel R, Goodyear C, et al. Large-vessel vasculitis. *Nat Rev Dis Primer.* (2022) 7:1–23. doi: 10.1038/s41572-021-00327-5

37. Robson J, Kiran A, Maskell J, Hutchings A, Arden N, Dasgupta B, et al. The relative risk of aortic aneurysm in patients with giant cell arteritis compared with the general population of the UK. *Ann Rheum Dis.* (2015) 74:129–35. doi: 10.1136/annrheumdis-2013-204113

38. Nuenninghoff D, Hunder G, Christianson T, McClelland R, Matteson E. Incidence and predictors of large-artery complication (aortic aneurysm, aortic dissection, and/or large-artery stenosis) in patients with giant cell arteritis: a population-based study over 50 years. *Arthritis Rheum.* (2003) 48:3522–31. doi: 10.1002/art.11353

39. García-Martínez A, Hernández-Rodríguez J, Arguis P, Paredes P, Segarra M, Lozano E, et al. Development of aortic aneurysm/dilatation during the followup of patients with giant cell arteritis: a cross-sectional screening of fifty-four prospectively followed patients. *Arthritis Rheum.* (2008) 59:422–30. doi: 10.1002/art.23315

40. Kermani T, Warrington K, Crowson C, Ytterberg S, Hunder G, Gabriel S, et al. Large-vessel involvement in giant cell arteritis: a population-based cohort study of the incidence-trends and prognosis. *Ann Rheum Dis.* (2013) 72:1989–94. doi: 10.1136/annrheumdis-2012-202408

41. Galli E, Muratore F, Mancuso P, Boiardi L, Marvisi C, Besutti G, et al. The role of PET/CT in disease activity assessment in patients with large vessel vasculitis. *Rheumatol Oxf Engl.* (2022) 8:keac125. doi: 10.1093/rheumatology/keac125

42. Blockmans D, Coudyzer W, Vanderschueren S, Stroobants S, Loeckx D, Heye S, et al. Relationship between fluorodeoxyglucose uptake in the large vessels and late aortic diameter in giant cell arteritis. *Rheumatol Oxf Engl.* (2008) 47:1179–84. doi: 10.1093/rheumatology/ken119

43. Grayson P, Alehashemi S, Bagheri A, Civelek A, Cupps T, Kaplan M, et al. 18 F-Fluorodeoxyglucose-Positron emission tomography as an imaging biomarker in a prospective, longitudinal cohort of patients with large vessel vasculitis. *Arthritis Rheumatol.* (2018) 70:439–49. doi: 10.1002/art.40379

44. Quinn K, Ahlman M, Alessi H, LaValley M, Neogi T, Marko J, et al. Association of 18F-fluorodeoxyglucose positron emission tomography and angiographic progression of disease in large-vessel vasculitis. *Arthritis Rheumatol.* (2022) 75:98–107. doi: 10.1002/art.42290

45. Hellmich B, Agueda A, Monti S, Buttgereit F, de Boysson H, Brouwer E, et al. 2018 Update of the EULAR recommendations for the management of large vessel vasculitis. *Ann Rheum Dis.* (2020) 79:19–30. doi: 10.1136/annrheumdis-2019-215672

46. Alba M, García-Martínez A, Prieto-González S, Tavera-Bahillo I, Corbera-Bellalta M, Planas-Rigol E, et al. Relapses in patients with giant cell arteritis: prevalence, characteristics, and associated clinical findings in a longitudinally followed cohort of 106 patients. *Medicine (Baltimore).* (2014) 93:194–201. doi: 10.1097/MD.0000000000000033

47. Kermani T, Warrington K, Cuthbertson D, Carette S, Hoffman G, Khalidi N, et al. Disease relapses among patients with giant cell arteritis: A prospective, longitudinal cohort study. *J Rheumatol.* (2015) 42:1213–7. doi: 10.3899/jrheum.141347

48. Both M, Ahmadi-Simab K, Reuter M, Dourvos O, Fritzer E, Ullrich S, et al. MRI and FDG-PET in the assessment of inflammatory aortic arch syndrome in complicated courses of giant cell arteritis. *Ann Rheum Dis.* (2008) 67:1030–3. doi: 10.1136/ard.2007.082123

49. van der Geest K, Treglia G, Glaudemans A, Brouwer E, Sandovici M, Jamar F, et al. Diagnostic value of [18F]FDG-PET/CT for treatment monitoring in large vessel vasculitis: a systematic review and meta-analysis. *Eur J Nucl Med Mol Imaging.* (2021) 48:3886–902. doi: 10.1007/s00259-021-05362-8

50. Nielsen B, Gormsen L, Hansen I, Keller K, Therkildsen P, Hauge E. Three days of high-dose glucocorticoid treatment attenuates large-vessel 18F-FDG uptake in large-vessel giant cell arteritis but with a limited impact on diagnostic accuracy. *Eur J Nucl Med Mol Imaging.* (2018) 45:1119–28. doi: 10.1007/s00259-018-4021-4

51. Schönau V, Roth J, Tascilar K, Corte G, Manger B, Rech J, et al. Resolution of vascular inflammation in patients with new-onset giant cell arteritis: data from the RIGA study. *Rheumatol Oxf Engl.* (2021) 60:3851–61. doi: 10.1093/rheumatology/keab332

52. Quinn K, Dashora H, Novakovich E, Ahlman M, Grayson P. Use of 18F-fluorodeoxyglucose positron emission tomography to monitor tocilizumab effect on vascular inflammation in giant cell arteritis. *Rheumatol Oxf Engl.* (2021) 60:4384–9. doi: 10.1093/rheumatology/keaa894

53. Imfeld S, Aschwanden M, Rottenburger C, Schegk E, Berger C, Staub D, et al. [18F]FDG positron emission tomography and ultrasound in the diagnosis of giant cell arteritis: congruent or complementary imaging methods? *Rheumatol Oxf Engl.* (2020) 59:772–8. doi: 10.1093/rheumatology/kez362

54. de Boysson H, Dumont A, Liozon E, Lambert M, Boutemy J, Maigné G, et al. Giant-cell arteritis: concordance study between aortic CT angiography and FDG-PET/CT in detection of large-vessel involvement. *Eur J Nucl Med Mol Imaging.* (2017) 44:2274–9. doi: 10.1007/s00259-017-3774-5

55. Olthof S, Krumm P, Henes J, Nikolaou K, la Fougère C, Pfannenberg C, et al. Imaging giant cell arteritis and Aortitis in contrast enhanced 18F-FDG PET/CT: Which imaging score correlates best with laboratory inflammation markers? *Eur J Radiol.* (2018) 99:94–102. doi: 10.1016/j.ejrad.2017.12.021

56. Vaidyanathan S, Chattopadhyay A, Mackie S, Scarsbrook A. Comparative effectiveness of 18F-FDG PET-CT and contrast-enhanced CT in the diagnosis of suspected large-vessel vasculitis. *Br J Radiol.* (2018) 91:20180247. doi: 10.1259/bjr.20180247

57. Meller J, Strutz F, Siefker U, Scheel A, Sahlmann C, Lehmann K, et al. Early diagnosis and follow-up of aortitis with [(18)F]FDG PET and MRI. *Eur J Nucl Med Mol Imaging.* (2003) 30:730–6.

58. Quinn K, Ahlman M, Malayeri A, Marko J, Civelek A, Rosenblum J, et al. Comparison of magnetic resonance angiography and 18F-fluorodeoxyglucose positron emission tomography in large-vessel vasculitis. *Ann Rheum Dis.* (2018) 77:1165–71. doi: 10.1136/annrheumdis-2018-213102

59. Toshihiko N. Current status of large and small vessel vasculitis in Japan. *Int J Cardiol.* (1996) 54 Suppl:S91–8. doi: 10.1016/s0167-5273(96)88777-8

60. Watanabe Y, Miyata T, Tanemoto K. Current clinical features of new patients with takayasu arteritis observed from cross-country research in japan: Age and sex specificity. *Circulation.* (2015) 132:1701–9. doi: 10.1161/CIRCULATIONAHA.114.012547

61. Saadoun D, Bura-Riviere A, Comarmond C, Lambert M, Redheuil A, Mirault T, et al. French recommendations for the management of Takayasu's arteritis. *Orphanet J Rare Dis.* (2021) 16(Suppl 3):311. doi: 10.1186/s13023-021-01922-1

62. Saadoun D, Vautier M, Cacoub P. Medium- and large-vessel vasculitis. *Circulation.* (2021) 143:267–82. doi: 10.1161/CIRCULATIONAHA.120.046657

63. Mason J. Takayasu arteritis–advances in diagnosis and management. *Nat Rev Rheumatol.* (2010) 6:406–15. doi: 10.1038/nrrheum.2010.82

64. Grayson P, Ponte C, Suppiah R, Robson J, Gribbons K, Judge A, et al. 2022 American College of Rheumatology/EULAR classification criteria for Takayasu arteritis. *Ann Rheum Dis.* (2022) 81:1654–60.

65. Santhosh S, Mittal B, Gayana S, Bhattacharya A, Sharma A, Jain S. F-18 FDG PET/CT in the evaluation of Takayasu arteritis: an experience from the tropics. *J Nucl Cardiol.* (2014) 21:993–1000. doi: 10.1007/s12350-014-9910-8

66. Duftner C, Dejaco C, Sepriano A, Falzon L, Schmidt W, Ramiro S. Imaging in diagnosis, outcome prediction and monitoring of large vessel vasculitis: a systematic literature review and meta-analysis informing the EULAR recommendations. *RMD Open.* (2018) 4:e000612. doi: 10.1136/rmdopen-2017-000612

67. Comarmond C, Biard L, Lambert M, Mekinian A, Ferfar Y, Kahn J, et al. Long-Term outcomes and prognostic factors of complications in takayasu arteritis. *Circulation.* (2017) 136:1114–22.

68. Janes A, Castro M, Arraes A, Savioli B, Sato E, de Souza A. A retrospective cohort study to assess PET-CT findings and clinical outcomes in Takayasu arteritis: does 18F-fluorodeoxyglucose uptake in arteries predict relapses? *Rheumatol Int.* (2020) 40:1123–31. doi: 10.1007/s00296-020-04551-2

69. Ishihara T, Haraguchi G, Tezuka D, Kamiishi T, Inagaki H, Isobe M. Diagnosis and assessment of Takayasu arteritis by multiple biomarkers. *Circ J.* (2013) 77:477–83.

70. Kerr G, Hallahan C, Giordano J, Leavitt R, Fauci A, Rottem M, et al. Takayasu arteritis. *Ann Intern Med.* (1994) 120:919–29.

71. Misra R, Danda D, Rajappa S, Ghosh A, Gupta R, Mahendranath K, et al. Development and initial validation of the Indian Takayasu Clinical Activity Score (ITAS2010). *Rheumatology.* (2013) 52:1795–801. doi: 10.1093/rheumatology/ket128

72. Barra L, Kanji T, Malette J, Pagnoux C, CanVasc. Imaging modalities for the diagnosis and disease activity assessment of Takayasu's arteritis: A systematic review and meta-analysis. *Autoimmun Rev.* (2018) 17:175–87. doi: 10.1016/j.autrev.2017.11.021

73. Alessi, H, Quinn K, Ahlman M, Novakovich E, Saboury B, Luo Y, et al. Longitudinal characterization of vascular inflammation and disease activity in takayasu's arteritis and giant cell arteritis: A single-center prospective study. *Arthritis Care Res.* (2022) 1–9. doi: 10.1002/acr.24976

74. Addimanda O, Spaggiari L, Pipitone N, Versari A, Pattacini P, Salvarani C. Pulmonary artery involvement in Takayasu arteritis. PET/CT versus CT angiography. *Clin Exp Rheumatol.* (2013) 31(1 Suppl 75):S3–4.

75. Gao W, Gong J, Guo X, Wu J, Xi X, Ma Z, et al. Value of 18F-fluorodeoxyglucose positron emission tomography/computed tomography in the evaluation of pulmonary artery activity in patients with Takayasu's arteritis. *Eur Heart J Cardiovasc Imaging.* (2021) 22:541–50. doi: 10.1093/ehjci/jeaa229

76. Ma L, Wu B, Jin X, Sun Y, Kong X, Ji Z, et al. A novel model to assess disease activity in Takayasu arteritis based on 18F-FDG-PET/CT: a Chinese cohort study. *Rheumatol Oxf Engl.* (2022) 61(SI):SI14–22.

77. Laurent C, Ricard L, Fain O, Buvat I, Adedjouma A, Soussan M, et al. PET/MRI in large-vessel vasculitis: clinical value for diagnosis and assessment of disease activity. *Sci Rep.* (2019) 9:12388.

78. van der Geest K, Sandovici M, Nienhuis P, Slart R, Heeringa P, Brouwer E, et al. Novel PET imaging of inflammatory targets and cells for the diagnosis and monitoring of giant cell arteritis and polymyalgia rheumatica. *Front Med.* (2022) 9:902155. doi: 10.3389/fmed.2022.902155

79. Liozon E. Place actuelle de l'imagerie non invasive des artères de gros calibre dans l'artérite à cellules géantes: du diagnostic au suivi. *Rev Méd Interne.* (2020) 41:756–68. doi: 10.1016/j.revmed.2020.06.004

80. Rinagel M, Chatelus E, Jousse-Joulin S, Sibilia J, Gottenberg J, Chasset F, et al. Diagnostic performance of temporal artery ultrasound for the diagnosis of giant cell arteritis: a systematic review and meta-analysis of the literature. *Autoimmun Rev.* (2019) 18:56–61.

81. Nielsen B, Hansen I, Keller K, Therkildsen P, Gormsen L, Hauge E. Diagnostic accuracy of ultrasound for detecting large-vessel giant cell arteritis using FDG PET/CT as the reference. *Rheumatol Oxf Engl.* (2020) 59:2062–73. doi: 10.1093/rheumatology/kez568

82. Hop H, Mulder D, Sandovici M, Glaudemans A, van Roon A, Slart R, et al. Diagnostic value of axillary artery ultrasound in patients with suspected giant cell arteritis. *Rheumatology.* (2020) 59:3676–84.

83. Skoog J, Svensson C, Eriksson P, Sjöwall C, Zachrisson H. The diagnostic performance of an extended ultrasound protocol in patients with clinically suspected giant cell arteritis. *Front Med.* (2021) 8:807996. doi: 10.3389/fmed.2021.807996

84. Bley T, Uhl M, Carew J, Markl M, Schmidt D, Peter H, et al. Diagnostic value of high-resolution MR imaging in giant cell arteritis. *AJNR Am J Neuroradiol.* (2007) 28:1722–7. doi: 10.3174/ajnr.A0638

85. Rhéaume M, Rebello R, Pagnoux C, Carette S, Clements-Baker M, Cohen-Hallaleh V, et al. High-Resolution magnetic resonance imaging of scalp arteries for the diagnosis of giant cell arteritis: Results of a prospective cohort study. *Arthritis Rheumatol Hoboken NJ.* (2017) 69:161–8. doi: 10.1002/art.39824

86. Kumar S, Radhakrishnan S, Phadke R, Gupta R, Gujral R. Takayasu's arteritis: evaluation with three-dimensional time-of-flight MR angiography. *Eur Radiol.* (1997) 7:44–50. doi: 10.1007/s003300050107

87. Yamada I, Nakagawa T, Himeno Y, Kobayashi Y, Numano F, Shibuya H. Takayasu arteritis: diagnosis with breath-hold contrast-enhanced three-dimensional MR angiography. *J Magn Reson Imaging JMRI.* (2000) 11:481–7. doi: 10.1002/(SICI)1522-2586(200005)11:5<481::AID-JMRI3>3.0.CO;2-4

Frontiers in Medicine

Translating medical research and innovation into improved patient care

A multidisciplinary journal which advances our medical knowledge. It supports the translation of scientific advances into new therapies and diagnostic tools that will improve patient care.

Discover the latest Research Topics

See more →

Frontiers

Avenue du Tribunal-Fédéral 34
1005 Lausanne, Switzerland
frontiersin.org

Contact us

+41 (0)21 510 17 00
frontiersin.org/about/contact